Diverse methods for integrable models

Fehér, G.

György Fehér

Diverse methods for integrable models

Diverse methods for integrable models

György Fehér

Diverse methods for integrable models

ACADEMISCH PROEFSCHRIFT
ter verkrijging van de graad van doctor
aan de Universiteit van Amsterdam
op gezag van de Rector Magnificus
prof. dr. ir. K.I.J. Maex
ten overstaan van een door het College voor Promoties ingestelde commissie,
in het openbaar te verdedigen in de Agnietenkapel
op dinsdag 28 november 2017, te 14.00 uur
door

György Fehér
geboren te Boedapest, Hongarije

Promotiecommissie:

Promotor:	Prof. dr. B.Nienhuis	Universiteit van Amsterdam
Overige leden:	Prof. dr. J.V.Stokman	Universiteit van Amsterdam
	Prof. dr. C.J.M.Schoutens	Universiteit van Amsterdam
	Prof. dr. J.-S.Caux	Universiteit van Amsterdam
	dr. V.Gritsev	Universiteit van Amsterdam
	Prof. dr. N.Reshetikhin	University of California, Berkeley, Universiteit van Amsterdam
	Prof. dr. J.-B.Zuber	Université Pierre et Marie Curie
	Prof. dr. P.Zinn-Justin	University of Melbourne

Faculteit der Natuurwetenschappen, Wiskunde en Informatica

List of Publications

This thesis is based on the following publications:

[1] G. Z. Feher and B. Nienhuis. Currents in the dilute $O(n = 1)$ model. 2015, math-ph/1510.02721., *preprint*

[2] Gyorgy Z. Feher, Paul A. Pearce, and Alessandra Vittorini-Orgeas. One-dimensional sums and finitized characters of 2×2 fused RSOS models. 2016, *unpublished*

[3] Jan de Gier, Gyorgy Z. Feher, Bernard Nienhuis, and Magdalena Rusaczonek. Integrable supersymmetric chain without particle conservation. 2015, math-ph/1510.02520, *J. Stat. Mech. (2016) 023104*

Contents

List of Figures

Chapter 1

Introduction

Statistical physics is the branch of physics which aims to describe the collective behavior of a large number of constituting pieces, typically particles. The precise, or near precise description of such a system (e.g. the trajectories of all the particles in an interacting classical system) is a hopelessly complicated task, and statistical physics does not aim for that. Its goal is to describe the system through average macroscopic quantities, such as temperature, density, magnetization, etc. To describe the intrinsic behavior of systems, correlations between different parts of the system are probed in the context of statistical physics. An example is how the correlation of local magnetization decays with the distance.

One important focus of statistical physical research is the description of phase transition: the phenomenon when some macroscopic quantity of the system undergoes a sudden change. It is observed that while usually the thermodynamic properties of the materials change smoothly, at certain values of the parameters, they undergo abrupt, often discontinuous changes. E.g. the density of the material changes drastically, or a magnet loses its magnetization. The phase transition happens at certain external conditions, e.g. at atmospheric pressure, the water boils at $T = 100°C$. These external conditions are characterized by intensive thermodynamic quantities. Intensive thermodynamic quantities are the thermodynamic quantities which –instead of adding together– equalize when some interaction is introduced between two previously separate systems.

Two types of phase transitions are distinguished, first (or discontinuous) and second order (or continuous) phase transition. To describe the difference between them, first we introduce the concept of correlation length.

Correlation length is an intrinsic length scale of the material, which can be observed, e.g. by scattering experiments. At distances less than the correlation

length, microscopic properties are correlated, while much further apart, they are not. Naturally, the correlation length depends on the external conditions, such as temperature, pressure, external magnetic field, etc. This property is used to characterize the phase transitions.
The correlation length behaves differently in the two types of phase transition. At the phase transition point, the correlation length either remains finite, or becomes effectively infinite.
In case of the first order phase transition, the correlation length remains finite. In this case, phase coexistence occurs, which means that two (or more) different phases of the material are in thermal equilibrium, e.g. water and steam are in equilibrium. This is in agreement with the finite correlation length, as one would expect that the different coexisting phases are uncorrelated.
For second order phase transition, the correlation length becomes infinite, correlations extend to the whole system. The system is said to be critical. In this case, the typical, exponentially decaying correlations disappear, and the correlations are ruled by power laws. The points in the phase diagram where a continuous transition takes place are called critical points. In the vicinity of the critical point, thermodynamic quantities are singular with simple non-integer powers. The scaling hypothesis further predicts simple algebraic relations between these exponents. As the whole system is correlated, one would expect the description at the critical points to be intrinsically difficult. Many approximation methods are expected to break down, as they are based on neglecting the correlations between components far apart (e.g. mean field theory).
Despite these difficulties, there are simplifications, which help to describe systems close to the critical point. It is observed that the critical exponents –the exponents appearing in the correlations and close to criticality– are independent of the microscopic details of the model. There are classes of systems with different Hamiltonians which seem to share the same exponents. These classes are based on a few properties of the Hamiltonian, like the dimensionality, the symmetry of the Hamiltonian.
Our main tool to probe the statistical properties of a system is the partition function. Define the partition function as follows

$$Z = \sum_s \mathrm{e}^{-\beta H(s)} \tag{1.1}$$

Here, the summation runs over all the possible states s of the system, H is the Hamiltonian of the system, and $\beta = \frac{1}{T}$ is the inverse temperature (in appropriate units). As the states might be labeled by continuous index, the summation is rather formal here, and might denote integration. The partition function is the

fundamental object to describe systems in thermal equilibrium with some further restriction, such as a fixed number of degrees of freedom. The probability that the system is in state s is proportional to the Boltzmann weight $\mathrm{e}^{-\beta H(s)}$, and in this context, Z acts as a normalization factor

$$P(s) = \frac{\mathrm{e}^{-\beta H(s)}}{Z} \tag{1.2}$$

The partition function is a useful tool to derive thermodynamic quantities. The average thermodynamic value of some observable A is computed as follows

$$\langle A \rangle = \frac{\sum_s A(s)\, \mathrm{e}^{-\beta H(s)}}{Z} \tag{1.3}$$

Thermodynamic quantities follow as derivatives of the partition function. For example, the internal energy – the average energy of the system – is

$$U = \langle H \rangle = \frac{\sum_s H(s)\, \mathrm{e}^{-\beta H(s)}}{Z} \tag{1.4}$$

$$= -\frac{\partial}{\partial \beta} \log Z \tag{1.5}$$

$$= T^2 \frac{\partial}{\partial T} \log Z \tag{1.6}$$

Another example is the free energy F of the system, which is given by the following equation in appropriate units

$$F = -T \log Z \tag{1.7}$$

One of the main challenges of statistical physics is the computation of the partition function. However, this is a tremendously difficult question for any nearly realistic system. In order to compute derivatives of Z, one needs analytic computations, which are even more hopeless. Nevertheless, perturbative methods are used to compute approximate results. Any of these perturbative methods which are somehow based on neglecting some of the correlations fail near critical point, which may lead one to think that computations are unmanageable here.

However, the idea of universality shines a light on this problem: In order to compute the universal properties of certain material, one does not need to consider the actual material, but equivalently might look at a much simpler model in the same universality class. This leads to a different approach to the same problem: Which are those simple systems where the partition function is

exactly computable, and what can we learn from these systems?
This question leads us to the two-dimensional lattice models. Two-dimensional lattice models are simple statistical physical models, where the degrees of freedom live on a two-dimensional lattice, e.g. spins on the vertices, or on the bonds. Usually the degrees of freedom take values from a finite set, and in general, these models are highly oversimplified compared to real world systems. Exactly solvable – here meaning that the partition function is computed exactly – models were found mainly in one and two spatial dimensions. Accepting the assumption that our world has three spatial dimensions, lower dimensional systems are generally less interesting: they might be considered as non-physical. However, this is not completely the case. In recent experimental settings, effectively one and two-dimensional systems are created with tunable parameters, relating these result to actual physical experiments. Also, these models are very valuable in understanding concepts and ideas in statistical physics. And let me quote a final motivation from Baxter: they are relevant and they can be solved, so why not do so and see what they tell us?
Systems that are exactly at critical point exhibit scale invariance. Due to the infinite correlation length and the power-law decay, the system is without any macroscopic length-scale, so as long as we stay above the length-scale of atomic distances, the system is scale invariant. In case of a local Hamiltonian, when the interaction is short ranged, the scale invariance leads to the much stronger conformal invariance. Based on conformal symmetry, and using the toolbox of the naturally arising quantum field theory (QFT), conformal field theory (CFT) is constructed. Conformal field theories describe statistical systems exactly at their critical point; however, there are other motivations to study them. Conformal field theories are most rich in two dimension, hence giving further reason to study two-dimensional lattice models.
One of the main method of computing the partition function of lattice models is based on the transfer matrix. Informally speaking, the transfer matrix –or T-matrix for short– is an operator, which represents a row of the lattice model, and the full lattice is built up, as T-matrices are multiplied with each other, corresponding to the graphical picture of building up the lattice row-by-row. Considering an $N \times M$ square lattice, the partition function is as follows

$$Z = \mathrm{Tr}\, T_M^N \tag{1.8}$$

where T_M is the transfer matrix describing one row of the $N \times M$ system. For sufficiently large N, or in the $N \to \infty$ limit, in case of a unique largest eigenvalue Λ, the following approximate expression is used for the partition function

$$Z = \mathrm{Tr}\, T_M^N \approx \Lambda^N \tag{1.9}$$

As we see, using the transfer matrix method, the search for the partition function simplifies to the search of the larges eigenvalue of T. There are numerous quantities which are computed in the context of T-matrix method. In this thesis, we consider two lattice models, the dilute $O(n)$ loop model and the Restricted Solid-On-Solid (RSOS) model.
In case of the dilute $O(n)$ loop model, the degrees of freedom are not local variables on the bonds or on the vertices, but are rather loops restricted to certain paths by the underlying lattice. The non-locality is inherent in the model, as statistical weight n is associated to the non-local loops. Nevertheless, we use techniques based on the previous approach, to compute a certain current in the context of dilute $O(n = 1)$ loop model.
The other lattice model we consider is the Restricted Solid-On-Solid model, which is a height model, originally developed to describe the fluctuating interface between different phases. In the context of the RSOS model, we probe the continuum limit, and the conformal field theory in the continuum limit of the model. As this is a well known result for the RSOS models, we consider fused versions of the RSOS model. The fusion is a procedure to define new lattice models from already existing ones. We consider the continuum limit of fused RSOS models, and identify the continuum CFTs.
Two-dimensional lattice models in statistical physics are closely related to one-dimensional quantum chains. The study of one-dimensional quantum chains started when Bethe solved the one-dimensional spin-$\frac{1}{2}$ Heisenberg spin chain – also known as spin-$\frac{1}{2}$ XXX spin chain– in 1931 [4]. He gave the solution by a method, which later became known as the coordinate Bethe ansatz. Bethe gave the multiparticle wavefunction in the terms of symmetrized plane waves. The momenta associated to the waves satisfy certain conditions, known as Bethe equations. This method solves exactly the eigenvalue problem of the spin chain in the following sense: For the spin-$\frac{1}{2}$ spin chain, assuming N sites, the Hilbert-space is 2^N dimensional. In principle, as the Hamiltonian is a finite matrix, there is no problem to diagonalize it. However, due to the exponential increase in the dimension, with the increasing system size, this approach quickly breaks down. Bethe ansatz reformulates the question of diagonalizing the $2^N \times 2^N$ matrix in terms of $\mathcal{O}(N)$ coupled nonlinear algebraic equations. The method was extended by the Leningrad school, introducing the algebraic Bethe ansatz (for a good review, and further literature, see [5]). The algebraic Bethe ansatz clearly shows the connection to two- dimensional lattice models. The idea of algebraic Bethe ansatz is to work with the so called monodromy matrix $\mathcal{T}$, and express the wavefunction in algebraic terms, instead of the complicated real-space wavefunction. The monodromy matrix is closely related to the transfer

matrix

$$T = \mathrm{Tr}_0 \mathcal{T} \tag{1.10}$$

where the partial trace is taken over the so called auxiliary space. Pictorially, the transfer matrix corresponds to a finite, approximate time evolution of the system. The connection to the lattice models is straightforward, as the two transfer matrices coincide. Also, typically the Hamiltonian of a quantum chain is the logarithmic derivative of the transfer matrix of the corresponding lattice model.

The method of Bethe ansatz was extended to include more then one species of particles by the nested Bethe ansatz (which has both coordinate and algebraic version). In this thesis, we consider a quantum chain model, and solve it by nested coordinate Bethe ansatz. The model is formulated in terms of spinless fermions; however the fermion number is not conserved, and the Bethe ansatz is done in other degrees of freedom.

Chapter 2

Spin-1 current in the dilute $O(n = 1)$ loop model

2.1 Introduction of loop models

The study of exactly solvable lattice models dates back to Ising and Bethe [4,6]. Loop models are two-dimensional integrable models, with non-local structure, based on loop representations of various algebras, including the Temperley-Lieb algebra, the dilute Temperley-Lieb algebra, and the Brauer algebra [7–9]. Loop models are defined by fixing the possible decorations on the tiles of the lattice, and imposing matching rules for neighboring tiles. In this non-technical introduction, we focus on the bulk properties of the model on a square lattice, leaving the boundary considerations for later.

The dense $O(n)$ loop model has been introduced in [7]. The model describes the statistical ensemble of densely packed, non-intersecting paths which either form closed loops or are attached to the boundary (given that we consider the model with appropriate boundary conditions). Every closed loop carries a statistical weight n, the loop fugacity. The dense $O(n)$ loop model has two possible faces

A typical configuration is in fig. 2.1. The model is closely related to the celebrated six-vertex (6V) model [10].

Historically, the six-vertex model was formed as a two-dimensional toy-model for the residual entropy of water ice: Ice (the I_h phase of ice) has a crystal

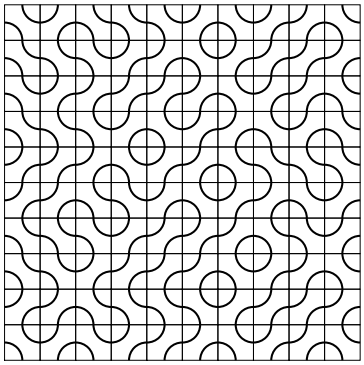

Figure 2.1: Typical dense $O(n)$ loop model configuration.

structure of stacked layers of tessellating hexagons. The vertices of the hexagons are occupied by the oxygen atoms. These planes and hexagons form a tetrahedral diamond lattice, with four oxygen atoms around every oxygen atom. Hydrogen atoms form bonds between the oxygen atoms. Four bonds correspond to every oxygen atom which are occupied by four hydrogen atoms. Energetically the most suitable is if two of these hydrogen atoms are closer to the oxygen, and two are farther, locally imitating the structure of the H_2O water molecule. This is the origin for the residual entropy of ice: Even at zero temperature, there are many microstates corresponding to the different arrangements of hydrogen atoms. Six-vertex model is a two-dimensional version of the problem formulated above: Consider a square lattice, with degrees of freedom living on the bonds of the lattice. Every bond is occupied by an arrow. The arrows satisfy the ice-rule: There are two arrows pointing in and two pointing out with respect to any vertex. Hence the name of the model, there are six possible arrow configurations around any vertex (fig. 2.2). The number of possible configurations and hence the residual entropy of the 6V model with periodic boundary conditions has been computed by Lieb [10].

The mapping between the 6V model and the dense $O(n)$ model is realized by an intermediate step, a dense directed loop model. In the directed loop model all loops have an orientation. The loop model is recovered by summing over the orientations, and the vertex model is obtained by summing over the loop configurations consistent with the orientation of the edges of the loop. An other interpretation of the six-vertex model is a spin-$\frac{1}{2}$ model, the arrows corresponding to the spins. This gives a possibility to generalize the model to higher spin, still

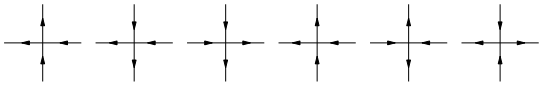

Figure 2.2: The six possible configurations of the six-vertex model.

satisfying the generalized version of the ice rule. The generalization to spin-1 gives rise to the nineteen vertex (19V) models: Every edge is either empty or occupied by an arrow pointing in or out. There are three integrable versions of 19V model: the Faddeev-Zamolodchikov (FZ) [11], the Izergin-Korepin (IK) [12] and the Bazhanov-Shadrikov model [13]. The Faddeev-Zamolodchikov model is constructed by fusion from the 6V model: Two spin-$\frac{1}{2}$ are fused, and projected to the spin-1 (triplet) representation. The other two models are constructed independently, not by fusion.

Dilute $O(n)$ loop models on square lattice have been introduced equivalent to the Izergin-Korepin 19V model [14, 15]. Again via a directed loop model this vertex model can be mapped onto a dilute loop model. The mapping is such that integrability is preserved, and the loop fugacity n becomes a free parameter, $-2 \leq n \leq 2$. The dilute loop model is defined as the statistical ensemble of the following nine plaquettes

Based on the same scheme, the Faddeev-Zamolodchikov 19V model is mapped to a loop model, with an extra plaquette of crossing loops, and with $n = 2$.

Since their introduction, loop models are the subject of growing interest. One of the most fruitful connection is with combinatorics. One of the early signs of the connection of integrable models to counting of certain objects was the discovery that $n \times n$ 6V configurations with domain wall boundary condition (DWBC) counts the number of $n \times n$ Alternating Sign Matrices (ASMs) [16–20]. Similar observations has been made in a number of cases [21, 22]. The most prominent result is the Razumov-Stroganov conjecture (Cantini-Sportiello theorem), which relates the groundstate elements of the dense $O(1)$ loop model to the counting of fully packed loop configurations (FPLs) [23]. The conjecture was proven by purely combinatorial methods [24]. The search for proof by algebraic methods led to new useful techniques [25,26]. Our approach to the computation of correlators is based on these methods.

Loop models form a natural basis for discretely holomorpic operators. Discrete holomorpicity is a lattice generalization of holomorphic functions: lattice contour

integrals of the function are expected to be zero. Discrete holomorphicity has been used to prove the conformal invariance of the Ising model [27], and to prove that the growth constant of the number of self-avoiding-walks on the honeycomb lattice is $\sqrt{2+\sqrt{2}}$ [28–30]. Surprisingly, prescribing a certain parafermionic observable to be discretely holomorphic results in the Boltzmann weights of the model to be Yang-Baxter integrable. This connection has been found in several models [31–36], and also for boundary cases [37].

In this chapter our main focus is to present our computation of a certain parafermionic observable, in the context of dilute $O(n=1)$ loop model on a strip with open boundary conditions. The strip is infinite vertically, and has finite width horizontally. The open boundary conditions allow the loops to connect to the boundaries. We compute the spin-1 boundary to boundary current on the infinite strip, with finite width. Every path, connecting the left and right boundary, carries an equal unit of current from the left boundary to the right boundary. Closed loops and paths connected only to one of the boundaries do not carry any current. In this chapter, we compute the mean current density induced by the statistics of the paths. We introduce the observable $F^{(x_1,x_2)}$, as the mean current between the points x_1 and x_2

$$F^{(x_1,x_2)} = \sum_{C\in\Gamma} P(C) N_C^{(x_1,x_2)} \mathrm{sign}_C^{(x_1,x_2)} \tag{2.1}$$

Here, Γ is the set of all configurations, $N_C^{(x_1,x_2)}$ is the number of paths passing in between the points x_1 and x_2 from the left to the right boundary, $P(C)$ is the ensemble probability of the configuration, and $\mathrm{sign}_C^{(x_1,x_2)}$ is $+1$ if x_1 lies in the region above the paths, and -1 if it lies below, as shown in fig. 2.3. Due to the non intersecting nature of the loop model, the quantities $N_C^{(x_1,x_2)}$ and $\mathrm{sign}_C^{(x_1,x_2)}$ are well defined. This observable is discretely holomorphic, antisymmetric, $F^{(x_1,x_2)} = -F^{(x_2,x_1)}$, and additive, $F^{(x_1,x_3)} = F^{(x_1,x_2)} + F^{(x_2,x_3)}$.

Up to an overall phase factor, F is the $s=1$ special case of the more general arbitrary s spin case

$$\tilde{F}^{s,(x_1,x_2)} = \sum_{C\in\Gamma} P(C) N_C^{(x_1,x_2)} \mathrm{e}^{\mathrm{i}s\phi(C)} \tag{2.2}$$

where $\phi(C)$ is the winding angle between the starting direction on the left boundary and the x_1, x_2 line.

Our result [1] is in close connection with the result of de Gier, Nienhuis and Ponsaing [38]. They computed the same spin-1 current for the dense $O(1)$ model, while here we compute it for the dilute $O(1)$ model.

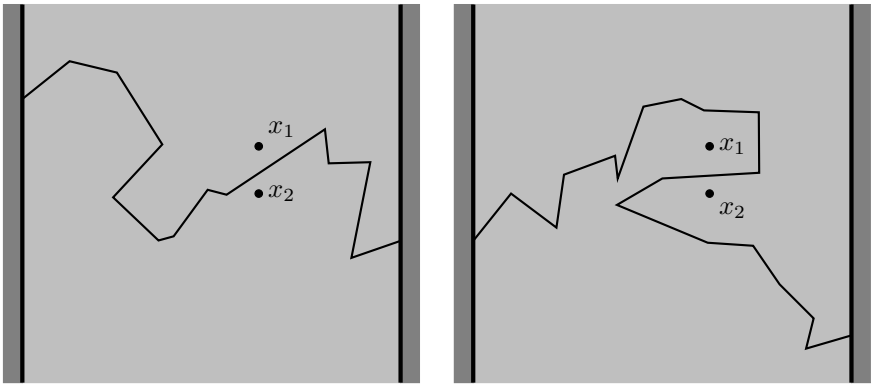

(a) Path with +1 contribution (b) Path with −1 contribution

Figure 2.3: The spin-1 property of the current: different paths contribute with different signs.

The continuum limit of such expressions was studied by Gorin and Panova [39]. They studied the $N \to \infty$ homogeneous limit of certain classes of symmetric polynomials.
This chapter is organized as follows: In section 2.2 we introduce the dilute $O(n)$ lattice models, with various boundary conditions. In section 2.3 we describe the integrable version of the model with open boundary conditions. This defines the R-matrix for generic n. In section 2.3.1, we fix the value of the loop fugacity to $n = 1$, and derive the Boltzmann weights (the elements of the R-matrix) for this case. In section 2.4, we introduce the vector space, where the transfer matrix (section 2.5) acts. We present our main computation tool, the quantum Knizhnik-Zamolodchikov equations in section 2.6. We show our main result on the current in section 2.7. The recursion relations needed for proving our statements are introduced in section 2.8. We discuss the symmetry structure of our expressions in section 2.9. Note that we do not prove all the observed symmetries, we use some assumptions in our final results. In section 2.10 we prove the main result under the aforementioned technical assumptions.
The model, we discuss is equivalent to a percolation model in a certain limit, the details of this mapping is in appendix A.2. We put some more technical calculations in the appendix.

2.2 Dilute $O(n)$ loop model

Consider a square lattice of width L and infinite height. Each tile of the lattice is decorated randomly by one of the nine plaquettes

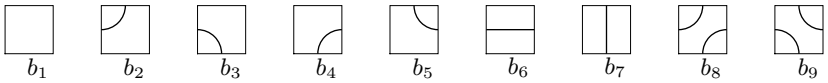

The decoration is subject to the restriction, that the formed paths have to be continuous. They form closed loops, or end on the boundaries, if the boundary conditions allow. Because adjacent tiles are thus not chosen independently, their Boltzmann weights can not be interpreted as probabilities. Closed loops carry a statistical weight n.

On the $L \times \infty$ geometry, we can introduce different boundary conditions. Here we discuss five different cases: two periodic, one closed and two open boundary conditions. In the case of the periodic boundary conditions, the continuity condition is extended to the left and right boundary, i.e. the right side of the right boundary has to have the same occupancy as the left side of the left boundary, and the configuration is considered, as these two sides are connected (fig. 2.4a). The vector spaces on which the transfer matrix act depend on the boundary conditions.

In the case of closed and open boundary conditions, the model is considered on an $L \times \infty$ strip, with left and right boundary. The interaction with the left and right boundary is described by the following plaquettes, respectively

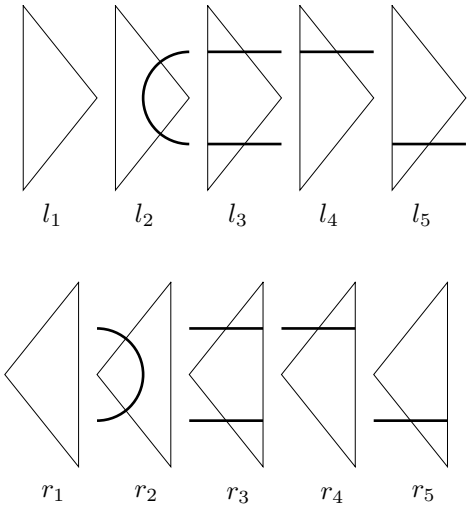

The closed boundary condition involves only the $\{l_1, l_2, r_1, r_2\}$ plaquettes, hence the choice is completely determined by the occupancy. Consequently their statistical weight is considered to be identically one. The loops cannot connect to the boundary, hence only loops are formed.
The first open boundary condition involves $\{l_1, l_2, l_3, r_1, r_2, r_3\}$, the second one all the ten plaquettes $\{l_1, \ldots, l_5, r_1, \ldots, r_5\}$. The main difference between the first and second open boundary condition is the number of global parameters: The first open boundary condition for the integrable version of the model allows larger freedom for the loop weights, while for the second one, all the loop weight have to be equal [37]. As our main interest involves the second open boundary case, we will refer as restricted open boundary condition and open boundary condition to the first and second one, respectively. Typical configurations with different boundary conditions are in fig. 2.4.
The statistical weight of a configuration C is given by the product of the weights of the constituent plaquettes and the weight of the loops. Every loop carries a weight, and depending on the boundary conditions, different type of loops carry different weights. We call the two periodic boundary conditions as PBC with puncture and PBC without puncture. The difference between these two cases is whether we topologically distinguish loops winding around the cylinder from contractible loops or not. For the case without puncture, there is only one type of loop, which carries the weight n. For the case with puncture there are two kind of loops, contractible and non-contractible, with loop weight n and b, respectively. For closed boundary conditions, there are only contractible loops, with weight n. For restricted open boundary condition, there are the most possible different loops. As the loops connected to the boundary only through l_3 and r_3, the boundary loops have certain "parity" properties. The topmost connection to the boundary is either at the top or bottom of the boundary plaquette, and the bottom connection is either at the bottom or the top, respectively (possibly on the same boundary plaquette, for the first case). There are four types of loops stretching between the left and right boundary, according to their connection on the left and right side: on both side, they can be connected via the top or bottom part of the boundary plaquette. These gives eight distinguishable boundary loops, two-two on the left and right boundary, and four connected to both. The largest freedom which can be consistent with exactly solvable version of the model distinguishes these eight types of boundary loops with weights $n_1, \ldots, n_8$, and the contractible loop with weight n.
For the open boundary conditions, such an abundance of free parameters does not generally permit exact solution. As loops attached to the boundary, we can distinguish three types of non-contractible loops: loops attached to the left boundary, loops attached to the right boundary, and loops stretching between

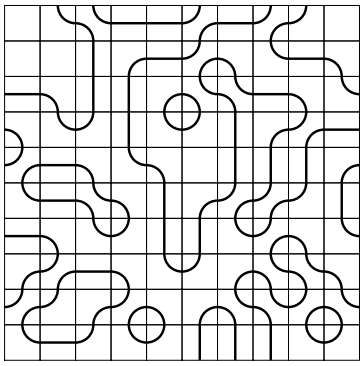

(a) Periodic boundary conditions (both)

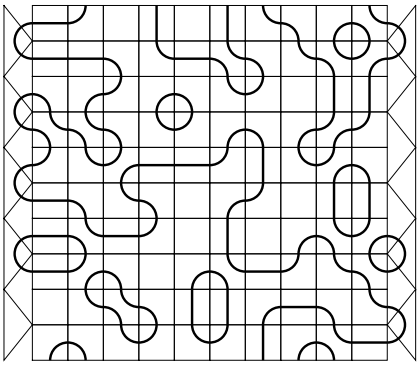

(b) Closed boundary conditions

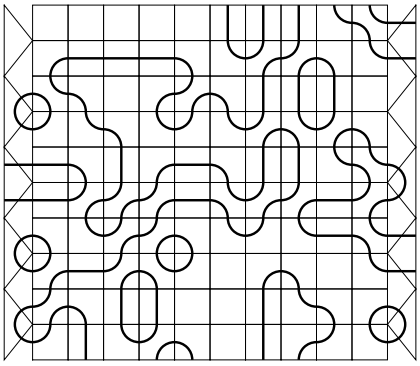

(c) Restricted open boundary conditions

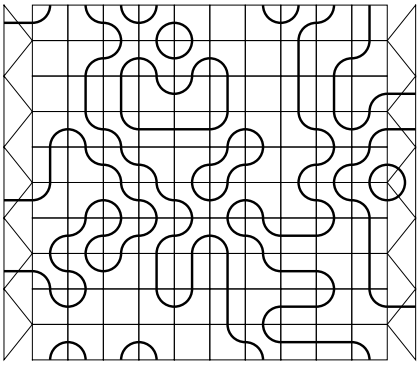

(d) Open boundary conditions

Figure 2.4: Typical configurations with different boundary conditions at $L = 10$.

the two boundaries. These carry the weights n_1, n_2, n_3, respectively.
The statistical weight of any configuration with any boundary condition is given by the product of the weights of the plaquettes constituting the configuration, multiplied by the weights of the loops formed in the configuration. Here, we show the explicit expression for a configuration C with all the five boundary condition

$$P^{(\mathrm{PBC})}_{\text{w/o punct.}}(C) = \left(\prod_{i=1}^{9} b_i^{\#b_i \text{ plaquettes}}\right) n^{\#\text{contr. loops}} \tag{2.3a}$$

$$P^{(\mathrm{PBC})}_{\text{w/ punct.}}(C) = \left(\prod_{i=1}^{9} b_i^{\#b_i \text{ plaquettes}}\right) n^{\#\text{contr. loops}} n_1^{\#\text{non-contr. loops}} \tag{2.3b}$$

$$P^{\mathrm{CBC}}(C) = \left(\prod_{i=1}^{9} b_i^{\#b_i \text{ plaquettes}}\right) n^{\#\text{contr. loops}} \tag{2.3c}$$

$$\begin{aligned} P^{(\mathrm{OBC})}_{\text{restricted}}(C) = &\left(\prod_{i=1}^{9} b_i^{\#b_i \text{ plaquettes}}\right)\left(\prod_{i=1}^{3} l_i^{\#l_i \text{ plaquettes}}\right)\times \\ &\times\left(\prod_{i=1}^{3} r_i^{\#r_i \text{ plaquettes}}\right)\left(\prod_{i=1}^{8} n_i^{\#n_i \text{ type loops}}\right) n^{\#\text{contr. loops}} \end{aligned} \tag{2.3d}$$

$$\begin{aligned} P_{\mathrm{OBC}}(C) = &\left(\prod_{i=1}^{9} b_i^{\#b_i \text{ plaquettes}}\right)\left(\prod_{i=1}^{5} l_i^{\#l_i \text{ plaquettes}}\right)\times \\ &\times\left(\prod_{i=1}^{5} r_i^{\#r_i \text{ plaquettes}}\right) n_1^{\#\text{left bndry loops}}\, n_2^{\#\text{right bndry loops}}\times \\ &\times n_3^{\#\text{stretching loops}}\, n^{\#\text{contr. loops}} \end{aligned} \tag{2.3e}$$

Note that for the closed boundary conditions, the boundary plaquettes do not carry any statistical weight, as they are entirely prescribed by the decoration of the normal plaquettes. By this, we defined the *homogeneous dilute $O(n)$ loop model* with different boundary conditions, i.e. with two periodic, closed, restricted open and open boundary conditions.
It is possible to define further versions of the model, e.g. with one boundary, on a half-plane, but our main focus is on the model with finite width.

2.3 Inhomogeneous weights

According to the standard technique in exactly solvable models [40], we introduce inhomogeneous weights corresponding to the tiles.

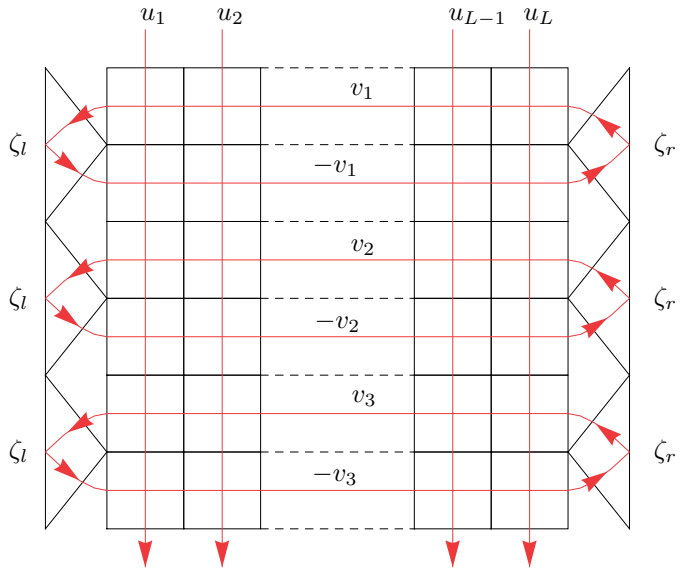

Figure 2.5: Rapidities for the open boundary case: $u_1, \ldots, u_L$ and v_i are the rapidities. The ζ_l and ζ_r are further parameters of the left and right K-matrices. As later we see, for many occasions we can threat them as rapidities, hence we will call them boundary rapidities. (More precisely, we express the ζ's in the boundary rapidities.)

As our main interest is the model with open boundary conditions, we focus on this case, the other cases are similar. In order to do so, we introduce rapidities –also called spectral parameters– flowing through the sites, as in fig. 2.5. The rapidities are complex parameters, associated with directed rapidity lines. Two rapidity lines crossing each other correspond to a square tile in the bulk. From the boundary, the lines "bounce back", while the rapidity changes sign. We make the weights of the tiles to be the function of the corresponding rapidities. The integrable version of the model is defined by the following R-matrix

$R(u,v) \equiv R(u-v) =$ 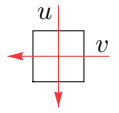

$=$

$= r_1(u-v)$ 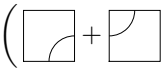 $+ r_2(u-v)$ 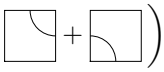 $+ r_3(u-v)$  $+$

 $+ r_4(u-v)$  $+ r_5(u-v)$  $+ r_6(u-v)$  , (2.4)

where the inhomogeneous weights are the following

$$r_1(x) = \sin(2\lambda)\sin(3\lambda - x) \tag{2.5a}$$
$$r_2(x) = \sin(2\lambda)\sin(x) \tag{2.5b}$$
$$r_3(x) = \sin(x)\sin(3\lambda - x) \tag{2.5c}$$
$$r_4(x) = \sin(x)\sin(3\lambda - x) + \sin(2\lambda)\sin(3\lambda) \tag{2.5d}$$
$$r_5(x) = \sin(2\lambda - x)\sin(3\lambda - x) \tag{2.5e}$$
$$r_6(x) = -\sin(x)\sin(\lambda - x) \tag{2.5f}$$

Here λ is a global parameter, related to the loop fugacity n

$$n = -2\cos(4\lambda) \tag{2.6}$$

The previously defined R-matrix can be regarded in two different way: as a Boltzmann weight of the tile, or as an operator. To define it as an operator, we introduce some more objects later. We consider the model with open boundary conditions, and define the inhomogeneous K-matrix as follows

$K_l(u,\zeta) = \zeta$ 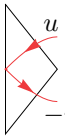

$= k_1^l(u,\zeta)$ 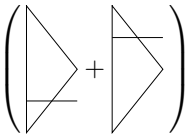 $+ k_2^l(u,\zeta)$ 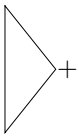 $+$ (2.7)

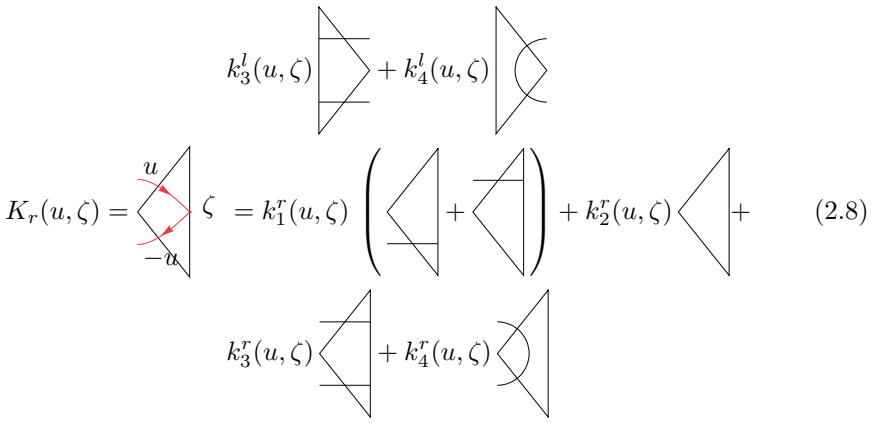

(2.8)

The weights of the left K-matrix elements are

$$k_1^l(u,\zeta) = \zeta \sin(2\lambda)\sin(2u) \tag{2.9a}$$

$$k_2^l(u,\zeta) = 2\cos\lambda \sin\left(\tfrac{3}{2}\lambda + u\right) - n_1\zeta^2 \sin\left(\tfrac{1}{2}\lambda + u\right)\sin\left(\tfrac{1}{2}\lambda - u\right)\sin\left(\tfrac{3}{2}\lambda - u\right) \tag{2.9b}$$

$$k_3^l(u,\zeta) = -\zeta^2 \sin(2\lambda)\sin(3u)\sin\left(\tfrac{1}{2}\lambda - u\right) \tag{2.9c}$$

$$k_4^l(u,\zeta) = \sin\left(\tfrac{3}{2}\lambda - u\right)\left(2\cos\lambda - n_1\zeta^2 \sin^2\left(\tfrac{1}{2}\lambda - u\right)\right) \tag{2.9d}$$

The weight of the right K-matrix elements are related to the left one by the following equation

$$k_i^r(u,\zeta) = k_i^l(-u,\zeta), \qquad i = 1\ldots 4, \tag{2.10}$$

where the $n_1 \to n_2$ substitution is also understood due to the different loop weights. By these definition, we defined the inhomogeneous dilute $O(n)$ model with open boundary conditions. The K-matrix weights for the restricted open boundary conditions are in [37].

2.3.1 Specialization of loop weights to $n = 1$

Our main interest is the dilute $O(n)$ loop model with open boundary conditions, when all the loop fugacities equal 1: $n = n_1 = n_2 = n_3 = 1$. In this section we derive the Boltzmann weights for this case, in multiplicative notation.
The weights shown in the previous section (eqs. (2.5a) to (2.5f), (2.9a) to (2.9d) and (2.10)) are in the additive notation: the R-matrix is a function of the

difference of the two rapidities. We introduce the multiplicative notation by introducing the following new variables

$$\begin{aligned} q &= \mathrm{e}^{\mathrm{i}\lambda} \\ z &= \mathrm{e}^{\mathrm{i}x} \end{aligned} \tag{2.11}$$

In the new variables, the eqs. (2.5a) to (2.5f) weights are the following (after multiplying by a common factor $4q^5z^2$)

$$r_1(z) = \left(q^4-1\right)\left(q^6-z^2\right)z \tag{2.12a}$$
$$r_2(z) = \left(q^4-1\right)\left(z^2-1\right)zq^3 \tag{2.12b}$$
$$r_3(z) = \left(z^2-1\right)\left(q^6-z^2\right)q^2 \tag{2.12c}$$
$$r_4(z) = \left(z^2-1\right)\left(q^6-z^2\right)q^2 + \left(q^4-1\right)\left(q^6-1\right)z^2 \tag{2.12d}$$
$$r_5(z) = \left(q^4-z^2\right)\left(q^6-z^2\right) \tag{2.12e}$$
$$r_6(z) = -\left(z^2-1\right)\left(q^2-z^2\right)q^4 \tag{2.12f}$$

The loop weight n is related to the new parameter q as

$$n = -2\cos 4\lambda = -q^4 - q^{-4} \tag{2.13}$$

Setting the loop fugacity to $n = 1$ means that q takes one of the following values

$$q_1^{(\pm)} = \mathrm{e}^{\pm \mathrm{i}\pi/6} \tag{2.14a}$$
$$q_2^{(\pm)} = \mathrm{e}^{\pm \mathrm{i}\pi/3} \tag{2.14b}$$
$$q_3^{(\pm)} = \mathrm{e}^{\pm 2\mathrm{i}\pi/3} \tag{2.14c}$$
$$q_4^{(\pm)} = \mathrm{e}^{\pm 5\mathrm{i}\pi/6} \tag{2.14d}$$

Out of these solutions, we will consider $q_2^{(\pm)}$. Using the property that $\left(q_2^{(\pm)}\right)^3 = -1$, the weights in this case simplify to the following (writing q instead of $q_2^{(\pm)}$)

$$r_1(z) = -\left(1+q\right)\left(1-z^2\right)z \tag{2.15a}$$
$$r_2(z) = -\left(1+q\right)\left(1-z^2\right)z \tag{2.15b}$$
$$r_3(z) = -\left(1-z^2\right)\left(1-z^2\right)q^2 \tag{2.15c}$$
$$r_4(z) = -\left(1-z^2\right)\left(1-z^2\right)q^2 \tag{2.15d}$$
$$r_5(z) = \left(-q-z^2\right)\left(1-z^2\right) \tag{2.15e}$$

$$r_6(z) = \left(1 - z^2\right)\left(q^2 - z^2\right)(-q) \tag{2.15f}$$

The solution $q_3^{(\pm)}$ gives the same weights, as here. The expressions are related to the previous expressions by a $q \to -q$ change, and $q_3^{(\pm)} = -q_2^{(\mp)}$. Consequently the two minus factors cancel each other, resulting in the same weights. After factorizing a common factor $(1 - z^2)$, we get the following weights

$$r_1(z) = r_2(z) = -\left(1 + q\right) z \tag{2.16a}$$
$$r_3(z) = r_4(z) = -\left(1 - z^2\right) q^2 \tag{2.16b}$$
$$r_5(z) = -q - z^2 \tag{2.16c}$$
$$r_6(z) = \left(q^2 - z^2\right)(-q) \tag{2.16d}$$

This defines the R-matrix for $n = 1$, in Regime I. The K-matrix is also computable similarly.
We will work in a different convention, defined by the following R-matrix for $n = 1$, in Regime I, in multiplicative notation

$R(z,w) \equiv R\left(\frac{w}{z}\right) =$ 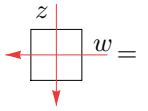

$=$

$$W_1\left(\tfrac{w}{z}\right)\Big($$  $$+$$  $$+$$  $$\Big) + W_t\left(\tfrac{w}{z}\right)\Big($$  $$+$$  $$+$$

$$+$$  $$+$$  $$\Big) + W_2\left(\tfrac{w}{z}\right)$$  $$+ W_m\left(\tfrac{w}{z}\right)$$  $$, \tag{2.17}$$

where the weights are defined as

$$W_1(z) = -1 + z^2\,, \tag{2.18a}$$
$$W_t(z) = \left(q + q^2\right) z\,, \tag{2.18b}$$
$$W_2(z) = q^2 + q z^2\,, \tag{2.18c}$$
$$W_m(z) = -q - q^2 z^2\,. \tag{2.18d}$$

As one can see, this convention is related to the previous one by a $z \to z^{-1}$ transformation and an overall factor $-q$.
We define the K-matrix for this case as follows

$K_l(z, z_B) = z_B$ 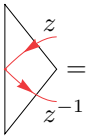

$= K_{id}^{l}(z, z_B)\Big($ 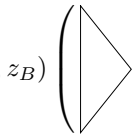 $+$ 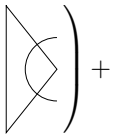 $\Big) +$ (2.19)

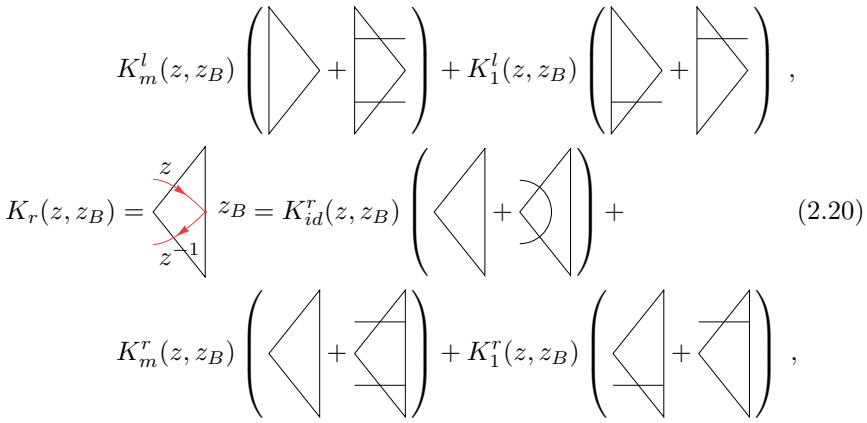

(2.20)

with the following weights

$$K_{id}^l(z, z_B) = k^2\left(z^{-1}\right) x^2\left(z_B\right) - 1 \,, \tag{2.21a}$$
$$K_m^l(z, z_B) = x^2(z_B) k\left(z^{-1}\right)\left(k(z) - k\left(z^{-1}\right)\right) \,, \tag{2.21b}$$
$$K_1^l(z, z_B) = x(z_B)\left(k(z) - k\left(z^{-1}\right)\right) \,, \tag{2.21c}$$

$$K_{id}^r(z, z_B) = 1 - k^2\left(z\right) x^2\left(z_B\right) \,, \tag{2.21d}$$
$$K_m^r(z, z_B) = x^2\left(z_B\right) k(z)\left(k\left(z\right) - k\left(z^{-1}\right)\right) \,, \tag{2.21e}$$
$$K_1^r(z, z_B) = x(z_B)\left(k(z) - k\left(z^{-1}\right)\right) \,, \tag{2.21f}$$

$$k(z) = qz - z^{-1} \,, \tag{2.21g}$$
$$x(z_B) = q\frac{z_B}{z_B^2 - 1} \,. \tag{2.21h}$$

This K-matrix is also gauge equivalent with the generic one, the precise derivation is in appendix A.1.
In the followings we use the R and K-matrix weights defined in eqs. (2.18a) to (2.18d) and (2.21a) to (2.21f). The R and K-matrix are stochastic operators with the following weights

$$W_R(z, w) \equiv W_R\left(\tfrac{w}{z}\right) = -1 + \left(q + q^2\right) + z^2 \,, \tag{2.22}$$
$$W_{K_l}(z, z_B) = \left(k(z)x(z_B) - 1\right)\left(1 + k(z^{-1})x(z_B)\right) \,, \tag{2.23}$$
$$W_{K_r}(z, z_B) = \left(1 - k(z^{-1})x(z_B)\right)\left(1 + k(z)x(z_B)\right) \tag{2.24}$$

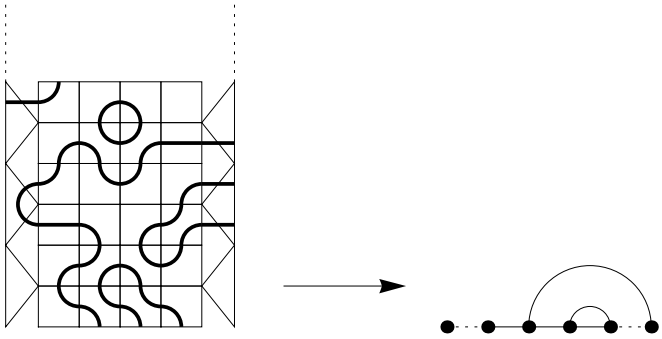

Figure 2.6: The mapping from loop configurations to dilute link patterns. The two outermost points –connected with dotted line to the others– represent the two boundaries. Here the image of the mapping is $|\bullet(()\rangle$

As the R and K-matrices are not defined yet as operators, the meaning of these normalizations will be clearer in the next section.

2.4 Vector space of link patterns

In this section, we introduce the vector space of link patterns, in which the R and K-matrices act as stochastic operators. Based on this description, we present the equations which are satisfied by the inhomogeneous model. The R and K-matrices act on the vector space as elements of the two boundary representation of the dilute Temperley-Lieb algebra (For a brief overview, see [9]).
We introduce dLP_L, the set of dilute link patterns of size L, the possible connectivities on a half-infinite strip with width $L \in \mathbb{N}$. The set is built up as follows: Consider L sites. Every site is either occupied or empty. An occupied site is connected to the left or right boundary, or to an other occupied site. As the underlying loop model is such that the paths are non-intersecting, the chords representing the connectivities are also non-intersecting. Consequently, every dilute loop configuration on the half-infinite strip with width L corresponds to one dilute link pattern. There are finitely many dilute link patterns, and infinitely many loop configurations, hence many (in fact infinitely many) loop configurations correspond to one dilute link pattern. An example of such a mapping is in fig. 2.6. The set dLP_L is in bijection with L long strings of the

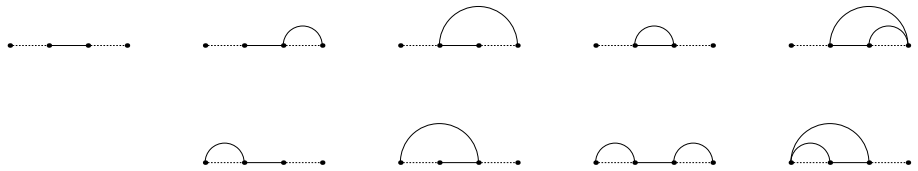

Figure 2.7: The elements of $dLP_{L=2}$. The two outermost points represent the boundaries, the inner ones the sites. The top row: $|\bullet\bullet\rangle$ (empty element), $|\bullet(\rangle$, $|(\bullet\rangle$, $|()\rangle$, $|((\rangle$ (fully nested element). The bottom row: $|)\bullet\rangle$, $|\bullet)\rangle$, $|)(\rangle$, $|))\rangle$ (fully nested element).

characters (, • and), consequently dLP_L contains 3^L elements. The bijection is the following: • represents an empty site, occupied sites are represented by the parentheses. As far as the parentheses are well nested, the matching parentheses represent connected edges. The unmatched right or left parentheses represent edges that are connected to the left or right boundary, respectively. The mapping for all the elements of $dLP_{L=2}$ are in fig. 2.7. There are three elements which have names because of their importance: The $|\bullet\,\bullet\ldots\bullet\rangle$ is the empty element, the $|))\ldots)\rangle$ and $|((\ldots(\rangle$ are the fully nested elements.
We define the vector space of link patterns V_L, as the vector space over $\mathbb{C}$ which is spanned by the elements of the dLP_L dilute link patterns: $V_L = \mathrm{span}(dLP_L)$. The result of the action of an R- or K-matrix on an element of dLP_L, typically denoted as $|\pi\rangle$, is a linear combination of link patterns that results by attaching the graphical representation of the operators below the picture of the link pattern, and keeping only the terms in which the occupancy matches. Left and right K-matrices act only on the connectivity of the left-most and right-most site, while for R-matrices, two consecutive sites are specified, where it acts. It acts, as it is tilted by 45 degree. If an R-matrix acts on the two consecutive sites i, $i+1$, we denote it in the subscript: $R_{i,i+1}$. Some examples of such mapping are in fig. 2.8. Note that every loop closed by this operation is a new loop which has to be considered. Consequently, the configuration is multiplied by n, n_1, n_2 or n_3, depending on the type of newly formed loop. As all these loop weights are 1 in our case, we do not have to take this into account.

The R and K-matrices are stochastic operators on V_L, with weights (2.22) to (2.24). To compute the correct weights, R-matrices (K-matrices) should be considered as they map from the two (one) sites, where the rapidities enter to the two (one), where they exit. Relations involving R and K-matrices can be

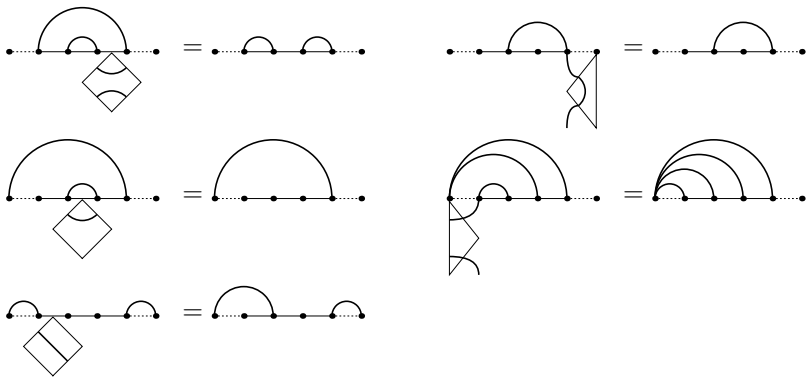

Figure 2.8: Some examples of R, and K-matrix elements acting on dilute link patterns.

represented by drawings. The directed red lines always represent rapidity flows. A crossing of two rapidity flows is an R-matrix, its weight is computed respecting the direction of lines. We introduce lines for the boundary rapidities too. It is helpful to treat rapidities and boundary rapidities in a more uniform way. By this, we give new pictorial representation for the K-matrices.

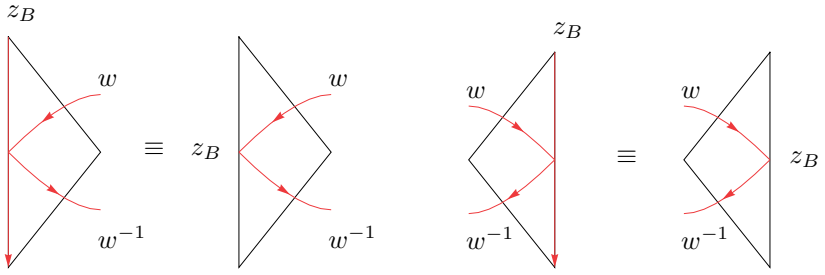

The reflection of a rapidity on a boundary represents a K-matrix. The order of the operators is prescribed by the direction of the rapidities. The rapidity lines uniquely determine the drawing, hence we draw tiles only in some of the pictures.

With these prescriptions, the R-matrix satisfies the following equations. (In the figures, for legibility, we omit the prefactors. The equations hold for $n = 1$, for

generic n, the same equations hold with different normalization.)

- the inversion/unitary relation:

$$R(z_2, z_1)R(z_1, z_2) = W_R(z_2, z_1)W_R(z_1, z_2) \cdot \mathrm{id} \tag{2.25}$$

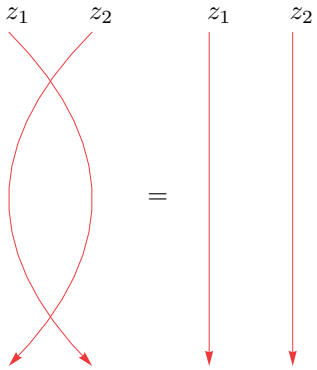

- the crossing relation:

$$R(z, w) = -\left(\frac{w}{z}\right)^2 R^{rot}(-w, z) \tag{2.26}$$

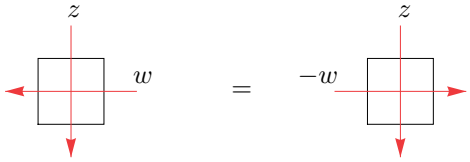

As the R-matrix only depends on the ratio $\frac{w}{z}$, an equivalent form of the crossing relation is

$$R(z, w) = -\left(\frac{w}{z}\right)^2 R^{rot}(w, -z). \tag{2.27}$$

- the Yang-Baxter equation (this equation holds for generic n without modification):

$$R_{23}(u, v)R_{12}(u, w)R_{23}(v, w) = R_{12}(v, w)R_{23}(u, w)R_{12}(u, v) \tag{2.28}$$

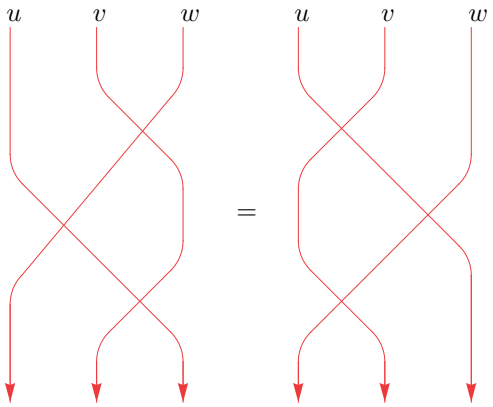

The K-matrix satisfies a similar set of equations. Similarly, we omit prefactors in the figures. These equations also generalize to generic n with minor modifications in the normalizations. The equations are the following:

- the boundary inversion/unitary relation:
  - left boundary:

$$K_l(w^{-1}, z_B)K_l(w, z_B) = W_{K_l}(w^{-1}, z_B)W_{K_l}(w, z_B) \cdot \mathrm{id} \tag{2.29}$$

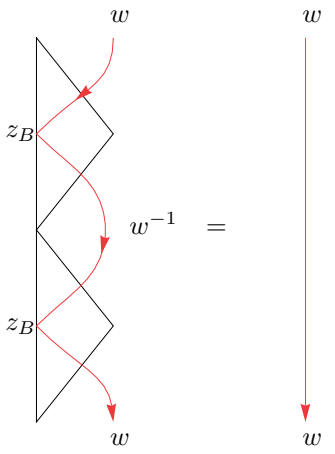

  - right boundary:

$$K_r(w^{-1}, z_B)K_r(w, z_B) = W_{K_r}(w^{-1}, z_B)W_{K_r}(w, z_B) \cdot \mathrm{id} \tag{2.30}$$

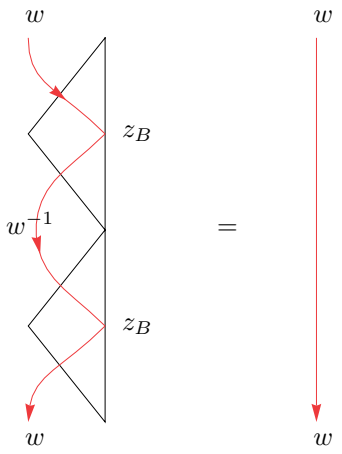

- the boundary crossing relation:

$$K_l(w, z_B) = -K_r(-w^{-1}, -z_B) \tag{2.31}$$

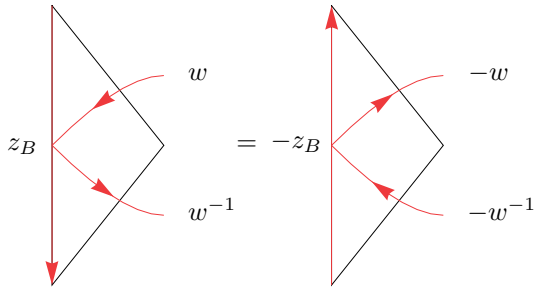

- the reflection equation:

  - left boundary:

$$R(v^{-1}, u^{-1})K_l(v, z_B)R(u^{-1}, v)K_l(u, z_B) = \\ = K_l(u, z_B)R(v^{-1}, u)K_l(v, z_B)R(u, v) \tag{2.32}$$

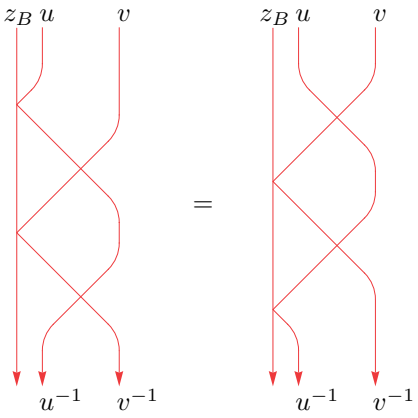

– right boundary:

$$R(v^{-1},u^{-1})K_r(u,z_B)R(u,v^{-1})K_r(v,z_B) = \\ = K_r(v,z_B)R(v,u^{-1})K_r(u,z_B)R(u,v) \quad (2.33)$$

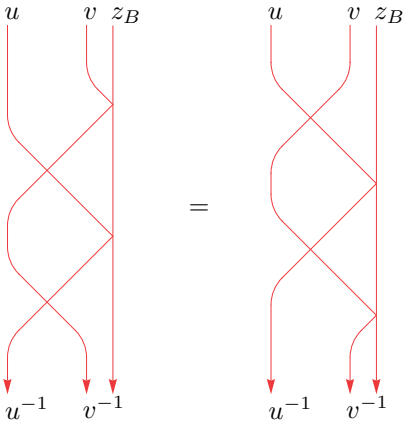

We consider the right reflection equation with a rapidity flowing in the opposite direction. With our definitions of the left and right K-matrices, this is only possible with a boundary rapidity which changes orientation. Note the direction of rapidities and boundary rapidities. The following equation holds

$$R(u,v^{-1})K_l(u,-z_B)R(v,u^{-1})K_r(v,z_B) = \\ = K_r(v,z_B)R(u,v)K_l(u,-z_B)R(v,u^{-1})\,. \quad (2.34)$$

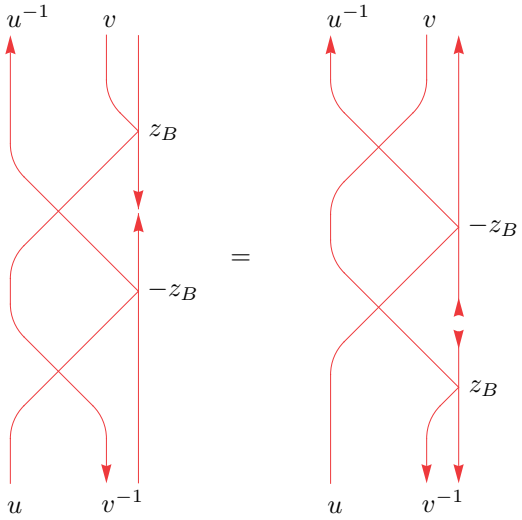

We restore the continuity of the orientation of the boundary rapidity line, by introducing the boundary-crossed left K-matrix. It is introduced by reversing the orientation of the boundary rapidity. The boundary-crossed K-matrix is as follows

$$K_l^{b.reversed}(w, -z_B) = K_r(w, z_B)\ . \tag{2.35}$$

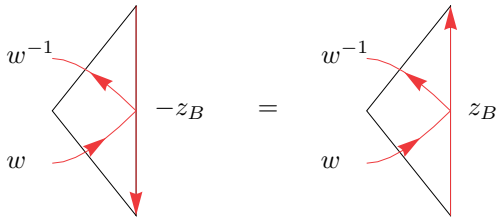

This definition leads to the following, preferred form of eq. (2.34) which restores the continuity of the boundary rapidity flow

$$\begin{aligned} R(u, v^{-1})K_l^{b.reversed}(u, z_B)R(v, u^{-1})K_r(v, z_B) = \\ = K_r(v, z_B)R(u, v)K_l^{b.reversed}(u, z_B)R(v, u^{-1})\ . \end{aligned} \tag{2.36}$$

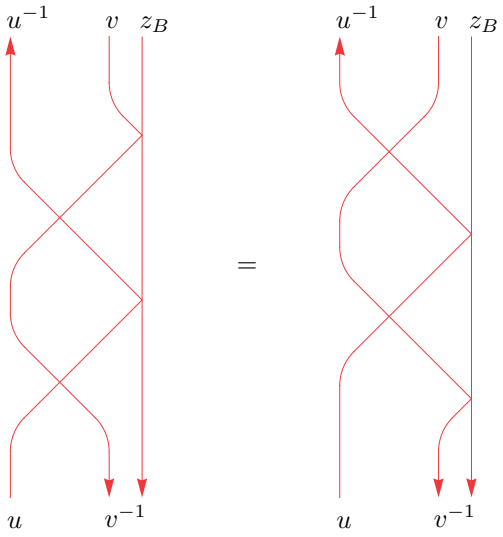

We would like to give some comments regarding the boundary rapidity. The boundary rapidity is a free parameter in the K-matrix of the model. It is not clear, why would we introduce a corresponding rapidity. As it turns out, this K-matrix is constructed from the closed boundary K-matrix, with the insertion of a rapidity line. The boundary rapidity corresponds to the rapidity of this inserted line. This computation is shown in details in appendix A.6. This explains, why a factor -1 relates the normal and the boundary-crossed K-matrix: The (2.26) crossing relation introduces the factor -1.
The boundary-crossed right K-matrix can be introduced analogously. We introduce the boundary-crossed K-matrix in order to define the transfer matrix.

2.5 Double row transfer matrix

We define the double row transfer matrix (T-matrix) as follows

$$T_L(w, z_0, z_1, \ldots, z_L, z_{L+1}) =$$

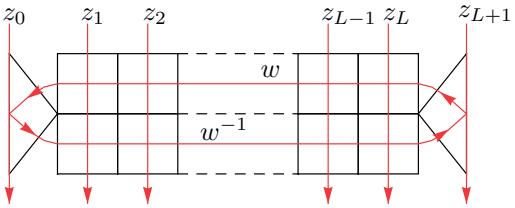

(2.37)

Note that a boundary-crossed left K-matrix is on the right side. By standard method, using the Yang-Baxter equation, the inversion relation, and the reflection equation, we can prove that such double row transfer matrices form a one-parameter family of commuting matrices [41]

$$[T_L(w_1, z_0, z_1, \ldots, z_L, z_{L+1}), T_L(w_2, z_0, z_1, \ldots, z_L, z_{L+1})] = 0\ . \tag{2.38}$$

The transfer matrix is a stochastic operator on V_L. The weight is defined by the R and K-matrices, constituting the T-matrix. A matrix element of the transfer matrix corresponds to a mapping from one element of dLP_L to another. Its value is the sum of the weights of all the possible T-matrix configurations (the R and K-matrix content of the transfer matrix) which maps the preimage link pattern to the image link pattern. As certain maps cannot be realized by one T-matrix configuration, some matrix elements are zero. The matrix element of the transfer matrix are Laurent polynomials in the rapidities $z_1, \ldots, z_L$ and the boundary rapidities z_0, z_{L+1}.
Take a half-infinite configuration, with finite width L and infinite height upward, with an edge at the bottom. The states of the edge map to the elements of V_L (fig. 2.6). We act on V_L by the transfer matrix, if we add the graphical representation of the T-matrix to the bottom, and consider the new edge. In fact, loosely speaking, the half infinite configuration can be considered as a tower of stacked T-matrices. The (unnormalized) probability distribution of the link patterns is given by the groundstate eigenvector of the T-matrix which we will denote by $|\Psi(z_0, z_1, \ldots, z_L, z_{L+1})\rangle$. The groundstate eigenvector is the eigenvector corresponding to the largest eigenvalue. The entries of the groundstate eigenvector are Laurent polynomials in $z_0, \ldots, z_{L+1}$, and due to the (2.38) commutation property, independent of the w spectral parameter. The existence and uniqueness of such a vector is provided by the Perron-Frobenius

theorem [42, 43]. The eigenvalue equation is the following

$$T(w, z_0, \ldots, z_{L+1}) |\Psi(z_0, \ldots, z_{L+1})\rangle = \\ = N(w, z_0, \ldots, z_{L+1}) |\Psi(z_0, \ldots, z_{L+1})\rangle \ . \quad (2.39)$$

Note that the eigenvector is not a function of w, which we call auxiliary rapidity. Here, N is the normalization of the T-matrix

$$N(w, z_0, \ldots, z_{L+1}) = \\ W_{K_l}(w, z_0) W_{K_l}(w^{-1}, -z_{L+1}) \prod_{i=1}^{L} W_R(w, z_i) W_R(z_i, w^{-1}) + \\ \tilde{W}_{K_l}(w, z_0) \tilde{W}_{K_l}(w^{-1}, -z_{L+1}) \prod_{i=1}^{L} \tilde{W}_R(w, z_i) \tilde{W}_R(z_i, w^{-1}) \ , \quad (2.40)$$

where W_R and W_{K_l} are defined in eqs. (2.22) and (2.23), and $\tilde{W}_R$ and $\tilde{W}_{K_l}$ are the following functions

$$\tilde{W}_R(z_1, z_2) = W_1(z_1, z_2) - W_t(z_1, z_2) \ , \quad (2.41a)$$

$$\tilde{W}_{K_l}(z, z_B) = K_{id}(z, z_B) + K_m(z, z_B) - K_1(z, z_B) \ . \quad (2.41b)$$

The derivation for N is in appendix A.3.
The groundstate vector is

$$|\Psi_L(z_0, \ldots, z_{L+1})\rangle = \sum_{\pi \in dLP_L} \psi_\pi(z_0, \ldots, z_{L+1}) |\pi\rangle \ . \quad (2.42)$$

This is a vector in V_L, with Laurent polynomial entries $\psi_\pi(z_0, \ldots, z_{L+1})$, where $|\pi\rangle \in dLP_L$ denotes the basis vector. We use the following shortened notation: $|\psi_\pi\rangle \equiv \psi_\pi |\pi\rangle$.
In order to compute quantities on the full strip, we introduce dLP_L^* and V_L^*, the dual basis of dLP_L and the dual vector space of V_L. The dual basis dLP_L^* consist of link patterns in the downward direction. The dual vector space is spanned by the dual basis over $\mathbb{C}$: $V_L^* = \mathrm{span}(dLP_L^*)$. We define the scalar product of $\langle\alpha| \in dLP_L^*$ and $|\beta\rangle \in dLP_L$

$$\langle\alpha|\beta\rangle = \begin{cases} 1 & \text{if the two link patterns match respecting the occupation,} \\ 0 & \text{otherwise.} \end{cases} \quad (2.43)$$

In an analogous fashion, we can built up the probabilistic picture for the dual vector space with a dual transfer-matrix.
Scalar products of vectors and dual vectors are considered as probabilities of certain configurations on the full strip. The dual transfer matrix acts "upward". In order to express the eigenvector of dLP_L^*, we relate the transfer matrices of dLP_L and dLP_L^*

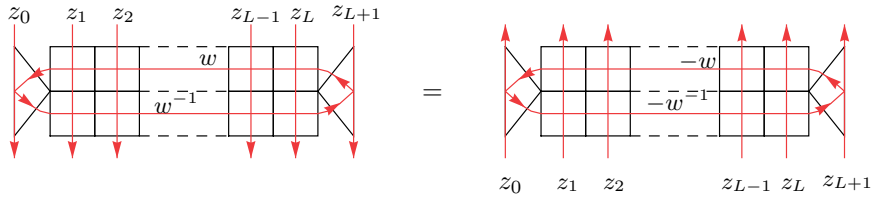

(2.44)

The transfer matrix of the dual space has a unique largest eigenvector, the dual groundstate

$$\langle \Psi | = \sum_{\pi \in dLP_L^*} \psi_\pi^* \langle \pi | \equiv \sum_{\pi \in dLP_L^*} \langle \psi_\pi | \,. \tag{2.45}$$

Equation (2.44) relates the groundstate and dual groundstate elements

$$\psi_\alpha(z_0, \ldots, z_{L+1}) = \psi^*_{r(\alpha)}(z_{L+1}, \ldots, z_0) \,, \tag{2.46}$$

where $\psi_\alpha \in V_L$ and $\psi^*_{r(\alpha)} \in V_L^*$. The two link patterns, $\alpha \in dLP_L$ and $r(\alpha) \in dLP_L^*$ are related by a 180 degree rotation, e.g.: $r\big(\,|\bullet\,\bullet\,\bullet()(\bullet\bullet)\rangle\,\big) = \langle\bullet\bullet)()\,\bullet\,\bullet\bullet|$. As the T and the dual T-matrix define the groundstate vector of both vector spaces, we can take the scalar product of the groundstate elements

$$\langle \psi_\alpha | \psi_\beta \rangle = \psi^*_\alpha(z_0, \ldots, z_{L+1}) \psi_\beta(z_0, \ldots, z_{L+1}) \langle \alpha | \beta \rangle \tag{2.47}$$

$$= \psi_{r(\alpha)}(z_{L+1}, \ldots, z_0) \psi_\beta(z_0, \ldots, z_{L+1}) \langle \alpha | \beta \rangle, \tag{2.48}$$

which is equal to the statistical weight of the full strip configuration given by $\langle \alpha | \beta \rangle$.
For further calculations, we define two quantities: the partition sum of the half strip and the partition sum of the full strip. The partition sum of the half strip is the sum of all groundstate elements

$$Z_{h.s.}(z_0, \ldots, z_{L+1}) = \sum_{\alpha \in dLP_L} \psi_\alpha(z_0, \ldots, z_{L+1}) \,. \tag{2.49}$$

The partition sum of the full strip is the normalization of the probabilities on the full strip. The partition sum of the full strip is

$$Z_{f.s.}(z_0,\ldots,z_{L+1}) = \langle\Psi(z_0,\ldots,z_{L+1})|\Psi(z_0,\ldots,z_{L+1})\rangle = \\ = \sum_{\substack{\alpha\in dLP_L \\ r(\beta)\in dLP_L^*}} \psi_\alpha(z_0,\ldots,z_{L+1})\psi^*_{r(\beta)}(z_0,\ldots,z_{L+1})\,\langle r(\beta)|\alpha\rangle = \\ = \sum_{\alpha,\beta\in dLP_L} \psi_\alpha(z_0,\ldots,z_{L+1})\psi_\beta(z_{L+1},\ldots,z_0)\ , \quad (2.50)$$

where we sum up to $\alpha,\beta\in dLP_L$ link patterns with matching occupation. These functions are normalization factors for the unnormalized probabilities.

2.6 The quantum Knizhnik – Zamolodchikov equations

Based on the properties of R and K-matrices, the transfer matrix satisfies the following equations (suppressing irrelevant notation)

$$R_{i,i+1}(z_i,z_{i+1})T\left(\ldots z_i,z_{i+1}\ldots\right) = T\left(\ldots z_{i+1},z_i\ldots\right)R_{i,i+1}(z_i,z_{i+1})\ , \quad (2.51a)$$
$$K_l\left(z_1,z_0\right)T\left(z_1,\ldots\right) = T\left(z_1^{-1},\ldots\right)K_l\left(z_1,z_0\right)\ , \quad (2.51b)$$
$$K_r\left(z_L,z_{L+1}\right)T\left(\ldots,z_L\right) = T\left(\ldots,z_L^{-1}\right)K_r\left(z_L,z_{L+1}\right)\ . \quad (2.51c)$$

Act with both sides on $|\Psi_L\rangle$, and the q-Knizhnik-Zamolodchikov equations follows [25, 44, 45] for the dilute $O(1)$ model, with open boundaries

$$R_{i,i+1}(z_i,z_{i+1})\left|\Psi\left(\ldots z_i,z_{i+1}\ldots\right)\right\rangle = W_R(z_i,z_{i+1})\left|\Psi\left(\ldots z_{i+1},z_i\ldots\right)\right\rangle\ , \quad (2.52a)$$
$$K_l\left(z_1,z_0\right)\left|\Psi\left(z_0,z_1,\ldots\right)\right\rangle = W_{K_l}\left(z_1,z_0\right)\left|\Psi\left(z_0,z_1^{-1},\ldots\right)\right\rangle\ , \quad (2.52b)$$
$$K_r\left(z_L,z_{L+1}\right)\left|\Psi\left(\ldots z_L,z_{L+1}\right)\right\rangle = W_{K_r}\left(z_L,z_{L+1}\right)\left|\Psi\left(\ldots z_L^{-1},z_{L+1}\right)\right\rangle\ , \quad (2.52c)$$

where the prefactors W's follow from the stochasticity and the normalization of the R and K-matrices.
We used the qKZ equations to compute the groundstate vector of the transfer matrix for $L=1,2,3$ system sizes. Starting from the fully nested elements, the full groundstate is computable, by the repeated application of the qKZ equations. The algorithm to generate the full groundstate vector from the fully nested elements is described in details in [46]. Further details are in [25, 47]. Explicit groundstate elements and partition sum for $L=1$ are presented in appendix A.4.

2.7 Definition of spin-1 current and main result

In this section we define precisely the spin-1 boundary to boundary current in the dilute $O(1)$ model, and we give our main result, the closed expression to it. In eq. (2.1), we introduced the spin-1 boundary to boundary current

$$F^{(x_1,x_2)} = \sum_{C\in\Gamma} P(C) N_C^{(x_1,x_2)} \mathrm{sign}_C^{(x_1,x_2)}$$

This current is the signed and weighted sum of all the full strip configurations which contain boundary to boundary paths passing through between points x_1 and x_2. $N_C^{(x_1,x_2)}$ is the number of paths passing through, $\mathrm{sign}_C^{(x_1,x_2)}$ is either $+1$ or -1, if x_1 is in the region above or below the path, respectively. $P(C)$ is the ensemble probability of the configuration. After introducing inhomogeneous weights, $P(C)$ and $F^{(x_1,x_2)}$ become a function of the rapidities. There are two cases to consider, all other expressions follow from the additivity. These two cases are when x_1 and x_2 are on two adjacent vertices of the square lattice, and either separated by a horizontal or a vertical line. Denote the position of the x_1 and x_2 markers by horizontal and vertical lattice indices. Denote the horizontal and vertically separated case by X and Y, respectively

$$X^{(k)} = F^{((k,i),(k+1,i))} \tag{2.53a}$$

$$Y^{(k)} = F^{((k,j),(k,j+1))} \tag{2.53b}$$

After introducing the rapidities, X and Y become a function of them. As T-matrices with different auxiliary rapidity commute, the X current cannot depend on them, and the Y current depends on the auxiliary rapidity between the points $(k,\, j)$ and $(k,\, j+1)$

$$X^{(k)} = X^{(k)}(z_0, \ldots, z_{L+1}) \,, \tag{2.54a}$$

$$Y^{(k)} = Y^{(k)}(w, z_0, \ldots, z_{L+1}) \,. \tag{2.54b}$$

The currents are computable by the introduction of operators $\hat{X}^{(k)}$ and $\hat{Y}^{(k)}$, as the following expectation values

$$X^{(k)}(z_0, \ldots, z_{L+1}) = \frac{\langle \Psi(z_0, \ldots, z_{L+1}) | \, \hat{X}^{(k)} \, | \Psi(z_0, \ldots, z_{L+1}) \rangle}{\langle \Psi(z_0, \ldots, z_{L+1}) | \Psi(z_0, \ldots, z_{L+1}) \rangle} \,, \tag{2.55a}$$

$$Y^{(k)}(w, z_0, \ldots, z_{L+1}) = \frac{\langle \Psi(z_0 \ldots z_{L+1}) | \, \hat{Y}^{(k)}(w, z_0 \ldots z_{L+1}) \, | \Psi(z_0 \ldots z_{L+1}) \rangle}{\langle \Psi(z_0 \ldots z_{L+1}) | \, T(w, z_0 \ldots z_{L+1}) \, | \Psi(z_0 \ldots z_{L+1}) \rangle} \,. \tag{2.55b}$$

Here $\hat{X}^{(k)}$ is a matrix, acting on dLP_L. Its matrix elements are 0 and ± 1. It has the ± 1 nonzero elements between $\langle\alpha| \in dLP_L^*$ and $|\beta\rangle \in dLP_L$ elements, if the $\langle\alpha|\beta\rangle$ link pattern configuration contains a boundary to boundary path on the kth site. The sign depends on weather position k or $k+1$ is above the path. $\hat{Y}^{(k)}$ has a more complicated structure, as only the two link patterns do not tell information about the horizontal connectivity. $\hat{Y}^{(k)}$ is a modified T-matrix. An element of $\hat{Y}^{(k)}$ is a weighted sum –with weights 0 and ± 1– of all T-matrix configuration with the proper occupancy on the top and bottom. The weight is ± 1 if a proper boundary to boundary path is formed with that T-matrix configuration. The ± 1 sign is chosen according to the current.

2.7.1 Main result

Our main result is an explicit closed expression for the X and Y spin-1 boundary to boundary current in the inhomogeneous dilute $O(1)$ model, defined on a strip, infinite in vertical direction (both upward and downward), with a finite width L. To present the expression, first we introduce some auxiliary functions. We use the standard definition of the elementary symmetric functions

$$e_k(z_1,\ldots,z_n) = \sum_{1\le i_1<\ldots<i_k\le n} z_{i_1}\ldots z_{i_n} \quad \text{for } 1\le k\le n \text{ , otherwise } 0 \ . \tag{2.56}$$

We introduce elementary symmetric functions over z_i and z_i^{-1}

$$E_i(z_0,z_1,\ldots,z_L,z_{L+1}) = e_i\left(z_0,z_1\ldots z_L,z_{L+1},z_0^{-1},z_1^{-1}\ldots z_L^{-1},z_{L+1}^{-1}\right) \ . \tag{2.57}$$

Note that these symmetric polynomials take the same value for indices i and $L+1-i$

$$E_i(z_0,z_1,\ldots,z_L,z_{L+1}) = E_{L+1-i}(z_0,z_1,\ldots,z_L,z_{L+1}) \ . \tag{2.58}$$

Define the following auxiliary polynomial

$$P_L^p(z_0,z_1,\ldots,z_{L+1}) = -\tfrac{\mathrm{i}^{L+1}}{2(q-q^{-1})}\left(\prod_{j=0}^{L+1}\tfrac{(qz_j+\mathrm{i})(q^{-1}z_j-\mathrm{i})}{z_j} \ - \prod_{j=0}^{L+1}\tfrac{(q^{-1}z_j+\mathrm{i})(qz_j-\mathrm{i})}{z_j}\right) . \tag{2.59}$$

With these definitions, Garbali and Nienhuis found closed expressions for the empty element and the partition sums (in [46, 47], where alternative definitions are also presented)

$$\psi_{L,EE}(z_0,\ldots,z_{L+1}) = \frac{\det_{1\le i,j\le L+1}\left(E_{3j-2i} - E_{3j+2i-4(L+2)}\right)}{P_L^p(z_0,\ldots,z_{L+1})} \ , \tag{2.60}$$

$$Z_{L,h.s.}(z_0,\ldots,z_{L+1}) = 2^L \psi_{L,EE}(z_0,\ldots,z_{L+1}) \ , \tag{2.61}$$

$$Z_{L,f.s.}(z_0,\ldots,z_{L+1}) = 2^L \left(\psi_{L,EE}(z_0,\ldots,z_{L+1})\right)^2 \ . \tag{2.62}$$

In [1], under some technical assumption, we prove that on an inhomogeneous lattice of width L

$$X_L^{(i)}(z_0,\ldots,z_{L+1}) = \frac{1-2q}{2}\left(z_i - \frac{1}{z_i}\right)\frac{1}{E_1(z_0,\ldots,z_{L+1})} \ , \tag{2.63}$$

$$\begin{aligned} Y_L^{(i)}(w,z_0,\ldots,z_{L+1}) = 3\,(-1)^{L+1}\left(w-\frac{1}{w}\right)^2 \frac{w^{2(L+2)}}{W_Y(w,z_0,\ldots,z_{L+1})}\times \\ \times\ \frac{\psi_{L+2,EE}(w,-w,z_0,\ldots,z_{L+1})}{E_1(z_0,\ldots,z_{L+1})\,\psi_{L,EE}(z_0,\ldots,z_{L+1})} \ . \end{aligned} \tag{2.64}$$

Note that $Y_L^{(i)}$ is independent of the index i. W_Y is an auxiliary function, similar to the normalization N of the T-matrix

$$W_Y(w,z_0,\ldots,z_{L+1}) = \prod_{i=0}^{L+1} W_R(z_i,w)W_R(w^{-1},z_i) + \prod_{i=0}^{L+1} \tilde{W}_R(z_i,w)\tilde{W}_R(w^{-1},z_i) \ . \tag{2.65}$$

Notice that W_Y is a symmetrized version of N. Instead of the normalization of the K-matrix, it contains R-matrix normalization, belonging to the boundary rapidities. X has the following equivalent form

$$X_L^{(i)}(z_0,\ldots,z_{L+1}) = \frac{1-2q}{2}\, z_i \frac{\partial}{\partial z_i} \log E_1(z_0,\ldots,z_{L+1}) \ . \tag{2.66}$$

2.8 Recursion relations

In this section, we derive recursion equations, relating systems with sizes L and $L-1$. For a special ratio of two consecutive rapidities, the possible configurations on the two sites are restricted in such a way that they effectively act as a single site. By setting the left (right) boundary rapidity and the first (last) rapidity to the special ratio, the same relation holds. This allows us to write down recursion equations, relating systems with system sizes L and $L-1$.
At the special ratio of the two rapidities, the polynomial weights of the forbidden link patterns are zero. If the link patter is allowed, the polynomial weight factorizes into a product of a symmetric prefactor and the polynomial weight of the one size smaller system.

This kind of equations show up in integrable quantum field theories, usually referred as fusion equation and boundary fusion equation [48].

2.8.1 Fusion equation

The R-matrix factorizes into the product of two "triangle operators", if we set the two rapidities to a ratio q^2, e.g. set them to zq^{-1} and zq

$$R\left(zq^{-1}, zq\right) = (-1-q)M \cdot S =$$
$$(-1-q)\left(\quad + \quad + \quad + \quad\right) \cdot \left(\quad + \quad + \quad + \quad\right) \tag{2.67}$$

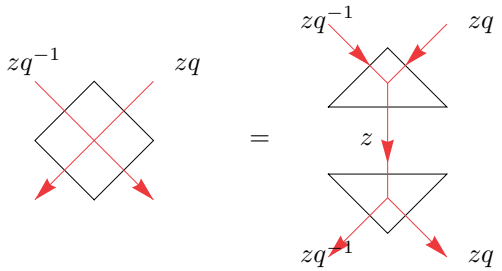

With the help of the operator M, the following fusion equation holds

$$R_i(zq, w)R_{i+1}(zq^{-1}, w)M_i = 2\frac{(w-z)(w+z)}{z^2}M_iR_i(z, w)\ . \tag{2.68}$$

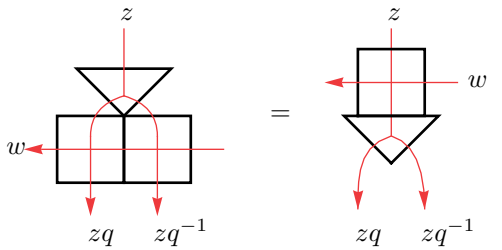

This equation is derived by Garbali and Nienhuis [46,47], and we give a detailed proof in appendix A.5. This equation should also be understood as the previous equations: the statistical weight of both configurations are the same, or equivalently, their action on V_L is the same. Intuitively, one can say that setting the two consecutive rapidities to the special ratio q^2, we can use the fusion equation from row to row which effectively decreases the system size by one. In

fact, the "triangle operators" are intertwiners between dLP_L and dLP_{L-1}. The fusion equation relates the transfer matrix of size L and $L-1$

$$M_i T_L(\ldots, z_{i-1}, zq, zq^{-1}, z_{i+2}, \ldots) = T_{L-1}(\ldots, z_{i-1}, z, z_{i+2}, \ldots) M_i \ . \tag{2.69}$$

Act by both sides on the $\left|\Psi_L(\ldots, zq, zq^{-1}, \ldots)\right\rangle$ eigenvector of T_L

$$\begin{aligned} N M_i \left|\Psi_L(\ldots, zq, zq^{-1}, \ldots)\right\rangle = \\ = T_{L-1}(\ldots, z, \ldots) \left(M_i \left|\Psi_L(\ldots, zq, zq^{-1}, \ldots)\right\rangle\right) \ , \end{aligned} \tag{2.70}$$

which means using the uniqueness of the eigenvector of T_{L-1}

$$\begin{aligned} M_i \left|\Psi_L(\ldots, z_{i-1}, zq, zq^{-1}, z_{i+2}, \ldots)\right\rangle = \\ = F(z; z_0, \ldots, z_{i-1}, z_{i+2}, \ldots, z_{L+1}) \left|\Psi_{L-1}(\ldots, z_{i-1}, z, z_{i+2}, \ldots)\right\rangle \ . \end{aligned} \tag{2.71}$$

Here $F(z; z_0, \ldots, z_{i-1}, z_{i+2}, \ldots, z_{L+1})$ is a proportionality factor [46]

$$F(z; z_1, \ldots, z_n) = \prod_{j=1}^{n} E_1(z, z_j) = \prod_{j=1}^{n} \frac{(1 + z_j z)(z_j + z)}{z_j z} \ . \tag{2.72}$$

The mapping of a dLP_L link configuration to a dLP_{L-1} configuration depends on the local configuration on sites $i, i+1$. There are five different local configurations: (), $\bullet\bullet$, $\bullet|$, $|\bullet$, and $||$. Here we use the notation with parentheses, with the addition that $|$ denotes a link connected somewhere outside the two sites. Elements with the local configuration $||$ are mapped to 0 (the corresponding groundstate weight become 0). The full list of mapping is the following

- Mapping to empty site:

$$\begin{aligned} M: \quad & () \to \bullet \\ & \bullet\bullet \to \bullet \end{aligned}$$

- Mapping to one occupied, one empty site:

$$\begin{aligned} M: \quad & \bullet| \to | \\ & |\bullet \to | \end{aligned}$$

- Disappearing elements:

$$M: \quad || \to 0$$

There is a simple argument for the existence of the recursion relation. Consider the following qKZ equation

$$R_{i,i+1}\left(zq^{-1},zq\right)\left|\Psi_L\left(\ldots zq^{-1},zq\ldots\right)\right\rangle=\left|\Psi_L\left(\ldots zq,zq^{-1}\ldots\right)\right\rangle\ . \tag{2.73}$$

On the r.h.s., the groundstate vector is set to the recursion ratio. On the l.h.s., $R_{i,i+1}\left(zq^{-1},zq\right)$ acts on the state. As at this value, the R matrix factorizes into the two triangle operators, $W_2\left(zq^{-1},zq\right)=0$. This sets the probability of any element with || local configuration to 0, and by removing the bottom triangle, we get the mapping from dLP_L link configurations to dLP_{L-1} configurations.

2.8.2 Boundary fusion equation

The fusion equation has a boundary version, involving the boundary rapidity and the first or last rapidity. Setting $z_0=zq$, $z_1=zq^{-1}$, or $z_L=zq$, $z_{L+1}=zq^{-1}$ effectively decreases the size of the system by one. The reasoning is basically identical for the left and right boundary, so here we present it only for the left side.
Setting $z_0=zq$, $z_1=zq^{-1}$, the left K-matrix factorizes into an upper and a lower triangle

$$K_l\left(zq^{-1},zq\right)=-\frac{-1+2q+z^2+qz^2}{-1+q+z^2}L_l\cdot U_l=$$
$$-\frac{-1+2q+z^2+qz^2}{-1+q+z^2}\left(\quad+\quad\right)\cdot\left(\quad+\quad\right) \tag{2.74}$$

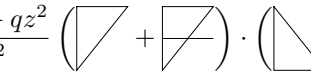

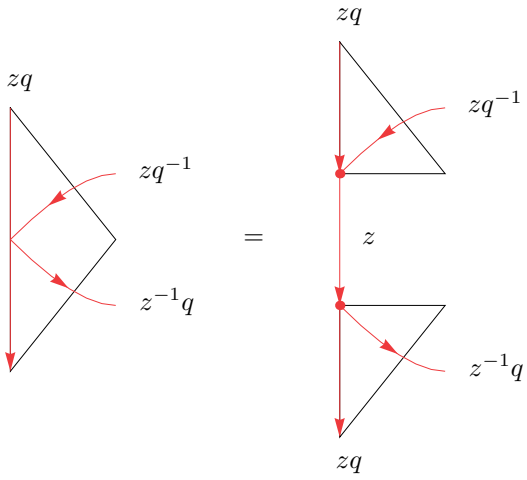

Using the operator U, the boundary reflection holds

$$U_l R_1\left(w^{-1}, zq^{-1}\right) K_l(w, zq) R_1\left(zq^{-1}, w\right) = \\ = \frac{q(w+z)(-1+wz)w^2(1+z^2)^2}{z^2(-w1+qw-qz+qw^2z-qz^2)} K_l(w,z) U_l \quad (2.75)$$

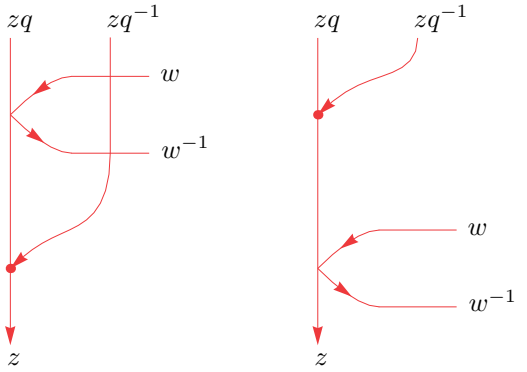

This is proved by combining the (2.68) fusion equation and the construction of the K-matrix described in appendix A.6. Consequently, the following intertwining equation holds

$$L_l T_L(w, zq, zq^{-1}, z_2, \ldots) = T_{L-1}(w, z, z_2 \ldots) L_l \,. \quad (2.76)$$

Similarly, as before, L_l effectively decreases the system size by one

$$L_l \left|\Psi_L(zq, zq^{-1}, z_2, \ldots)\right\rangle = F(z, z_2, \ldots, z_{L+1}) \left|\Psi_{L-1}(z, z_2 \ldots)\right\rangle \ , \tag{2.77}$$

where $F(z, z_0, \ldots, z_{i-1}, z_{i+2}, \ldots, z_{L+1})$ is the same proportionality factor as in eq. (2.72). This recursion relation decreases the system size by erasing the first site. The rule for the mapping is the following

- Elements with erased first site:

$$\begin{aligned} L_l : \quad & |\bullet \ldots\rangle \to |\ldots\rangle \\ & |) \ldots\rangle \to |\ldots\rangle \end{aligned}$$

- Disappearing element:

$$L_l : \quad |(\ldots\rangle \to 0$$

A completely analogous derivation holds for the right boundary, with an analogous $K_r\left(zq, zq^{-1}\right) \sim L_r U_r$ right boundary fusion equation.
As a consequence, based on the fusion and boundary fusion equations, regarding the fusion properties, we can treat all the rapidities and boundary rapidities on the same footing.
The fusion equations leads to the following recursion relations, satisfied by the partition sums (without the rapidities not participating in the fusion)

$$Z_{L,h.s.}\left(z_{i-1}, zq, z_q^{-1}, z_{i+2}\right) = 2 \left(\prod_{k \neq i, i+1} E_1(z, z_k) \right) Z_{L-1,h.s}\left(z_{i-1}, z, z_{i+2}\right) \ , \tag{2.78}$$

$$Z_{L,f.s.}\left(z_{i-1}, zq, zq^{-1}, z_{i+2}\right) = 2 \left(\prod_{k \neq i, i+1} E_1^2(z, z_k) \right) Z_{L-1,f.s}\left(z_{i-1}, z, z_{i+2}\right) \ . \tag{2.79}$$

The prefactor 2 is a consequence of the mappings realized by M, L_l and L_r: Every image in dLP_{L-1} has two preimage. The F^2 proportionality factor for $Z_{L-1,f.s.}$ is the result of $Z_{f.s.}$ being a sum of products of two groundstate elements. The recursion acts on the dual space dLP_L^* in the flipped order, hence the recursion only takes place after the action with M to project out the extra site.

2.8.3 The missing recursion by size two

In the previous section, we introduced a recursion by system size one. For generic n, there are two recursions, with increment one and two in the size of the system. The recursion by system size two is missing in the case $n = 1$.
These two recursions are based on the zeros of the unitarity/inversion relation (eq. (2.25)). The inversion relation for general n, in additive notation is as follows

$$R(u)R(-u) = \sin(u - 3\lambda)\sin(u - 2\lambda)\sin(u + 2\lambda)\sin(u + 3\lambda) \tag{2.80}$$

This equation in the multiplicative notation is

$$R(z)R(z^{-1}) = \frac{1}{16z^2q^{10}}\left(z^2 - q^6\right)\left(z^2 - q^4\right)\left(z^2q^4 - 1\right)\left(z^2q^6 - 1\right) \tag{2.81}$$

As we take the loop weight to $n = 1$, the factor $(z^2 - 1)$ is one that all R-matrix elements have in common (and we divide it out), so it is not the result of a projection of the R-operator.As for $n = 1$, $q^3 = -1$, this leads to the following equation

$$R(z)R(z^{-1}) = \frac{1}{16z^2q^{10}}\left(z^2 - q^4\right)\left(z^2q^4 - 1\right) \tag{2.82}$$

As one can see, this equation does not have zeros at $z = q^{\pm 3}$, and the other possibility is covered by the discussed recursion.

2.9 Symmetries

The (2.63, 2.64) expressions for the $X^{(k)}$ and $Y^{(k)}$ exhibit a number of symmetries, most arising from the unitarity relations and the qKZ and boundary qKZ equations.
$X^{(k)}$ and $Y^{(k)}$ are symmetric under $z_i \leftrightarrow z_j$ (for $X^{(k)}$, $i, j \neq k$), and under $z_i \to z_i^{-1}$ (for $X^{(k)}$, $i \neq k$). We prove these symmetries in the following steps.
(i) First, we prove that $X^{(k)}$ and $Y_L^{(k)}$ are symmetric under $z_i \leftrightarrow z_j$ for certain sets of indices, namely

$$\begin{aligned} X^{(k)}: \quad & 1 \le i, j \le k-1 \text{ or} \\ & k+1 \le i, j \le L \end{aligned}$$

$$\begin{aligned} Y^{(k)}: \quad & 1 \le i, j \le k-1 \text{ or} \\ & k \le i, j \le L \end{aligned}$$

We did not find a way to extend the symmetry to the boundary rapidities (with indices 0 and $L+1$), we checked these cases for small system analytically and numerically: We computed the $X^{(k)}$ current analytically for $L = 1, 2, 3$, and found it symmetric in all the variables. We computed the $Y^{(k)}$ current analytically for $L = 0, 1$ and found it symmetric, and numerically checked the symmetry for the boundary rapidity for $L = 2, 3$.
(ii) Using this, we prove the $z_i \to z_i^{-1}$ symmetry, for $X^{(k)}$, $0 \le i \le L+1$, $i \neq k$, and for $Y^{(k)}$, $0 \le i \le L+1$.
(iii) We use the $z_i \to z_i^{-1}$ inversion symmetry as an ingredient to prove the full symmetry of $Y_L^{(k)}$ under $z_i \leftrightarrow z_j$ without restriction on the indices.
We did not find a proof for the full symmetry of $X_L^{(k)}$, so in the proof of the main result for X, we use it as a necessary assumption. As the symmetry for the boundary rapidities is also an assumption, our statements hold up to these assumption.

2.9.1 Partial symmetry of X and Y

We prove the symmetry of $X^{(k)}$ and $Y^{(k)}$ under $z_i \leftrightarrow z_j$, given that $i, j < k$ or $k < i, j$. The proof is based on the (2.25) unitarity relation and the (2.52a) qKZ equation. The proof is the same for both expressions, so here we present the one for X. Use the operator form of X (suppressing irrelevant notations and normalization)

$$\begin{aligned} X^{(k)}(z_i, z_{i+1}) &\simeq \langle \Psi(z_i, z_{i+1})| \hat{X}^{(k)} |\Psi(z_i, z_{i+1})\rangle \\ &\simeq \langle \Psi(z_i, z_{i+1})| \hat{X}^{(k)} R_{i,i+1}(z_{i+1}, z_i) R_{i,i+1}(z_i, z_{i+1}) |\Psi(z_i, z_{i+1})\rangle \\ &\simeq \langle \Psi(z_i, z_{i+1})| R_{i,i+1}(z_{i+1}, z_i) \hat{X}^{(k)} |\Psi(z_{i+1}, z_i)\rangle \\ &\simeq \langle \Psi(z_{i+1}, z_i)| \hat{X}^{(k)} |\Psi(z_{i+1}, z_i)\rangle \simeq X^{(k)}(z_{i+1}, z_i) \,. \end{aligned} \tag{2.83}$$

The R-matrix and the $\hat{X}^{(k)}$ operators commute, if $i+1 < k$ or $k < i$. By repeating this procedure, we extend the symmetry to $z_1, \ldots, z_{k-1}$ and $z_{k+1}, \ldots, z_L$. We did not find a way to extend the proof to the z_0, z_{L+1} boundary rapidities. The same proof with the same flaw applies for $Y^{(k)}$, the only difference is in the restriction for the indices, i.e. for $Y^{(k)}$, $z_i \leftrightarrow z_{i+1}$, $i+1 \le k$ or $k < i$.
To give evidence of the symmetry involving the bulk rapidities, we made the following analytic and numerical check: We checked analytically the expression for X with $L = 1, 2, 3$, and for Y with $L = 0, 1$. For larger system sizes, we made numerical checks, namely for $L = 2, 3$. Due to the largely increasing terms –especially in Y– in these expressions, these checks are strong evidences

supporting our assumption.
The symmetry of X and Y under $z_i \to z_i^{-1}$ is based on the (2.29, 2.30) unitarity relations of the K-matrix and on the (2.52b, 2.52c) boundary qKZ equations. The proof is again the same for $X^{(k)}$ and $Y^{(k)}$, so we present it for $X^{(k)}$. Derive the inversion symmetry for z_1 , using the unitarity of the left K-matrix (assume $k \neq 1$)

$$\begin{aligned} X^{(k)}(z_1) &\simeq \langle \Psi(z_1)| \hat{X}^{(k)} |\Psi(z_1)\rangle \\ &\simeq \langle \Psi(z_1)| \hat{X}^{(k)} K_l(z_1^{-1}, z_0) K_l(z_1, z_0) |\Psi(z_1)\rangle \\ &\simeq \langle \Psi(z_1)| K_l(z_1^{-1}, z_0) \hat{X}^{(k)} \left|\Psi(z_1^{-1})\right\rangle \\ &\simeq \left\langle \Psi(z_1^{-1})\right| \hat{X}^{(k)} \left|\Psi(z_1^{-1})\right\rangle \simeq X^{(k)}(z_1^{-1}) \ . \end{aligned} \quad (2.84)$$

The proof for the $z_L \to z_L^{-1}$ symmetry goes the same way, using the unitarity of the right K-matrix. The inversion symmetry extends to the other rapidities on the two sides of the position of the current by the consecutive application of $z_i \leftrightarrow z_j$ symmetry. By this we extend the inversion symmetry to $0 \leq i \leq k-1$ and $k+1 \leq i \leq L+1$ for $X^{(k)}$, and for all $0 \leq i \leq L+1$ for $Y^{(k)}$.

2.9.2 Full symmetry of Y

In this section, we show that $Y_L^{(k)}$ is independent of the position k, and symmetric in the variables $z_0, \ldots, z_{L+1}$.
Define p as a path going from the left boundary to the right boundary. The path is defined as a set of K and R-matrix elements which constitute the line connecting the two boundaries. Regard two paths to be different, if the line connecting the two boundaries are the same, but there is difference between the content of the K and R-matrix elements, as on fig. 2.9. By this definition, we identify configurations which only differ in their position, and which are related by a vertical translation. The weight of the p path is the weight of the constituting matrices. Since Y depends only on one auxiliary rapidity, we set all the auxiliary rapidities to the same value w. Denote the weight of p by $\Omega_p(w, z_0 \ldots z_{L+1})$.
The set of all paths, P is a union of two disjoint sets, P_T and P_B. P_T contains the paths starting from the top of the left K-matrix, P_B contains the ones starting from the bottom of it. Every path, $p \in P_T$ is in bijection with a path $\tilde{p} \in P_B$, by a horizontal mirroring, as in fig. 2.10). By the properties of the R and K-matrices, it is easy to see that $\Omega_p(w, z_0 \ldots z_{L+1}) = \Omega_{\tilde{p}}(w, z_0^{-1} \ldots z_{L+1}^{-1})$. We introduce $m_{p,k,x}$, where p denotes the path, $0 \leq k \leq L$ the horizontal position of $Y_L^{(k)}$, and

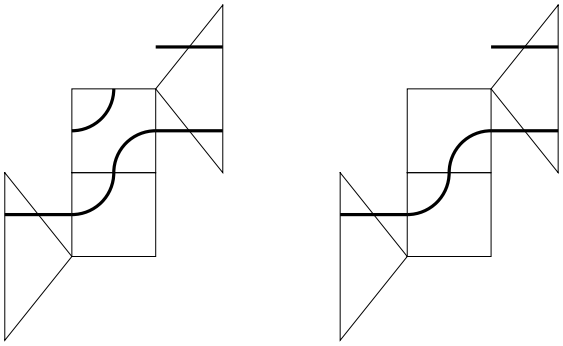

Figure 2.9: These two paths are not equivalent.

$x \in T, B$ is stands for 'top' or 'bottom'. Define $m_{p,k,x}$ as the signed crossing of the path p at horizontal line k on the 'top' or 'bottom' section, i.e. at the top or bottom of the double row transfer matrix (See in fig. 2.11). Signed crossing means that if the line crosses from left to right, it counts as 1, if from right to left, it counts as -1. Since a path is crossing once more from left to right then to right to left, $m_{p,k,T} + m_{p,k,B} = 1$ (as in fig. 2.11).

By the mirroring, the crossing from the top of the path p maps to the crossing to the bottom of the path $\tilde{p}$, and vice versa. This means that $m_{p,k,x} = m_{\tilde{p},k,\bar{x}}$, where $\bar{T} = B$, $\bar{B} = T$. Combining these features, it is clear that $m_{p,k,x} + m_{\tilde{p},k,x} = 1$. Denote by $Y_L^{(k,T)}$ and $Y_L^{(k,B)}$ the current through the top and the bottom of the T-matrix, respectively. By this definitions, the Y current is given by

$$\begin{aligned} Y_L^{(k,x)}(w, z_0, \dots z_{L+1}) = \\ &= \sum_{p \in P_T} m_{p,k,x} \Omega_p \left(w, z_0, \dots z_{L+1}\right) + \sum_{\tilde{p} \in P_B} m_{\tilde{p},k,x} \Omega_{\tilde{p}} \left(w, z_0, \dots z_{L+1}\right) \\ &= \sum_{p \in P_T} m_{p,k,x} \Omega_p \left(w, z_0, \dots z_{L+1}\right) + m_{\tilde{p},k,x} \Omega_p \left(w, z_0^{-1}, \dots z_{L+1}^{-1}\right) \ . \end{aligned} \tag{2.85}$$

Using that Y is symmetric under $z_i \to z_i^{-1}$, we consider the following construction

$$Y_L^{(k,x)}(w, z_0, \dots z_{L+1}) = \frac{1}{2} \left(Y_L^{(k,x)} \left(w, \{z_i\}\right) + Y_L^{(k,x)} \left(w, \{z_i^{-1}\}\right) \right) =$$

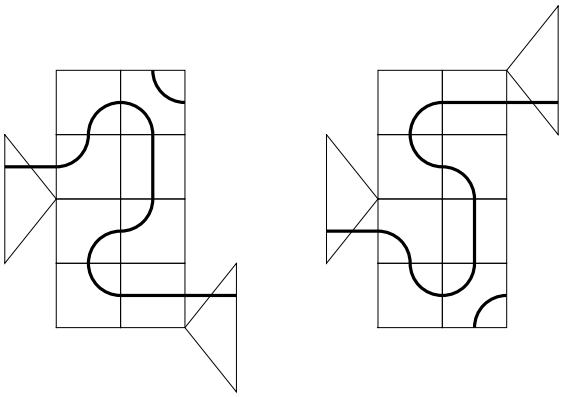

Figure 2.10: Path p and the mirrored path $\tilde{p}$.

$$
\begin{aligned}
=&\frac{1}{2}\left(\sum_{p\in P_T} m_{p,k,x}\ \Omega_p\left(w,\{z_i\}\right) + m_{\tilde{p},k,x}\Omega_p\left(w,\left\{z_i^{-1}\right\}\right) + \right.\\
&\left. + \sum_{p\in P_T} m_{p,k,x}\Omega_p\left(w,\left\{z_i^{-1}\right\}\right) + m_{\tilde{p},k,x}\Omega_p\left(w,\{z_i\}\right)\right) = \qquad (2.86)\\
=&\frac{1}{2}\left(\sum_{p\in P_T} (m_{p,k,x} + m_{\tilde{p},k,x})\Omega_p\left(w,\{z_i\}\right) + \right.\\
&\left. + \sum_{p\in P_T} (m_{p,k,x} + m_{\tilde{p},k,x})\Omega_p\left(w,\left\{z_i^{-1}\right\}\right)\right) =\\
=&\frac{1}{2}\sum_{p\in P_T} \Omega_p\left(w,\{z_i\}\right) + \Omega_p\left(w,\left\{z_i^{-1}\right\}\right)\ .
\end{aligned}
$$

It thus follows that each path in P_T contribute to Y, by the average of the weights of p and $\tilde{p}$. It is also clear from this reasoning that $Y^{(k)}$ is independent of k. This means that there is no further restriction on its symmetries, so it is symmetric in z_i, and under $z_i \to z_i^{-1}$, $\forall i$.

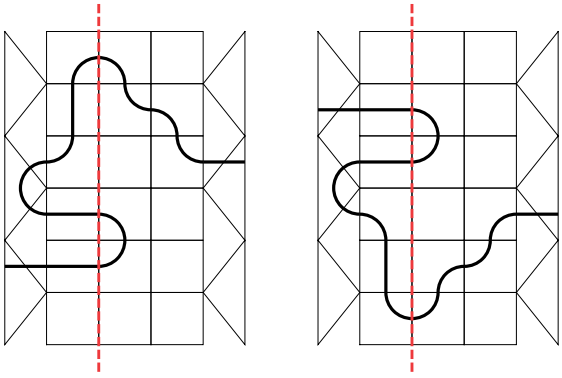

Figure 2.11: $m_{p,k=1,T}=2$, $m_{p,k=1,B}=-1$, $\quad m_{\tilde{p},k=1,T}=-1$, $m_{\tilde{p},k=1,B}=2$

2.10 Proof of the main result

In order to prove our (2.63, 2.64) main result, we utilize the symmetries and the recursion relations.
The X and Y currents satisfy the following recursion relations

$$X_L^{(i)}\left(\ldots,z_{j-1},zq,zq^{-1},z_{j+2},\ldots\right)=X_{L-1}^{(i)}(\ldots,z_{j-1},z,z_{j+2},\ldots),\quad \forall i\neq j,j+1\,, \tag{2.87a}$$

$$Y_L\left(\ldots,z_{j-1},zq,zq^{-1},z_{j+2},\ldots\right)=Y_{L-1}(\ldots,z_{j-1},z,z_{j+2},\ldots),\quad \forall i\neq j,j+1\,. \tag{2.87b}$$

Note that depending on the relative position of j compared to i, the actual position of the current might change, however, we misuse the $X^{(i)}$ notation for both cases. The symmetry property extends to non-adjacent rapidities.
To prove our main result, we list the recursion relations for the *unnormalized* expressions $X_{u.n.}$and $Y_{u.n.}$, and use that to prove the recursion relation for the normalized cases.

2.10.1 Proof for the Y current

In this section we prove that Y is indeed in the (2.64) form.
We define the unnormalized version of Y as follows

$$Y_L^{(i),u.n.}=\langle\Psi_L|\,\hat{Y}_L^{(i)}\,|\Psi_L\rangle=\sum_{\alpha,\beta,\gamma}(-1)^{\mathrm{sign}(\alpha,\beta,\gamma)}\psi_\alpha T_\beta\psi_\gamma\,. \tag{2.88}$$

Here, $\alpha \in dLP_L$, $\gamma \in dLP_L^*$, and T_β is a T-matrix configuration which provides the necessary tiling to form a path through the top row of the T-matrix, at position i. The $\text{sign}(\alpha, \beta, \gamma) = \pm 1$ term encodes the spin-1 property. The relation between the normalized and unnormalized Y current is

$$Y_L^{(i)} = \frac{Y_L^{(i),u.n.}}{Z_{L,f.s.} N_L} \,, \tag{2.89}$$

where N_L is the T-matrix normalization.
The (2.87b) and (2.79) recursion relations for Y and $Z_f.s.$ lead to the following recursion relation for the unnormalized Y current

$$\left.\frac{Y_L^{(i),u.n.}}{W_{T,L}}\right|_{z_j = zq, z_{j+1} = zq^{-1}} = 2 \left(\prod_{k \neq j, j+1} E_1^2 \left(z, z_k\right) \right) \frac{Y_{L-1}^{(i),u.n.}}{W_{T,L-1}} \,. \tag{2.90}$$

As Y is fully symmetric, and N is not fully symmetric, $Y^{u.n.}$ is not symmetric. To exploit the symmetric properties, we introduce an auxiliary Laurent polynomial function which is symmetric by construction

$$\tilde{Y}_L^{u.n.} = Y_L^{u.n.} \frac{W_{Y,L}}{N_L} = Y_L W_Y Z_{f.s.} \,. \tag{2.91}$$

W_Y is the quantity defined in eq. (2.65) which satisfies the following recursion relation

$$W_{Y,L}(\ldots, zq, zq^{-1}, \ldots) = -w^2 E_1(w, z) E_1(-w1, z) W_{Y,L-1}(\ldots, z, \ldots) \,. \tag{2.92}$$

These lead to the following recursion relation for the symmetrized, unnormalized current $\tilde{Y}_{u.n.}$

$$\tilde{Y}_L^{u.n.}(z_i = zq \ldots z_j = zq^{-1}) = -2w^2 E_1(w, z) E_1(-w, z) \prod_{k \neq i, j} E_1^2(z, z_k) \tilde{Y}_{L-1}^{u.n.}(z) \,. \tag{2.93}$$

As Y, the normalized current is fully symmetric in the rapidities $z_0, \ldots, z_{L+1}$, any two of them set to the recursion ratio leads to a recursion relation. The recursion relation holds for two additional value, following from the $z_i \to z_i^{-1}$ symmetry. The complete set of recursions involving two chosen rapidities z_i, z_j is the following

$$Y_L(z_i = zq \ldots z_j = zq^{-1}) = Y_{L-1}(\ldots z \ldots) \,, \tag{2.94a}$$

$$Y_L(z_i = zq^{-1} \ldots z_j = zq) = Y_{L-1}(\ldots z \ldots) \,, \tag{2.94b}$$

$$Y_L(z_i = (zq)^{-1} \dots z_j = z^{-1}q) = Y_{L-1}(\dots z \dots) \,, \tag{2.94c}$$
$$Y_L(z_i = z^{-1}q \dots z_j = (zq)^{-1}) = Y_{L-1}(\dots z \dots) \,. \tag{2.94d}$$

Involving two fixed variables leads to 4 recursion relations. Involving one fixed variable and leaving the other one freely chosen leads to $4(L+1)$ recursion relations, relating Y_L and Y_{L-1}, fully exploiting the symmetry in the variables and the inversion symmetry.
We calculated $\tilde{Y}^{u.n.}$ for $L = 0, 1$, giving starting elements for the following conjectured form

$$\tilde{Y}^{u.n.}(w, z_0, \dots, z_{L+1}) = 2^L \, 3(-1)^{L+1} \, w^{2(L+2)} \left(w - \frac{1}{w}\right)^2 \times \\ \times \frac{\psi_{L,EE}(z_0 \dots, z_{L+1}) \psi_{L+2,EE}(w, -w, z_0 \dots, z_{L+1})}{E_1(z_0, \dots, z_{L+1})} \,. \tag{2.95}$$

The degree width of this expression is $4(L+1) - 1$ for size L which means that the recursion fully fixes $\tilde{Y}^{u.n.}$ for any system size, as a Lagrange interpolation. Based on eq. (2.91), we get Y for any system size. This proves that the Y current has the proposed (2.64) form

$$Y_L^{(i)}(w, z_0, \dots, z_{L+1}) = 3(-1)^{L+1} \left(w - \frac{1}{w}\right)^2 \\ \frac{w^{2(L+2)}}{W_Y(w, z_0, \dots, z_{L+1})} \frac{\psi_{L+2,EE}(w, -w, z_0, \dots, z_{L+1})}{E_1(z_0, \dots, z_{L+1}) \psi_{L,EE}(z_0, \dots, z_{L+1})} \,.$$

By this, based on the recursion relation, under the assumption of the symmetry of the bulk and boundary rapidities, we proved that the unique solution which satisfies eq. (2.87b) with the computed starting element, is indeed eq. (2.64).

2.10.2 Proof for the X current

In this section, under some technical assumption, we prove the (2.63) form of the X current. We use the same method as for the Y current.
We define the unnormalized version of the X current as follows

$$X_L^{(i),u.n.} = \langle \Psi_L | \, \hat{X}_L^{(i)} \, | \Psi_L \rangle = \sum_{\alpha,\beta} (-1)^{\mathrm{sign}(\alpha,\beta)} \psi_\alpha \psi_\beta \,, \tag{2.96}$$

where $\alpha \in dLP_L$, $\beta \in dLP_L^*$ are such that $\langle \alpha | \beta \rangle$ link pattern forms a boundary to boundary path through the ith site. The factor $\mathrm{sign}(\alpha, \beta) = \pm 1$ is chosen

according to the direction of the path. The normalized and unnormalized X currents are related as follows

$$X_L^{(i)} = \frac{X_L^{(i),u.n.}}{Z_{L,f.s.}} \,. \tag{2.97}$$

As the partition sum $Z_{L,f.s.}$ is fully symmetric, $X_L^{(i)}$ and $X_L^{(i),u.n.}$ share the same symmetry properties. The recursion relation for the unnormalized $X_L^{(i),u.n.}$ current is

$$X_L^{(i),u.n.}(z_j = zq \dots z_k = zq^{-1}) = 2 \prod_{n \neq j,k} E_1^2(z, z_n) X_{L-1}^{(i)u.n.}(z) \,. \tag{2.98}$$

We computed this quantity explicitly for $L = 1, 2, 3$ which lead us to the following conjectured form

$$X_L^{(i)u.n.}(z_0, \dots, z_{L+1}) = (2-q)2^{L-1} \left(z_i - \frac{1}{z_i}\right) \frac{\psi_{L,EE}^2(z_0, \dots, z_{L+1})}{E_1(z_0, \dots, z_L)} \,. \tag{2.99}$$

The computation for $L = 1$ is in appendix A.4. Based on the recursion properties of $\psi_{L,EE}$ and E_1, this form clearly satisfies eq. (2.87a). To prove the uniqueness of the solution, we assume the symmetry in all the variables expect z_i. The degree width of $X^{(i)u.n.}$ in any $z_j \neq z_i$ rapidity is $4L - 1$. Based on a similar counting as in the Y, there are $4L$ recursion relations relating systems L and $L - 1$. All the arguments hold as for Y, only the number of variables is smaller by one (since X^i is not symmetric in z_i, but all the other z.). By this, we see that under the aforementioned assumption, we found the unique solution for X presented in eq. (2.63)

$$X_L^{(i)}(z_0, \dots, z_{L+1}) = \frac{(1-2q)}{2} \left(z_i - \frac{1}{z_i}\right) \frac{1}{E_1(z_0, \dots, z_{L+1})} \,.$$

2.11 Conclusion

In this chapter, we showed our calculation on a boundary to boundary spin-1 current in the context of the dilute $O(n = 1)$ model on a strip, with open boundary conditions. We introduced the generic $O(n)$ model with different boundary conditions, and then specialized the loop weight to $n = 1$. This specializations allows us to do analytic computation on finite size systems. Due to the additivity of the current, it was sufficient to focus on two cases, which we denoted by X and Y. We have conducted the computation for the inhomogeneous

case, i.e. our expressions are symmetric rational functions in the rapidities and boundary rapidities of the model.
We have found a construction for the open boundary from closed boundary case, with the insertion of a rapidity line. This construction explains many observed properties of our model, however it is not sufficient to prove the symmetry of the current in the bulk and boundary rapidity. We also proved the fusion equation. From the fusion equation, and construction of the open boundary case, the boundary recursion relation follows, as a corollary.
Using similar methods to the one of Gorin and Panova, the homogeneous continuum limit of the current expressions is a topic of further interest.

Chapter 3

One-dimensional sums and finitized characters of 2×2 fused RSOS models

3.1 Introduction

Minimal model conformal field theories (CFTs) and certain statistical lattice models, RSOS models were introduced around the same time, and soon the connection was also established. An infinite family of conformal field theories was introduced by Belavin-Polyakov-Zamolodchikov [49], when they introduced the minimal model conformal field theories $\mathcal{M}(m,\, m')$, with central charge

$$c = c^{m,m'} = 1 - \frac{6(m-m')^2}{mm'}, \quad 2 \leq m < m', \quad m,\, m' \text{ coprime.} \tag{3.1}$$

In the same year, Andrews-Baxter-Forrester [50] introduced an infinite family of two-dimensional exactly solvable lattice models, the Restricted Solid-on-Solid models, parametrized by integer m', denoted by RSOS$(m'-1, m')$ by defining the infinite family of R-matrices, satisfying the Yang-Baxter equation. The result has been generalized in [51] to introduce RSOS(m, m') models, depending on two integer parameters m, m'. RSOS(m, m') models are height models on a lattice, with integer heights range from $1, \ldots, m'-1$.
It was shown in [52] by Friedan-Qiu-Schenker that unitarity –the conservation of probability in scattering processes– requires $m = m' - 1$ for the $\mathcal{M}(m,\, m')$

minimal models. Based on critical exponents, Huse could identify the universality class of the RSOS$(m'-1, m')$ models as the universality class of multicritical Ising-model [53], hence in the continuum limit, they realize the unitary minimal models $\mathcal{M}(m'-1, m')$. The generic RSOS(m, m') models have been identified as the lattice realizations of the non-unitary $\mathcal{M}(m, m')$ models [54, 55]. The minimal models include some of the most prominent studied models, including the Ising model $\mathcal{M}(3, 4)$ [6,56,57], the tricritical Ising model $\mathcal{M}(4, 5)$ [58–61] and the Lee-Yang model $\mathcal{M}(2, 5)$ [62–65].

By the method of fusion, new exactly solvable models are defined, by taking an $n \times n$ (or more generally $n \times m$) block of R-matrices, and regarding this block as the new R-matrix for the model [66]. This was carried out for RSOS models in [67], defining the $n \times n$ fused RSOS models RSOS$(m,\, m')_{n\times n}$.

On the CFT side, the corresponding field theories are expected to be the higher fusion level minimal models $\mathcal{M}(M,\, M',\, n')$, with integer fusion level $n' \in \mathbb{N}$, and fractional fusion level $k \in \mathbb{Q}$, which are constructed as GKO cosets [68]

$$\mathrm{COSET}(k, n'): \quad \frac{(A_1^{(1)})_k \oplus (A_1^{(1)})_{n'}}{(A_1^{(1)})_{k+n'}}, \tag{3.2}$$

$$k = \frac{n'M}{M'-M} - 2, \quad \gcd\left(\frac{M'-M}{n'},\, M'\right) = 1$$

Setting $n' = 1$ gives the usual minimal models, $\mathcal{M}(M,\, M', 1) = \mathcal{M}(M,\, M')$, $n' = 2$ gives the superconformal minimal models [69]. The identification is known for the unitary cases [70–72]. The parameters of the CTF corresponding to the unitary RSOS$(m'-1,\, m)_{n\times n}$ are given by $n' = n$, $(M,\, M') = (m'-n, m')$.

This chapter is based on results which are part of a larger project. The ultimate goal of the project is to identify the continuum limit of the non-unitary fused RSOS$(m,\, m')_{n\times n}$ models, for all values of $(m,\, m')$ and the fusion level n. This program has started by Tartaglia and Pearce in [73], where $n \times n$ fused RSOS models were probed for values of the crossing parameter $0 < \lambda = \frac{(m'-m)\pi}{m'} < \frac{\pi}{n}$. It was conjectured that the RSOS$(m,\, m')_{n\times n}$ models are lattice realizations of $\mathcal{M}(M,\, M',\, n')$ models with $(M,\, M') = (nm-(n-1)m',\, m')$ and $n = n'$ in the interval $0 < \lambda < \pi/n$.

The identification of the CFT follows from the correspondence between the one-dimensional sums of the RSOS model and the branching functions of the CFT. One-dimensional sums are partition functions of the RSOS model in the low temperature, critical limit, where the model is effectively one-dimensional. These are computed in the framework of the corner transfer matrix (CTM) method, and approximate the characters of the CFT. Tartaglia and Pearce carried out explicit calculations for $n = 2,\, 3$, which supports their general conjecture.

Here, based on these earlier works, we identify the CFTs for $n = 2$, $\pi/2 < \lambda < \pi$. In the continuum limit, the RSOS$(m, m')_{2\times 2}$ models are described by the $\mathcal{M}(m, m', 1) = \mathcal{M}(m, m')$ minimal models, for the crossing parameter $\pi/2 < \lambda < \pi$.
Following a similar method, we compute the local energy functions of the model, i.e. the exponents of the Boltzmann weights in the low temperature limit. Based on this, one-dimensional sums are computed. The one-dimensional sums are identified with finitized characters, up to the leading power. The conjectured correspondence can be proven as follows. One-dimensional sums satisfy certain recursion relations and initial conditions. Based on small system results, closed expressions can be conjectured for one-dimensional sums. Knowing these and the groundstate energies (the leading powers of the finitized characters), it can be proven that the closed expressions satisfy the recursion relations with the initial conditions. This program was used in the $n = 1$ unfused case in [51]. However, we are not able to replicate this proof for the $n = 2$ case, as we are missing the groundstate energies and scertain one-dimensional sums which do not coincide with characters.
In their paper of 2007, Jacob and Matthieu studied one-dimensional sums of certain paths with half-integer steps [74]. Their one-dimensional sums are not based on a lattice model. However, they reproduce the Virasoro characters of the non-unitary minimal models $\mathcal{M}(m, 2m + 1)$, for $m \geq 2$, $m \in \mathbb{N}$. By a bijection between the JM paths and the fused RSOS paths, we show that these one-dimensional sums are reproduced by the fused RSOS$(m, 2m+1)_{2\times 2}$ models. Thus we find the underlying lattice model for their one-dimensional sums. This is an interesting discovery in its own right.
This chapter organized as follows: In section 3.2 we introduce minimal models and higher-level coset model conformal field theories, in section 3.3 we define both unfused and fused (section 3.3.1) RSOS models. In sections 3.3.2 to 3.3.5 we build up the necessary machinery for making the correspondence with the conformal field theory. In section 3.4 we give the identification with the Jacob-Mathieu theory. In section 3.5 we describe the conjectured finitized characters (section 3.5.1) from [73] and our result (section 3.5.2) reported in [2].

3.2 Minimal models and higher-level minimal coset models

In this section we give a brief overview of minimal models and the corresponding coset models as their higher-level generalizations. We introduce the conformal

data, the central charge, the Virasoro characters and the branching functions. The minimal models, $\mathcal{M}(m,\, m') = \mathcal{M}(m,\, m',\, 1)$, have been introduced in [49]. These are rational conformal field theories which are parametrized by the two coprime integers, $m,\, m'$. The central charge is given by

$$c = c^{m,m'} = 1 - \frac{6(m-m')^2}{mm'}, \quad 2 \le m < m', \quad \gcd(m, m') = 1. \tag{3.3}$$

The minimal models are characterized by a finite number of primary fields, which are indexed by the $(r,\, s)$ Kac labels. The conformal weights of the primary fields and the corresponding Virasoro characters are given by

$$\Delta_{r,s}^{m,m'} = \frac{(rm'-sm)^2-(m-m')^2}{4mm'}, \quad 1 \le r \le m-1,\ 1 \le s \le m'-1, \tag{3.4}$$

$$\mathrm{ch}_{r,s}^{m,m'} = \frac{q^{-c/24+\Delta_{r,s}^{m,m'}}}{(q)_\infty} \sum_{k=-\infty}^{\infty} \left(q^{kmm'+rm'-sm} - q^{(km+r)(km'+s)} \right), \tag{3.5}$$

where the (infinite) q-factorials are defined by

$$(q)_n = \prod_{k=1}^{n} (1-q^k), \quad (q)_\infty = \prod_{k=1}^{\infty} (1-q^k). \tag{3.6}$$

Here, $q = \mathrm{e}^{\mathrm{i}\pi\tau}$ is the modular nome, and τ is the modular parameter, determined by geometry.
Higher-level minimal models $\mathcal{M}(M,\, M', n')$ with $n' > 1$ are constructed as GKO cosets [68, 69]:

$$\mathcal{M}(M, M', n') \equiv \mathrm{COSET}\left(\frac{n'M}{M'-M} - 2, n' \right), \tag{3.7}$$

$$\gcd\left(\frac{M'-M}{n'},\, M' \right) = 1, \quad 2 \le M < M', \quad n', M, M' \in \mathbb{N}$$

where n' is the integer fusion level and $\frac{n'M}{M'-M} - 2$ is the fractional fusion level. The GKO cosets are Wess-Zumino-Witten (WZW) models [75–78], built on the following affine Lie algebra

$$\mathrm{COSET}(k,\, n') : \ \frac{(A_1^{(1)})_k \oplus (A_1^{(1)})_{n'}}{(A_1^{(1)})_{k+n'}}, \quad k = \frac{\hat{p}}{\hat{p}'} - 2, \quad \gcd(\hat{p},\, \hat{p}') = 1, \quad n',\, \hat{p},\, \hat{p}' \in \mathbb{N} \tag{3.8}$$

where the level of the affine $su(2)$ current algebra $A_1^{(1)}$ is given by the subscripts k, n' and $k+n'$. A brief overview on the coset construction is given in appendix B.1.

The central charge of the $(A_1^{(1)})_k$ current algebra is given by

$$c_k = \frac{3k}{k+2}. \tag{3.9}$$

The central charge of the COSET(k, n') model follows from the coset construction. It is given in terms of the $(A_1^{(1)})_k$ central charge

$$c = c_k + c_{n'} - c_{k+n'} = \frac{3kn'(k+n'+4)}{(k+2)(n'+2)(k+n'+2)} \quad . \tag{3.10}$$

Following eqs. (3.7) and (3.10), the central charge of the fused higher level minimal models $\mathcal{M}(M, M', n')$ is expressed by

$$c^{M,M',n'} = \frac{3n'}{n'+2}\left(1 - \frac{2(n'+2)(M'-M)^2}{n'^2 MM'}\right). \tag{3.11}$$

The $n' = 1$ minimal models are given by $M = m$, $M' = m'$. The $n' = 2$ minimal models coincide with superconformal minimal models.
The characters of the higher fusion level coset models are presented in appendix B.2.

3.3 RSOS models

In this section we introduce Restricted Solid-on-Solid (RSOS) lattice models [50,51]. We define the face weights of the model, satisfying the Yang-Baxter, the unitarity and the crossing equations. We define the $n \times n$ fused RSOS models, and consider the $n = 2$, 3 cases in more details.
The RSOS(m, m') models are statistical physical models, defined on a square lattice, where the degrees of freedom are height variables taking positive integer values $a = 1, 2, \ldots, m'-1$ on the vertices of the lattice. Furthermore, the neighboring sites have height difference ± 1. Hence, the connectivity graph of the heights is the Dynkin diagram of the simple Lie algebra $A_{m'-1}$. The model is integrable, satisfying the Yang-Baxter equation with the following Boltzmann weights, associated to the plaquettes of the model in Regime III

$$W\left(\begin{matrix} a\pm 1 & a \\ a & a\mp 1 \end{matrix}\middle| u\right) = \quad = s(\lambda - u) \tag{3.12a}$$

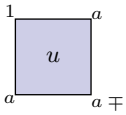

$$W\left(\begin{matrix} a & a\pm 1 \\ a\mp 1 & a \end{matrix}\middle| u\right) = \quad = \frac{g_{a\pm 1}}{g_{a\mp 1}} \frac{s\left((a\pm 1)\lambda\right) s(u)}{s(a\lambda)} \tag{3.12b}$$

$$W\left(\begin{matrix} a & a\pm 1 \\ a\pm 1 & a \end{matrix}\middle| u\right) = \quad = \frac{s(a\lambda \pm u)}{s(a\lambda)} \tag{3.12c}$$

where $s(u)$ is a quotient of standard elliptic functions

$$s(u) = \frac{\vartheta_1(u,t)}{\vartheta_1(\lambda,t)} \tag{3.13}$$

$$\vartheta_1(u,t) = 2t^{1/4} \sin u \prod_{n=1}^{\infty} (1-2t^{2n}\cos(2u)+t^{4n})(1-t^{2n}), \tag{3.14}$$

$$0 < u < \lambda,\ 0 < t < 1,$$

where u is the spectral parameter, and g_a is an arbitrary gauge function. The restriction

$$0 < u < \lambda, \quad 0 < t < 1 \tag{3.15}$$

indicates that we consider the model in Regime III. We use $g_a = 1$, unless otherwise stated. The elliptic nome t is a temperature-like global variable, where t^2 measures the departure from criticality through a $\varphi_{1,3}$ integrable perturbation [79–81].The crossing parameter λ is a global parameter

$$\lambda = \frac{(m'-m)\pi}{m'}, \quad 2 \le m < m', \quad m, m' \text{ coprime.} \tag{3.16}$$

The weights satisfy the Yang-Baxter equation (in additive notion)

$$\sum_g W\left(\begin{matrix} f & g \\ a & b \end{matrix}\middle| u\right) W\left(\begin{matrix} e & d \\ f & g \end{matrix}\middle| u+v\right) W\left(\begin{matrix} d & c \\ g & b \end{matrix}\middle| v\right) =$$

$$= \sum_g W\left(\begin{matrix} e & g \\ f & a \end{matrix}\middle| v\right) W\left(\begin{matrix} g & c \\ a & b \end{matrix}\middle| u+v\right) W\left(\begin{matrix} e & d \\ g & c \end{matrix}\middle| u\right) \tag{3.17}$$

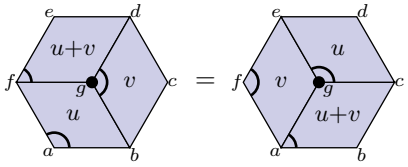

Here we use a different notation from the notation of rapidities for loop models: There the direction of the two arrows sets the direction of the R-matrix, here the arch sets it. We do not always denote the arch. In the rest of the chapter, we refer to R-matrix elements as face weights. The weights also satisfy the regularity (or initial condition) and the inversion relation (or unitarity)

$$W\left(\begin{matrix} d & c \\ a & b \end{matrix}\middle| 0\right) = \delta_{a,c} \tag{3.18}$$

$$\sum_g W\left(\begin{matrix} d & g \\ a & b \end{matrix}\middle| u\right) W\left(\begin{matrix} d & c \\ g & b \end{matrix}\middle| -u\right) = \delta_{a,c} \frac{s(\lambda-u)s(\lambda+u)}{s^2(\lambda)} \tag{3.19}$$

Further properties are the symmetry under reflection about the main diagonal and height reversal symmetry

$$W\left(\begin{matrix} d & c \\ a & b \end{matrix}\middle| u\right) = W\left(\begin{matrix} b & c \\ a & d \end{matrix}\middle| u\right) \tag{3.20}$$

$$W\left(\begin{matrix} d & c \\ a & b \end{matrix}\middle| u\right) = W\left(\begin{matrix} m'-d & m'-c \\ m'-a & m'-b \end{matrix}\middle| u\right). \tag{3.21}$$

3.3.1 Fused RSOS models and fused weights

Fused RSOS models were considered in [67]. The construction is based on the Yang-Baxter equation, and the following fusion property. Consider two plaquettes, forming a 2×1 block, with spectral parameters u and $u + \lambda$, respectively. Define the 2×1 fused weights as

$$W_{2,1}\left(\begin{matrix} d & c \\ a & b \end{matrix}\middle| u\right) = \sum_{a'} W\left(\begin{matrix} d & c' \\ a & a' \end{matrix}\middle| u\right) W\left(\begin{matrix} c' & c \\ a' & b \end{matrix}\middle| u+\lambda\right). \tag{3.22}$$

$W_{2,1}\left(\begin{matrix} d & c \\ a & b \end{matrix}\middle| u\right) =$

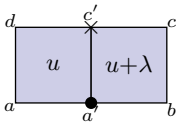

This is a proper definition of the 2×1 fused weight, as in the $g_a = 1$ gauge, after summing up to a', this weight is independent of the choice of c', provided that $|c' - c| = |c' - d| = 1$. In the figure, the dot indicates summation over all admissible heights, and the cross indicates independence of the allowed height. Equation (3.22) is proved by the Yang-Baxter equation, and other properties of the weights.

The fusion generalizes to the $n \times n$ case, and gives a systematic method to define the $n \times n$ fused Boltzmann weights as

$$W_{n,n}\left(\begin{matrix} d & c \\ a & b \end{matrix}\middle| u\right) = \frac{1}{\eta^{n,n}(u)}$$

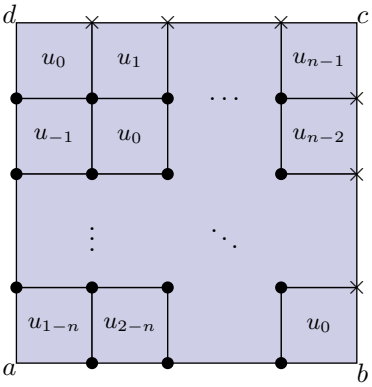

(3.23)

Here again, we sum over the vertices marked with a dot, and the weight is independent of the choice of heights on vertices marked with a cross, in the $g_a = 1$ gauge. The notation of u_k denotes the shifted u: $u_k = u + k\lambda$. The normalization factor is

$$\eta^{n,n}(u) = \prod_{k=2}^{n} s(k\lambda) \prod_{k=1}^{n-1} s^{n-k}(u - k\lambda) s^{n-k}(u + (k-1)\lambda). \tag{3.24}$$

The adjacency restrictions on corner heights of the $n \times n$ heights are

$$\sigma - \sigma' = -n, -n+2 \ldots, n, \tag{3.25}$$

$$\sigma + \sigma' = n+2, n+4, \ldots, 2m' - n - 2 \tag{3.26}$$

where σ, σ' are any two corner heights. The latter restriction follows since $W_{n,n}\left(\begin{matrix} a & a \\ a & a \end{matrix}\middle| u\right)$ has a pole for $a = 1$ and $m' - 1$ which we need to exclude. Based on the properties of the RSOS weights, the $n \times n$ fused weights also satisfy the regularity, the inversion relation and the Yang-Baxter equation (in additive convention)

$$W_{n,n}\left(\begin{matrix} d & c \\ a & b \end{matrix}\middle| 0\right) = \delta_{a,c} \tag{3.27a}$$

$$\sum_g W_{n,n}\left(\begin{matrix} d & g \\ a & b \end{matrix}\middle| u\right) W_{n,n}\left(\begin{matrix} d & c \\ g & b \end{matrix}\middle| -u\right) = \delta_{a,c} \prod_{k=1}^{n} \frac{s(k\lambda - u)s(k\lambda + u)}{s^2(k\lambda)} \tag{3.27b}$$

$$\sum_g W_{n,n}\left(\begin{matrix} f & g \\ a & b \end{matrix}\middle| u\right) W_{n,n}\left(\begin{matrix} e & d \\ f & g \end{matrix}\middle| u+v\right) W_{n,n}\left(\begin{matrix} d & c \\ g & b \end{matrix}\middle| v\right) = \tag{3.27c}$$

$$= \sum_g W_{n,n}\left(\begin{matrix} e & g \\ f & a \end{matrix}\middle| v\right) W_{n,n}\left(\begin{matrix} g & c \\ a & b \end{matrix}\middle| u+v\right) W_{n,n}\left(\begin{matrix} e & d \\ g & c \end{matrix}\middle| u\right)$$

The $n \times n$ fused weights also satisfy the symmetry under reflection about the main diagonal and the height reversal symmetry

$$W_{n,n}\left(\begin{matrix} d & c \\ a & b \end{matrix}\middle| u\right) = W_{n,n}\left(\begin{matrix} b & c \\ a & d \end{matrix}\middle| u\right) \tag{3.28}$$

$$W_{n,n}\left(\begin{matrix} d & c \\ a & b \end{matrix}\middle| u\right) = W_{n,n}\left(\begin{matrix} m'-d & m'-c \\ m'-a & m'-b \end{matrix}\middle| u\right) \tag{3.29}$$

Our main interests are the 2×2 and 3×3 fused cases which we further examine.

2×2 case

The normalized 2×2 RSOS face weights are the following

$$W_{2,2}\left(\begin{matrix} d & c \\ a & b \end{matrix}\middle| u\right) = \frac{1}{\eta^{2,2}(u)}$$

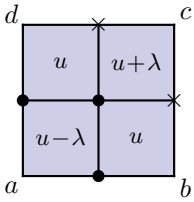

(3.30)

where $\eta^{2,2}(u) = s(2\lambda)s(u)s(u-\lambda)$ is the common normalization factor. Here again, the dot marks summation, the cross marks independence. There are nineteen allowed face configurations, with the following explicit weights

$$W_{2,2}\left(\begin{matrix} a \pm 2 & a \\ a & a \mp 2 \end{matrix}\middle| u\right) = \frac{s(u-2\lambda)s(u-\lambda)}{s(2\lambda)} \tag{3.31a}$$

$$W_{2,2}\left(\begin{matrix} a & a \\ a & a \pm 2 \end{matrix}\middle| u\right) = W_{2,2}\left(\begin{matrix} a \pm 2 & a \\ a & a \end{matrix}\middle| u\right) = -\frac{s(u-\lambda)s((a \pm 1)\lambda \mp u)}{s((a \pm 1)\lambda)} \tag{3.31b}$$

$$W_{2,2}\left(\begin{matrix} a & a \\ a \pm 2 & a \end{matrix}\middle| u\right) = -\frac{s((a \mp 1)\lambda)s(u)s(a\lambda \pm u)}{s(2\lambda)s(a\lambda)s((a \pm 1)\lambda)} \tag{3.31c}$$

$$W_{2,2}\left(\begin{matrix}a & a\pm 2\\ a & a\end{matrix}\middle| u\right) = -\frac{s(2\lambda)s((a\pm 2)\lambda)s(u)s(a\lambda\pm u)}{s((a-1)\lambda)s((a+1)\lambda)} \tag{3.31d}$$

$$W_{2,2}\left(\begin{matrix}a & a\mp 2\\ a\pm 2 & a\end{matrix}\middle| u\right) = \frac{s((a\mp 2)\lambda)s((a\mp 1)\lambda)s(u)s(\lambda+u)}{s(2\lambda)s(a\lambda)s((a\pm 1)\lambda)} \tag{3.31e}$$

$$W_{2,2}\left(\begin{matrix}a & a\pm 2\\ a\pm 2 & a\end{matrix}\middle| u\right) = \frac{s(a\lambda\pm u)s((a\pm 1)\lambda\pm u)}{s(a\lambda)s((a\pm 1)\lambda)} \tag{3.31f}$$

$$W_{2,2}\left(\begin{matrix}a & a\\ a & a\end{matrix}\middle| u\right) = \frac{s(a\lambda\pm u)s((a\pm 1)\lambda\mp u)}{s(a\lambda)s((a\pm 1)\lambda)} + \tag{3.31g}$$

$$+\frac{s((a\pm 1)\lambda)s((a\mp 2)\lambda)s(u)s(u-\lambda)}{s(2\lambda)s(a\lambda)s((a\mp 1)\lambda)}$$

$$W_{2,2}\left(\begin{matrix}a & a\pm 2\\ a & a\pm 2\end{matrix}\middle| u\right) = W_{2,2}\left(\begin{matrix}a\pm 2 & a\pm 2\\ a & a\end{matrix}\middle| u\right) = \frac{s((a\pm 3)\lambda)s(u)s(u-\lambda)}{s(2\lambda)s((a\pm 1)\lambda)} \tag{3.31h}$$

Note that the two versions of the weight $W_{2,2}\left(\begin{matrix}a & a\\ a & a\end{matrix}\middle| u\right)$ with the upper and lower sign are equal. The $\pm$ signs in the other expressions correspond to the upper or lower sign on the left hand side. Here we see explicitly, why adjacent 1, 1 and $m'-1$, $m'-1$ are excluded: for these cases, the denominator is 0 in the aforementioned expressions.
Following from the general statement, the 2×2 fused weights satisfy regularity, the inversion relation and the Yang-Baxter equation (in the additive convention)

$$W_{2,2}\left(\begin{matrix}d & c\\ a & b\end{matrix}\middle| 0\right) = \delta_{a,c}\ , \tag{3.32}$$

$$\sum_g W_{2,2}\left(\begin{matrix}d & g\\ a & b\end{matrix}\middle| u\right)W_{2,2}\left(\begin{matrix}d & c\\ g & b\end{matrix}\middle| -u\right) = \delta_{a,c}\frac{s(2\lambda-u)s(\lambda-u)s(\lambda+u)s(2\lambda+u)}{s^2(\lambda)s^2(2\lambda)}\ , \tag{3.33}$$

$$\sum_g W_{2,2}\left(\begin{matrix}f & g\\ a & b\end{matrix}\middle| u\right)W_{2,2}\left(\begin{matrix}e & d\\ f & g\end{matrix}\middle| u+v\right)W_{2,2}\left(\begin{matrix}d & c\\ g & b\end{matrix}\middle| v\right) =$$

$$= \sum_g W_{2,2}\left(\begin{matrix}e & g\\ f & a\end{matrix}\middle| v\right)W_{2,2}\left(\begin{matrix}g & c\\ a & b\end{matrix}\middle| u+v\right)W_{2,2}\left(\begin{matrix}e & d\\ g & c\end{matrix}\middle| u\right)\ . \tag{3.34}$$

The 2×2 case also possesses the reflection about the main diagonal and the height reversal symmetry

$$W_{2,2}\left(\begin{matrix} d & c \\ a & b \end{matrix}\middle| u\right) = W_{2,2}\left(\begin{matrix} b & c \\ a & d \end{matrix}\middle| u\right) , \tag{3.35}$$

$$W_{2,2}\left(\begin{matrix} d & c \\ a & b \end{matrix}\middle| u\right) = W_{2,2}\left(\begin{matrix} m'-d & m'-c \\ m'-a & m'-b \end{matrix}\middle| u\right) . \tag{3.36}$$

3×3 case

The normalized 3×3 RSOS face weights are the following

$$W_{3,3}\left(\begin{matrix} d & c \\ a & b \end{matrix}\middle| u\right) = \frac{1}{\eta^{3,3}(u)} \tag{3.37}$$

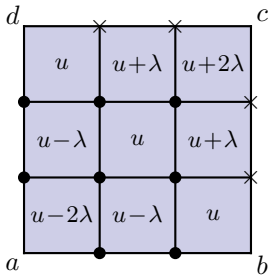

As previously, dots denote summation, crosses independence. The common normalization is

$$\eta^{3,3}(u) = s(2\lambda)s(3\lambda)s(u-2\lambda)s^2(u-\lambda)s^2(u)s(u+\lambda) . \tag{3.38}$$

The explicit 3×3 weights are in appendix B.3. As it follows from the generic case, the 3×3 weights satisfy the usual equations, i.e the regularity, the inversion, the Yang-Baxter equation, and the reflection and height reversal symmetry (eqs. (3.27a) to (3.27c)).

3.3.2 Corner transfer matrix

Following Baxter [82–84], we define corner transfer matrices (CTMs). There are four kinds of corner transfer matrices, as in fig. 3.1.

Each corner transfer matrix, A, B, C and D is defined in a similar fashion, so we describe only A in detail. The corner transfer matrix is an operator which maps a string of admissible heights $\boldsymbol{\sigma} = \{\sigma_0, \ldots, \sigma_N\}$ to an other string of admissible heights $\boldsymbol{\sigma'} = \{\sigma'_0, \ldots, \sigma'_N\}$. A matrix element of the CTM is realized

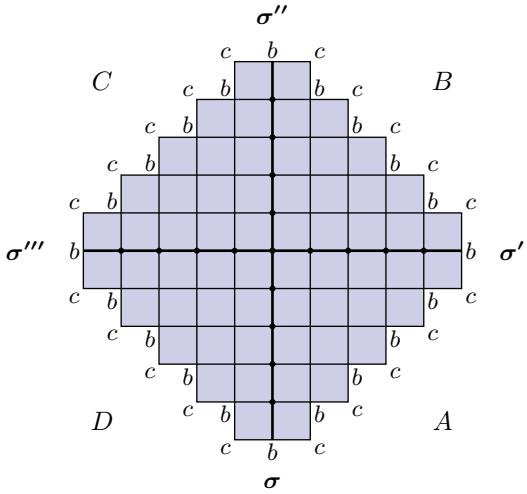

Figure 3.1: The four corner transfer matrices (CTMs). Each quadrant of the plane corresponds to a CTM, A, B, C and D, counterclockwise from the lower right quadrant.

by summing over all internal heights in the quadrant

$$A^{(N)}_{\boldsymbol{\sigma},\boldsymbol{\sigma'}} = \sum \prod W\left(\begin{matrix}\sigma_{i,j+1} & \sigma_{i,j} \\ \sigma_{i+1,j} & \sigma_{i+1,j+1}\end{matrix}\middle| u\right) \quad =$$

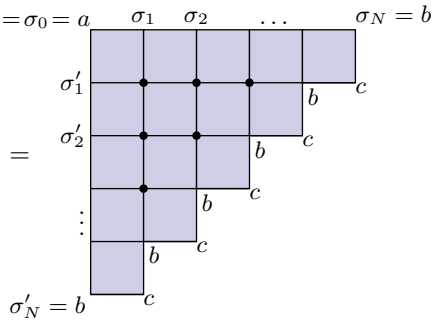

(3.39)

where the product runs over all internal faces, and the sum runs over all allowed configurations with internal heights $\sigma_{i,j}$ and with the boundary conditions ($\sigma_0 = \sigma'_0 = a$, $\sigma_N = \sigma'_N = b$, c). The boundary conditions fix the central height value a and the b, c height values along the outer diagonal. When it is denoted, N

refers to the size of the corner transfer matrix. The previous definition of the CTM applies both for unfused and fused RSOS models. The height strings $\boldsymbol{\sigma}$ and $\boldsymbol{\sigma'}$ satisfy the adjacency restriction according to the fusion level. The other transfer matrices B, C, and D are defined in a similar way. The partition function of the diamond shaped region of the lattice model (fig. 3.1) with fixed boundary conditions (b, c) is given by summing over all internal configurations, hence taking the trace over the product of the CTMs

$$Z^{(N)}_{b,c} = \sum_{\boldsymbol{\sigma},\boldsymbol{\sigma'},\boldsymbol{\sigma''},\boldsymbol{\sigma'''}} A^{(N)}_{\boldsymbol{\sigma},\boldsymbol{\sigma'}} B^{(N)}_{\boldsymbol{\sigma'},\boldsymbol{\sigma''}} C^{(N)}_{\boldsymbol{\sigma''},\boldsymbol{\sigma'''}} D^{(N)}_{\boldsymbol{\sigma'''},\boldsymbol{\sigma}} = \mathrm{Tr}\, A^{(N)} B^{(N)} C^{(N)} D^{(N)} \,. \tag{3.40}$$

The CTMs commute in the $N \to \infty$ limit [82,83]. Hence, it is sufficient to probe the spectrum of only one CTM which will be the lower right one, denoted by A. In the low temperature limit the Boltzmann-weights become diagonal along the counter-diagonal, i.e. $W\left(\begin{smallmatrix} d & c \\ a & b \end{smallmatrix}\middle| u\right)\Big|_{\text{low } T} \sim \delta_{a,c}$. Hence, A become a diagonal matrix, and taking Tr A simplifies to taking the one-dimensional sums of the RSOS model.

3.3.3 RSOS paths, and shaded bands

In this section we introduce RSOS paths, and shaded bands, to understand the low temperature limit of the RSOS models. We introduce these concepts both for the unfused and fused models. The low temperature limit is taken as follows

$$t = e^{-\epsilon} \to 1, \quad u \to 0, \quad \frac{u}{\epsilon} \text{ fixed.} \tag{3.41}$$

In this limit the face weights become diagonal along the counter-diagonal (the SW-NE direction) of the face, and a power of e^{-u}

$$W_{2,2}\left(\begin{smallmatrix} d & c \\ a & b \end{smallmatrix}\middle| u\right)\Big|_{\text{low } T} \sim \frac{g_a g_c}{g_b g_d} w^{H(d,a,b)} \delta_{a,c}, \qquad w \sim \mathrm{e}^{-2\pi u/\epsilon}. \tag{3.42}$$

Here we introduced the function $H(d,a,b)$ which is the local energy function.
In the low temperature limit, the two-dimensional lattice model becomes effectively one-dimensional, as the degrees of freedom freeze in the SW-NE direction. Consequently, the lower right corner transfer matrix A become a diagonal matrix. The diagonal elements are labeled by the string of heights $\boldsymbol{\sigma} = \{\sigma_0, \sigma_1, \ldots, \sigma_N, \sigma_{N+1}\}$, where we included $\sigma_{N+1} = c$.
Define the $n \times n$ (fused) RSOS lattice path $\boldsymbol{\sigma} = \{\sigma_0, \sigma_1, \ldots, \sigma_N, \sigma_{N+1}\}$ as a

sequence of integers, corresponding to the height variable, hence taking values on the relevant Dynkin-diagram: $\sigma_i \in A_{m'-1}$. The adjacency conditions are inherited from the $n \times n$ fused RSOS weights, and hold for the fused paths too

$$\sigma_{j+1} - \sigma_j = -n,\ -n+2, \ldots, n-2,\ n,$$
$$\sigma_{j+1} + \sigma_j = n+2,\ n+4, \ldots, 2m'-n-2.$$

Note that for even fusion level n the second condition means that there are no $\{\ldots, 1, 1, \ldots\}$ or $\{\ldots, m'-1, m'-1, \ldots\}$ segments in a path. Unlike in the unfused case, the connectivity graph of the fused model is not $A_{m'-1}$. Some examples are given in section 3.4.1. We define the boundary conditions of a (fused) path by fixing the first and the two last height variables

$$(\sigma_0, \sigma_N, \sigma_{N+1}) = (a,\ b,\ c), \qquad c - b = -n,\ -n+2, \ldots, n-2,\ n, \tag{3.43}$$

which is equivalent to the boundary condition of the corner transfer matrix. The paths are in bijection with the low temperature lower right CTM configurations. The path in N steps starts at height a and finishes at heights b, c, where steps can only be taken in accordance with the adjacency conditions of the model. For even fusion levels n, all the heights σ_j take values with the same parity, while for odd n's, the parity alternates along the path. An example of a 2×2 fused path is in fig. 3.2.

We introduce the notation of shaded and unshaded bands. The shaded bands play a role in determining the groundstate boundary conditions for the one-dimensional sums. A band is a range of heights, and as in fig. 3.2, certain bands are shaded. Define the sequence

$$\rho(r) = \left\lfloor \frac{rm'}{m} \right\rfloor, \qquad r = 1, 2, \ldots, m-1, \tag{3.44}$$

and define the shaded bands as the bands between heights $\rho(r)$ and $\rho(r) + 1$, following [85]. Define a k-band as k contiguous bands, without restricting whether these bands are shaded, unshaded or both. A shaded (unshaded) k-band is an k-band which only contains shaded (unshaded) 1-bands.
The shaded and unshaded bands interchange under the duality $m \leftrightarrow m' - m$, and as they only depend on $(m,\ m')$, they are the same for all RSOS$(m,\ m')_{n\times n}$ model, regardless the fusion level n.
In [73], it was shown that shaded k-bands only exist for $0 < \lambda < \frac{\pi}{k}$, and there are no shaded k-bands for $\frac{\pi}{k} < \lambda < \pi$. The number of shaded k-bands is given by

$$\#\text{ of shaded } k\text{-bands} = M - 1 = \begin{cases} km - (k-1)m' - 1, & 0 < \lambda < \frac{\pi}{k} \\ 0, & \frac{\pi}{k} < \lambda < \pi \end{cases} \tag{3.45}$$

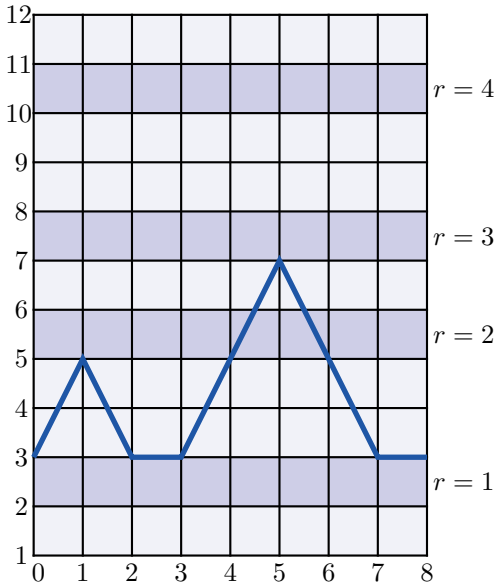

Figure 3.2: A typical path $\sigma = \{3,5,3,3,5,7,5,3,3\}$ in model $(m,m') = (5,13)$ with boundary conditions $(s,\rho,\rho') = (3,3,3)$ and $N = 7$ steps from $s = 3$ to $\rho = 3$. The shaded 1-bands are labelled by $r = 1,2,3,\ldots$ from the bottom.

This expression depends on m, m' through $\lambda = \frac{(m-m')\pi}{m'}$. In the unitary cases, with $m = m' - 1$ all of the 1-bands are shaded. For non-unitary cases, with $2 \leq m \leq m' - 1$, there are both shaded and unshaded bands. Despite the ease with which the position of shaded k-bands can be computed diagrammatically for any given case and k, there is no known general expression for it.
For the interval $\frac{\pi}{2} < \lambda < \pi$ which is our primary interest here, there are only shaded 1-bands, and no shaded k-bands for $k > 1$. The shaded bands are separated by contiguous unshaded k-bands with $k \geq 1$.

3.3.4 Low temperature limit and local energy functions

In [82, 83], Baxter argued that the corner transfer matrices commute in the $N \to \infty$ massive, low temperature limit.
The low temperature limit is realized by the limit

$$t = \mathrm{e}^{-\epsilon} \to 1, \quad u \to 0, \quad \frac{u}{\epsilon} \text{ is fixed.} \tag{3.46}$$

In this limit, the Boltzmann weights become diagonal along the counter-diagonal

$$W_{2,2}\left(\begin{matrix} d & c \\ a & b \end{matrix}\middle| u\right) \sim \frac{g_a g_c}{g_b g_d} w^{H(d,a,b)} \delta_{a,c}, \tag{3.47}$$
$$w = \mathrm{e}^{-2\pi u/\epsilon},\ t = \mathrm{e}^{-\epsilon},\ \epsilon \to 0,\ u \to 0,\ \frac{u}{\epsilon} \text{ fixed.}$$

This defines the local energy functions $H(d,a,b)$ which inherits reflection and height reversal symmetry from the Boltzmann weights

$$H(d,a,b) = H(b,a,d) = H(m'-d, m'-a, m'-b) \tag{3.48}$$

There is a gauge freedom from the arbitrary gauge functions g_a which allows us to put the local energy functions in a convenient form.

1×1 local energy function

The 1×1 RSOS local energy functions were computed by Forrester and Baxter [51], in the $g_a = 1$ gauge

$$H^{FB}(a, a \mp 1, a) = \pm \left\lfloor \frac{a\lambda}{\pi} \right\rfloor \tag{3.49}$$

$$H^{FB}(a \pm 1, a, a \mp 1) = \frac{1}{2} \tag{3.50}$$

By changing the gauge, a more suitable set of local energy functions is constructed [73]

$$H(a+1, a, a+1) = \frac{1}{2}(h_{a+1} - h_a) \tag{3.51}$$

$$H(a-1, a, a-1) = \frac{1}{2}(h_a - h_{a-1}) \tag{3.52}$$

$$H(a \pm 1, a, a \mp 1) = \frac{1}{2} - \frac{1}{4}(h_{a+1} - h_{a-1}) \tag{3.53}$$

$$\tag{3.54}$$

where we introduce the auxiliary function

$$h_a = \left\lfloor \frac{a(m'-m)}{m'} \right\rfloor = \left\lfloor \frac{a\lambda}{\pi} \right\rfloor \tag{3.55}$$

This function counts the number of unshaded 1-bands below the height a. With

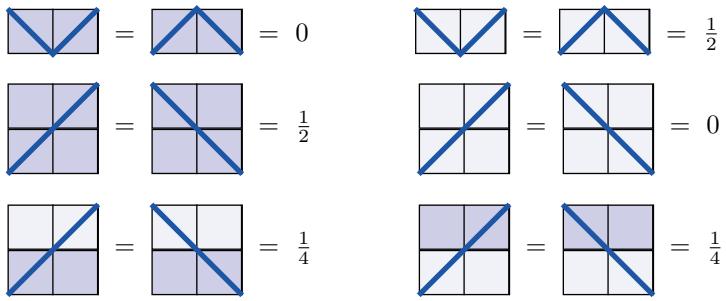

Figure 3.3: The gauged local energies of the 1×1 RSOS models in the interval $0 < \lambda < \pi$. In this gauge, the local energies take the values $0, \frac{1}{4}, \frac{1}{2}$.

this choice of gauge, the groundstate paths indeed have minimal, 0 energy, and all the local energy functions are fractional values: $0, \frac{1}{4}, \frac{1}{2}$. The local energy functions for RSOS$(m, m')_{1\times 1}$ are depicted in fig. 3.3.

There is a duality, described by

$$\begin{aligned} m &\leftrightarrow m' - m, \\ \lambda &\leftrightarrow \pi - \lambda, \\ \text{shaded 1-bands} &\leftrightarrow \text{unshaded 1-bands}, \\ h_a &\leftrightarrow a - 1 - h_a \end{aligned} \tag{3.56}$$

which leads to the identity

$$H^{m,m',1}(a,b,c) = \tfrac{1}{2} H^{m'-m,m',1}(a,b,c) \ . \tag{3.57}$$

2×2 local energy function

The 2×2 local energy functions are computed after a conjugate modulus transformation is performed on the Boltzmann weights. The conjugate modulus transformation was originally used by Forrester and Baxter to make the computation feasible [51]. The conjugate modulus transformation involves a change from elliptic nome $t = \mathrm{e}^{-\epsilon}$ to conjugate nome $p = \mathrm{e}^{-\pi^2/\epsilon}$ and the replacement of λ and u with x and w, respectively

$$x = \mathrm{e}^{-2\pi\lambda/\epsilon} = p^{\lambda/\pi} \ , \tag{3.58}$$

$$w = \mathrm{e}^{-2\pi u/\epsilon} \ . \tag{3.59}$$

The conjugate modulus transformation is the following

$$\theta_1(u, t = \mathrm{e}^{-\epsilon}) = \mathrm{i}\mathrm{e}^{-\epsilon/4}\mathrm{e}^{-\mathrm{i}u}E(\mathrm{e}^{2\mathrm{i}u}, \mathrm{e}^{-2\epsilon}) = \sqrt{\frac{\pi}{\epsilon}}\mathrm{e}^{-(u-\pi/2)^2/\epsilon}E(\mathrm{e}^{-2\pi u/\epsilon}, \mathrm{e}^{-2\pi^2/\epsilon}) \ . \tag{3.60}$$

where we introduce the function

$$E(w) = E(w, p) = \sum_{k=-\infty}^{\infty} (-1)^n p^{n(n-1)/2} w^n = \prod_{n=1}^{\infty} (1-p^{n-1}w)(1-p^n w^{-1})(1-p^n) \ . \tag{3.61}$$

The diagonal fused weights are expressed as such

$$W_{2,2}\begin{pmatrix} a \pm 2 & a \\ a & a \mp 2 \end{pmatrix} = \frac{g_a^2}{g_{a-2}g_{a+2}} \frac{wE(x^2w^{-1})E(w^{-1}x)}{E(x^2)E(x)} \ , \tag{3.62a}$$

$$W_{2,2}\begin{pmatrix} a & a \\ a & a \pm 2 \end{pmatrix} = W_{2,2}\begin{pmatrix} a \pm 2 & a \\ a & a \end{pmatrix} = \frac{g_a}{g_{a\pm 2}} \frac{E(xw^{-1})E(x^{a\pm 1}w^{\mp 1})}{E(x)E(x^{a\pm 1})} \ , \tag{3.62b}$$

$$W_{2,2}\begin{pmatrix} a & a \pm 2 \\ a \pm 2 & a \end{pmatrix} = \frac{g_{a\pm 2}^2}{g_a^2} \frac{E(x^a w^{\pm 1})E(x^{a\pm 1}w^{\pm 1})}{E(x^a)E(x^{a\pm 1})} \ , \tag{3.62c}$$

$$W_{2,2}\begin{pmatrix} a & a \\ a & a \end{pmatrix} = \frac{xwE(w^{-1})E(xw^{-1})E(x^{a-1})E(x^{a+2})}{E(x)E(x^2)E(x^a)E(x^{a+1})} + \frac{E(x^{a-1})E(x^a w^{-1})}{E(x^{a-1})E(x^a)} \ . \tag{3.62d}$$

where the gauge factors g_a are arbitrary. The low temperature limit is taken as $x \to 0$, or equivalently $p \to 0$ with w kept constant. The function E satisfies the following relations which are used for taking the limit

$$E(w, p) = E(pw^{-1}, p) = -wE(w^{-1}, p) \ , \tag{3.63a}$$

$$E(p^n w, p) = p^{-n(n-1)/2}(-w)^{-n}E(w, p) \ , \tag{3.63b}$$

$$\lim_{p\to 0} E(p^a w, p^b) = \begin{cases} 1, & 0 < a < b \\ 1 - w, & a = 0 \end{cases} \tag{3.63c}$$

$$\lim_{x\to 0} \frac{E(x^a w^{-1})}{x^a} = w^{\lfloor a\lambda/\pi \rfloor} \ . \tag{3.63d}$$

where n is an integer. These identities are used to derive the limit. By choosing the gauge $g_a = w^{a(a\lambda-\pi)/(4\pi)}$, after removing an overall scale factor $\mathrm{e}^{-2u(\lambda-u)/\epsilon}$ the local energy functions are

$$0 < \lambda < \tfrac{\pi}{2} : \quad H(a \pm 2, a, a \mp 2) = 1 \tag{3.64a}$$

$$H(a\pm 2,a,a) = H(a,a,a\pm 2) = \frac{1}{2} \pm h_{a\pm 1} \tag{3.64b}$$

$$H(a,a\pm 2,a) = \mp\big(h_a + h_{a\pm 1}\big) \tag{3.64c}$$

$$H(a,a,a) = \begin{cases} 0, & h_{a-1} = h_a = h_{a+1} \\ 1, & \text{otherwise} \end{cases} \tag{3.64d}$$

$$\tfrac{\pi}{2} < \lambda < \pi: \quad H(a\pm 2,a,a\mp 2) = 2 \tag{3.65a}$$

$$H(a\pm 2,a,a) = H(a,a,a\pm 2) = \frac{1}{2} \pm h_{a\pm 1} \tag{3.65b}$$

$$H(a,a\pm 2,a) = \mp(h_a + h_{a\pm 1}) \tag{3.65c}$$

$$H(a,a,a) = \begin{cases} 0, & h_{a-1} = h_a \text{ or } h_a = h_{a+1} \\ 1, & \text{otherwise} \end{cases} \tag{3.65d}$$

Note that the local energy functions take different values for the intervals $0 < \lambda < \frac{\pi}{2}$ and $\frac{\pi}{2} < \lambda < \pi$. These local energies can be put in a more desirable form, with only non-negative, half-integer values by a gauge transformation. In present form, they also take negative and positive values. We introduce a new gauge $g'_a = w^{G_a}$ which defines the new local energies

$$H'(a,b,c) = H(a,b,c) + 2G_b - G_a - G_c\ . \tag{3.66}$$

The requirement $H'(a,b,c) \geq 0$ is satisfied by the following choice for G_a

$$G_a = \begin{cases} h_1 + h_3 + \ldots h_{a-1}, & a \text{ even} \\ h_2 + h_4 + \ldots h_{a-1}, & a \text{ odd} \end{cases} \qquad G_{a+1} - G_{a-1} = h_a \tag{3.67}$$

This gauge-transformation can be defined through defining $G(a,b) = G_b - G_a$ and applying

$$H'(a,b,c) = H(a,b,c) + G(a,b) - G(b,c), \quad G(a,b) = \frac{1}{2}(b-a)h_{(a+b)/2}\ . \tag{3.68}$$

These local energies are depicted in figs. 3.4 and 3.5. They take non-negative half-integer values, namely $0, \frac{1}{2}, 1$. They take the following values for the two intervals (leaving the prime)

$$0 < \lambda < \tfrac{\pi}{2}: \quad H(a\pm 2,a,a\mp 2) = 1 - (h_{a+1} - h_{a-1}) \tag{3.69a}$$

$$H(a\pm 2,a,a) = H(a,a,a\pm 2) = \frac{1}{2} \tag{3.69b}$$

$$H(a,a\pm 2,a) = \pm\big(h_{a\pm 1} - h_a\big) \tag{3.69c}$$

$$H(a,a,a) = \begin{cases} 0, & h_{a-1} = h_a = h_{a+1} \\ 1, & \text{otherwise} \end{cases} \tag{3.69d}$$

$\frac{\pi}{2} < \lambda < \pi$:

$$H(a \pm 2, a, a \mp 2) = 2 - (h_{a+1} - h_{a-1}) \tag{3.70a}$$

$$H(a \pm 2, a, a) = H(a, a, a \pm 2) = \frac{1}{2} \tag{3.70b}$$

$$H(a, a \pm 2, a) = \pm(h_{a\pm 1} - h_a) \tag{3.70c}$$

$$H(a,a,a) = \begin{cases} 0, & h_{a-1} = h_a \text{ or } h_a = h_{a+1} \\ 1, & \text{otherwise} \end{cases} \tag{3.70d}$$

The shaded band structure, hence the h_a functions differ for the two intervals, $0 < \lambda < \frac{\pi}{2}$ and $\frac{\pi}{2} < \lambda < \pi$. Hence, the h_a dependent choice of G_a leads to the two sets of equations (3.69) and (3.70). The $H(a,b,c)$ functions depend on differences of the h_a function which is in fact a dependence on the shaded band structure, as

$$\delta_a = h_{a+1} - h_a = \begin{cases} 0, & \text{the 1-band } (a, a+1) \text{ is shaded} \\ 1, & \text{the 1-band } (a, a+1) \text{ is unshaded} \end{cases} \tag{3.71}$$

This means the local energies can be associated to height independent local configurations, as in figs. 3.4 and 3.5.The duality relation, described for the 1×1 case (eq. 3.56) interchanges the two intervals, $0 < \lambda < \frac{\pi}{2}$ and $\frac{\pi}{2} < \lambda < \pi$. The shaded and unshaded bands are also interchanged, hence $\delta_a \leftrightarrow 1 - \delta_a$. The duality leads to the following equation for the local energy functions

$$H^{m,m',2}(a,b,c) = 1 - H^{m'-m,m',2}(a,b,c) \ . \tag{3.72}$$

3×3 local energy function

The 3×3 local energy functions are computed for the interval $0 < \lambda < \frac{\pi}{3}$ in [73]. By the duality eq. (3.56), the local energies of the interval $\frac{2\pi}{3} < \lambda < \pi$ follow. The local energies in the intermediate interval $\frac{\pi}{3} < \lambda < \frac{2\pi}{3}$ has not yet been found.

The computation for the interval $0 < \lambda < \frac{\pi}{3}$ is the same as for the 2×2 case. We use initially the $g_a = w^{a(a\lambda-\pi)/(4\pi)}$ gauge, use the conjugate modulus

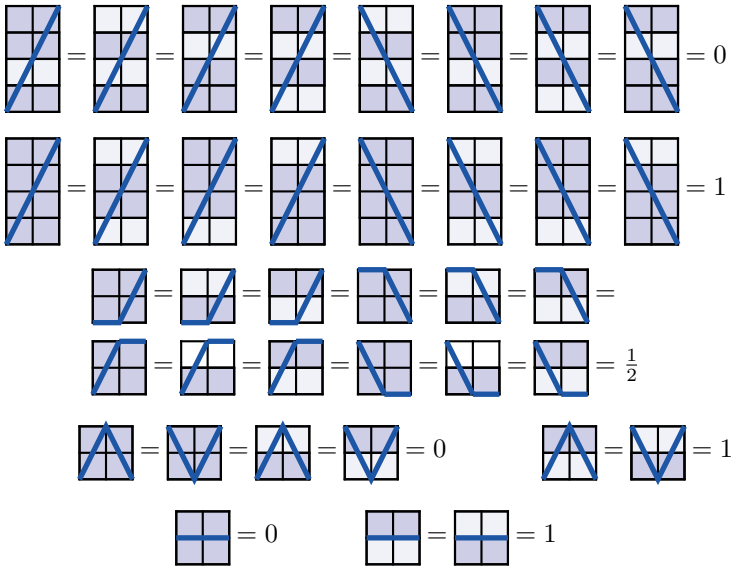

Figure 3.4: Local energies for 2×2 fused RSOS models in the interval $0 < \lambda < \frac{\pi}{2}$.

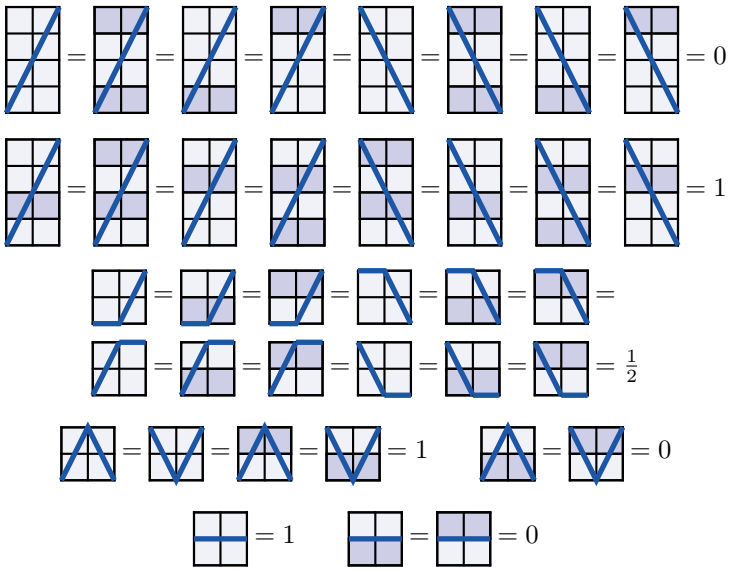

Figure 3.5: Local energies for 2×2 fused RSOS models in the interval $\frac{\pi}{2} < \lambda < \pi$.

transformation, and normalize by a factor $\mathrm{e}^{3u(\lambda-u)/\epsilon}$. In the low temperature limit $x \to 0$, initially the local energies take the following values

$$H(a \pm 3, a, a \pm 3) = \pm(h_{a\pm1} + h_{a\pm2} + h_{a\pm3}) \tag{3.73a}$$
$$H(a \pm 3, a, a \pm 1) = H(a \pm 1, a, a \pm 3) = \tfrac{1}{2} \pm (h_{a\pm1} + h_{a\pm2}) \tag{3.73b}$$
$$H(a \pm 3, a, a \mp 1) = H(a \mp 1, a, a \pm 3) = 1 \pm h_{a\pm1} \tag{3.73c}$$
$$H(a \pm 3, a, a \mp 3) = \tfrac{3}{2} \tag{3.73d}$$
$$H(a \pm 1, a, a \pm 1) = \begin{cases} 1 \pm h_{a\pm1}, & h_{a+1} = h_{a+1} = h_{a-1} + 1 = h_{a-2} + 1 \\ \pm h_{a\pm2}, & \text{otherwise} \end{cases} \tag{3.73e}$$
$$H(a \pm 1, a, a \mp 1) = \tfrac{1}{2} + h_{a+1} - h_{a-1} \tag{3.73f}$$

To introduce non-negative, fractional weights, we perform a similar transformation, as before, to introduce $H'(a, b, c)$

$$H'(a, b, c) = H(a, b, c) + 2G_b - G_a - G_c \,, \tag{3.74}$$

where we use the gauge function

$$G_a = \tfrac{1}{4} \sum_{k=1}^{a-1} h_{a+1} + h_a, \qquad G_{a+1} - G_a = \tfrac{1}{4}(h_{a+1} + h_a). \tag{3.75}$$

The change of gauge leads to the following local energies (again, we omit the prime)

$$H(a \pm 3, a, a \pm 3) = \pm\tfrac{1}{2}(h_{a\pm3} - h_a) \tag{3.76a}$$
$$H(a \pm 3, a, a \pm 1) = H(a \pm 1, a, a \pm 3) = \tag{3.76b}$$
$$= \tfrac{1}{2} \pm \tfrac{1}{4}(-2h_a + h_{a\pm1} + 2h_{a\pm2} - h_{a\pm3})$$
$$H(a \pm 3, a, a \mp 1) = H(a \mp 1, a, a \pm 3) = \tag{3.76c}$$
$$= 1 \pm \tfrac{1}{4}(h_{a\mp1} + 2h_{a\pm1} - 2h_{a\pm2} - h_{a\pm3})$$
$$H(a \pm 3, a, a \mp 3) = \tfrac{3}{2} + \tfrac{1}{4}(h_{a-3} + 2h_{a-2} + 2h_{a-1} - \tag{3.76d}$$
$$- 2h_{a+1} - 2h_{a+2} - h_{a+3})$$
$$H(a \pm 1, a, a \pm 1) = \begin{cases} \pm(h_{a\pm2} - h_{a\pm1}), & h_{a+1} = h_a = h_{a-1} \\ 1 \pm \tfrac{1}{2}(h_{a\pm1} - h_a), & h_{a+1} = h_{a-1} + 1 \end{cases} \tag{3.76e}$$
$$H(a \pm 1, a, a \mp 1) = \tfrac{1}{2} + \tfrac{3}{4}(h_{a+1} - h_{a-1}) \tag{3.76f}$$

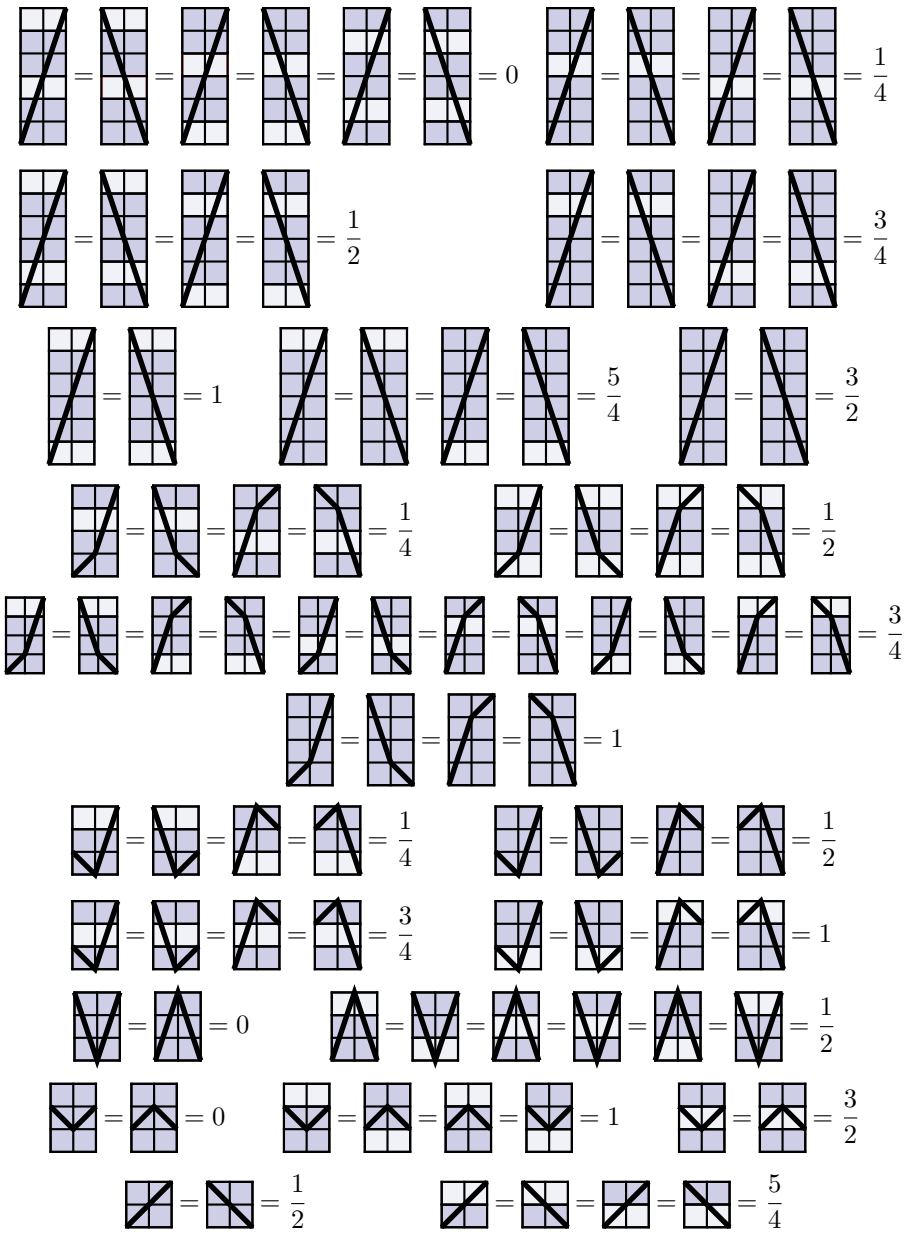

Figure 3.6: The gauged local energies of the $n = 3$ RSOS models in the interval $0 < \lambda < \frac{\pi}{3}$. In this gauge, the local energies take the values $0, \frac{1}{4}, \frac{1}{2}, \frac{3}{4}, 1, \frac{5}{4}, \frac{3}{2}$.

The local energy functions, expressed in the last gauge, are listed in fig. 3.6.

In the dual interval, $\frac{2\pi}{3} < \lambda < \pi$ the local energy functions follow from the duality

$$H^{m,m',3}(a,b,c) = \frac{3}{2} - H^{m'-m,m',3}(a,b,c) \; . \tag{3.77}$$

In general, the duality is conjectured [2] to be

$$H^{m,m',n}(a,b,c) = \frac{n}{2} - H^{m'-m,m',n}(a,b,c) \; . \tag{3.78}$$

3.3.5 One-dimensional sums and energy statistics

Utilizing Baxter's corner transfer matrix (CTM) method [82–84] we define the energy statistics of an RSOS path

$$E(\sigma) = \sum_{j=1}^{N} jH(\sigma_{j-1}, \sigma_j, \sigma_{j+1}) \; . \tag{3.79}$$

The energy statistics is the statistical weight of the corresponding CTM configuration in the lower-right (SE) quadrant in the low temperature limit. As in the low temperature limit, the configuration is diagonal in the SW-NE direction, the configuration of the CTM is described by a path. The boundary conditions (a, b, c) of the path correspond to the boundary conditions of the CTM, i.e. to the value of the central height, and the boundary values of the CTM, respectively. The summation runs from the center to the edge of the CTM. Hence the factor j in the summands is due to the increasing number of faces.

With the help of the energy statistics, we define the one-dimensional sum, by summing over every path with boundary conditions (a, b, c)

$$X^{(N)}_{a,b,c}(q) = \sum_{\sigma} q^{E(\sigma)} = \sum_{\sigma} q^{\sum_{j=1}^{N} jH(\sigma_{j-1},\sigma_j,\sigma_{j+1})} \; , \tag{3.80}$$
$$\sigma_0 = a,\, \sigma_N = b,\, \sigma_{N+1} = c \; .$$

The one-dimensional sums satisfy the recursion relation

$$X^{(N)}_{a,b,c}(q) = \sum_{d \sim b} q^{NH(d,b,c)} X^{(N-1)}_{a,d,c}(q), \tag{3.81}$$

where $d \sim b$ means that we sum over all values of d which can form an allowed path with b. The recursion relations satisfy the following boundary and initial conditions

$$X^{(N)}_{a,0,c}(q) = X^{(N)}_{a,m',c}(q) = 0, \qquad X^{(0)}_{a,b,c}(q) = \delta_{a,b}. \tag{3.82}$$

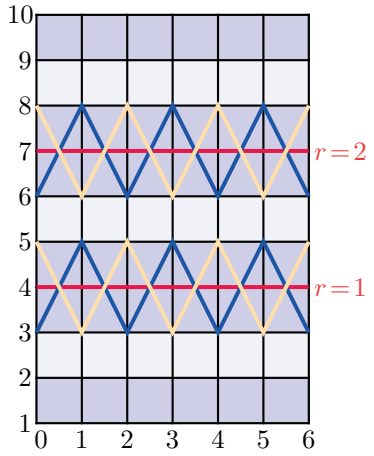

(a) Flat and alternating groundstates for $0 < \lambda < \pi/2$.

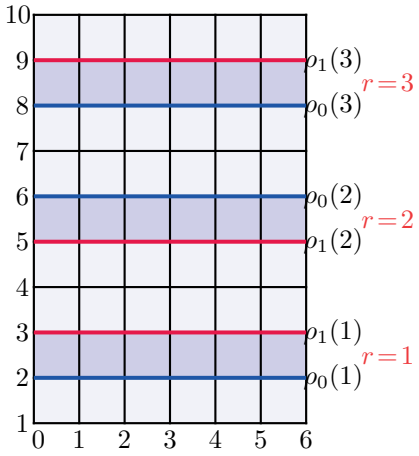

(b) Flat groundstates for $\pi/2 < \lambda < \pi$.

Figure 3.7: A comparison of groundstate RSOS paths for dual RSOS$(m, m')_{2\times 2}$ models with (a) $(m, m') = (7, 11)$ and (b) $(m, m') = (4, 11)$
(a) For $(m, m') = (7, 11)$, the shaded 1-bands occur at heights $\lfloor \frac{11r}{7} \rfloor = 1, 3, 4, 6, 7, 9$ for $r = 1, 2, \ldots, 6$. The 6 groundstate (shaded) 2-bands occur centered at heights $a = 4, 7$. The groundstates are either flat of the form $\{a, a, \ldots, a\}$ or alternating of the form $\{a \pm 1, a \mp 1, a \pm 1, a \mp 1, \ldots\}$.
(b) For $(m, m') = (4, 11)$, there are no shaded 2-bands. The groundstate (shaded) 1-bands occur at heights $\lfloor \frac{11r}{4} \rfloor = 2, 5, 8$ for $r = 1, 2, 3$. The 6 groundstates are flat of the form $\{a, a, \ldots, a\}$ with a belonging to the even or odd sequences $\rho_0(r) = 2, 6, 8$ or $\rho_1(r) = 3, 5, 9$.

The energy statistics and the one-dimensional sums are defined for arbitrary fusion level n.

Groundstates and finitized characters

In this section, based on the shaded band structure, local energy functions and the one-dimensional sums, we define groundstate boundary conditions and groundstate paths. As local energies are known explicitly only for $n = 1, 2$ and for $n = 3$ in the interval $0 < \frac{\lambda}{\pi} < \frac{1}{3}$, we restrict our statements to these cases. As a conjecture, we extend our statements to generic n in the interval $0 < \frac{\lambda}{\pi} < \frac{1}{n}$. Loosely speaking, groundstate boundary conditions are boundary conditions where the lowest energy path can be extended in length without increment in its

energy statistics.
We define a boundary condition $(a,\, b,\, c)$ to be groundstate boundary for RSOS fusion level n and $0 < \frac{\lambda}{\pi} < \frac{1}{n}$, if b and c are in the same shaded n-band, and they are symmetrically placed about its center. The further necessary condition for $(a,\, b,\, c)$ that the fused paths can be actually formed (e.g. for fusion level $n = 2$, $a,\, b,\, c$ have to share the same parity).
If n is even, then the central value d is an integer height, and $(b,\, c)$ can take the following values: $(d,\, d),\ (d \pm 1,\, d \mp 1),\ (d \pm 2,\, d \mp 2), \ldots, (d \pm \frac{n}{2},\, d \mp \frac{n}{2})$. If n is odd, the central value d of the shaded n-band is a half integer, and the allowed $(b,\, c)$ values are $(d \pm \frac{1}{2},\, d \mp \frac{1}{2}),\ (d \pm \frac{3}{2},\, d \mp \frac{3}{2}), \ldots, (d \pm \frac{n}{2},\, d \mp \frac{n}{2})$.
Shaded n-bands occur for $0 < \frac{\lambda}{\pi} < \frac{1}{n}$, and not for larger λ. This means that the $(d \pm \frac{n}{2},\, d \mp \frac{n}{2})$ values of $(b,\, c)$ are not supported here, and we cannot extend our definition here. However, we expect that the other elements of the previous lists are groundstate boundary condition, with some d which is not necessary central. Out primary interest is fusion level $n = 2$ which means that the fused path, a and b share the same parity.
For the interval $0 < \frac{\lambda}{\pi} < \frac{1}{2}$ there are shaded 2-bands, and at fusion level $n = 2$, the associated groundstates are related to the superconformal minimal models in the Neveu-Schwarz and Ramond sectors.
In the interval $\frac{1}{2} < \frac{\lambda}{\pi} < 1$, there are no shaded 2-bands, only shaded 1-bands. Consider the union of two sequences $\rho(r)$ and $\rho(r) + 1$. Separate this union into the union of two new sequences $\rho_0(r)$ and $\rho_1(r)$ consisting of the even and odd members respectively (fig. 3.7). As there are only shaded 1-bands, if we wish to end a 2×2 fused path in the same, we must have

$$b = c = \rho_\mu(r), \qquad \mu = 0,\, 1 \tag{3.83}$$

for some $r = 1,\, 2, \ldots, m - 1$. The supported zero energy groundstate paths are flat paths $\boldsymbol{\sigma} = \{\rho, \rho, \ldots, \rho\}$ with $\rho = \rho_0(r)$ or $\rho = \rho_1(r)$ with some r.
Based on *Physical Combinatorics* [74,85–92] and the *correspondence principle* of the Kyoto school [67, 93–95], one-dimensional sums with groundstate boundary conditions are interpreted as finitized conformal characters

$$\chi_\Delta^{(N)}(q) = q^{-c/24+\Delta} X_{abc}^N(q) = q^{-c/24+\Delta} \sum_{\boldsymbol{\sigma}} q^{E(\sigma)}\ , \tag{3.84}$$

where on the CFT side, $E(\sigma)$ are identified as conformal energies of the infinite system. These are spectrum generating functions for a finite truncated set of conformal energy levels in a given sector labeled by $(a,\, b,\, c)$. The connection between the one-dimensional sum with boundary conditions $(a,\, b,\, c)$ and conformal character with Kac indices (r, s) is the following: $s = a$, and

$(b,\, c)$ is in the rth continuous shaded band, in other words, in the shaded band associated to $\rho(r)$. The precise value of b and c depend on the type of groundstate and the fusion level and the length N.
For fusion level $n = 2$ and $\frac{1}{2} < \frac{\lambda}{\pi} < 1$, the correspondence is given by

$$a = s, \quad b = c = \rho_\mu(r), \quad \mu = s \bmod 2\ . \tag{3.85}$$

Here, the previous definition of ρ_0 and ρ_1 ensures the required parity property.

3.4 RSOS$(m, 2m+1)_{2\times 2}$ sequence

In [74], Jacob and Mathieu (JM) defined one-dimensional sums associated with a particular choice of local energy functions for RSOS lattice paths with half-integer steps. These local energy functions were not related to integrable lattice models. However quite remarkably, in the thermodynamic limit, these one-dimensional sums reproduce the Virasoro characters of the sequence of non-unitary minimal models $\mathcal{M}(m, 2m+1)$ with $m = 2, 3, 4, \ldots$. Here, we present an energy preserving bijection between the JM paths and RSOS$(m, 2m+1)_{2\times 2}$ paths. Hence we show that the underlying lattice models of the JM paths are the RSOS$(m,\, 2m+1)_{2\times 2}$ fused models.

3.4.1 Adjacency graph for RSOS$(m,\, 2m+1)_{2\times 2}$ models

The heights of the unfused model RSOS$(m,\, m')$ live on the Dynkin diagram $A_{m'-1}$, which possesses a $\mathbb{Z}_2$ symmetry. Specifically, the Boltzmann weights are invariant under the height reversal $\sigma \leftrightarrow m' - \sigma$. As a consequence, when nodes related by the symmetry are identified, the connectivity graph of the 1×1 unfused models with odd m' folds into a $T_{\frac{m'-1}{2}}$ tadpole diagram. Examples are shown in fig. 3.8.
At fusion level $n = 2$, the allowed adjacent heights fulfill the following conditions

$$\sigma - \sigma' = 0,\, \pm 2 \tag{3.86}$$

$$\sigma + \sigma' = 4,\, 6,\, \ldots, 2m' - 4 \tag{3.87}$$

For $m' = 2m + 1$ models, this means that their adjacency diagram split into the product of two tadpole diagrams $T_m^{(n=2)}$. For the RSOS$(m,\, 2m+1)$ series, the unfused tadpole diagrams T_m have only one self-connected node (figs. 3.8a and 3.8c), while the 2×2 fused tadpole diagrams $T_m^{(n=2)}$ have only one not self-connected node (figs. 3.8b and 3.8d). Hence, the fused and unfused tadpole diagrams do not coincide, with the exception of RSOS(2, 5) (fig. 3.8b), where the fused and unfused models are equivalent, as one can easily prove.

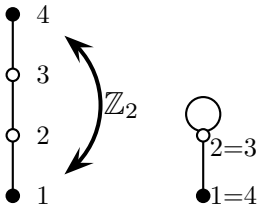

(a) RSOS$(2,5)_{1\times1}$: folding of the $A_4 = A_4^{(n=1)}$ and the corresponding T_2 tadpole.

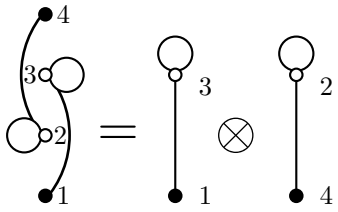

(b) RSOS$(2,5)_{2\times2}$: decomposition of $A_4^{(n=2)}$ into the tensor product of two T_2 tadpoles.

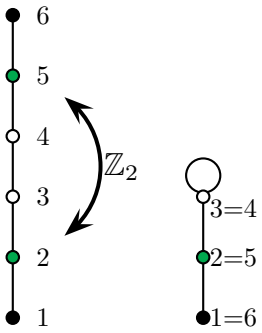

(c) RSOS$(3,7)_{1\times1}$: folding of the $A_6 = A_6^{(n=1)}$ and the corresponding $T_3^{(n=1)}$ tadpole.

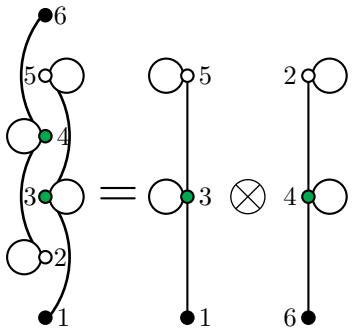

(d) RSOS$(3,7)_{2\times2}$: decomposition of $A_6^{(n=2)}$ into the tensor product of two $T_3^{(n=2)}$ tadpoles.

Figure 3.8: The RSOS$(2,5)$ and RSOS$(3,7)$ lattice models are identified with tadpole diagrams which encode the adjacency rules between heights. The RSOS$(2,5)_{1\times1}$ (a) and RSOS$(2,5)_{2\times2}$ (b) models share the same tadpole diagram. This results from the fact that the 2×2 lattice fusion gives back the original lattice model. Instead, the RSOS$(3,7)_{1\times1}$(c) and RSOS$(3,7)_{2\times2}$ (d) models show different tadpole diagrams because the 2×2 lattice fusion produces a new lattice model. In all figures, we denoted the $\sigma^{(RSOS)}$ heights.

3.4.2 Bijection between the JM and 2×2 RSOS paths

Jacob and Mathieu defined their path as follows: It is a sequence of half-integer heights $\sigma_j^{(JM)}$, with half integer steps. The heights are restricted to $1 \leq \sigma_j^{(JM)} \leq m,\ \sigma_j^{(JM)} \in \frac{1}{2}\mathbb{Z}$, and the steps goes from 0 to L: $0 \leq j \leq L,\ j \in \frac{1}{2}\mathbb{Z}$. The steps are either up or down by half unit: $|\sigma_{j+\frac{1}{2}}^{(JM)} - \sigma_j^{(JM)}| = \frac{1}{2}$ The path must start at integer value, $\sigma_0^{(JM)} \in \mathbb{N}$, and the local maxima occur at integer j's with integer height $\sigma_j^{(JM)}$. Every path of length $N + \frac{1}{2}$ ends at a half-integer value $\sigma_{N+\frac{1}{2}}^{(JM)} = \frac{1}{2}, \frac{3}{2}, \ldots, m - \frac{3}{2}$ with a down step.
The energy of a JM path is given by

$$E = \sum_{j=\frac{1}{2}, j\in\frac{1}{2}\mathbb{N}}^{N} jw(j), \quad w(j) = \frac{1}{2}\left|\sigma_{j+\frac{1}{2}}^{(JM)} - \sigma_{j-\frac{1}{2}}^{(JM)}\right|, \qquad (3.88)$$

$$1 \leq \sigma_j^{(JM)} \leq m,\ \sigma_j^{(JM)} \in \frac{1}{2}\mathbb{N}\,.$$

To understand the bijection between the RSOS and JM path, consider the RSOS path as a walk on the fused tadpole diagram $T_m^{(n=2)}$, where we relabel the nodes corresponding to the heights as $\sigma^{(TP)} = 1, 2, \ldots, m$. Every $\sigma^{(TP)}$ value corresponds to two original RSOS heights, $\sigma_1^{(RSOS)} = 2\sigma^{(TP)} - 1,\ \sigma_2^{(RSOS)} = 2m + 2 - 2\sigma^{(TP)}$. As $2\sigma^{(TP)} - 1$ is odd and $2m + 2 - 2\sigma^{(TP)}$ is even, a path expressed in the $\sigma^{(TP)}$ variables corresponds to two –an odd and an even– paths in the $\sigma^{(RSOS)}$ variables. These two paths are equivalent: the corresponding energy statistics are the same, what follows from the height reversal symmetry (eq. 3.29). The two paths are also equivalent walks on the two copies of the $T_m^{(n=2)}$ tadpole diagrams.
Consider the RSOS path, as a path in the $\sigma^{(TP)}$ variables. The bijecton between the RSOS and the JM path is given as follows. The RSOS path on the tadpole diagram –in the $\sigma_j^{(TP)}$ variables– takes values of the JM path at integer positions, so that two JM steps become one RSOS step

$$\sigma_j^{(TP)} = \sigma_j^{(JM)} \qquad j \in \mathbb{N} \qquad (3.89)$$

Where the JM path has a local minimum at a half integer position and value, the RSOS path has a horizontal step. As a result, the RSOS path follows almost completely the JM path, with the exception of local minima, as shown in fig. 3.9.

To prove the bijection, we prove that the energy defined by JM is gauge

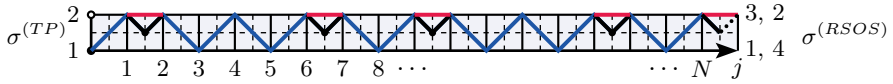

(a) JM(2,5) and $RSOS(2,5)_{2\times 2}$ paths with $N = 17$ integer steps. Due to the 2×2 fusion, RSOS paths have definite parity, with only even or odd heights. Due to the $\mathbb{Z}_2$ symmetry of the A_4 Dynkin diagram we made the identification: $\sigma^{(TP)} = \sigma^{(JM)} = 1, 2$ correspond to $\sigma^{(RSOS)} = 1, 4$ and $\sigma^{(RSOS)} = 3, 2$, respectively.

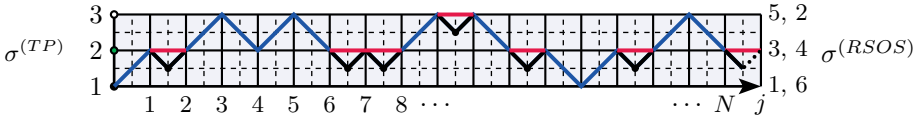

(b) JM(3,7) and $RSOS(3,7)_{2\times 2}$ paths with $N = 17$ integer steps: $\sigma^{(TP)} = \sigma^{(JM)} = 1, 2, 3$ correspond to $\sigma^{(RSOS)} = 1, 6$, $\sigma^{(RSOS)} = 3, 4$ and $\sigma^{(RSOS)} = 5, 2$, respectively.

Figure 3.9: Two examples of the bijection between JM and RSOS paths. The shared path is highlighted in blue. The edges of JM paths are in black while their equivalent in the RSOS description in purple. The bijection between the JM and RSOS paths preserves the contour of the path except at local minima where RSOS path replaces two consecutive steps with a single straight step.

equivalent with the corresponding RSOS energy

$$\sum_{j=\frac{1}{2}, j\in\mathbb{Z}}^{N+\frac{1}{2}} jw(j) = \tag{3.90}$$

$$= \tfrac{1}{2}\sum_{j=1}^{N} j\big(w(j-\tfrac{1}{2}) + 2w(j) + w(j+\tfrac{1}{2})\big) + \tfrac{1}{2}(N+1)w(N+\tfrac{1}{2})$$

$$= \sum_{j=1}^{N} j\big(H(\sigma_{j-1}, \sigma_j, \sigma_{j+1}) - 2G_j + G_{j-1} + G_{j+1}\big) + E_0\ , \tag{3.91}$$

where the constant energy shift is

$$E_0 = \tfrac{1}{2}(N+1)w(N+\tfrac{1}{2}) = \tfrac{1}{4}(N+1)|c-b| \tag{3.92}$$

with boundary conditions $(\sigma_N, \sigma_{N+1}) = (b, c)$.
To prove the bijection between the JM and the fused RSOS description, we need to find a gauge $G_j = g(\sigma_j)$ such that eq. (3.91) holds

$$H(\sigma_{j-1}, \sigma_j, \sigma_{j+1}) = \tfrac{1}{2}\big(w(j-\tfrac{1}{2}) + 2w(j) + w(j+\tfrac{1}{2})\big) + 2G_j - G_{j-1} - G_{j+1}. \tag{3.93}$$

To find the appropriate gauge transformation, consider $\sigma_j = a$, $\sigma_{j+1}, \sigma_{j-1} = a \pm 2$, $\sigma_{j+1/2}, \sigma_{j-1/2} = a \pm 1$, where a is the height in the equivalent RSOS description (in the original height variables), write out eq. (3.93) for each possible local energy function, and substitute the correct value of $w(j)$ from eq. (3.88)

$a \in 2\mathbb{N} - 1$:

$$H(a \pm 2, a, a \mp 2) = 1 + 2g(a) - g(a+2) - g(a-2) \tag{3.94a}$$
$$H(a+2, a, a) = H(a, a, a+2) = \tfrac{3}{4} + g(a) - g(a+2) \tag{3.94b}$$
$$H(a-2, a, a) = H(a, a, a-2) = \tfrac{1}{4} + g(a) - g(a-2) \tag{3.94c}$$
$$H(a, a+2, a) = \tfrac{1}{2} + 2g(a+2) - 2g(a) \tag{3.94d}$$
$$H(a, a-2, a) = \tfrac{1}{2} + 2g(a-2) - 2g(a) \tag{3.94e}$$
$$H(a, a, a) = 0 \tag{3.94f}$$

Now, we solve all these equations together. This computation was performed for a odd; the case where a is even follows from the $\mathbb{Z}_2$ symmetry $\sigma \leftrightarrow m' - \sigma$. The last equation (3.94f) is an identity, whenever $h_a = h_{a+1}$ or $h_{a-1} = h_a$ which is the case for the RSOS$(m,\, 2m+1)_{2\times 2}$ series described in JM theory. The sequence of integers, describing the shaded bands is explicitly computable for this case

$$\rho = \lfloor \tfrac{r(2m+1)}{m} \rfloor = \lfloor 2r + \tfrac{r}{m} \rfloor = 2r \qquad r = 1, 2, \ldots, m-1 \; . \tag{3.95}$$

This shows that every other band is shaded starting from the lowest one $a = 1$, what implies that eq. (3.94f) is satisfied.
Excluding this identity, the remaining equations simplify to

$a \in 2\mathbb{N} - 1$:

$$h_{a+1} - h_{a-1} = 1 \tag{3.96a}$$
$$g(a+2) - g(a) = \tfrac{1}{4} \tag{3.96b}$$
$$g(a-2) - g(a) = -\tfrac{1}{4} \tag{3.96c}$$
$$h_{a+1} - h_a = 1 \tag{3.96d}$$
$$h_{a-1} - h_a = 0 \tag{3.96e}$$

Here eqs. (3.96a), (3.96d) and (3.96e) are again satisfied because of the shaded band structure of the JM series. Finally, the desired solution to the gauge is the solution to eqs. (3.96b) and (3.96c), where C is an arbitrary constant

$$a \in 2\mathbb{N} - 1 : \qquad g(a) = \frac{1}{8} a + C \; . \tag{3.97}$$

This solutions completes the bijection between the RSOS$(m,\, 2m+1)_{2\times 2}$ models and the JM models, proving that these fused models are indeed the underlying lattice models of the JM one-dimensional sums.

3.5 Finitized characters

In this section, we present the known results on the finitized characters. In [73], a formula was conjectured for RSOS$_{n\times n}(m,\, m')$ for $0 < \lambda < \frac{\pi}{n}$ which based on explicit calculations carried out for $n = 2,\, 3$. In [2], we conjectured the finitized characters for $n = 2,\, \frac{\pi}{2} < \lambda < \pi$. Neither of these conjectures is proven using the recursion relation: The groundstate energies and certain one-dimensional sums which do not correspond to characters have not been calculated.

3.5.1 Conjectured finitized branching functions corresponding to $n \times n$ fused RSOS models at $0 < \lambda < \frac{\pi}{n}$

Finitized characters of RSOS$(m,\, m')_{n\times n}$ models with $0 < \lambda < \frac{\pi}{n}$ were considered in [73]. These give the finitized branching functions for non-unitary minimal cosets $\mathcal{M}(M,\, M',\, n')$ with $n' = n$, establishing the correspondence between them. The unitary case was considered in [72].
For simplicity, we assume that the system size N is even and consequently $b-a$ also even. Following Schilling [72] we introduce q-multinomials

$$T_\ell^{(n)}(N,\mu) = \sum_{\tilde{v}\in\mathbb{Z}_{\geq 0}^{n+1}} q^{vC^{-1}v - e_\ell C^{-1} v} (q)_N \prod_{i=0}^{n} \frac{1}{(q)_{v_i}} \tag{3.98}$$

where

$$\tilde{v} = (v_0, v_1, \ldots, v_n), \tag{3.99}$$

$$v = (v_1, v_2, \ldots, v_{n-1}), \qquad v_i \in \mathbb{Z},\ \ i = 0, \ldots, n \tag{3.100}$$

and the sum means summing over all $v_i \in \mathbb{Z}_{\geq 0},\ i = 0, \ldots, n$ with the constrains

$$v_0 = \frac{N}{2} - \frac{\mu}{n} - e_1 C^{-1} v, \tag{3.101a}$$

$$v_n = \frac{N}{2} + \frac{\mu}{n} - e_{n-1} C^{-1} v, \tag{3.101b}$$

$$\mu = -\frac{nN}{2}, -\frac{nN}{2}+1, \ldots, \frac{nN}{2} \tag{3.101c}$$

The matrix C^{-1} is the inverse of the Cartan matrix C with entries $C_{i,j} = 2 - \delta_{i,j+1} - \delta_{i,j-1}$. The vectors e_ℓ are standard $(n-1)$ dimensional basis vectors

$$C^{-1}_{i,j} = \begin{cases} \frac{(n-i)j}{n}, & j \le i \\ \frac{(n-j)i}{n}, & j > i \end{cases} \qquad (e_i)_j = \begin{cases} \delta_{i,j}, & i,j = 1,\ldots,n-1 \\ 0, & \text{otherwise} \end{cases} \tag{3.102}$$

The q-factorials are defined in eq. (3.6) as

$$(q)_n = \prod_{k=1}^{n}(1-q^k), \qquad (q)_\infty = \prod_{k=1}^{\infty}(1-q^k).$$

The q-multinomials satisfy the following recursion relation and initial condition which is an equivalent definition of them

$$\begin{aligned} T^{(n)}_\ell(N,\,\mu) =& \sum_{k=0}^{\ell-1} q^{(\ell-k)(\frac{N}{2}+\frac{\mu}{n})} T^{(n)}_{n-k}(N-1,\,\frac{n}{2}+\mu-k) + \\ &+ \sum_{k=\ell}^{n} q^{(k-\ell)(\frac{N}{2}-\frac{\mu}{n})} T^{(n)}_{n-k}(N-1,\,\frac{n}{2}+\mu-k) \end{aligned} \tag{3.103}$$

$$T^{(n)}_\ell(0,\,\mu) = \delta_{\mu,0} \tag{3.104}$$

The finitized branching functions of the $\mathcal{M}(M,\,M',n)$ models corresponding to one-dimensional sums of RSOS$(m,\,m')_{n\times n}$ models are

$$\begin{aligned} b^{M,M',n,(N)}_{r,s,\ell}(q) \cong \sum_{k=-\infty}^{\infty} \Big(& q^{\frac{k}{n}(kMM'+M'r-Ms)} T_{(n+b-c)/2}(N,\,\tfrac{1}{2}(b-a)+kM') \\ & - q^{\frac{1}{n}(kM+r)(kM'+s)} T^{(n)}_{(n+b-c)/2}(N,\,\tfrac{1}{2}(b+a)+kM') \Big) \end{aligned} \tag{3.105}$$

where $\cong$ means that the equality holds up to the leading power of q. The relations between the parameters of the equation

$$M = nm - (n-1)m' \,, \tag{3.106}$$

$$M' = m' \,, \tag{3.107}$$

$$s = a \,, \tag{3.108}$$

$$r = r(\rho) = r^{m,m',n}(\rho) \,, \tag{3.109}$$

$$\ell = \tfrac{1}{2}(n + (-1)^{h_b}(b - c)) \tag{3.110}$$

Note that in the case h_b is odd, b and c are interchanged. Whenever $\gcd(m,\, m') = 1$, $\gcd(\frac{M'-M}{n},\, M') = \gcd(m'-m,\, m') = 1$ also. In case, $nm-(n-1)m' = M = 1$, the fused model is not defined. For the unitary cases $m = m' - 1$, the formula reduces to the one in Schilling [72]. This formula has been checked for $n = 1, 2, 3$, for many different models, for different branching functions, up to $N = 14$.
Setting $q \to 1$ gives the correct counting of states. The $N \to \infty$ limit correctly recovers the full branching function, as it was proven in [73].

3.5.2 Conjectured finitized minimal characters corresponding to 2×2 fused RSOS models at $\frac{\pi}{2} < \lambda < \pi$

For the $\mathrm{RSOS}(m, m')_{2\times 2}$ models, two intervals are distinguished: $0 < \lambda < \frac{\pi}{2}$ and $\frac{\pi}{2} < \lambda < \pi$, which are covered in [73] and [2] respectively. Here, we consider the latter one.
Define the q-trinomial coefficients in terms of q-factorials

$$\begin{bmatrix} n \\ \ell, m \end{bmatrix}_q = \begin{cases} \frac{(q)_n}{(q)_\ell (q)_m (q)_{n-\ell-m}} & \ell,\, m,\, n-\ell-m \in \mathbb{Z}_{\geq 0} \\ 0 & \text{otherwise} \end{cases} \tag{3.111}$$

The $\begin{bmatrix} n \\ \ell, m \end{bmatrix}_q$ trinomial is a q-deformed counting of 2×2 fused paths with ℓ up steps, m down steps, and $n - \ell - m$ flat steps. The counting does not respect the height restrictions eqs. (3.25) and (3.26).
In the $q \to 1$ limit, the q-deformed trinomials simplify to trinomial coefficients

$$\lim_{q\to 1} \begin{bmatrix} n \\ \ell, m \end{bmatrix}_q = \binom{n}{\ell,\, m} = \frac{n!}{\ell! m! (n-\ell-m)!} \tag{3.112}$$

Introduce an auxiliary function, a special case of a trinomial, originally introduced in [96]

$$T_k^{(N)}(q) = \sum_{j=0}^{N} q^{j(j+k)} \begin{bmatrix} N \\ j, j+k \end{bmatrix}_q . \tag{3.113}$$

Note that it does not have direct connection to the $T_\ell^{(n)}(N, \mu)$ Schilling multinomials. The $T_k^{(N)}(q)$ function is a q-deformed counting of an other set of 2×2 fused paths. It counts the N step long 2×2 fused paths on A_∞ Dynkin-diagram, only respecting $\sigma_{i+1} - \sigma_i = 0, \pm 2$, with $2k$ height difference between

the initial and final height: $\sigma_N - \sigma_0 = 2k$. This ensures correct counting, as $j+k$ is the number of up-steps, j is the number of down-steps, and $N-2j-k$ is the number of flat steps.
The finitized characters corresponding to $\mathcal{M}(m,m')$ minimal models, realized by RSOS$(m,m')_{2\times 2}$ model, with $\frac{\pi}{2} < \lambda = \frac{(m'-m)\pi}{m'} < \pi$ are the following

$$\mathrm{ch}^{m,m',(N)}_{r,s}(q) \cong X^{m,m',(N)}_{a,b,c}(q) = \\ = \sum_{k=-\infty}^{\infty} \left(q^{k(kmm'+m'r-ms)} T^{(N)}_{km'+\frac{\rho-s}{2}}(q) - q^{(km+r)(km'+s)} T^{(N)}_{-km'-\frac{\rho+s}{2}}(q) \right) \tag{3.114}$$

where

$$a = s, \qquad b = c = \rho_\mu(r), \quad \mu \equiv 0 \mod 2 \tag{3.115}$$

as it is defined in section 3.3.5.
This result was extensively checked for numerous RSOS$(m,\, m')_{2\times 2}$ models, for for all possible $1 \le r \le m$, $1 \le s \le m'-1$ (r,s) Kac indices, up to size $N = 12$, for $(m,\, m') = (2,\, 5)$, $(2,\, 7)$, $(3,\, 7)$, $(3,\, 8)$, up to size $N = 11$ for $(m,\, m') = (2,\, 9)$, $(4,\, 9)$, up to size $N = 10$ for $(m,\, m') = (3,\, 10)$ and up to size $N = 9$ for $(m,\, m') = (2,\, 11)$, $(3,\, 11)$, $(4,\, 11)$, $(5,\, 11)$.
The result correctly recover the counting of the paths in the $q \to 1$ limit.
In the $N \to \infty$ limit the finitized characters are expected to recover the full CFT character, up to an overall factor. The q-deformed trinomial $T^{(N)}_k(q)$ takes the following value in the $N \to \infty$ limit

$$\lim_{N\to\infty} T^{(N)}_k(q) = \lim_{N\to\infty} \sum_{j=0}^{\infty} \begin{bmatrix} N \\ j, j+k \end{bmatrix}_q = \frac{1}{(q)_\infty} \tag{3.116}$$

To prove this, first we take the limit inside the summation. Then we take the limit of the trinomial inside

$$\lim_{N\to\infty} \begin{bmatrix} N \\ j, j+k \end{bmatrix}_q = \lim_{N\to\infty} \frac{(q)_N}{(q)_j (q)_{j+k} (q)_{N-2j-k}} = \frac{1}{(q)_j (q)_{j+k}} \tag{3.117}$$

This shows that $\lim_{N\to\infty} T^{(N)}_k(q) = \sum_{j=0}^{\infty} \frac{q^{j(j+k)}}{(q)_j (q)_{j+k}}$. Use the q-deformed version of Kummer's theorem (see (2.2.8) of [97]), which is

$$\sum_{j=0}^{\infty} \frac{q^{j(j-1)z^j}}{(1-q)\ldots(1-q^j)(1-z)(1-zq)\ldots(1-zq^{j-1})} = \prod_{j=0}^{\infty} \frac{1}{1-zq^j}, \tag{3.118}$$

with $z = q^{k+1}$, to obtain the identity

$$\lim_{N\to\infty} T_k^{(N)}(q) = \sum_{j=0}^{\infty} \frac{q^{j(j+k)}}{(q)_j (q)_{j+k}} = \frac{1}{(q)_\infty}. \tag{3.119}$$

From here, it is straightforward to prove that the finitized characters reconstruct the $n' = 1$ Virasoro characters in the $N \to \infty$ limit

$$\lim_{N\to\infty} q^{-c/24+\Delta_{r,s}^{m,m'}} \mathrm{ch}_{r,s}^{m,m',(N)}(q) = \mathrm{ch}_{r,s}^{m,m'}(q). \tag{3.120}$$

The $n' = 1$ Virasoro characters are symmetric under the change $(r,\, s) \;\leftrightarrow (m - r,\, m' - s)$, which means

$$\mathrm{ch}_{r,s}^{m,m'}(q) = \mathrm{ch}_{m-r,m'-s}^{m,m'}(q) \tag{3.121}$$

This symmetry also holds for the finitized characters

$$X_{a,b,c}^{m,m',(N)}(q) = X_{m'-a,m'-b,m'-c}^{m,m',(N)}(q) \tag{3.122}$$

The shaded band structure is symmetric, hence the Kac-indices corresponding to the right hand side of the equation are $(m - r,\, m' - s)$. To prove eq. (3.122), we use the property

$$T_k^{(N)}(q) = T_{-k}^{(N)}(q) \tag{3.123}$$

which follows from direct calculation.
By direct calculation, using eq. (3.123), we prove eq. (3.122)

$$\begin{aligned}
X_{m'-a,m'-b,m'-c}^{m,m',(N)} &= \\
&= \sum_{k=-\infty}^{\infty} \Big(q^{k(kmm'+m'(m-r)-m(m'-s))} T^{(N)}_{km'+\frac{m'-b-m'+a}{2}}(q) - \qquad (3.124a)\\
&\quad - q^{(km+m-r)(km'+m'-s)} T^{(N)}_{-km'-\frac{m'-b+m'-a}{2}}(q) \Big) = \\
&= \sum_{k=-\infty}^{\infty} \Big(q^{k(kmm'-m'r+ms)} T^{(N)}_{km'-\frac{b-a}{2}}(q) - \qquad (3.124b)\\
&\quad - q^{((k+1)m-r)((k+1)m'-s)} T^{(N)}_{-(k+1)m'+\frac{b+a}{2}}(q) \Big) = \\
&= \sum_{k=-\infty}^{\infty} \Big(q^{k(kmm'+m'r-ms)} T^{(N)}_{km'+\frac{b-a}{2}}(q) - \qquad (3.124c)
\end{aligned}$$

$$- q^{(km+r)((km'+s)m'-s)} T^{(N)}_{-km'-\frac{b+a}{2}}(q)\Big) =$$
$$= X^{m,m',(N)}_{a,b,c}(q) \tag{3.124d}$$

where in eq. (3.124d), we modified the summation indices, $k \to -k$ in the first summand and $k \to -(k+1)$ in the second summand. This proves that the finitized characters $X^{m,m',(N)}_{a,b,c}(q)$ are symmetric under $(r,\, s) \leftrightarrow (m-r,\, m'-s)$.

3.6 Conclusion and outlook

In this chapter, we considered fused RSOS$(m,\, m')_{n\times n}$ models. These models are lattice realizations of higher level non-unitary minimal models $\mathcal{M}(M,\, M',\, n')$. We considered fusion level $n = 2$ in the regime $\frac{\pi}{2} < \lambda < \pi$, for crossing parameter $\lambda = \frac{m'-m}{m'}$, and found that in this interval the lattice models are new realizations of $n' = 1$ minimal models.

Our calculation is based on Baxter's corner transfer matrix method, making correspondence between the low temperature one-dimensional sums of the statistical physical model and finitized versions of the conformal characters. We found explicit expressions for the one-dimensional sums, expressed in terms of q-deformed trinomials. These one-dimensional sums correspond to the finitized characters up to on overall factors. We checked our result for numerous models up to system size $N = 12$, to support our conjecture. Our result is a conjecture. In order to prove it we need to make use of recursion relations, which require certain other one-dimensional sums that do not correspond to CFT characters.

The project has some clear directions to continue: To finalize the $n = 2$ case, we have to find the groundstate energies, and some more one-dimensional sums. This has started, and some partial results on the required one-dimensional sums are achieved. Higher fusion levels n are also in the focus of further research.

Chapter 4

Supersymmetric fermion chain without particle conversation

4.1 Introduction

The study of supersymmetric lattice models dates back to the $\mathcal{N} = 1$ supersymmetry in the tricritical Ising model [52, 98, 99] and the fully frustrated XY-model [100]. In the introduction of [101], the historical development is further detailed.

The interest in the construction of the model originates from the model of Fendley, Schoutens, and de Boer [102], where the supersymmetric M_1 model was introduced. The model is an exactly solvable $\mathcal{N} = 2$ supersymmetric model. There are two supercharges, $Q_1 = Q + Q^\dagger$ and $Q_2 = \mathrm{i}(Q - Q^\dagger)$, where Q and its Hermitian conjugate $Q^\dagger$ are nilpotent: $Q^2 = (Q^\dagger)^2 = 0$. The Hamiltonian is defined as $H = \{Q, Q^\dagger\}$. For generic $\mathcal{N}$, there are $\mathcal{N}$ fermionic algebra generators with the properties $Q_k^2 = Q_n^2$, and every anticommutator $\{Q_k, Q_n\}$ is a central element of the algebra.

The consequences of the supersymmetry include the absence of negative energy states, that all positive energy states come in doublets, with the same eigenvalue, but differing in the number of fermions by one. The zero energy states (the lowest possible) might be degenerate, but form singlets with respect to the supersymmetry. This choice for the supercharge generator Q in the M_1 model

[102] results in a repulsive hardcore potential, i.e. fermions have to be apart at least two sites, with an empty site in between. Later, this model has been generalized to M_k models, where k long strings of fermions are allowed [103].
We modify the original M_1 model in a different way: we change Q and $Q^\dagger$ such that we restore fermion–hole symmetry. This simply means that we add extra terms to $Q^\dagger$ (and Q) which create (annihilate) solitary holes. This modifies the nature of the model to a large extent, e.g. fermion number is not conserved anymore. Instead, we identify domain walls with Majorana-like properties, as conserved degrees of freedom. The spectrum also changes drastically. The high degeneracy of the ground state is a common feature of supersymmetric lattice models [104–107], but here this high degeneracy is no longer limited to the ground state. While in the original model, all energy levels are two-fold degenerate, here all energy levels show *extensive* degeneracy: the degeneracy is a power of two, with an exponent growing linearly in the system size. Most surprisingly, despite the change in Q, the model preserves both supersymmetry and integrability.
The original motivation for this work comes from understanding the high degeneracy of the model. During our investigation, we identified one symmetry in terms of zero energy Cooper pair like excitations –similar to excitations in [108]– which explains the degeneracy of the groundstate. We further show that the energy gap of the system scales as $\sim 1/L^2$ with the system size L, which is usually associated to classical diffusive models.
This chapter is organized as follows: In section 4.2 we introduce the model. In section 4.3 we present the solution by means of the nested coordinate Bethe ansatz [109, 110]. First we expose the Bethe equations (section 4.3.1), and after that we derive them. Our derivation is pedagogical, we derive gradually more and more complicated cases. In section 4.4, we list the known symmetries of the model, including the most prominent one, coined as zero mode Cooper pairs (section 4.4.9), which explains the extensive degeneracy of the model. The Cooper pair description relies on the Bethe ansatz solution of the model. In section 4.5, we investigate further properties of the model and the Bethe ansatz solution. We examine the question of completeness in certain cases in sections 4.5.1 and 4.5.2. We give the exact groundstate and first excited state for $L = 4n$ system sizes in section 4.5.3. We finish with a conclusion in section 4.6. In appendix C.1 we carefully address the question of the extensiveness of the groundstate for $L = 4n$ and the highest energy level for $L = 4n + 2$ systems.

4.2 Definition of the model

Define the usual fermionic creation and annihilation operators satisfying the usual anticommutation relations

$$\{c_i^\dagger, c_j\} = \delta_{ij}, \qquad \{c_i^\dagger, c_j^\dagger\} = \{c_i, c_j\} = 0. \tag{4.1}$$

These operators create and annihilate spinless fermions on a one-dimensional chain, indexed by the site-index i and j. We introduce the usual fermion- and hole-number operators

$$n_i = c_i^\dagger c_i, \qquad p_i = 1 - n_i. \tag{4.2}$$

Define another number operator, $\mathcal{N}_i$ which counts the fermions from site 1 to i, and $\mathcal{N}_F$, as the total fermion number operator

$$\mathcal{N}_i = \sum_{j=1}^{i} n_j, \qquad \mathcal{N}_\mathrm{F} := \mathcal{N}_L. \tag{4.3}$$

Here and in the following L denotes the length of the system. These operators act on a Fock space built on the vacuum state $|\mathbf{0}\rangle$, spanned by the vectors

$$|\tau\rangle =: \prod_{i=1}^{L} \left(c_i^\dagger\right)^{\tau_i} : |\mathbf{0}\rangle . \tag{4.4}$$

The semicolons indicate the normal-ordering of the product according to their position. The vacuum state is defined by the relations

$$c_i |\mathbf{0}\rangle = 0 \qquad i = 1, \ldots, L \tag{4.5}$$

The $\tau_i = 0, 1$ indices represent a hole and fermion at site i, respectively. Hence, we trivially get $n_i |\tau\rangle = \tau_i |\tau\rangle$. We use the following notation for the vectors of the Hilbert space

$$|\tau_1\, \tau_2 \ldots \tau_L\rangle \equiv: \prod_{i=1}^{L} \left(c_i^\dagger\right)^{\tau_i} : |\mathbf{0}\rangle \tag{4.6}$$

To define the modified version of the M_1 model, we introduce the operators $d_i^\dagger$ and e_i

$$d_i^\dagger = p_{i-1} c_i^\dagger p_{i+1}, \qquad e_i = n_{i-1} c_i n_{i+1}. \tag{4.7}$$

These operators create solitary fermion and hole at the ith site, respectively. The operator $d_i^\dagger$ creates a fermion at site i, given that $i \pm 1$ are empty. Similarly, e_i

creates a hole at site i, given that $i\pm1$ are occupied. Due to the anti-commutation relations and normal ordering, the following relations hold

$$d_i^\dagger \left|\tau_1 \dots \tau_{i-2}\, 000\, \tau_{i-2} + \dots \tau_L\right\rangle = (-1)^{\mathcal{N}_{i-1}} \left|\tau_1 \dots \tau_{i-2}\, 010\, \tau_{i+2} \dots \tau_L\right\rangle, \quad (4.8)$$

$$e_i \left|\tau_1 \dots \tau_{i-2}\, 111\, \tau_{i+2} \dots \tau_L\right\rangle = (-1)^{\mathcal{N}_{i-1}} \left|\tau_1 \dots \tau_{i-2}\, 101\, \tau_{i+2} \dots \tau_L\right\rangle, \quad (4.9)$$

while acting on other states results in 0.
We define the supercharges and the Hamiltonian as follows

$$Q = \sum_{i=1}^{L} (d_i^\dagger + e_i), \qquad Q^2 = 0 \quad (4.10)$$

$$Q^\dagger = \sum_{i=1}^{L} (d_i + e_i^\dagger), \qquad (Q^\dagger)^2 = 0 \quad (4.11)$$

$$H = \{Q^\dagger, Q\} \quad (4.12)$$

Here and in the rest of the paper, unless otherwise stated, we assume periodic boundary conditions

$$c_{i+L}^\dagger = c_i^\dagger. \quad (4.13)$$

The nilpotent properties eqs. (4.10) and (4.11) also hold with antiperiodic boundary conditions, defined by

$$c_{i+L}^\dagger = c_i. \quad (4.14)$$

Our definition of Q is the fermion-hole symmetric extension of the supercharge $Q_{\mathrm{FSdB}} = \sum_i d_i^\dagger$ of Fendley, Schoutens and de Boer [102]. Unexpectedly, our modification on Q_{FSdB} keeps supersymmetry, which is checked by direct calculation.
To analize the system defined by eq. (4.12), we expand the Hamiltonian, and group the summands according to their content. H_I contains terms involving d-type operators, H_{II} contains e-type operators, H_{III} contains mixed terms

$$H = H_I + H_{II} + H_{III}, \quad (4.15a)$$

$$H_I = \sum_i \left(d_i^\dagger d_i + d_i d_i^\dagger + d_i^\dagger d_{i+1} + d_{i+1}^\dagger d_i \right), \quad (4.15b)$$

$$H_{II} = \sum_i \left(e_i e_i^\dagger + e_i^\dagger e_i + e_i e_{i+1}^\dagger + e_{i+1} e_i^\dagger \right), \quad (4.15c)$$

$$H_{III} = \sum_i \left(e_i^\dagger d_{i+1}^\dagger \ + d_{i+1} e_i + e_{i+1}^\dagger d_i^\dagger + d_i e_{i+1} \right), \tag{4.15d}$$

where we assume periodic boundary conditions $c_{i+L}^\dagger = c_i^\dagger$. H_I is the Hamiltonian of the M_1 model, considered in [102]. H_{II} is the same expression, as H_I, after a $d_i^\dagger \leftrightarrow e_i$ change. As the only difference that the role of fermions and holes are exchanged, physically it is equivalent to H_I. H_{III} contains the mixed terms. Since d and e are not simple fermionic operators, they do not obey the usual anticommutation relations. This means, eq. (4.15a) bilinear Hamiltonian cannot be solved by taking linear combinations of d- and e-type operators.
H_I and H_{II} contain terms, which are pairs of creation and annihilation operators, hence they preserve the fermion number. H_{III} contains terms, which break the fermion conservation: e.g. $d_{i+1}e_i$ sends the state $|\dots 1110 \dots\rangle$ to $|\dots 1000 \dots\rangle$, annihilating two fermions. Hence, the fermions are not good quantum numbers for the Bethe ansatz. In the next section we introduce other type of excitations which are conserved: domain walls.

4.2.1 Domain walls

Introduce the 01-domain wall, as an interface between a string of 0's followed by a string of 1's, and similarly, the 10-domain wall, as an interface between a string of 1's followed by a string of 0's. We index the domain wall by the index of the site to the left of it. For example, the next state contains 8 domain walls, four-four of both type

$$00|11|0|1|0|111|0|1111| \tag{4.16}$$

To describe a state $|\tau_1 \, \tau_2 \dots \tau_L\rangle$, we list the positions of the domain walls, and the type of the first domain wall. This is sufficient to make the description bijective. Let us revisit the terms in the Hamiltonian with respect to the domain walls. H_{III} corresponds to the hopping of a domain wall, creating or annihilating two fermions

$$|\dots 1|000 \dots\rangle \underset{d_{i+1}e_i}{\overset{e_i^\dagger d_{i+1}^\dagger}{\rightleftharpoons}} |\dots 111|0 \dots\rangle \,, \tag{4.17}$$

$$|\dots 0|111 \dots\rangle \underset{e_{i+1}^\dagger d_i^\dagger}{\overset{d_i e_{i+1}}{\rightleftharpoons}} -|\dots 000|1 \dots\rangle \,, \tag{4.18}$$

where the minus sign arises because of the fermionic nature of the model. In H_I and H_{II}, there are diagonal and nondiagonal terms. The diagonal terms are $d_i^\dagger d_i + d_i d_i^\dagger$ and $e_i e_i^\dagger + e_i^\dagger e_i$. These terms count the number of 010, 000, 101 and

111 strings. The nondiagonal terms describe the hopping of a fermion or a hole

$$|\ldots 00|1|0\ldots\rangle \underset{d_{i+1}^\dagger d_i}{\overset{d_i^\dagger d_{i+1}}{\rightleftharpoons}} |\ldots 0|1|00\ldots\rangle \tag{4.19}$$

$$|\ldots 11|0|1\ldots\rangle \underset{e_i^\dagger e_{i+1}}{\overset{e_i e_{i+1}^\dagger}{\rightleftharpoons}} -|\ldots 1|0|11\ldots\rangle \tag{4.20}$$

The hopping of a fermion or hole is equivalent to the interaction between two domain walls. As we see, all the processes, included in H, preserve the number of domain walls. The coordinate of any domain wall changes by two during these processes, hence on an even sized system $L = 2n$, $n \in \mathbb{N}$, with periodic boundary conditions, the number of domain walls at odd and even positions are separately conserved. We call these two types of domain walls simply odd and even domain walls. The total number of domain walls is even, due to periodic boundary conditions. In the following, unless otherwised stated, we consider even sized systems. Hence the Hilbert space is naturally divided into the direct sum of sectors. An (m, k) sector contains m domain walls, $m - k$ domain walls with even positions, k with odd. The Hamiltonian is consequently block-diagonal in these sectors.

4.3 Solution by Bethe ansatz

In this section we derive the solution to the supersymmetric chain by means of the nested coordinate Bethe ansatz [109,110]. First, we expose the most general Bethe equations, and give some notes on it. Then we derive these equations gradually: We start from the simplest case, i.e. the Bethe solution for the (2, 0) sector, and case by case derive solutions to more complicated cases, ending up at the most general (m, k) sector.

4.3.1 Bethe equations

Consider a generic (m, k) sector for an even L sized system, with m domain walls (m must be even) and k odd domain walls, with periodic boundary conditions ($c_i = c_{L+i}$). The Bethe ansatz is performed in the domain walls, as particles. There are two kind of particles, even and odd domain walls. Each domain wall is associated with a Bethe root z_j, where $\log z_j$ is proportional to the momentum of the particle, and each odd domain wall carries an additional nested Bethe root,

u_l. The eigenenergy of H for a Bethe solution is given in terms of z_j's

$$\Lambda = L + \sum_{i=1}^{m} (z_i^2 + z_i^{-2} - 2) \tag{4.21}$$

The set of $z_1, z_2, \ldots, z_m$ and $u_1, u_2, \ldots u_k$ satisfies the equations

$$z_j^L = \pm \mathrm{i}^{-L/2} \prod_{l=1}^{k} \frac{u_l - (z_j - 1/z_j)^2}{u_l + (z_j - 1/z_j)^2}, \qquad j = 1, \ldots, m \tag{4.22}$$

$$1 = \prod_{j=1}^{m} \frac{u_l - (z_j - 1/z_j)^2}{u_l + (z_j - 1/z_j)^2}, \qquad l = 1, \ldots, k \tag{4.23}$$

where the choice of $\pm$ is the same for all j in the first equation.
Certain solutions of the Bethe equations belong to the same Bethe vector: If $z_1, \ldots, z_m; u_1, \ldots, u_k$ and $z'_1, \ldots, z'_m; u'_1, \ldots, u'_k$ are two solutions, they correspond to the same Bethe vector, if there is a set of signs $\delta_i = \pm$, and permutations $\pi \in S_m$, $\sigma \in S_k$, such that $z_j = \delta_j z'_{\pi(j)}$, $j = 1, \ldots, m$ and $u_l = u'_{\sigma(l)}$. In other words, the solutions are invariant under permutations of the Bethe roots, and the sign of z's. In order to have nonzero Bethe vector, all the u's have to be different, and all the z's differ up to a sign, $u_r \neq u_s$ and $z_i \neq \pm z_j$.
In the absence of odd domain walls, the second set of equations is missing, and the first set simplifies to the free-fermionic equations

$$z_j^L = \pm \mathrm{i}^{-L/2}, \qquad j = 1, \ldots, m \tag{4.24}$$

This is physically clear, if we take into account that only with even domain walls, the domain walls satisfy simple hardcore repulsion. The solution to the free-fermion case is

$$z_j = \mathrm{i}^{-1/2} \mathrm{e}^{2\mathrm{i}\pi I_j / L}, \quad j = 1, \ldots, m \tag{4.25}$$

where I_j's are (half-)integers.
Having the odd domain walls at the nested level is an arbitrary choice: we can chose the even domain walls to be nested. Hence, the sectors (m, k) and $(m, m-k)$ display the same physics after an odd–even change. This is not apparent in the Bethe equations, however, this will be clear during the discussion of the symmetries of the model.
As a preparation for the derivation, introduce the domain wall notation for the $|\tau_1 \tau_2 \ldots \tau_L\rangle$ basis vectors of the Fock space. Let $1 \leq x_1 < x_2 < \ldots < x_m \leq L$

denote the position of the m domain walls, of which $p_1, \ldots, p_k$ are the indices of odd domain walls

$$|x_1, x_2, \ldots, x_m; p_1, \ldots p_k\rangle_\epsilon \tag{4.26}$$

To fully specify the vector, the type of the first domain wall is encoded in $\epsilon = 0, 1$, 0 denoting 01-type domain wall, and 1 denoting 10-type domain wall. The information contained in $p_1, \ldots, p_k$ is redundant, but it is useful during the derivation of the Bethe equations. The following equation is an example for this notation

$$|000110010011\rangle = |3, 5, 7, 8, 10, 12; 1, 2, 3\rangle_0 \,. \tag{4.27}$$

To conveniently describe how the Hamiltonian acts on a state, introduce two operators, $S_i^\pm$ which by definition shifts the ith domain wall

$$S_i^\pm \, |x_1, \ldots, x_i, \ldots, x_m; p_1, \ldots, p_k\rangle = |x_1, \ldots, x_i \pm 1, \ldots, x_m; p_1, \ldots, p_k\rangle \,. \tag{4.28}$$

The $S_i^\pm$ operators change the p content of the vector, which we did not denote here.

To diagonalize the Hamiltonian in the $(m,\, k)$ sector, introduce eigenvectors of H expanded in the domain wall notation. Define $|\Psi(m,k)\rangle$ as an eigenvector in the sector $(m,\, k)$

$$H \, |\Psi(m,k)\rangle = \Lambda \, |\Psi(m,k)\rangle \,, \tag{4.29}$$

where we give the most general form to the vector by

$$|\Psi(m,k)\rangle = \sum_{\{x_i\}} \sum_{\{p_j\}} \sum_{\epsilon=0,1} \psi_\epsilon(x_1, \ldots, x_m; p_1, \ldots, p_k) \, |x_1, \ldots, x_m; p_1, \ldots, p_k\rangle_\epsilon \,. \tag{4.30}$$

Here we sum up for all possible domain wall configurations with m domain walls and k odd domain walls. The Bethe ansatz takes place in the wavefunction amplitudes $\psi_\epsilon(x_1, \ldots, x_m; p_1, \ldots, p_k)$. We start with the simplest case, the two even, no odd domain wall case.

4.3.2 Two domain walls, no odd domain wall $(m,\, k) = (2,\, 0)$

We start by examining, what is the effect of H on a state with two even domain walls. If the two domain walls are far apart ($|x_1 - x_2| > 2$), both domain walls can move in both direction. If they are close, they cannot move towards each other

$$H \, |x_1, x_2\rangle_\epsilon = \left(L - 4 + \sum_{i=1,2} (-1)^{i+\epsilon} \left(S_i^{+2} + S_i^{-2} \right) \right) |x_1, x_2\rangle_\epsilon \,, \tag{4.31}$$

$$H\,|x,x+2\rangle_\epsilon = (L-4+(-1)^\epsilon(-S_1^{-2}+S_2^{+2})\;\;|x,x+2\rangle_\epsilon\,. \tag{4.32}$$

The diagonal terms $(L-4)\,|x_1,x_2\rangle_\epsilon$ and $|x,x+2\rangle_\epsilon$ come from the diagonal terms in the Hamiltonian. The only terms without contribution are the 001, 011, 110 and 100 strings around the domain walls. Taking the scalar product with an eigenstate $\langle\Psi(2,0)|$, it follows from the first equation

$$\begin{aligned}\Lambda\psi_\epsilon(x_1,x_2) = (L-4)\psi_\epsilon(x_1,x_2) + (-1)^\epsilon\big(&-\psi_\epsilon(x_1+2,x_2)-\psi_\epsilon(x_1-2,x_2)\\ &+\psi_\epsilon(x_1,x_2+2)+\psi_\epsilon(x_1,x_2-2)\big)\end{aligned} \tag{4.33}$$

From the second equation, a similar equation follows

$$\Lambda\psi_\epsilon(x,x+2) = (L-4)\psi_\epsilon(x,x+2)+(-1)^\epsilon\big(\psi_\epsilon(x-2,x+2)+\psi_\epsilon(x,x+4)\big) \tag{4.34}$$

Analytically continue eq. (4.33) to $x_2 = x_1+2$ and by subtracting eq. (4.34), we get

$$-\psi_\epsilon(x-2,x-2)+\psi_\epsilon(x,x) = 0 \tag{4.35}$$

We use the following ansatz to satisfy eqs. (4.33) and (4.35)

$$\psi_\epsilon(x_1,x_2) = c_\epsilon\left(A^{12}(\mathrm{i}^{1-\epsilon}z_1)^{x_1}(\mathrm{i}^\epsilon z_2)^{x_2}+A^{21}(\mathrm{i}^{1-\epsilon}z_2)^{x_1}(\mathrm{i}^\epsilon z_1)^{x_2}\right) \tag{4.36}$$

The z_j variables are the Bethe roots, complex parameters to be determined by further conditions. By substituting the ansatz, we find that the eigenvalue Λ and the amplitudes A satisfy the conditions

$$\Lambda = L+\sum_{i=1}^{2}(z_i^2+z_i^{-2}-2), \qquad A^{12}+A^{21}=0 \tag{4.37}$$

The periodic boundary condition on a chain of even length L imposes the following further condition

$$\psi_\epsilon(x,L+2) = \psi_{1-\epsilon}(2,x) \tag{4.38}$$

Substituting the ansatz in this equation results in

$$\begin{aligned} c_0A^{12}z_2^L &= c_1A^{21} & \qquad c_1A^{12}(\mathrm{i}z_2)^L &= c_0A^{21}\\ c_0A^{21}z_1^L &= c_1A^{12} & \qquad c_1A^{21}(\mathrm{i}z_1)^L &= c_0A^{12}\end{aligned} \tag{4.39}$$

Hence we find that $(c_0/c_1)^2 = \mathrm{i}^L$ and

$$z_1^{2L} = z_2^{2L} = \mathrm{i}^{-L}. \tag{4.40}$$

Taking the square root of the equation, we find two different sets of solutions

$$\frac{c_0}{c_1} = \mathrm{i}^{L/2} \qquad \frac{c_0}{c_1} = -\mathrm{i}^{L/2} \tag{4.41a}$$

$$z_1^L = -\frac{c_1}{c_0} = -\mathrm{i}^{-L/2} \qquad z_1^L = -\frac{c_1}{c_0} = \mathrm{i}^{-L/2} \tag{4.41b}$$

$$z_2^L = -\frac{c_1}{c_0} = -\mathrm{i}^{-L/2} \qquad z_2^L = -\frac{c_1}{c_0} = \mathrm{i}^{-L/2} \tag{4.41c}$$

For certain solutions, the wavefunction amplitude is identically zero, which is a manifestation of the Pauli principle: $z_1 \neq \pm z_2$. Two solutions, $(z_1,\, z_2)$ and $(z_1',\, z_2')$ are independent and the corresponding Bethe vectors are orthogonal, if taking the squares of the Bethe roots are not equal up to interchange. If z is a solution, $-z$ is also a solution, but does not give new Bethe vector. Hence it is enough to deal with half of the solutions of eq. (4.41b). This gives $2\binom{L/2}{2}$ different solutions (where the prefactor 2 is coming from the two different set of solutions). The dimension of the (2, 0) sector is $2\binom{L/2}{2}$, consequently the Bethe ansatz gives the full solution in the free-fermionic (2, 0) sector.

4.3.3 Two domain walls, one odd domain wall $(m,\, k) = (2,\, 1)$

Probe the effect of H on a state with two domain walls, the first being an odd domain wall. Similarly as in the previous case, we distinguish two cases. The walls are either far apart ($|x_1 - x_2| > 1$), and they diffuse without interaction, or next to each other and they interact

$$H\,|x_1, x_2; 1\rangle_\epsilon = \left(L - 4 + \sum_{i=1,2} (-1)^{i+\epsilon} \left(S_i^{+2} + S_i^{-2} \right) \right) |x_1, x_2; 1\rangle_\epsilon\,, \tag{4.42a}$$

$$\begin{aligned} H\,|x, x+1; 1\rangle_\epsilon =& \big(L - 2 + (-1)^\epsilon (-S_1^{-2} + S_2^{+2}) \big)\, |x, x+1; 1\rangle_\epsilon \\ &+ (-1)^\epsilon \big(|x-1, x; 2\rangle_\epsilon + |x+1, x+2; 2\rangle_\epsilon \big). \end{aligned} \tag{4.42b}$$

In the second case, there is no hardcore exclusion as for two even domain walls close to each other, but the walls can pass each other. Similar equations hold for the case when the second domain wall is the odd one.
From eq. (4.42a), the same way, as previously, by taking the scalar product with an eigenstate $\langle \Psi(2,1)|$ we derive the following equation

$$\begin{aligned} \Lambda \psi_\epsilon(x_1, x_2; 1) = (L-4)\psi_\epsilon(x_1, x_2; 1) + (-1)^\epsilon \big(&- \psi_\epsilon(x_1 + 2, x_2; 1) - \psi_\epsilon(x_1 - 2, x_2; 1) \\ &+ \psi_\epsilon(x_1, x_2 + 2; 1) + \psi_\epsilon(x_1, x_2 - 2; 1) \big). \end{aligned} \tag{4.43}$$

For eq. (4.42b), when the domain walls are distance one apart, we derive the following equation

$$\Lambda\psi_\epsilon(x,x{+}1;1) = (L{-}2)\psi_\epsilon(x,x{+}1;1){+}(-1)^\epsilon\big(-\psi_\epsilon(x{-}2,x{+}1;1){+}\psi_\epsilon(x,x{+}3;1) + \psi_\epsilon(x-1,x;2)+\psi_\epsilon(x+1,x+2;2)\big). \quad (4.44)$$

Analytically continue eq. (4.43) to $x_2 = x_1 + 1$, and by subtracting eq. (4.44), it follows

$$2\psi_\epsilon(x,x+1;1) + (-1)^\epsilon\big(\psi_\epsilon(x+2,x+1;1) - \psi_\epsilon(x,x-1;1) + \psi_\epsilon(x-1,x;2)+\psi_\epsilon(x+1,x+2;2)\big) = 0. \quad (4.45)$$

The previous derivation is for the case, when out of the two domain walls, the first one is at the odd position. The same equation is derived for the case, when the odd domain wall is the second one

$$2\psi_\epsilon(x,x+1;2) + (-1)^\epsilon\big(\psi_\epsilon(x+2,x+1;2) - \psi_\epsilon(x,x-1;2) + \psi_\epsilon(x-1,x;1)+\psi_\epsilon(x+1,x+2;1)\big) = 0. \quad (4.46)$$

To solve these equations (eqs. (4.43), (4.45) and (4.46)), we use a nested wavefunction ansatz. With a view to later generalization, we make the following ansatz

$$\psi_\epsilon(x_1,x_2;p) = \sum_{\pi\in S_2} B_\epsilon^{\pi_1\pi_2}(p)(\mathrm{i}^{1-\epsilon}z_{\pi_1})^{x_1}(\mathrm{i}^{\epsilon}z_{\pi_2})^{x_2}, \quad (4.47)$$

where $B_\epsilon^{\pi_1\pi_2}(p)$ is the nested amplitude in the wavefunction

$$B_\epsilon^{\pi_1\pi_2}(p) = c_\epsilon(-1)^{\lfloor(p+\epsilon-1)/2\rfloor}A^{\pi_1\pi_2}g(u,z_{\pi_p})\prod_{j=1}^{p-1}f(u,z_{\pi_j}). \quad (4.48)$$

Here the extra phase factors have the purpose of canceling the (-1) factors of the Hamiltonian.
We assume the same form of the eigenenergy and the wavefuncion amplitudes as previously

$$\Lambda = L + \sum_{i=1}^{2}(z_i^2 + z_i^{-2} - 2), \qquad A^{12} + A^{21} = 0. \quad (4.49)$$

Substituting these assumptions leads to the following equations for the nested ansatz functions f and g of eqs. (4.45) and (4.46)

$$\sum_{\pi\in S_2} A^{\pi_1\pi_2}\big(z_{\pi_2}g(u,z_{\pi_1})(2 - z_{\pi_1}^2 - z_{\pi_2}^{-2}) - \mathrm{i}z_{\pi_1}f_\epsilon(u,z_{\pi_1})g(u,z_{\pi_2})(z_{\pi_1}^{-2} - z_{\pi_2}^2)\big) = 0, \quad (4.50)$$

$$\sum_{\pi\in S_2} A^{\pi_1\pi_2}\big(z_{\pi_2} f_\epsilon(u,z_{\pi_1})g(u,z_{\pi_2})(2-z_{\pi_1}^2-z_{\pi_2}^{-2}) - \mathrm{i}z_{\pi_1} g(u,z_{\pi_1})(z_{\pi_1}^{-2}-z_{\pi_2}^2)\big) = 0. \tag{4.51}$$

These equations are solved by the following expressions, which is checked by direct calculation

$$f(u,z) = \mathrm{i}\frac{u-(z-1/z)^2}{u+(z-1/z)^2}, \tag{4.52}$$

$$g(u,z) = \frac{z-1/z}{u+(z-1/z)^2}. \tag{4.53}$$

Here u is a additional complex parameter, the nested Bethe root, associated only with odd domain walls.
Imposing periodic boundary conditions leads to further conditions, where again we have to carefully take minus signs into account

$$\psi_\epsilon(x,L+2;1) = \psi_{1-\epsilon}(2,x;2), \qquad \psi_\epsilon(x,L+1;2) = (-1)^{\mathcal{N}_F-1}\psi_{1-\epsilon}(1,x;1). \tag{4.54}$$

As for this case, we have odd number of fermions, this leads to

$$B_\epsilon^{\pi_1\pi_2}(1)(\mathrm{i}^\epsilon z_{\pi_2})^L = B_{1-\epsilon}^{\pi_2\pi_1}(2), \qquad B_\epsilon^{\pi_1\pi_2}(2)(\mathrm{i}^\epsilon z_{\pi_2})^L = B_{1-\epsilon}^{\pi_2\pi_1}(1). \tag{4.55}$$

Substituting this into eq. (4.48) we arrive to the following equation

$$c_0/c_1 = \pm\mathrm{i}^{L/2+1}. \tag{4.56}$$

The following equations are derived from eq. (4.55), after substituting the ansatz

$$z_{\pi_2}^L = -\frac{c_1}{c_0}\frac{A^{\pi_2\pi_1}}{A^{\pi_1\pi_2}} f(u,z_{\pi_2}) = \frac{c_1}{c_0}\frac{A^{\pi_2\pi_1}}{A^{\pi_1\pi_2}} f(u,z_{\pi_1})^{-1} \tag{4.57}$$

Using the previous results, we derive the following Bethe equations

$$z_1^L = \pm\mathrm{i}^{-L/2}\frac{u-(z_1-1/z_1)^2}{u+(z_1-1/z_1)^2}, \tag{4.58}$$

$$z_2^L = \pm\mathrm{i}^{-L/2}\frac{u-(z_2-1/z_2)^2}{u+(z_2-1/z_2)^2}, \tag{4.59}$$

with the further nested Bethe equation

$$1 = -f(u,z_1)f(u,z_2) = \frac{u-(z_1-1/z_1)^2}{u+(z_1-1/z_1)^2}\frac{u-(z_2-1/z_2)^2}{u+(z_2-1/z_2)^2}. \tag{4.60}$$

The simultaneous solution of eqs. (4.58) to (4.60) gives the Bethe vectors for the (2, 1) sector. The same exclusion rules apply for these solutions, as for the (2, 0) sector: $z_1 \neq \pm z_2$. For the (2, 0) sector, the Bethe equations are free-fermionic. In the (2, 1) sector, the free-fermionic spectrum is produced by the $u = 0$ or $u = \infty$ solutions.

4.3.4 Arbitrary number of domain walls, no odd domain wall $(m,\, k = 0)$

Taking a solution with an arbitrary number of domain walls, without odd domain wall is the straightforward generalization of the (2, 0) case. If all the walls are far apart ($|x_i - x_j| > 2$, $\forall i,\, j \in 1, \ldots, m$), the following equation holds for the wavefunction amplitudes

$$\begin{aligned}\Lambda\psi_\epsilon(x_1, \ldots, x_m) = (L - 2m)\psi_\epsilon(x_1, \ldots, x_m) + \\ + (-1)^\epsilon \sum_{j=1}^{m} (-1)^j \psi_\epsilon(\ldots, x_j - 2, \ldots) + (-1)^j \psi_\epsilon(\ldots, x_j + 2, \ldots)\end{aligned} \quad (4.61)$$

If the distance between two walls is 2, $x_{i+1} = x_i + 2$, then $\psi_\epsilon(\ldots, x_i, x_{i+1} - 2)$ and $\psi_\epsilon(x_i + 2, x_{i+1}, \ldots)$ are not present in the sum. This, and taking the $x_{i+2} = x_i + 2$ limit in eq. 4.61 leads to

$$0 = (-1)^\epsilon (-1)^i \psi_\epsilon(\ldots, x_i + 2, x_i + 2, \ldots) + (-1)^\epsilon (-1)^{i+1} \psi_\epsilon(\ldots, x_i, x_i, \ldots) \quad (4.62)$$

In the absence of odd domain walls, we use the generalization of the simple version of the ansatz

$$\psi_\epsilon(x_1, \ldots, x_m) = c_\epsilon \sum_{\pi \in S_m} A^\pi \prod_{j=1}^{m/2} (\mathrm{i}^{1-\epsilon} z_{\pi_{2j-1}})^{x_{2j-1}} (\mathrm{i}^\epsilon z_{2j})^{x_{2j}}. \quad (4.63)$$

This generalized ansatz solves the conditions with the generalizations on the eigenvalue and amplitudes

$$\Lambda = L + \sum_{j=1}^{m} (z_j^2 + z_j^{-2} - 2), \quad A^\pi = \mathrm{sign}(\pi). \quad (4.64)$$

Periodic boundary conditions fully specify the solution. Prescribing PBC leads to

$$\psi_\epsilon(x_2, \ldots, x_m, x_1 + L) = \psi_{1-\epsilon}(x_1, \ldots, x_m), \quad (4.65)$$

which results in one of the following equations

$$z_j^L = -\mathrm{i}^{-L/2}, \qquad \forall\, j = 1, \ldots, m, \tag{4.66}$$

$$z_j^L = \mathrm{i}^{-L/2}, \qquad \forall\, j = 1, \ldots, m. \tag{4.67}$$

These are the Bethe equations for m free-fermionic particle, where all the Bethe roots have to satisfy the equations either with $+$ or $-$ sign. As for the (2, 0) sector, certain solutions for the Bethe equations lead to identical or zero Bethe vectors. If two roots are equal up to a sign, the corresponding vector is identically zero, which is the same manifestation of the Pauli principle as before. If $z_1, \ldots, z_m$ and $z'_1, \ldots, z'_m$ are two solutions of eq. 4.66, they give the same vector, if for a set of signs $\delta_i = \pm 1$ and permutation $\pi \in S_m$, $\{z_1, \ldots, z_m\} = \{\delta_1 z'_{\pi(1)}, \ldots, \delta_m z'_{\pi(m)}\}$. In other words, if the two sets only differ by signs up to permutation, the two Bethe vectors coincide. There are $2\binom{L/2}{m}$ states in the $(m, 0)$ sector. Since z and $-z$ give the same solution, out of the L roots of the Bethe equation, only $L/2$ should be taken into account. This leads to $2\binom{L/2}{m}$ different solutions, fully determining the spectrum of these sectors.

4.3.5 Arbitrary number of domain walls, one odd domain wall $(m,\, k = 1)$

Consider the case where one odd wall is present at position x_p, the pth wall is odd. Analogously, as before, we can derive an equation for the case, when all the walls are well separated ($x_{i+1} - x_i > 2$, and particularly $|x_p - x_{p\pm1}| > 3$). This equation is essentially the same as eq. (4.61), with the only difference that the pth wall is odd. Taking the $x_{p+1} = x_p + 1$ case, when otherwise everything else is well separated, and subtracting the two equations leads to

$$\begin{aligned} &2\psi_\epsilon(\ldots, x_p, x_p + 1, \ldots; p) + \\ &\quad + (-1)^{\epsilon+p-1}\big[\psi_\epsilon(\ldots, x_p + 2, x_p + 1, \ldots; p) - \psi_\epsilon(\ldots, x_p, x_p - 1, \ldots; p) \\ &\quad + \psi_\epsilon(\ldots, x_p - 1, x_p, \ldots; p + 1) + \psi_\epsilon(\ldots, x_p + 1, x_p + 2, \ldots; p + 1)\big] = 0. \end{aligned} \tag{4.68}$$

In this case, the odd wall is the start of the 1-long string of fermion or hole. The other possibility that the odd wall is the end of the 1-long string, which leads to (denoting the original position of the odd wall by x_{p+1})

$$\begin{aligned} &2\psi_\epsilon(\ldots, x_p, x_p + 1, \ldots; p + 1) + \\ &\qquad + (-1)^{\epsilon+p-1}\big[\psi_\epsilon(\ldots, x_p + 2, x_p + 1, \ldots; p + 1) - \\ &\qquad - \psi_\epsilon(\ldots, x_p, x_p - 1, \ldots; p + 1) + \psi_\epsilon(\ldots, x_p - 1, x_p, \ldots; p) + \end{aligned} \tag{4.69}$$

$$+\psi_\epsilon(\dots,x_p+1,x_p+2,\dots;p)\big]=0.$$

There are three additional cases to consider, i.e. three wall the closest possible to each other, the odd one being in the middle, being the last one, or being the first one.
The first case is, when $x_{p+2}=x_{p+1}+1=x_p+2$, the domain wall at position x_{p+1} is the odd wall. This leads to the following equation

$$\begin{aligned}&4\psi_\epsilon(\dots,x_p,x_p+1,x_p+2,\dots;p+1)+\\&+(-1)^{\epsilon+p-1}\big[\psi_\epsilon(\dots,x_p+2,x_p+1,x_p+2,\dots;p+1)+\\&+\psi_\epsilon(\dots,x_p,x_p+1,x_p,\dots;p+1)-\psi_\epsilon(\dots,x_p,x_p-1,x_p+2;p+1)-\\&-\psi_\epsilon(\dots,x_p,x_p+3,x_p+2;p+1)+\psi_\epsilon(\dots,x_p-1,x_p,x_p+2,\dots;p)-\\&-\psi_\epsilon(\dots,x_p,x_p+2,x_p+3,\dots;p+2)\big]=0.\end{aligned}\tag{4.70}$$

In the case when $x_{p+2}=x_{p+1}+1=x_p+3$, with $x_{p+2}=x_p+3$ being the odd domain wall, we derive the following equation

$$\begin{aligned}&2\psi_\epsilon(\dots,x_p,x_p+2,x_p+3,\dots;p+2)+\\&+(-1)^{\epsilon+p-1}\big[\psi_\epsilon(\dots,x_p,x_p+2,x_p+1,\dots;p+2)-\\&-\psi_\epsilon(\dots x_p,x_p+4,x_p+3\dots;p+2)+\psi_\epsilon(\dots x_p+2,x_p+2,x_p+3\dots;p+2)\\&-\psi_\epsilon(\dots,x_p,x_p,x_p+3,\dots;p+2)-\psi_\epsilon(\dots,x_p,x_p+1,x_p+2,\dots;p+1)+\\&+\psi_\epsilon(\dots,x_p,x_p+3,x_p+4;p+1)\big]=0.\end{aligned}\tag{4.71}$$

A similar equation holds for the $x_{p+2}=x_{p+1}+2=x_p+3$ case, with x_p being the odd wall. These equations are satisfied by a similar ansatz as in the (2, 1) case: The f and g functions take the same form, and the full wavefunction ansatz is in the following form

$$\psi_\epsilon(x_1,\dots,x_{2n};p)=c_\epsilon\sum_{\pi\in S_n}A^{\pi_1\dots\pi_{2n}}\phi_p^{(\epsilon)}(u;\pi)\prod_{j=1}^{n}\left[(\mathrm{i}^{1-\epsilon}z_{\pi_{2j-1}})^{x_{2j-1}}(\mathrm{i}^{\epsilon}z_{\pi_{2j}})^{x_{2j}}\right],\tag{4.72}$$

where the one odd domain wall wave function is given by

$$\phi_p^{(\epsilon)}(u;\pi)=g(z_{\pi_p})(-1)^{\lfloor(p+\epsilon-1)/2\rfloor}\prod_{j=1}^{p-1}f(u,z_{\pi_j}).\tag{4.73}$$

The solution for the eigenvalue and amplitudes are

$$\Lambda=L+\sum_{i=1}^{2n}(z_i^2+z_i^{-2}-2),\qquad A^{\pi_1\dots\pi_{2n}}=\mathrm{sign}(\pi_1\dots\pi_{2n}).\tag{4.74}$$

Periodic boundary conditions lead to the conditions

$$\psi_\epsilon(x_1,\ldots,x_{2n-1},L+2;p)=\psi_{1-\epsilon}(2,x_1,\ldots,x_{2n-1};p+1), \tag{4.75}$$

$$\psi_\epsilon(x_1,\ldots,x_{2n-1},L+1;2n)=(-1)^{\mathcal{N}_F-1}\psi_{1-\epsilon}(1,x_1,\ldots,x_{2n-1};1). \tag{4.76}$$

The parity of the number of fermions $\mathcal{N}_F$ is equal to the number of odd domain walls, hence we conclude the following conditions

$$\begin{aligned} c_\epsilon A^{\pi_1\ldots\pi_{2n}}(\mathrm{i}^\epsilon z_{\pi_{2n}})^L(-1)^{\lfloor(p+\epsilon-1)/2\rfloor}= \\ =c_{1-\epsilon}A^{\pi_{2n}\pi_1\ldots\pi_{2n-1}}(-1)^{\lfloor(p+1-\epsilon)/2\rfloor}f(u,z_{\pi_{2n}}), \end{aligned} \tag{4.77}$$

$$\begin{aligned} c_{1-\epsilon}(-1)^{\lfloor(1-\epsilon)/2\rfloor}A^{\pi_{2n}\pi_1\ldots\pi_{2n-1}}= \\ =c_\epsilon A^{\pi_1\ldots\pi_{2n}}(\mathrm{i}^\epsilon z_{\pi_{2n}})^L(-1)^{\lfloor(2n+\epsilon-1)/2\rfloor}\prod_{j=1}^{2n-1}f(u,z_{\pi_j}). \end{aligned} \tag{4.78}$$

Using the $(-1)^{\lfloor(p+\epsilon-1)/2\rfloor}=(-1)^{\epsilon-1}(-1)^{\lfloor(p+1-\epsilon)/2\rfloor}$ identity, we obtain the same condition as before

$$c_0/c_1=\pm\mathrm{i}^{L/2+1}, \tag{4.79}$$

and similar consistency conditions, which are the Bethe equations for this case

$$z_j^L=\pm\mathrm{i}^{-L/2-1}f(u,z_j)=\pm\mathrm{i}^{-L/2}\frac{u-(z_j-1/z_j)^2}{u+(z_j-1/z_j)^2}\qquad(j=1,\ldots,2n) \tag{4.80}$$

$$\prod_{j=1}^{2n}f(u,z_j)=(-1)^n\quad\Leftrightarrow\quad\prod_{j=1}^{2n}\frac{u-(z_j-1/z_j)^2}{u+(z_j-1/z_j)^2}=1, \tag{4.81}$$

Here again, we have free-fermionic solutions, corresponding to the $u=0$ and $u=\infty$ solution.

4.3.6 Arbitrary number of domain walls, two odd domain walls (m, $k=2$)

With similar technique, the equivalent equation of eq. (4.70) describes three wall being together, the two outermost being odd. The indices of the odd walls are $p_1\equiv p$ and p_2, hence $p_2=p_1+2\equiv p+2$. There are two extra terms due to two more prohibited processes (the two odd walls cannot hop towards each other due to exclusion)

$$4\psi_\epsilon(\ldots,x_p,x_p+1,x_p+2,\ldots;p,p+2)+ \tag{4.82}$$

$$+(-1)^{\epsilon+p-1}\big[\psi_\epsilon(\dots,x_p+2,x_p+1,x_p+2,\dots;p,p+2)+$$
$$+\psi_\epsilon(\dots,x_p,x_p+1,x_p,\dots;p,p+2)-\psi_\epsilon(\dots,x_p,x_p-1,x_p+2,\dots;p,p+2)$$
$$-\psi_\epsilon(\dots,x_p,x_p+3,x_p+2,\dots,\dots;p,p+2)+$$
$$+\psi_\epsilon(\dots,x_p-1,x_p,x_p+2,\dots;p+1,p+2)-$$
$$-\psi_\epsilon(\dots,x_p,x_p+2,x_p+3,\dots;p,p+1)\big]=0.$$

The equivalent equation of eq. (4.71) is similar. These equations are satisfied by the two particle generalization of the nested ansatz

$$\psi_\epsilon(x_1,\dots,x_{2n};p_1,p_2)=c_\epsilon\sum_{\pi\in S_{2n}}A^{\pi_1\dots\pi_{2n}}\sum_{\sigma\in S_2}B^{\sigma_1\sigma_2}$$
$$\phi^{(\epsilon)}_{p_1}(u_{\sigma_1};\pi)\phi^{(\epsilon)}_{p_2}(u_{\sigma_2};\pi)\prod_{j=1}^{n}\left[(\mathrm{i}^{1-\epsilon}z_{\pi_{2j-1}})^{x_{2j-1}}(\mathrm{i}^{\epsilon}z_{\pi_{2j}})^{x_{2j}}\right],\quad(4.83)$$

Here the eigenvalue and the wavefunction amplitudes are

$$\Lambda=L+\sum_{i=1}^{m}(z_i^2+z_i^{-2}-2),\quad A^\pi=\mathrm{sign}(\pi),\quad B^\sigma=\mathrm{sign}(\sigma).\qquad(4.84)$$

Periodic boundary conditions lead to

$$\psi_\epsilon(x_1,\dots,x_{2n-1},L+2;p_1,p_2)=\psi_{1-\epsilon}(2,x_1,\dots,x_{2n-1};p_1+1,p_2+1),\quad(4.85)$$
$$\psi_\epsilon(x_1,\dots,x_{2n-1},L+1;p_1,2n)=(-1)^{\mathcal{N}_F-1}\psi_{1-\epsilon}(1,x_1,\dots,x_{2n-1};1,p_1+1).\quad(4.86)$$

These result in $c_0/c_1=\pm\mathrm{i}^{L/2+2}$, and the Bethe equations for two odd particles follow

$$z_j^L=\pm\mathrm{i}^{-L/2}\prod_{k=1,2}\frac{u_k-(z_j-1/z_j)^2}{u_k+(z_j-1/z_j)^2},\qquad j=1,\dots,2n\qquad(4.87)$$

$$1=\prod_{j=1}^{2n}\frac{u_k-(z_j-1/z_j)^2}{u_k+(z_j-1/z_j)^2},\qquad k=1,2.\qquad(4.88)$$

4.3.7 Arbitrary number of domain walls, arbitrary number of odd domain walls ($m=2n$, k)

This is a straightforward generalization of the previous cases. The similar, but more general equations are solved by the general form of the ansatz

$$\psi_\epsilon(x_1,\dots,x_{2n};p_1,\dots p_m) = c_\epsilon \sum_{\pi\in S_{2n}} A^{\pi_1\dots\pi_{2n}} \sum_{\sigma\in S_m} B^{\sigma_1\dots\sigma_m} \prod_{j=1}^{m} \phi^{(\epsilon)}_{p_j}(u_{\sigma_j};\pi) \prod_{j=1}^{n} \left[(\mathrm{i}^{1-\epsilon} z_{\pi_{2j-1}})^{x_{2j-1}} (\mathrm{i}^{\epsilon} z_{\pi_{2j}})^{x_{2j}}\right], \quad (4.89)$$

where the nested wavefunction of the odd domain walls is

$$\phi^{(\epsilon)}_p(u;\pi) = g(z_{\pi_p})(-1)^{\lfloor (p+\epsilon-1)/2\rfloor} \prod_{j=1}^{p-1} f(u, z_{\pi_j}). \quad (4.90)$$

The amplitudes and the eigenvalue take the usual form

$$\Lambda = L + \sum_{i=1}^{2n} (z_i^2 + z_i^{-2} - 2), \quad A^\pi = \mathrm{sign}(\pi), \quad B^\sigma = \mathrm{sign}(\sigma). \quad (4.91)$$

and the Bethe equations take their most general form

$$z_j^L = \pm \mathrm{i}^{-L/2} \prod_{k=1}^{m} \frac{u_k - (z_j - 1/z_j)^2}{u_k + (z_j - 1/z_j)^2}, \qquad j = 1,\dots,2n \quad (4.92)$$

$$1 = \prod_{j=1}^{2n} \frac{u_k - (z_j - 1/z_j)^2}{u_k + (z_j - 1/z_j)^2}, \qquad k = 1,\dots,m. \quad (4.93)$$

By this, we derived the Bethe equations for the most general case.

4.4 Symmetries

The original motivation of this work is to understand the high degeneracy at all energy levels. Table 4.1 shows the degeneracy of the groundstate, the least degenerate energy level and the number of energy levels both for periodic and antiperiodic boundary conditions. The degeneracies seem to be *extensive*: the degeneracy of all energy levels scales exponentially with the system size.
For a better understanding we also consider the model with antiperiodic boundary conditions (APBC), defined by $c_{i+L} = c_i^\dagger$. Table 4.2 shows the groundstate energies for both boundary conditions. As table 4.2 suggests, with periodic boundary conditions (PBC), for $L = 4n$, the groundstate energies are 0, while for $L = 4n-2$, they are positive. However, the antiperiodic groundstate energies are 0 for $L = 4n-2$. The groundstate degeneracy G shows the following extensiveness with PBC and APBC for $L = 4n$ and $L = 4n-2$, respectively

$$\#\text{ of GS: } 2^{\frac{L}{2}+1}. \quad (4.94)$$

	periodic			antiperiodic		
L	G	ℓ	e	G	ℓ	e
4	8	8	2	4	4	3
5	8	4	5	8	4	5
6	16	16	4	16	16	4
7	16	8	15	16	8	15
8	32	16	7	16	8	19
9	32	8	56	32	8	56
10	16	16	45	64	16	45
11	64	8	215	64	8	215
12	128	32	79			

Table 4.1: The degeneracy G of the groundstate, the degeneracy ℓ of the least degenerate energy level and the number of energy levels e both for periodic and antiperiodic boundary conditions.

Later we give a natural explanation why we consider periodic and antiperiodic BC for $L = 4n$ and $L = 4n - 2$, respectively.
The abundance of degeneracies suggests a high number of symmetries. There are many symmetries in the model, most obviously the supersymmetry and the fermion–hole symmetry. The extensive degeneracy is explained by a process similar to Cooper pairs in the BCS theory of superconductivity [108, 111]. From an existing solution a new one is created by turning two even domain walls into odd ones, with u and $-u$ as nested Bethe roots. Such pairs of odd domain walls are much like Cooper pairs.

4.4.1 Supersymmetry

By construction, the model possesses supersymmetry, the Hamiltonian exchanges with the supersymmetry generators

$$[H,\, Q] = 0, \qquad [H,\, Q^\dagger] = 0. \tag{4.95}$$

Examine the effect of these generators on a sector $(m,\, k)$. As they are sums of $d_i^\dagger + e_i$ and $d_i + e_i^\dagger$ respectively, they add or remove a fermion or hole, introducing or removing two domain walls, one even and one odd

$$Q:\ (m,k) \mapsto (m+2, k+1), \qquad Q^\dagger:\ (m,k) \mapsto (m-2, k-1). \tag{4.96}$$

	periodic		antiperiodic	
L	G	Λ_{GS}	G	Λ_{GS}
4	8	0.000	4	0.000
5	8	0.000	8	0.000
6	16	0.268	16	0.000
7	16	0.000	16	0.000
8	32	0.000	16	0.000
9	32	0.000	32	0.000
10	16	0.087	64	0.000
11	64	0.000	64	0.000
12	128	0.000		

Table 4.2: The degeneracy G of the groundstate, and the Λ_{GS} groundstate energy both for periodic and antiperiodic boundary conditions.

4.4.2 Domain wall number conversation and translation symmetry

The Bethe ansatz solution based on the property of the model that for even system sizes L, the number of domain walls ($\mathcal{D}$), and separately the number of even and odd domain walls ($\mathcal{D}_e$ and $\mathcal{D}_o$) are conserved

$$[H, \mathcal{D}] = 0, \quad [H, \mathcal{D}_e] = 0, \quad [H, \mathcal{D}_o] = 0. \tag{4.97}$$

By the periodic boundary conditions, the model is also invariant under the translation operator T. By applying T, the role of even and odd domain walls is exchanged, hence

$$T : (m, k) \mapsto (m, m - k). \tag{4.98}$$

4.4.3 Fermion parity symmetry

Despite the number of fermions is not conserved, the number of fermions always changes by two, hence the parity of the fermions is conserved. Define the fermion parity operator

$$P \left|\tau_1, \ldots, \tau_L\right\rangle = (-1)^{\mathcal{N}_L} \left|\tau_1, \ldots, \tau_L\right\rangle. \tag{4.99}$$

The supersymmetry generators change the parity, hence they anti-commute

$$\{P, Q\} = 0, \qquad \{P, Q^\dagger\} = 0. \tag{4.100}$$

From this, the symmetry is a trivial consequence

$$[P, H] = 0. \tag{4.101}$$

4.4.4 Fermion–hole symmetry

The model is introduced in a fermion–hole symmetric way. Define the Majorana operators

$$\Gamma =: \prod_{i=1}^{L} \gamma_i :, \qquad \gamma_i = c_i + c_i^\dagger. \tag{4.102}$$

The operator Γ acts on a state $|\tau_1\tau_2\ldots\rangle$ as exchanging fermions and holes. It is easy to prove that this is symmetry of the model,

$$[H, \Gamma] = 0. \tag{4.103}$$

Depending on system size, Γ either commutes or anticommutes with the generators

$$Q\Gamma + (-1)^L \Gamma Q = 0, \qquad Q^\dagger\Gamma + (-1)^L \Gamma Q^\dagger = 0. \tag{4.104}$$

4.4.5 Domain wall–non-domain wall symmetry

Define non-domain walls, as particles on the dual lattice of domain walls, occupying sites without domain walls. Non-domain walls have similar properties to domain walls: Their number and parity are conserved.
It is physically motivated that a domain wall–non-domain wall symmetry is present in the model: The displacement of domain walls (eqs. (4.17) and (4.18)), e.g. $|\ldots 1|000\ldots\rangle \leftrightarrow |\ldots 111|0\ldots\rangle$ and the interaction of even and odd domain walls (eqs. (4.19) and (4.20)), e.g. $|\ldots 0|1|00\ldots\rangle \leftrightarrow |\ldots 00|1|0\ldots\rangle$ are identical of interaction of even and odd non-domain walls, and displacement of non-domain walls, respectively. Define the domain wall–non-domain wall symmetry operator

$$E =: \prod_{i=1}^{L/2} (c_{2i} - c_{2i}^\dagger) :, \tag{4.105}$$

which satisfies the following commutation relations

$$EQ = Q^\dagger E, \quad EQ^\dagger = QE, \quad [E, H] = 0. \tag{4.106}$$

The domain wall–non-domain wall symmetry maps the sectors (m, k) and $(L - m, L/2 - m + k)$ into each other. This solves the so called "over the equator" problem [112–114]. Finding Bethe solutions over half-filling of the pseudo-vacuum raises difficulties, but utilizing the domain wall–non-domain wall symmetry, it is enough to probe the states up to half-filling.

4.4.6 Shift symmetry

A further symmetry is found, by examination of small systems. Define the shift operator

$$S = \sum_{i=1}^{L} n_{i-1}\gamma_i p_{i+1} + p_{i-1}\gamma_i n_{i+1}, \qquad \gamma_i = c_i + c_i^\dagger. \tag{4.107}$$

This operator shifts a domain wall either to the left or to the right by one. S is self-adjoint by construction, and easy to see that it is a symmetry

$$\{Q,\, S\} = 0, \quad \{Q^\dagger,\, S\} = 0, \qquad [H, S] = 0. \tag{4.108}$$

The shift operator relates the sector $(m,\, k)$ with the sectors $(m,\, k \pm 1)$.

4.4.7 Reflection symmetry of the spectrum for $L = 4n$

For $L = 4n$, $n \in \mathbb{N}$ the groundstate energy is exactly zero: $\Lambda_0 = 0$, which we compute in section 4.5.3. Similarly, the largest energy level is given by $\Lambda_{\max} = L$. We observed that the spectrum has a reflection symmetry, i.e. for every energy level $\Lambda = L - \Delta\Lambda$ there is a corresponding reflected one $\tilde{\Lambda} = \Delta\Lambda$ with the same degeneracy. The states on these two energy levels are related by a bijective operator, defined in the following way. Define an other type of Majorana operator

$$\delta_j = \mathrm{i}\,(c_j - c_j^\dagger), \qquad \delta_j^\dagger = \delta_j. \tag{4.109}$$

The reflection operator then defined as

$$M =: \prod_{i=0}^{n-1} \delta_{4i+1}\delta_{4i+2} := (-1)^n : \prod_{i=0}^{n-1} (c_{4i+1} - c_{4i+1}^\dagger)(c_{4i+2} - c_{4i+2}^\dagger) : . \tag{4.110}$$

The operator M is (anti)hermitian depending on the parity of n, and squares to a multiple of the identity,

$$M^\dagger = (-1)^n M, \qquad M^2 = (-1)^n \mathbb{I}. \tag{4.111}$$

Obviously, this operator is not expected to commute with H, rather the reflecting property is encoded in the following equation

$$M(L\mathbb{I} - H) = HM, \tag{4.112}$$

which means exactly that for every eigenstate, there is a corresponding reflected one

$$H\,|\Psi\rangle = \Lambda\,|\Psi\rangle \Leftrightarrow HM\,|\Psi\rangle = (L - \Lambda)M\,|\Psi\rangle\,. \tag{4.113}$$

A good example of the pairing is the pseudo-vacuum state $|00\ldots0\rangle$, which maps into the half-filled true groundstate, $M|00\ldots0\rangle = \pm|110011001\ldots100\rangle$, where the sign depends on the system size. It is easy to see that the pseudo-vacuum has energy $\Lambda = L$, while the other state is indeed a groundstate, $\Lambda = 0$.

4.4.8 Antiperiodic boundary conditions and reflection symmetry of the spectrum for $L = 4n - 2$

The reflection symmetry can be extended to $L = 4n - 2$ system sizes by taking into account the model with antiperiodic boundary conditions. The intuition is the following: Compare the same mapping for $L = 4n$ and $L = 4n - 2$

$$M|00\ldots0\rangle_{L=4n} = \pm|110011001\ldots100\rangle_{L=4n} \tag{4.114}$$

$$M|00\ldots0\rangle_{L=4n-2} = \pm|110011001\ldots011\rangle_{L=4n-2} \tag{4.115}$$

For $L = 4n$ systems, the 1100 pattern is repeated, while for the $L = 4n - 2$ systems, there is a "defect", an "accumulated" 1111 or 0000 string. This intuitively shows that this state is not a $\Lambda = 0$ state (as it is indeed not). Considering the model with antiperiodic boundary conditions removes this "defect", as under antiperiodic boundary conditions, the role of fermions and holes exchanges under a full turn.
Introduce antiperiodic boundary conditions by

$$c^\dagger_{i+L} = c_i. \tag{4.116}$$

This modifies the Hamiltonian which we denote by H_{AP}. The spectrum of the antiperiodic Hamiltonian has the same reflection symmetry as the periodic for $L = 4n$. M is boundary condition independent. The following equation describes the antiperiodic case for $L = 4n$ system size

$$M(L\mathbb{I} - H^{(L=4n)}_{AP}) = H^{(L=4n)}_{AP} M, \tag{4.117}$$

where for clarity we emphasized the system size $L = 4n$.
More interestingly, for $L = 4n-2$, the period and antiperiodic cases are related: For an eigenstate of H_{AP} with energy Λ_{AP}, there is a corresponding state of H with energy $L-\Lambda_{AP}$. The largest energy for H is $\Lambda_{P,max} = L$, which corresponds to the antiperiodic groundstate with zero energy, $\Lambda_{AP,GS} = 0$. This reflection is realized by the following operator equation

$$M(L\mathbb{I} - H^{(L=4n-2)}_{AP}) = H^{(L=4n-2)}_{P} M, \tag{4.118}$$

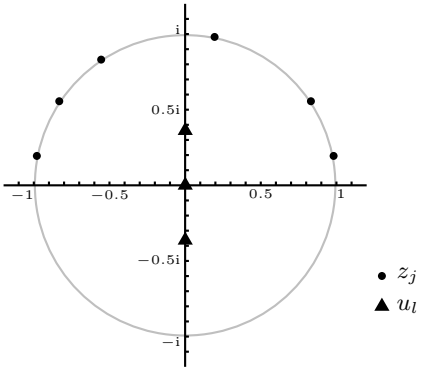

Figure 4.1: $L = 16$, (6, 3) sector, $\Lambda = 6.613$, free-fermionic solution. The six z_j's take six values of the 8th unit roots. Two u_l's form a zero mode Cooper pair, hence they are imaginary and each others negative.

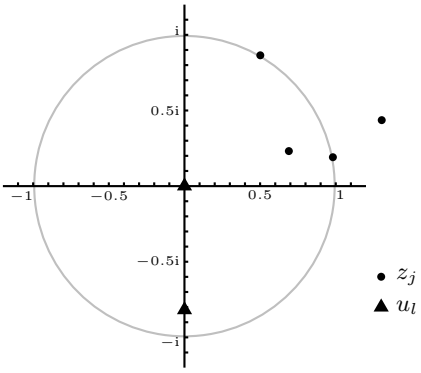

Figure 4.2: $L = 10$, (4, 2) sector, $\Lambda = 6.721$, non free-fermionic solution. The z_j's not on the unit circle are related as $z \to (z^*)^{-1}$.

where we stressed the system size $L = 4n - 2$ and the periodic Hamiltonian by H_P.
A good example again if we take e.g. the state $|000\ldots00\rangle$ with $L = 4n - 2$, which is an eigenvector of H_P with the largest eigenvalue $\Lambda_P = L$. This state is mapped to $|1100110\ldots0011\rangle$, where the first two and last two sites are occupied. This is a groundstate of the antiperiodic Hamiltonian, as the role of fermions and holes exchanges during a full round.

4.4.9 Zero mode Cooper pairs

Consider a free-fermionic solution of the Bethe equations, satisfying the equation

$$z_j^L = \pm \mathrm{i}^{-L/2}, \quad j = 1, \ldots, m. \tag{4.119}$$

The same equation is satisfied, if we turn two even domain walls into odd ones (and keep the total number of domain walls the same) with nested rapidities

which are each other's negative, $u_2 = -u_1$. The new Bethe equations are

$$z_j^L = \pm \mathrm{i}^{-L/2} \frac{u_1 - (z_j - 1/z_j)^2}{u_1 + (z_j - 1/z_j)^2} \frac{u_2 - (z_j - 1/z_j)^2}{u_2 + (z_j - 1/z_j)^2}, \qquad j = 1, \ldots, m \tag{4.120}$$

$$1 = \prod_{j=1}^{m} \frac{u_l - (z_j - 1/z_j)^2}{u_l + (z_j - 1/z_j)^2}, \qquad l = 1, 2. \tag{4.121}$$

The first equations are automatically satisfied, if $u_2 = -u_1$, since the product of the two fractions is one

$$\frac{u_1-(z_j-1/z_j)^2}{u_1+(z_j-1/z_j)^2} \times \frac{u_2-(z_j-1/z_j)^2}{u_2+(z_j-1/z_j)^2} = \frac{u_1-(z_j-1/z_j)^2}{u_1+(z_j-1/z_j)^2} \times \frac{u_1+(z_j-1/z_j)^2}{u_1-(z_j-1/z_j)^2} = 1. \tag{4.122}$$

Since the set of z's is already given, we can regard the second equations as rational equations for the unknown u's, and hence determine the possible u_1, u_2 pairs. Starting from a free-fermionic z solution, the solutions always contain such pairs which are each other's negative.
We can continue like this, introducing new pairs of u's, as long as m is large enough to generate new solutions from the $1 = \prod_{j=1}^{m} \frac{u-(z_j-1/z_j)^2}{u+(z_j-1/z_j)^2}$ equation. We address this question in more details in appendix C.1. Similarly, we can start from a non free-fermionic sector, with $k \neq 0$. Some typical solutions to the Bethe equations are shown in figs. 4.1 to 4.3.
We have not found an explicit operator that creates the Cooper pairs, acting on appropriate states. If such an operator can be constructed, it must either select one of the solution pairs $(u, -u)$ of eq. (4.121), or more likely create a linear combination of all such solution pairs. Since the pairs do not affect the energy, such linear combination is an eigenstate of the Hamiltonian, but not a pure Bethe state.

4.5 Completeness of the Bethe solution and exact solutions

One of the main question regarding the Bethe ansatz solution is its completeness: Whether all the eigenvectors are Bethe vectors with associated Bethe roots. We have addressed this question in certain finite size cases. We found that the Bethe solutions only form a subset of all the eigenvectors, and utilizing symmetry operators, we recover the full Hilbert space. Our examination is based on comparing the direct diagonalization results with numerical solutions to the Bethe equations.

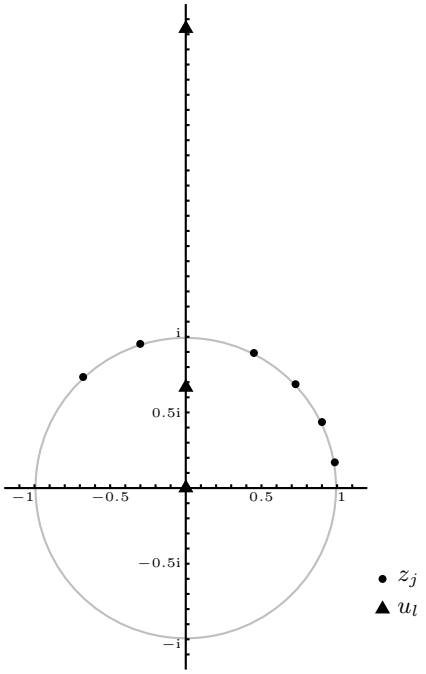

Figure 4.3: $L = 16$, (6, 3) sector, $\Lambda = 2.226$, non free-fermionic solution on the complex plane. The six z_j's are on the unit circle, but do not take the values of the 8^{th} unit roots.

There are two symmetries which are systematically used: the translation symmetry T and the domain wall–non-domain wall symmetry E. T maps the (m, k) sector to $(m, m-k)$, while E maps it to $(L-m, L/2-k)$. Applying both, the image of $(m\,k)$ is $(L-m, L/2-m+k)$

$$T: \qquad (m, k) \to (m, m-k) \tag{4.123a}$$
$$E: \qquad (m, k) \to (L-m, L/2-k) \tag{4.123b}$$
$$ET = TE \; (m, k) \to (L-m, L/2-m+k) \tag{4.123c}$$

These mappings allow us to reduce our examination to sectors with $m \leq L/2$ domain walls, and $k \leq m/2$ odd domain walls.
We recovered all the states in the probed cases, but other then T and E, we

Λ	deg.
0.268	16
2.000	16
3.732	16
6.000	16

Table 4.3: $L = 6$ sector energy levels and degeneracies.

m	k	dim.
0	0	2
2	0, 2	6, 6
2	1	18
4	2	18
4	1, 3	6, 6
6	3	2

Table 4.4: $L = 6$ sectors. Certain sectors have the same dimensions and are listed in the same line.

did not find a general scheme to do it: the application of the various symmetry operators was otherwise *ad hoc* without any apparent pattern. To address this question more carefully, much more extensive studies of small systems is needed, which might be a subject of further research.
The studied examples were the full spectrum of the $L = 6$ system and the most degenerate eigenvalue of $L = 10$, the $\Lambda = 6$ eigenvalue.

4.5.1 $L = 6$, full spectrum

The $L = 6$ Hamiltonian is easily solved by direct diagonalization. There are four energy levels, all of them are 16-folded degenerate (table 4.3).
There are eight sectors in the Hilbert space, and three of them should be considered: (0, 0), (2, 0), and (2, 1), the rest follows via T and E. The list of the sectors is in table 4.4.

$\Lambda = 6$ eigenvalue

The (0, 0) sector contains two trivial Bethe vectors: $|b_1\rangle = |000000\rangle$ and $|b_2\rangle = |111111\rangle$, both are eigenvectors with $\Lambda = 6$. By applying Q, two more states are created in (2, 1), $Q|b_1\rangle$ and $Q|b_2\rangle$. By applying E, we create four more states, two in (4, 2) and two in (6, 3): $EQ|b_1\rangle = Q^\dagger E|b_1\rangle$, $EQ|b_2\rangle = Q^\dagger E|b_2\rangle$, $E|b_1\rangle$, $E|b_2\rangle$.
In the (2, 1) sector, the Bethe equations are

$$z_j^6 = \pm \mathrm{i}^{-3} \frac{u - (z_j - 1/z_j)^2}{u + (z_j - 1/z_j)^2}, \qquad j = 1, 2, \tag{4.124}$$

$$1 = \prod_{j=1}^{2} \frac{u - (z_j - 1/z_j)^2}{u + (z_j - 1/z_j)^2}. \tag{4.125}$$

This has two independent non-free-fermionic solutions, with $\Lambda = 6$ eigenvalues

$$\left(z_1^2, z_2^2, u_\pm\right) = \left(\frac{\sqrt{3}}{2}\left(\sqrt{3} + \mathrm{i}\right), \frac{1}{2\sqrt{3}}\left(\sqrt{3} + \mathrm{i}\right), \frac{1}{39}\left(-9 \pm 14\sqrt{3}\right)\right). \tag{4.126}$$

Denote the corresponding two Bethe vectors by $|b_3\rangle$ and $|b_4\rangle$. Starting from these two, we generate all the remaining eight vectors. There are four vectors in (2, 1), namely: $|b_3\rangle$, $|b_4\rangle$, $Q^\dagger E\,|b_3\rangle = EQ\,|b_3\rangle$, $Q^\dagger E\,|b_4\rangle = EQ\,|b_4\rangle$, and these vectors mapped to (4, 2) by E: $E\,|b_3\rangle$, $E\,|b_4\rangle$, $Q\,|b_3\rangle$, $Q\,|b_4\rangle$, respectively.
With using all these symmetries, we recovered all the sixteen eigenvectors corresponding to $\Lambda = 6$, for $L = 6$.

Other eigenvalues

The (2, 0) sector is completely determined by the free-fermionic solution. The Bethe equations here are $z_j^6 = \pm\mathrm{i}^{-3}$, $j = 1, 2$. The (+) equation has 3 distinct solution, 1-1-1 for the three lowermost eigenvalues ($\Lambda_1 = 0.268$, $\Lambda_2 = 2$, $\Lambda_3 = 3.732$). The same hold for the (−) solution. These solutions are mapped to (2, 2), (4, 1) and (4, 3) by T, E and TE respectively. So far, we have found an 8-fold degeneracy for the lower three eigenvalues, we need to find a further 8-fold degeneracy. There are indeed four-four states in sectors (2, 1) and (4, 2) belonging to each of the lower three eigenvalues. These four-four solutions are achieved as follows: $u = 0$ and $u = \infty$ leads to one-one free-fermionic solution for each eigenvalues, call them $|f_1^{(i)}\rangle$ and $|f_2^{(i)}\rangle$, where $i = 1, 2, 3$ denotes the corresponding eigenvalue. In this case, $\{|f_1^{(i)}\rangle$, $|f_2^{(i)}\rangle\, EQ|f_1^{(i)}\rangle$, $EQ|f_2^{(i)}\rangle\}$ and $\{E|f_1^{(i)}\rangle$, $E|f_2^{(i)}\rangle\, Q|f_1^{(i)}\rangle$, $Q|f_2^{(i)}\rangle\}$, $i = 1, 2, 3$ are the sets of remaining states in (2, 1) and (4, 2) respectively.
These concludes that we indeed recovered the full Hilbert space from the Bethe solutions via symmetries.

4.5.2 $L = 10$, $\Lambda = 6$ eigenvalue

The other example, we probed, is the $\Lambda = 6$ eigenvalue of $L = 10$, which is the most, 64-fold degenerate eigenvalue of the system. The domain wall–non-domain wall symmetry E alows us, to consider only the sectors (m, k) with $m < L/2 = 4$. The sector by sector degeneracies are listed in table 4.5. The four states in (2, 0) are Bethe states, this is always the case for (m, 0) sectors. Denote the subspace

m	k	deg. of $\Lambda = 6$
0	0	0
2	0,2	4
2	1	8
4	0	0
4	1,3	4
4	2	8

Table 4.5: $L = 10$, $\Lambda = 6$ degeneracies sector by sector. The unlisted sectors follow by DW–nonDW symmetry.

of these four solutions by $\mathcal{B}^{(2,\,0)}$. By translation, we create the corresponding subspace in (2, 2), $\mathcal{B}^{(2,\,2)} = T\mathcal{B}^{(2,\,0)}$. There are further four free-fermionic solutions in (2, 1), spanning $\mathcal{B}^{(2,\,1)}$. Acting with Q on these three subspaces, we generate 4-4-4 further solutions: Action of Q is $(m,\,k) \mapsto (m+2,\,k+1)$, hence $Q\mathcal{B}^{(2,\,0)}$, $Q\mathcal{B}^{(2,\,1)}$, $Q\mathcal{B}^{(2,\,2)}$ are subspaces in (4, 1), (4, 2), (4, 3), respectively.
S is a symmetry operator which shifts the walls by one position, hence it maps $(m,\,k) \mapsto (m,\,k+1) \oplus (m,\,k-1)$. Acting with S on $Q\mathcal{B}^{(2,0)}$ creates two linearly independent vector in (4, 2) (and two linearly dependent one). Similarly, $SQ\mathcal{B}^{(2,2)}$ creates further two linearly independent vector in (4, 2) (and again, two linearly dependent one). This gives the expected 8-fold degeneracy of the sector (4, 2). From these four vectors, Q creates four further independent vectors in (2, 1). $QSQ\mathcal{B}^{(2,0)}$ and $QSQ^{\dagger}\mathcal{B}^{(2,2)}$ contain 2-2 linearly independent vectors in (2, 1). This gives the expected degeneracy in the sector (2, 1), and the remaining degeneracy is constructed by the domain wall–non-domain wall symmetry, E. The scheme of the full process is in fig. 4.4.
It would be interesting to find the full underlying symmetry algebra, i.e. the general algorithm to create all the eigenvectors. This is however seems fairly nontrivial as there is no obvious similarity in the discussed examples.

4.5.3 The groundstate and first excited state for $L = 4n$

In the half-filled sector $(2n,\,0)$ with $L = 4n$, the Bethe equations are

$$z_j^{4n} = \pm \mathrm{i}^{-4n/2} = \pm(-1)^n = \pm 1, \quad j = 1, \ldots, 2n, \tag{4.127}$$

which are satisfied by the free-fermionic solutions:

$$z_j^{(+)} = \mathrm{e}^{\frac{\mathrm{i}\pi j}{2n}} \quad (j = 1, \ldots, 2n), \qquad z_j^{(-)} = \mathrm{e}^{\frac{\mathrm{i}\pi(2j+1)}{4n}} \quad (j = 1, \ldots, 2n). \tag{4.128}$$

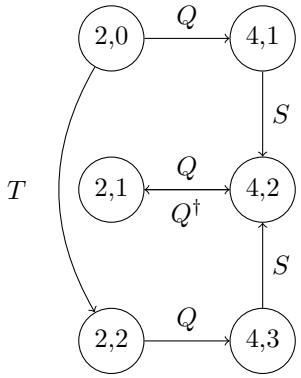

Figure 4.4: Action of symmetries between domain wall sectors

Both solutions produce a groundstate, as it is easy to check

$$\Lambda^{(\pm)} = 4n + \sum_{j=1}^{2n} (z_j^2 + z_j^{-2} - 2) = 0. \tag{4.129}$$

These two solutions span the subspace $(2n,\, 0)$, which is 2 dimensional, where an other basis is formed by $|0011\ldots0011\rangle$ and $|1100\ldots1100\rangle$.
There are further groundstates in the $(2n,\, k)$ sectors which are generated by the described Cooper-pair process. In the presence of k odd domain walls, the u's satisfy the constrain

$$1 = \prod_{j=1}^{2n} \frac{u - (z_j - 1/z_j)^2}{u + (z_j - 1/z_j)^2} \quad (l = 1, \ldots, k). \tag{4.130}$$

Setting $z_j = z_j^{(+)}$ or $z_j = z_j^{(-)}$ in eq. (4.130) gives the rational function for u's to satisfy. This has purely imaginary roots in complex conjugate pairs. Any combination of these pairs forms a new, valid solution, due to zero mode Cooper pairs.
The Cooper pairs give an overall degeneracy to the groundstate which grows exponentially with the system size L. This is intuitively clear, since $L = 4n$, and in a sector $(2n,\, k)$, (with even k) there are roughly $\binom{n}{k/2}$ states, generated by zero modes. Summing over k gives the full degeneracy which is consequently exponential. A detailed examination is in appendix C.1.

Based on the explicit solutions of the $L = 4,\ 8,\ 12$ systems, we observed that the first excited states occur in the sectors $(2n \pm 2,\ k)$, with arbitrary k, and$(2n,\ k)$ with $k \neq 0,\ 2n$. As for the $(2n - 2,\ 0)$ sector, the Bethe equations are free-fermionic, we can determine the the first excited state energy.
The Bethe equations for $L = 4n$, in the $(2n - 2,\ 0)$ sector are

$$z_j^L = \pm \mathrm{i}^{-L/2} = \pm(-1)^n = \pm 1, \quad j = 1, \ldots, 2n-2 \tag{4.131}$$

which have the solutions as described in eq. (4.128). The only difference is that out of the $2n$ solutions, we have to choose $2n - 2$ which minimizes the energy $\Lambda = 4 + \sum_{i=1}^{2n-2} z_i^2 + z_i^{-2}$. To do so, we have to leave out the two Bethe roots contributing the most. The two largest contribution is coming from the Bethe roots $z_{2n}^{(+)} = 1$, $z_1^{(+)} = \mathrm{e}^{\mathrm{i}\pi/(2n)}$ for the $(+)$ case and $z_1^{(-)} = \mathrm{e}^{\mathrm{i}\pi/(4n)}$, $z_{2n-1}^{(-)} = \mathrm{e}^{-\mathrm{i}\pi/(4n)}$ for the $(-)$ case. The two associated energy levels are

$$\Lambda^{(+)}(L = 4n) = 4 - 2 - 2\cos(\pi/n) = 2(1 - \cos(\pi/n)) \tag{4.132}$$

$$\Lambda^{(-)}(L = 4n) = 4 - 4\cos(\pi/2n) = 4(1 - \cos(\pi/2n)) \tag{4.133}$$

As $\Lambda^{(-)} < \Lambda^{(+)}$ gives the lower energy, $\Lambda^{(-)}$is the energy of the first excited state. This result correctly reproduces the $L = 4,\ 8,\ 12$ first excited state energies. Note that this investigation is based on the assumption that the $(2n - 2,\ 0)$ sector contains first excited states.
The groundtate energy is $\Lambda_0 = 0$, hence the energy gap of the system is

$$\Delta\Lambda_n = \Lambda_n^{(-)} - \Lambda_0 = 4(1 - \cos(\pi/2n)) \approx \frac{\pi^2}{2n^2}. \tag{4.134}$$

The gap vanishes as $\sim 1/L^2$, which is a sign of classical diffusive mode. As this is strictly speaking a conjecture, this result is strictly speaking an upper bound on the energy gap.

4.6 Conclusion and outlook

We have introduced a new lattice supersymmetric chain in which fermion number conservation is violated. The model turns out to be integrable and we give a detailed derivation of the equations governing the spectrum using nested coordinate Bethe ansatz. The energy spectrum is highly degenerate, all states with a finite density have an extensive degeneracy. This degeneracy is explained by the identification of several symmetry operators, but most significantly by the possibility at each level to create modes that do not cost any energy. These modes

are analoguous to Cooper pairs in BCS theory, and our model contains a direct realisation of these which can be explicitly identified in the Bethe equations. The class of finite solutions to the Bethe ansatz does not provide all eigenvectors. We give circumstantial evidence that all eigenvectors are obtained by the application of the symmetry operators on Bethe vectors. We furthermore find that the energy gap to the first excited state scales as $\sim 1/L^2$ where L is the system size which is a signature of classical diffusion.

Chapter 5

Conclusion and outlook

During my doctorate, my research focused on three main topics. The common theme in all three projects is integrability. Being involved in diverse researches during the four years of my doctorate allowed me to learn many techniques to probe integrable systems.
I studied integrable quantum field theories during my MSc, and my interest turned towards integrable lattice models and integrable quantum chains after starting my doctorate. Lattice models and quantum chains are closely related. This is most apparent in the transfer matrix formalism, as typically the logarithmic derivative of the transfer matrix of the lattice model corresponds to the Hamiltonian of the related quantum chain.
In the first and second main chapters I studied two different lattice models in statistical physics. The first model, I studied, is the dilute $O(n = 1)$ loop model, a model which is based on the dilute version of the Temperley-Lieb algebra, and related to the Izergin-Korepin 19-vertex model. I considered the model on a strip with finite width and infinite height, with open boundary conditions. The model describes the statistical ensemble of closed loops, possibly connected to the boundaries.
We considered the boundary to boundary spin-1 current. On the lattice, the current between two arbitrary points is expressed in terms of two "elementary" currents, X and Y which describe the current through a horizontal or a vertical edge, respectively. We found explicit expressions for these two types of currents on the inhomogeneous lattice. The Y current turned out to be translation invariant. We expressed these currents in terms of the partition sum of the model, and symmetric polynomials.
Our solution is based on the quantum Knizhnik-Zamolodchikov equations. The

qKZ equations give relations between the eigenvector of the transfer matrix with different permutations of the inhomogeneities. Based on the qKZ equations and some plausible minimal assumption on certain elements of the goundstate vector, we recovered the full groundstate vector of transfer matrix – a program similar to form factor bootstrap in integrable field theories. This method was found to be powerful to compute exact results in a number of cases, including our result for the spin-1 current. There is no Bethe ansatz approach directly for loop models, for the Temperley-Lieb algebra, Bethe ansatz was considered in the vertex (or spin) basis. Lacking of Bethe ansatz makes qKZ equations particularly important for loop models. However, this technique has some limitations: The loop weight is limited to $n = 0$ or 1, otherwise the eigenvector does not constitute polynomial entries, making the computation practically impossible. Achieving the analytic result also includes considerable amount of guesswork.

There are some further possibilities to consider: We can investigate further to compute different quantities with the same technique. We made some sizable efforts to compute different one point functions and correlators, however, these attempts did not lead to success. As the current was computed on the lattice, the continuum limit of the current is naturally interesting.

In the second chapter, we considered a whole family of lattice models, the $n \times n$ fused RSOS models, and studied the $n = 2$ case in more detail. These fused RSOS models are characterized by the λ crossing parameter, and the fusion level n. The nth level fused RSOS model is constructed based on the $n = 1$ unfused RSOS model, by considering the $n \times n$ configurations of the unfused R-matrix. We investigated the continuum limit of fused models via the Corner Transfer Matrix method, and finitized characters. The continuum limit is a higher level minimal model, where the exact correspondence depends on n and λ. The identification is based on the comparison of one-dimensional sums computed by Corner Transfer Matrix method and finitized characters of the conformal field theory. According to the Correspondence Principle, the low-temperature one-dimensional sums approximate the characters of the field theory. We found that the $n = 2$ fused RSOS models for the interval $\frac{\pi}{2} < \lambda < \pi$ correspond to minimal models $\mathcal{M}(m,\, m')$, where m and m' are coprime integers, and $\lambda = \frac{(m'-m)\pi}{m}$.

By the same method, Tartaglia and Pearce conjectured that for $n \times n$ RSOS models, for $0 < \lambda < \pi/n$, the corresponding models are $\mathcal{M}(M, M', n)$ higher level minimal models, where $\lambda = \frac{(m'-m)\pi}{m}$ and $(M,\, M') = (nm-(n-1)m',\, m')$. The conjecture is based on calculations performed on the $n = 2,\, 3$ cases.

Considering the project on the fused RSOS models, a clear further direction is the full exploration of the tower of models: for $n \geq 3$, only partial results are known even as a conjecture. As the 3×3 fused R-matrix is known for all values

of λ, there is no obvious obstacle to extend our investigation there. However, taking the low temperature limit does not lead to the expected form for the R-matrix. This problem has to be resolved in order to make further steps in finding the corresponding conformal field theory.

The third main chapter is focuses on the exact solution of a spinless supersymmetric fermionic chain with periodic boundary conditions. The model is a supersymmetric extension of the M_1 model of Fendley, Schoutens and de Boer. One striking feature of the model that fermion number is not conserved. However domain walls – separating particles from empty sites– are conserved degrees of freedom. The parity of domain walls (regarding that they occupy an even or odd site on the dual lattice) is also conserved which is a result of the parity conservation of the number of fermions. We solved the model by nested coordinate Bethe ansatz, and found the Bethe equations for the model. We checked back our result by comparison to direct diagonalization results. We checked the completeness of the Bethe ansatz, for small systems. We found that with supplementary use of the symmetries of the model, the whole spectrum is recovered. The model exhibit large number of symmetry, which we studied in details. The energy levels are extensively degenerate, i.e. the degeneracy of the levels exponentially increases with the system size. We explained the extensive degeneracy in terms of Bethe ansatz, in zero energy Cooper pair like excitations. The model is solved in terms of Bethe roots, however, there are many open questions: Mainly, the algebraic structure and the R-matrix are still to be discovered. There is a possible mapping of the model to a different chain model, which could help answering these questions.

Appendix A

Currents in the dilute $O(n=1)$ loop model

A.1 Derivation of the $n = 1$ K-matrix from the generic one

In this section, we derive the (2.21a, 2.21b, 2.21c) $n = 1$ left K-matrix weights from the (2.9a, 2.9b, 2.9c, 2.9d) generic weights.
The generic K-matrix weights are the following

$$k_1^l(u,\zeta) = \zeta \sin(2\lambda)\sin(2u) \tag{A.1a}$$

$$k_2^l(u,\zeta) = 2\cos\lambda \sin\left(\tfrac{3}{2}\lambda + u\right) - \\ - n_1\zeta^2 \sin\left(\tfrac{1}{2}\lambda + u\right)\sin\left(\tfrac{1}{2}\lambda - u\right)\sin\left(\tfrac{3}{2}\lambda - u\right) \tag{A.1b}$$

$$k_3^l(u,\zeta) = -\zeta^2 \sin(2\lambda)\sin(3u)\sin\left(\tfrac{1}{2}\lambda - u\right) \tag{A.1c}$$

$$k_4^l(u,\zeta) = \sin\left(\tfrac{3}{2}\lambda - u\right)\left(2\cos\lambda - n_1\zeta^2 \sin^2\left(\tfrac{1}{2}\lambda - u\right)\right) \tag{A.1d}$$

We change from additive to multiplicative notation by introducing new variables (eq. (2.11))

$$q = \mathrm{e}^{\mathrm{i}\lambda}$$
$$z = \mathrm{e}^{\mathrm{i}x}$$

In these new variables, the K-matrix elements are the following

$$k_1^l(z,\zeta) = \tfrac{\zeta}{4}\tfrac{(q^4-1)(z^4-1)}{q^2z^2} \tag{A.2a}$$
$$k_2^l(z,\zeta) = \tfrac{(q^2+1)(q^3z^2-1)}{2q^{5/2}z} - \zeta^2 n_1 \tfrac{(qz^2-1)(q-z^2)(q^3-z^2)}{8q^{5/2}z^3} \tag{A.2b}$$
$$k_3^l(z,\zeta) = -\zeta^2\,\tfrac{(q^4-1)(z^4-1)(q-z^2)}{8q^{5/2}z^3} \tag{A.2c}$$
$$k_4^l(z,\zeta) = \tfrac{q^3-z^2}{2q^{3/2}z}\left(\tfrac{q^2+1}{q} - \zeta^2 n_1 \tfrac{(q-z^2)^2}{4qz^2}\right) \tag{A.2d}$$

For Regime I, we take the (2.14b) solutions $q_2^{(\pm)}$, set the boundary loop weight $n_1 = 1$, and simplify the weights for the following form

$$k_1^l(z,\zeta) = -\tfrac{\zeta}{4}\tfrac{(1+q)(z^2-1)(1+z^2)}{q^2z^2} \tag{A.3a}$$
$$k_2^l(z,\zeta) = -\tfrac{(q^2+1)(1+z^2)}{2q^{5/2}z} + \zeta^2\tfrac{(qz^2-1)(q-z^2)(1+z^2)}{8q^{5/2}z^3} \tag{A.3b}$$
$$k_3^l(z,\zeta) = \zeta^2\,\tfrac{(1+q)(z^2-1)(1+z^2)(q-z^2)}{8q^{5/2}z^3} \tag{A.3c}$$
$$k_4^l(z,\zeta) = -\tfrac{(1+q^2)(1+z^2)}{2q^{5/2}z} + \zeta^2\tfrac{(1+z^2)(q-z^2)^2}{8q^{5/2}z^3} \tag{A.3d}$$

Here, ζ is a free parameter, which we relate to the function $x(z_B)$ defined in eq. (2.21h) as follows

$$\zeta(z_B) = -2q^{1/2}x(z_B) \tag{A.4}$$

With this substitution, the weights take the following form

$$k_1^l(z,\zeta) = \tfrac{x(z_B)}{2}\tfrac{(1+q)(z^2-1)(1+z^2)}{q^{3/2}z^2} \tag{A.5a}$$
$$k_2^l(z,\zeta) = -\tfrac{(1+z^2)}{2q^{3/2}z} + x^2(z_B)\tfrac{(qz^2-1)(q-z^2)(1+z^2)}{2q^{3/2}z^3} \tag{A.5b}$$
$$k_3^l(z,\zeta) = x^2(z_B)\,\tfrac{(1+q)(z^2-1)(q-z^2)(1+z^2)}{2q^{3/2}z^3} \tag{A.5c}$$
$$k_4^l(z,\zeta) = -\tfrac{(1+z^2)}{2q^{3/2}z} + x^2(z_B)\tfrac{(1+z^2)(q-z^2)^2}{2q^{3/2}z^3} \tag{A.5d}$$

where we also used the identity $1+q^2 = q$. These are the $n = 1$ weights up to a factor $\frac{1+z^2}{2q^{3/2}z}$.
To make this statement explicit, here we list the $n = 1$ weights reported in eqs. (2.21a) to (2.21c). They read as follows after substituting the function k

(for simplicity, in the same order as in eq. (A.5))

$$K^l_{OpCl}(z, z_B) = x(z_B)\frac{(1+q)(z^2-1)}{z} \tag{A.6a}$$

$$K^l_{id}(z, z_B) + K^l_m(z, z_B) = -1 + x^2(z_B)\frac{(q-z^2)(qz^2-1)}{z^2} \tag{A.6b}$$

$$K^l_m(z, z_B) = x^2(z_B)\frac{(1+q)(z^2-1)(q-z^2)}{z^2} \tag{A.6c}$$

$$K^l_{id}(z, z_B) = -1 + x^2(z_B)\frac{(z^2-q)^2}{z^2} \tag{A.6d}$$

This shows that the used weights are gauge equivalent.

A.2 The dilute O(n=1) model and the site percolation on a triangular lattice

The dilute O(n=1) loop model on a rectangular lattice maps to the critical site percolation on a triangular lattice. The site percolation is defined as such: Consider a triangular lattice, where every site is either red or blue, both with $p_c = \frac{1}{2}$ probability. This model maps to the dilute loop model in a certain limit. The mapping is depicted in fig. A.1. The loops became the domain walls of the percolation model. Since the domain walls live on the dual lattice of the triangular lattice, they live on a honeycomb lattice. The mapping takes place in a way that out of the nine possible plaquettes of the loop model one has to be zero, and all the others have equal weights. Since a plaquette belongs to four sites of the site percolation, if all the remaining eight plaquette configurations have equal weights, this gives back independent site probabilities. This is required, since the $2^4 = 16$ possible four-site percolation configurations have equal weights, and after a factorization of the two colors, each corresponds to a loop plaquette. Since one of the weights disappears, and the others have equal weight, this corresponds to the loop model after we take the fusion limit, and the R-matrix elements factorize. The mapping can be realized in two different ways, setting either the weight of  or  to 0. This is realized by setting $W_2(z, w) = 0$ or $W_m(z, w) = 0$, which means $w = zq^2$ or $w = zq^{-2}$, respectively. In the figure, the later realization is depicted. Either way, the remaining eight configurations have equal weights, hence the independent probabilities of the percolation model are guaranteed.

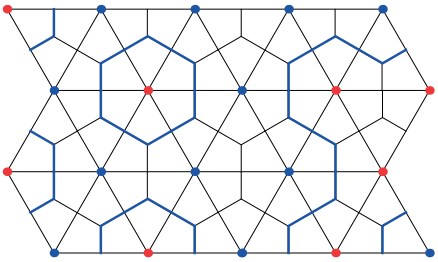

(a) The site percolation on a triangular lattice, with the domain walls

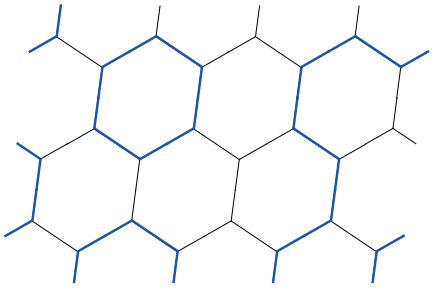

(b) The domain walls form loops on a honeycomb lattice

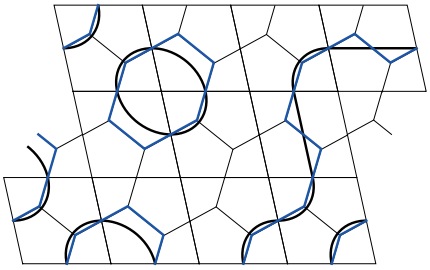

(c) This maps to the dilute loops in the appropriate limit

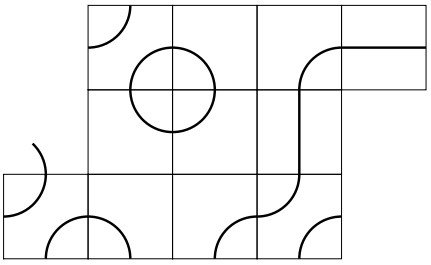

(d) The corresponding loop configuration

Figure A.1: The mapping of a site percolation configuration on a triangular lattice to a dilute loop configuration on the square lattice. For convenience, the figures are distorted, in order to have the usual triangular and square lattice on the two sides of the mapping.

A.3 Normalization of the transfer-matrix

In order to prove the (2.40) form of the normalization, first, we map the dilute $O(1)$ loop model to a site percolation model, and compute the normalization in the percolation model, using the all-1 left eigenvector.
There is a mapping between the dilute $O(1)$ loop model, and an unusual site percolation model, different from the one presented in appendix A.2. The site percolation model is built up from randomly distributed spins taking the values $s = \pm 1$ on the vertices of the tiles. The mapping takes place, as the lines of the loop model are mapped to the domain walls of the site percolation. To implement the R and K-matrix weights, we introduce the following plaquette-interactions

- For the R-matrix: $R = a + bs_1s_2s_3s_4$
- For the K-matrix: $K = A + Bs_1s_3$

Here s_1, s_2, s_3, s_4 are the four spins in the corner of the R-matrix, and s_1, s_3 are the vertices in the upper and lowermost corner of the K-matrix. The aforementioned definitions coincide with the loop weights, if

$$a = \frac{1}{2}\left(W_e + W_{R_1}\right) \equiv \frac{1}{2}W_R \ , \tag{A.7a}$$

$$b = \frac{1}{2}\left(W_e - W_{R_1}\right) := \frac{1}{2}\tilde{W}_R \ , \tag{A.7b}$$

$$A = \frac{1}{2}\left(W_{K_e} + W_{K_{OpCl}}\right) \equiv \frac{1}{2}W_K \ , \tag{A.7c}$$

$$B = \frac{1}{2}\left(W_{K_e} - W_{K_{OpCl}}\right) := \frac{1}{2}\tilde{W}_K \ . \tag{A.7d}$$

We define a percolation state, as a sequence of spins along the bottom edge of the T-matrix. A percolation state is equal to the sum of loop states with the same occupations, regardless the connectivity of occupied sites. There are two choices to map the occupied, and empty sites to the ± 1 spins. If we choose to map the occupied sites to -1, and the empty ones to $+1$, e.g. $|-1,-1,1,1\rangle_{\text{perco}} = |() \bullet \bullet\rangle + |((\bullet\bullet\rangle + |)) \bullet \bullet\rangle + |)(\bullet\bullet\rangle$. Even the states are not in bijection, the T-matrix configurations are, consequently the normalization for both T-matrices are the same.
By definition, the T-matrix is a left stochastic matrix, so all the columns of it sum up to N. Consequently, the left eigenvector is the $(1, 1, \ldots, 1)$ vector. The corresponding normalization is proportional to the weight of summing over all possible spin configurations of the sites, with the exception of the bottom line,

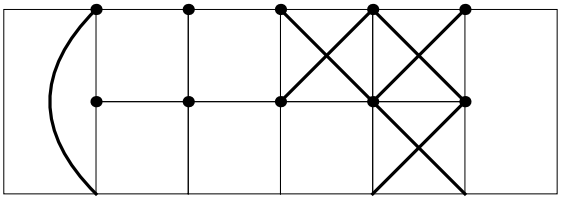

Figure A.2: Graphical representation of a summand in the normalization of the percolation transfer-matrix. For better understanding, we denote the K-matrices by rectangulars, instead of triangles. The spins –we sum up to– are emphasized by dots.

where the resulting state is. The weight of a T-matrix configuration is $\prod R \prod K$, and the normalization is

$$N = \frac{\sum_{\text{all config.}} \prod R \prod K}{\sum_{\text{all config.}} 1} = 2^{-2(L+1)} \sum_{\text{all config.}} \prod (a + b s_1 s_2 s_3 s_4) \prod (A + B s_1 s_3) \; . \tag{A.8}$$

Expanding the products, the $\prod(a + bs_1s_2s_3s_4)\prod(A + Bs_1s_3)$ summands of N are polynomials in s_i, and because s_i is summed over $+1$ and -1, if at least one s_i has odd power, the contribution of that summand cancels out as we sum over all the configurations. It is easy to see that all the summands have at least one odd-powered s_i, with the exception of $\prod a \prod A$ and $\prod b \prod B$. If we represent the $bs_1s_2s_3s_4$ term by a cross at the given square, and Bs_1s_3 as a line connecting s_1 and s_3, a given summand is a partial filling of the T-matrix with crosses and lines (fig. A.2). The power of a spin is equal to the lines starting from that vertex. By putting somewhere a cross or a line, it is clear that the full T-matrix has to be filled in order to not to have vertex with odd lines (regardless the bottom edge). By this, we see that the only non-vanishing contributions are $\prod a \prod A$ (the "empty" T-matrix) and $\prod b \prod B$ (the "completely filled" T-matrix). Consequently, the normalization is $N = 2^{-2(L+1)} \sum_{\text{all config.}} \prod a \prod A + \prod b \prod B = \prod a \prod A + \prod b \prod B$. The $2^{-2(L+1)}$ prefactor is canceled by the summation over all configuration. Including

inhomogeneous weights, we get the following expression for the normalization

$$\begin{aligned} &N(w, z_0, \ldots, z_{L+1}) = \qquad (A.9)\\ &= W_{K_l}(w, z_0) W_{K_l}(w^{-1}, -z_{L+1}) \prod_{i=1}^{L} W_R(w, z_i) W_R(z_i, w^{-1}) + \\ &\quad + \tilde{W}_{K_l}(w, z_0) \tilde{W}_{K_l}(w^{-1}, -z_{L+1}) \prod_{i=1}^{L} \tilde{W}_R(w, z_i) \tilde{W}_R(z_i, w^{-1}) \, . \end{aligned}$$

A.4 $L = 1$ groundstate elements and X current

As an example, here we present the $L = 1$ groundstate elements, and the computation of the X current for this case

$$\begin{aligned} \psi_\bullet(z_0, z_1, z_2) \equiv &\psi_{EE, L=1}(z_0, z_1, z_2) = \qquad (A.10a)\\ = &z_0 + z_1 + z_2 + z_0^{-1} + z_1^{-1} + z_2^{-1} = \\ = &\frac{z_0 z_1 + z_0 z_2 + z_1 z_2 + z_0^2 z_1 z_2 + z_0 z_1^2 z_2 + z_0 z_1 z_2^2}{z_0 z_1 z_2} \, , \\ \psi_(z_0, z_1, z_2) = &\frac{(q z_0 + z_1)(q + z_0 z_1)}{q z_0 z_1} \, , \qquad (A.10b)\\ \psi_)(z_0, z_1, z_2) = &\frac{(q z_1 + z_2)(1 + q z_1 z_2)}{q z_1 z_2} . \qquad (A.10c) \end{aligned}$$

The normalization of the full strip follows by summing up for all the allowed connectivity

$$\begin{aligned} &Z_{f.s., L=1}(z_0, z_1, z_2) = \\ &\quad = \psi_\bullet(z_0, z_1, z_2) \psi_\bullet^*(z_0, z_1, z_2) + \big(\psi_(z_0, z_1, z_2) + \psi_)(z_0, z_1, z_2)\big) \times \\ &\qquad \times \Big(\psi_(^*(z_0, z_1, z_2) + \psi_)^*(z_0, z_1, z_2)\Big) = \\ &\quad = \psi_\bullet(z_0, z_1, z_2) \psi_\bullet(z_2, z_1, z_0) + \big(\psi_(z_0, z_1, z_2) + \psi_)(z_0, z_1, z_2)\big) \times \\ &\qquad \times \big(\psi_)(z_2, z_1, z_0) + \psi_)(z_2, z_1, z_0)\big) = \\ &\qquad = \frac{2(z_0 z_1 + z_0 z_2 + z_1 z_2 + z_0^2 z_1 z_2 + z_0 z_1^2 z_2 + z_0 z_1 z_2^2)^2}{z_0^2 z_1^2 z_2^2} \, . \qquad (A.11) \end{aligned}$$

Here and in the followings, we utilize eq. (2.46) to relate the groundstate and the dual groundstate elements. The unnormalized current is

$$\begin{aligned} X^{(1)u.n.}_{L=1}(z_0,z_1,z_2) &= \psi_{)}(z_0,z_1,z_2)\psi^*_{(}(z_0,z_1,z_2) - \psi_{(}(z_0,z_1,z_2)\psi^*_{)}(z_0,z_1,z_2) \\ &= \psi_{)}(z_0,z_1,z_2)\psi_{)}(z_2,z_1,z_0) - \psi_{(}(z_0,z_1,z_2)\psi_{(}(z_2,z_1,z_0) = \\ (1-2q)\,&\frac{(z_1^2-1)(z_0z_1+z_0z_2+z_1z_2+z_0^2z_1z_2+z_0z_1^2z_2+z_0z_1z_2^2)}{z_0z_1^2z_2}. \end{aligned} \tag{A.12}$$

The normalized current follows after dividing by the partition sum of the full strip

$$\begin{aligned} X^{(1)}_{L=1}(z_0,z_1,z_2) &= \frac{1-2q}{2}\left(z_1-\frac{1}{z_1}\right)\ \frac{1}{E_1(z_0,z_1,z_2)} = \\ &= \frac{1-2q}{2}\ \frac{z_1^2-1}{z_1}\ \frac{1}{z_0+z_1+z_2+z_0^{-1}+z_1^{-1}+z_2^{-1}} = \\ &\frac{1-2q}{2}\frac{z_1^2-1}{z_1}\ \frac{z_0z_1z_2}{z_0z_1+z_0z_2+z_1z_2+z_0^2z_1z_2+z_0z_1^2z_2+z_0z_1z_2^2}. \end{aligned} \tag{A.13}$$

A.5 Proof of the fusion equation

In this section, we prove the (2.68) fusion equation

$$R_i(zq,w)R_{i+1}(zq^{-1},w)M_i = 2\frac{(w-z)(w+z)}{z^2}M_iR_i(z,w)\ . \tag{A.14}$$

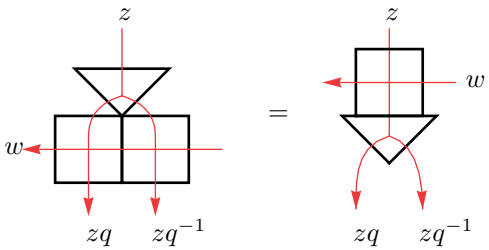

If such an equation holds, every RR configuration belongs to one of the nine possible faces of the R-matrix. In other words, we should be able to group the RR configurations such a way that the sum of their weight at the fusion values $(zq,\, zq^{-1})$ are proportional to the corresponding R-matrix weight.
First, according to the l.h.s. of the fusion equation, we group the RR

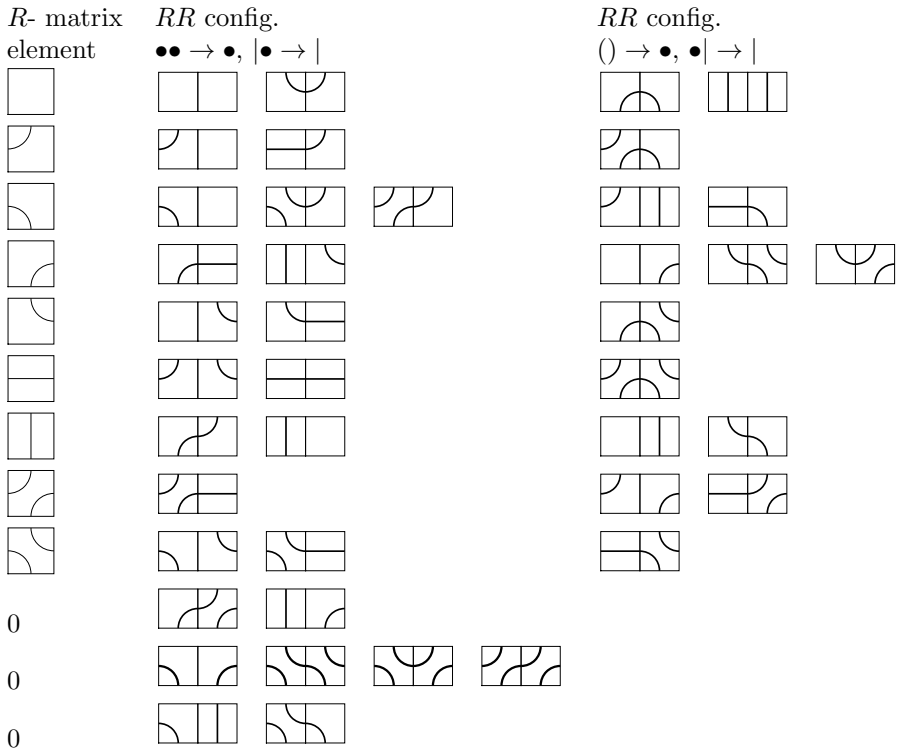

Table A.1: The classification of RR configurations in the fusion equation. The first column contains the resulting R-matrix element, the second and third column contain the corresponding RR-configurations, grouped according to their external connectivity. The connectivity is taken on the pentagon, i.e. on the external sides of the l.h.s. of the fusion equation. The top triangle is not drawn, as it is determined by the top two sites of the RR configuration.

configurations according to their external connectivity on the pentagon, i.e. on the five external sides of the l.h.s of eq. (A.14). This classification puts the possible 41 RR configurations in 21 sets.
At the value $z_1 = z\omega$, $z_2 = z\omega^{-1}$, 3 of these sets have vanishing weights.
The remaining 18 sets can be grouped into the expected 9 groups, according to the connectivity on the bottom, i.e. two empty sites or the two sites connected to each other turn into an empty site, one empty site and one occupied site turn into an occupied site, connected to the original connection of the occupied site. The grouping is exactly the same, as the elements of dLP_L maps to dLP_{L-1} under the recursion.
The disappearing elements are exactly the ones with two not linked lines on the bottom, which cannot be mapped to a proper one site.
The classification is depicted on Tab. A.1. The first column is the corresponding R-matrix (the r.h.s. of the equation), the second and third are the corresponding RR configurations, where we keep the original classification to 18 sets according to the external connectivity on the pentagon. The top triangle operator is not shown, as it is uniquely defined by the top two sites. Also, as the triangles have equal weights, we do not have to take them into account at computing the weight. The proportionality factor $2\frac{(z-w)(z+w)}{z^2}$ is exposed in eq. (A.14). It is even true that the 18 sets independently proportional to their corresponding R-matrix weight, with factor $\frac{(z-w)(z+w)}{z^2}$.
All of the aforementioned statements are computed directly.

A.6 Construction of the open boundary K-matrix from the closed boundary K-matrix via insertion of a line

In this section, we show the construction of the open boundary K-matrix weights from the closed boundary case, by the well known method of insertion of a line. This description of the open boundary K-matrix allows us to extend certain symmetry arguments to the boundary rapidity. Unfortunately, we cannot use this construction to prove the symmetry of the bulk and boundary rapidity in the currents. Using the fusion equation, we get the boundary fusion equation as a corollary.
The closed boundary K-matrix consist two elements, with identical weights, and

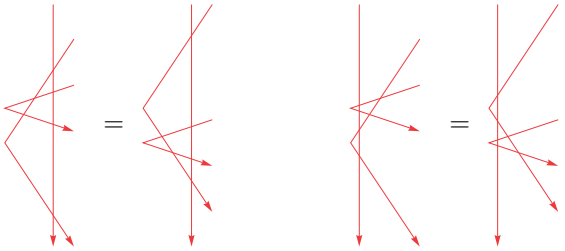

(a) (b)

Figure A.3: The construction of a new K-matrix via insertion of a line. In this figure –for convenience– we use different style, then in the previous equations. Straight lines represent the rapidity-lines, a crossing of two rapidity lines is an R-matrix, a cusp in a line is a K-matrix.

satisfies the reflection equation

$$K_{\text{closed b.c.}} = \quad + \qquad \text{(A.15)}$$

$$K_{\text{cbc}}R\left(v^{-1},u\right)K_{\text{cbc}}R\left(u,v\right) = R\left(v^{-1},u^{-1}\right)K_{\text{cbc}}R\left(u^{-1},v\right)K_{\text{cbc}}\,. \qquad \text{(A.16)}$$

The idea of the insertion of a line is as in fig. A.3. We multiply the closed boundary reflection equation from the right with a column of four R-matrices, and by the means of the Yang-Baxter equation, we move the R-matrices inside (fig. A.3, (b)). In this configuration we regard the KRR blocks, as the elements of the new K-matrix, and the weight of the new K-matrix is equal to the sum of the weights of the corresponding KRR blocks (fig. A.4). Our aim is to follow this procedure to create the open boundary (left) K-matrix. The procedure is the same for the right boundary. Since we want to create *independent* weights, and the possible KRR configurations depend on if a line or an empty site enters on the top of the top R-matrix, we can elaborate our procedure. For every open boundary K-matrix element, we want to have two groups of KRR configurations, one with an entering line on the top, one without, and we expect the sum of these weights to be equal, in order to produce independent open K-matrix weights. Since we expect the right sides of the two R-matrices to be the top and bottom half of the open boundary K-matrix, the occupancy on the left and on the top

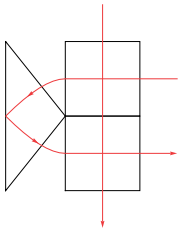

Figure A.4: A KRR block. The vertical rapidity is the boundary rapidity of the open BC K-matrix, the bouncing rapidity is the normal one.

already defines the six groups associated with the empty, the top, and the bottom type K-matrix. (First three row of table A.2.)

Distinguishing the two remaining elements (the "line":  and the "monoid": ) is a bit more tricky, and done in the following way: We look at configurations with a line entering, and we group them according to their connectivity on the left: If the two left side are connected, they belong to the "line", if not, they belong to the "monoid". Now we have to choose the other two groups according to the criteria that with and without the line, the weights should be the same. Based on this criteria, we can uniquely make the choice, however, there is one KRR configuration which has to "divided" between the line and the monoid. Regardless these divided cases, the following statement holds for the weight of the open BC K-matrix and the weight of the KRR configuration

$$\frac{\left(1+z_B^2\right)^2 z_1^2}{zB^2} W_{K_{OBC}}(z_1, z_B) = \sum_{i \in G_{K_{OBC}}} R_{i,\mathrm{top}}(z_B, z_1) R_{i,\mathrm{bottom}}(z_1^{-1}, z_B) \; . \tag{A.17}$$

Here $W_{K_{obc}}$ denotes the weigh of a specific open B.C. K-matrix element, and the sum on the other side runs over the KRR configurations which contribute to the given open BC K-matrix element (As given on Table A.2). The divided cases have the prefactors $\frac{3}{4}$ and $\frac{1}{4}$ in the homogeneous case, in the inhomogeneous

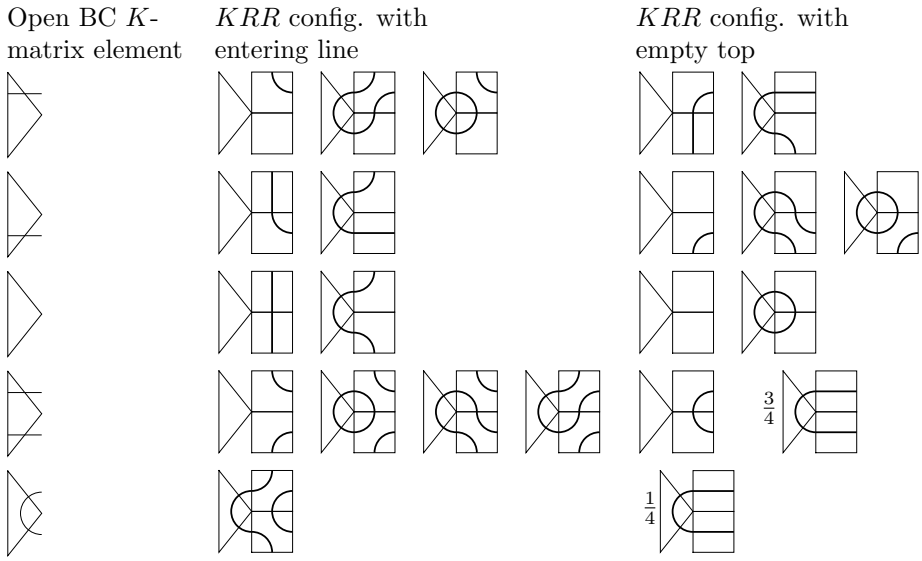

Table A.2: Open B.C. K-matrix elements expressed by closed B.C. KRR configurations. Note the $\frac{3}{4}$ and $\frac{1}{4}$ factors: In order to reproduce the open B.C. weights, we have to split the configuration into two part, with certain probabilities. These probabilities goes into $\frac{3}{4}$ and $\frac{1}{4}$ in the homogenous limit. For the general expression, consult the text.

case, the following relations hold

$$\frac{\left(1+z_B^2\right)^2 z_1^2}{zB^2} W_m^l(z_1,z_B) = W_t(z_B,z_1) W_t\left(z_1^{-1},z_B\right) + \left(\frac{1}{f\left(z_1^{-1},z_B\right)+1} + \frac{1}{\left(f\left(z_B,z_1\right)+1\right)\left(f\left(z_B,z_1^{-1}\right)+1\right)}\right) \times \times W_1(z_B,z_1) W_1\left(z_1^{-1},z_B\right) , \tag{A.18}$$

$$\frac{\left(1+z_B^2\right)^2 z_1^2}{zB^2} W_i^l d(z_1,z_B) = \frac{f\left(z_B,z_1^{-1}\right)+1}{f\left(z_1,z_B\right)+1} W_1(z_B,z_1) W_1\left(z_1^{-1},z_B\right) . \tag{A.19}$$

Here f is defined as

$$f(z_1,z_2) = \frac{W_2(z_1,z_2)}{W_m(z_1,z_2)} , \tag{A.20}$$

with the property: $f^{-1}(z_1,z_2) = f(z_2,z_1)$. The prefactors, involving the f's turn into $\frac{3}{4}$ and $\frac{1}{4}$, if the rapidities are equal to 1.
An intuitive understanding of the division of this KRR configuration is missing, however, the aforementioned relations have been thoroughly checked analytically. Since the vertical rapidity becomes the boundary rapidity, the previous argument about the symmetry in the rapidities in certain cases –e.g. the partition sum– extends to the boundary rapidities too.
It is easy to prove the boundary fusion relation, based on this construction and the fusion relation. If we extend the KRR configuration into a $KRRRR$ configuration, and we apply the recursion relation on the four R-matrix, we get the boundary fusion relation, as a corollary.

Appendix B

One-dimensional sums and finitized characters of 2×2 fused RSOS models

B.1 Coset construction

In this appendix, we give a brief overview of the GKO (Goddard-Kent-Olive) coset construction [68]. For a more complete introduction, we suggest standard textbooks, as [115, 116]. The GKO cosets are constructed based on quotients of affine Lie algebras. Affine Lie algebra arises from the central extension of the loop algebra, where a $\tilde{g}$ loop algebra is generated as a tensor product of a simple Lie algebra g and Laurent polynomials in a variable t

$$\tilde{g} = g \otimes \mathbb{C}[t,\, t^{-1}] \tag{B.1}$$

The generators of the loop algebra are expressed in terms of the $\{J^a\}$ generators of the Lie algebra as

$$J^a_n \equiv J^a \otimes t^n, \qquad n \in \mathbb{Z}, \tag{B.2}$$

with the following commutation relations

$$[J^a_n,\, J^b_m] = \sum_c \mathrm{i} f^{ab}_c J^c_{n+m} \tag{B.3}$$

Consider the central extension of the loop algebra, which leads to the following commutation relation

$$[J_n^a,\, J_m^b] = \sum_c \mathrm{i} f_c^{ab} J_{n+m}^c + \hat{k} n \delta_{ab} \delta_{n+m,0} \tag{B.4}$$

$$[J_n^a,\, \hat{k}] = 0 \tag{B.5}$$

where $\hat{k}$ is the central element. The $\hat{g}$ affine Lie algebra is defined as the central extension of the $\tilde{g}$ loop algebra, supplemented with an element L_0 which measures the grade, the polynomial degree of t

$$L_0 := -t\frac{\mathrm{d}}{\mathrm{d}t} \tag{B.6}$$

$$[L_0,\, J_n^a] = -n J_n^a \tag{B.7}$$

$$[L_0,\, \hat{k}] = 0 \tag{B.8}$$

With this definitions, the untwisted affine Lie algebra is defined as follows

$$\hat{g} = \tilde{g} \oplus \mathbb{C}\hat{k} \oplus \mathbb{C}L_0 \tag{B.9}$$

Considering the representation theory of affine Lie algebras, there are major differences compared to the simple Lie algebras. Every representation of an affine algebra is characterized by its $\hat{k}$ eigenvalue, denoted by k, which is called the level of the representation. The physically interesting highest-weight representations are infinite dimensionals, and are such that any $su(2)$ subalgebra associated with real roots are finite. These are called integrable highest-weight representations. For any integrable highest-weight representation, k must be a positive integer. The number of integral highest-weight representation is bounded by k.
Consider the current algebra, with the following OPE

$$J^a(z)J^b(w) \sim \tfrac{k\delta_{ab}}{(z-w)^2} + \sum_c i f_{abc} \tfrac{J^c(w)}{(z-w)} \tag{B.10}$$

Here $J^a(z)$ is expanded in the Laurent modes of the generators of the underlying affine Lie algebra

$$J^a(z) = \sum_{n\in\mathbb{Z}} z^{-n-1} J_n^a \tag{B.11}$$

Similarly to the aforementioned holomorphic module, depending on $z = x^0 + \mathrm{i}x^1$, there is an antiholomorphic section, depending on $\bar{z} = x^0 - \mathrm{i}x^1$, which commutes with the holomorphic section. We define the Wess-Zumino-Witten

(WZW) models in the Sugawara construction, based on the energy-momentum tensor, defined as

$$T(z) = \frac{1}{2(k+g)} \sum_a (J^a J^a)(z) \tag{B.12}$$

where k is the level of the algebra, and g is the dual Coxeter number. The normal ordering $(\ldots)$ is defined by contour integral. The central charge of this model is given by

$$c = \frac{k \dim g}{k+g} \tag{B.13}$$

where dim g is the dimension of the Lie algebra corresponding to the $\hat{g}$ affine algebra.
In terms of the affine generators, we define the following Virasoro generators

$$L_n = \frac{1}{2(k+g)} \sum_a \sum_m : J^a_m J^a_{n-m} : \tag{B.14}$$

where the normal order defined by the semicolons as the term with larger subindex is placed on the rightmost position. These Virasoro generators satisfy the following commutation relations

$$[L_n,\, L_m] = (n-m)L_{n+m} + \tfrac{c}{12}(n^3 - n)\delta_{n+m,0} \tag{B.15}$$

$$[L_n,\, J^a_m] = -m J^a_{n+m} \tag{B.16}$$

Consider the affine Lie algebra $\hat{g}$, and $\hat{p} < \hat{g}$ subalgebra of $\hat{g}$. The $\{\tilde{J}^{a'}_n\}$ generators of $\hat{p}$ are linear combinations of the $\{J^a_n\}$ generators of $\hat{g}$

$$\tilde{J}^{a'}_n = \sum_a m_{a'a} J^a_n \tag{B.17}$$

Using the definition of L^g_m and L^p_m, the Virasoro generators of the affine algebras $\hat{g}$ and $\hat{p}$ respectively

$$[L^g_m,\, \tilde{J}^{a'}_n] = -n\tilde{J}^{a'}_n \tag{B.18}$$

$$[L^p_m,\, \tilde{J}^{a'}_n] = -n\tilde{J}^{a'}_n \tag{B.19}$$

Define the Virasoro generators of the $\hat{g}/\hat{p}$ coset model, as

$$L^{(g/p)}_m := L^g_m - L^p_m \tag{B.20}$$

which leads to the following commutation relation

$$[L^{(g/p)}_m,\, L^{(g/p)}_n] = (m-n)L^{(g/p)}_{m+n} + (c(\hat{g}_k) - c(\hat{p}_{x_e k}))\tfrac{m(m^2-1)}{12}\delta_{m+n,0} \tag{B.21}$$

Here $c(\hat{g}_k)$ and $c(\hat{p}_{x_e k})$ are the central charges of the two affine algebras, and k and $x_e k$ are the levels, respectively. The level of the subalgebra $\hat{p}$ is necessarily an integer multiply of k, which is encoded in the x_e embedding index. Hence, $L_n^{(g/p)}$ satisfies the Virasoro algebra, and the central charge of it is the difference of the constituent pieces

$$c(\hat{g}_k/\hat{p}_{x_e k}) = \frac{k\dim\, g}{k+g} - \frac{x_e k \dim\, p}{x_e k+p} \tag{B.22}$$

where g and p are the dual Coxeter numbers of the two models, respectively. This construction is the GKO coset construction.
Coset construction based on the form $\frac{\hat{g}\oplus\hat{g}}{\hat{g}}$ is called diagonal coset construction. The generators of the direct sum algebra are given by simply the sum of the two copies of $\hat{g}$

$$J^a_{\rm diag} = J^a_{(1)} + J^a_{(2)} \tag{B.23}$$

where (1) and (2) refers to the first and second copy of $\hat{g}$. As they commute

$$[J^a_{(1)}, J^a_{(2)}] = 0 \tag{B.24}$$

the embedding index is always 1. Consequently, the levels of the three copies are k, n' and $k+n'$, and such a diagonal coset construction is denoted as $\frac{\hat{g}_k\oplus\hat{g}_{n'}}{\hat{g}_{k+n'}}$. The central charge of this coset is given as

$$c = c(\hat{g}_k) + c(\hat{g}_{n'}) - c(\hat{g}_{k+n'}) = \tag{B.25}$$

$$= \dim g \left(\frac{k}{k+g} + \frac{n'}{n'+g} - \frac{k+n'}{k+n'+g} \right) . \tag{B.26}$$

Current algebras with fractional level k do not have integrable highest-weight representations. Rather, they are represented in admissible representations which are highest-weight representations with certain modular transformation properties.

B.2 Characters of higher fusion level coset models

The Virasoro characters of the higher fusion level minimal models $\mathcal{M}(M, M', n')$ are given by the branching functions $b^{M,M',n'}_{r,s,\ell}(q)$ [117, 118] of the coset (3.7). The branching functions are expressed in terms of the string functions of $\mathbb{Z}_{n'}$ parafermionic models with central charges $c = \frac{2n'-2}{n'+2}$. The $\mathbb{Z}_{n'}$ parafermionic

model is constructed as the $\hat{su}(2)_{n'}/\hat{u}(1)$ coset model. The string function is given by the expression

$$c^{\ell}_{\bar{m}}(q) = \frac{q^{-\frac{1}{24}\frac{2n'-2}{n'+2}+\frac{\ell(\ell+2)}{4(n'+2)}-\frac{\bar{m}^2}{4n'}}}{(q)^3_\infty} \sum_{i,j=0}^{\infty} (-1)^{i+j} q^{ij(n'+1)+\frac{1}{2}i(i+1)+\frac{1}{2}j(j+1)} \times$$
$$\times \left(q^{\frac{i}{2}(\ell+\bar{m})+\frac{j}{2}(\ell-\bar{m})} - q^{n'-\ell+1+\frac{i}{2}(2n'+2-\ell-\bar{m})+\frac{j}{2}(2n'+2-\ell+\bar{m})} \right), \quad \text{(B.27)}$$

for the fundamental domain

$$0 \leq \bar{m} \leq \ell \leq n', \qquad \ell - \bar{m} \in 2\mathbb{Z}, \qquad \bar{m},\, \ell = 0,\, 1,\, \ldots,\, n', \qquad n' \in \mathbb{N}. \quad \text{(B.28)}$$

Note that the parameter $\bar{m}$ of the parafermionic model should not be confused with the $n' = 1$ minimal model parameter m. The previous definition is extended to general values $\ell = 0, 1, \ldots, n'$, $m \in \mathbb{Z}$, $\bar{m} \in \mathbb{Z}$, $n' \in \mathbb{N}$ by setting

$$c^{\ell}_{\bar{m}}(q) = 0 \text{ if } \ell - \bar{m} \notin 2\mathbb{Z} \quad \text{(B.29)}$$
$$c^{\ell}_{\bar{m}}(q) = c^{\ell}_{-\bar{m}}(q) = c^{n'-\ell}_{n'-\bar{m}}(q) = c^{\ell}_{\bar{m}+2n'}(q). \quad \text{(B.30)}$$

By this extension, $c^{\ell}_{\bar{m}}$ is an even and periodic function in $\bar{m}$ with period $2n'$. The branching functions are defined as follows [119–123] , for the values $r + s = \ell \bmod 2$

$$b^{M,M',n'}_{r,s,\ell}(q) = q^{\Delta^{M,M',n'}_{r,s} - \frac{c^{M,M',n'}}{24} + \frac{n'-1}{12(n'+2)}} \sum_{\substack{0 \leq \bar{m} \leq n/2 \\ \bar{m} = \ell/2 \bmod 1}} c^{\ell}_{2\bar{m}}(q) \times \quad \text{(B.31)}$$

$$\times \left(\sum_{\substack{j \in \mathbb{Z} \\ m_{r-s}(j) = \\ = \pm\bar{m} \bmod n'}} q^{\frac{j}{n'}(jMM'+rM'-sM)} - \sum_{\substack{j \in \mathbb{Z} \\ m_{r+s}(j) = \\ = \pm\bar{m} \bmod n'}} q^{\frac{1}{n'}(jM'+s)(jM+r)} \right)$$

$$1 \leq r \leq M-1, \qquad 1 \leq s \leq M'-1, \qquad \ell = 0, 1, \ldots, n \quad \text{(B.32)}$$

where the mod 1 notation in the first sum over $\bar{m}$ indicates summing over either integer or half-integer values, and in the second and third sum, $m_{r\pm s}(j)$ is defined as follows

$$m_a(j) = \frac{a}{2} + jM'. \quad \text{(B.33)}$$

The branching functions satisfy the branching rules [117–119] of the characters of the $A_1^{(1)}$ affine current algebras

$$\widehat{\mathrm{ch}}^{\hat{p},\hat{p}'}_{r,s}(q,z)\widehat{\mathrm{ch}}^{n'+2,1}_{r',0}(q,z) = \sum_{\substack{\sigma=1 \\ \sigma=r+\ell \bmod 2}}^{\hat{p}+n'\hat{p}'-1} b^{\hat{p},\hat{p}+n'\hat{p}',n'}_{r,\sigma,\ell}(q)\widehat{\mathrm{ch}}^{\hat{p}+n'\hat{p}',\hat{p}'}_{\sigma,s}(q,z), \tag{B.34}$$

$$\hat{p} = M, \quad \hat{p}' = \frac{M'-M}{n'}. \tag{B.35}$$

The branching rules relate admissible characters of affine current algebras $(A_1^{(1)})_k$, $(A_1^{(1)})_{n'}$, $(A_1^{(1)})_{k+n'}$, where

$$r' = \begin{cases} n'+1-\ell, & s \text{ odd} \\ \ell+1, & s \text{ even} \end{cases} \qquad \ell = 0,1,\ldots,n. \tag{B.36}$$

For $n' = 1, 2$, the branching functions give back the Virasoro minimal and superconformal characters, respectively.

B.3 3×3 fused RSOS face weights

$$W_{3,3}\left(\begin{matrix} a\pm 3 & a \\ a & a\pm 3 \end{matrix}\middle| u\right) = \frac{s\big((a\pm 1)\lambda \mp u\big)\, s\big((a\pm 2)\lambda \mp u\big)\, s\big((a\pm 3)\lambda \mp u\big)}{s\big((a\pm 1)\lambda\big)\, s\big((a\pm 2)\lambda\big)\, s\big((a\pm 3)\lambda\big)} \tag{B.37a}$$

$$W_{3,3}\left(\begin{matrix} a\mp 3 & a \\ a & a\pm 3 \end{matrix}\middle| u\right) = \frac{s\big(\lambda - u\big)\, s\big(2\lambda - u\big)\, s\big(3\lambda - u\big)}{s\big(2\lambda\big)\, s\big(3\lambda\big)} \tag{B.37b}$$

$$W_{3,3}\left(\begin{matrix} a\pm 1 & a \\ a & a\pm 3 \end{matrix}\middle| u\right) = W_{3,3}\left(\begin{matrix} a\pm 3 & a \\ a & a\pm 1 \end{matrix}\middle| u\right) = \tag{B.37c}$$

$$= \frac{s\big(\lambda - u\big)\, s\big((a\pm 1)\lambda \mp u\big)\, s\big((a\pm 2)\lambda \mp u\big)}{s\big((a\pm 1)\lambda\big)\, s\big((a\pm 2)\lambda\big)}$$

$$W_{3,3}\left(\begin{matrix} a\mp 1 & a \\ a & a\pm 3 \end{matrix}\middle| u\right) = W_{3,3}\left(\begin{matrix} a\pm 3 & a \\ a & a\mp 1 \end{matrix}\middle| u\right) = \tag{B.37d}$$

$$= \frac{s\big(\lambda - u\big)\, s\big(2\lambda - u\big)\, s\big((a\pm 1)\lambda \mp u\big)}{s\big(2\lambda\big)\, s\big((a\pm 1)\lambda\big)}$$

$$W_{3,3}\left(\begin{matrix} a\pm 1 & a \\ a & a\pm 1 \end{matrix}\middle| u\right) = \frac{s\big((a\pm 1)\lambda \mp u\big)\, s\big((a\pm 1)\lambda \pm u\big)\, s\big((a\pm 2)\lambda \mp u\big)}{s\big((a\pm 1)\lambda\big)^2\, s\big((a\pm 2)\lambda\big)} - \tag{B.37e}$$

$$- \frac{s\big(2\lambda\big)s\big((a-2)\lambda\big)s\big((a+2)\lambda\big)s\big(\lambda-u\big)s\big(u\big)s\big((a\pm1)\lambda\mp u\big)}{s\big(3\lambda\big)s\big((a\mp1)\lambda\big)s\big((a\pm1)\lambda\big)^2}$$

$$W_{3,3}\Big(\begin{matrix}a\mp1 & a\\ a & a\pm1\end{matrix}\Big|u\Big) = \frac{s\big(2\lambda\big)^2 s\big((a\mp2)\lambda\big)s\big(\lambda-u\big)s\big(a\lambda\pm u\big)s\big((a\pm1)\lambda\mp u\big)}{s\big(3\lambda\big)s\big((a\mp1)\lambda\big)^2 s\big((a\pm1)\lambda\big)} - \tag{B.37f}$$

$$- \frac{s\big((a\mp3)\lambda\big)s\big((a\pm1)\lambda\big)s\big(2\lambda-u\big)s\big(\lambda-u\big)s\big(\lambda+u\big)}{s\big(2\lambda\big)s\big(3\lambda\big)s\big((a\mp1)\lambda\big)^2}$$

$$W_{3,3}\Big(\begin{matrix}a\pm3 & a\pm6\\ a & a\pm3\end{matrix}\Big|u\Big) = -\frac{s\big((a\pm4)\lambda\big)s\big((a\pm5)\lambda\big)s\big((a\pm6)\lambda\big)s\big(u\big)s\big((\lambda+u)\big)s\big((2\lambda+u)\big)}{s\big(2\lambda\big)s\big(3\lambda\big)s\big((a\pm1)\lambda\big)s\big((a\pm2)\lambda\big)s\big((a\pm3)\lambda\big)} \tag{B.37g}$$

$$W_{3,3}\Big(\begin{matrix}a\pm3 & a\pm4\\ a & a\pm3\end{matrix}\Big|u\Big) = \frac{s\big((a\pm4)\lambda\big)s\big((a\pm5)\lambda\big)s\big(u\big)s\big(\lambda+u\big)s\big((a\pm3)\lambda\mp u\big)}{s\big(2\lambda\big)s\big(3\lambda\big)s\big((a\pm1)\lambda\big)s\big((a\pm2)\lambda\big)s\big((a\pm3)\lambda\big)} \tag{B.37h}$$

$$W_{3,3}\Big(\begin{matrix}a\pm1 & a\pm4\\ a & a\pm3\end{matrix}\Big|u\Big) = W_{3,3}\Big(\begin{matrix}a\pm3 & a\pm4\\ a & a\pm1\end{matrix}\Big|u\Big) = \tag{B.37i}$$

$$= -\frac{s\big((a\pm4)\lambda\big)s\big((a\pm5)\lambda\big)s\big(u\big)s\big(u-\lambda\big)s\big(\lambda+u\big)}{s\big(2\lambda\big)s\big(3\lambda\big)s\big((a\pm1)\lambda\big)s\big((a\pm2)\lambda\big)}$$

$$W_{3,3}\Big(\begin{matrix}a\pm3 & a\pm2\\ a & a\pm3\end{matrix}\Big|u\Big) = -\frac{s\big((a\pm4)\lambda\big)s\big(u\big)s\big((a\pm2)\lambda\mp u\big)s\big((a\pm3)\lambda\mp u\big)}{s\big(3\lambda\big)s\big((a\pm1)\lambda\big)s\big((a\pm2)\lambda\big)s\big((a\pm3)\lambda\big)} \tag{B.37j}$$

$$W_{3,3}\Big(\begin{matrix}a\pm1 & a\pm2\\ a & a\pm3\end{matrix}\Big|u\Big) = W_{3,3}\Big(\begin{matrix}a\pm3 & a\pm2\\ a & a\pm1\end{matrix}\Big|u\Big) = \tag{B.37k}$$

$$= \frac{s\big((a\pm4)\lambda\big)s\big(u\big)s\big(u-\lambda\big)s\big((a\pm2)\lambda\mp u\big)}{s\big(3\lambda\big)s\big((a\pm1)\lambda\big)s\big((a\pm2)\lambda\big)}$$

$$W_{3,3}\Big(\begin{matrix}a\mp1 & a\pm2\\ a & a\pm3\end{matrix}\Big|u\Big) = W_{3,3}\Big(\begin{matrix}a\mp3 & a\mp2\\ a & a\pm1\end{matrix}\Big|u\Big) = \tag{B.37l}$$

$$= -\frac{s\big((a\mp4)\lambda\big)s\big(2\lambda-u\big)s\big(\lambda-u\big)s\big(u\big)}{s\big(2\lambda\big)s\big(3\lambda\big)s\big((a\mp1)\lambda\big)}$$

$$W_{3,3}\Big(\begin{matrix}a\pm1 & a\pm4\\ a & a\pm1\end{matrix}\Big|u\Big) = \frac{s\big(3\lambda\big)s\big((a\pm3)\lambda\big)(s\big((a\pm4)\lambda\big)s\big(u\big)s\big(u+\lambda\big)s\big((a\pm1)\lambda\pm u\big)}{s\big(2\lambda\big)s\big((a-1)\lambda\big)s\big((a+1)\lambda\big)s\big((a\pm2)\lambda\big)} \tag{B.37m}$$

$$W_{3,3}\left(\begin{matrix} a\pm 1 & a\pm 2 \\ a & a\pm 1 \end{matrix}\middle| u\right) = -\frac{s\big(a\lambda\big)s\big((a\pm 3)\lambda\big)s\big((a\pm 4)\lambda\big)s\big(u\big)^2 s\big(u-\lambda\big)}{s\big(2\lambda\big)s\big(3\lambda\big)s\big((a\pm 1)\lambda\big)^2 s\big((a\pm 2)\lambda\big)} - \tag{B.37n}$$

$$- \frac{s\big((a\pm 3)\lambda\big)s\big(u\big)s\big(a\lambda\pm u\big)s\big((a\pm 1)\lambda\mp u\big)}{s\big((a\mp 1)\lambda\big)s\big((a\pm 1)\lambda\big)^2}$$

$$W_{3,3}\left(\begin{matrix} a\mp 1 & a\pm 2 \\ a & a\pm 1 \end{matrix}\middle| u\right) = W_{3,3}\left(\begin{matrix} a\mp 1 & a\mp 2 \\ a & a\pm 1 \end{matrix}\middle| u\right) = \tag{B.37o}$$

$$= \frac{s\big((a\pm 3)\lambda\big)s\big(u\big)s\big(u-\lambda\big)s\big(a\lambda\pm u\big)}{s\big((a-1)\lambda\big)s\big((a+1)\lambda\big)}$$

$$W_{3,3}\left(\begin{matrix} a\pm 1 & a\mp 2 \\ a & a\pm 1 \end{matrix}\middle| u\right) = -\frac{s\big(3\lambda\big)s\big(a\mp 2\lambda\big)s\big(u\big)s\big(a\lambda\mp u\big)s\big((a\pm 1)\lambda\mp u\big)}{s\big((a-1)\lambda\big)s\big((a+1)\lambda\big)s\big((a\pm 2)\lambda\big)} \tag{B.37p}$$

Appendix C

Supersymmetric fermion chain without particle conservation

C.1 Groundstate degeneracy for $L = 4n$

In this appendix we discuss the degeneracy of the $L = 4n$ groundstates in details. We give comments on the $L = 4n + 2$ case, and give a conjecture on the exact groundstate degeneracy based on numerical studies.
For $L = 4n$, the groundstate energy $\Lambda_G S^{(L=4n)} = 0$. Our aim is to explain the extensiveness of the groundstate degeneracy, based on the counting of zero mode solutions built on the groundstates in sector $(2n, 0)$, described in section 4.5.3. A solution in sector $(2n, k)$ satisfies the following equations

$$z_j^L = \pm \mathrm{i}^{-L/2} \prod_{l=1}^{k} \frac{u_l - (z_j - 1/z_j)^2}{u_l + (z_j - 1/z_j)^2}, \qquad j = 1, \ldots, 2n \tag{C.1a}$$

$$1 = \prod_{j=1}^{k} \frac{u_l - (z_j - 1/z_j)^2}{u_l + (z_j - 1/z_j)^2}, \qquad l = 1, \ldots, k. \tag{C.1b}$$

Plugging in the groundstate solution (eq. 4.128), as $\left(z_j^{(\pm)}\right)^L = \pm 1$, from eq. (C.1a) we get the consistency conditions

$$\prod_{l=1}^{k} \frac{u_l - (z_j - 1/z_j)^2}{u_l + (z_j - 1/z_j)^2} = \pm 1. \tag{C.2}$$

This can be satisfied by $u = 0$, $u = \infty$ and by purely imaginary complex conjugate u pairs, as for these

$$\frac{u - (z_j - 1/z_j)^2}{u + (z_j - 1/z_j)^2} \, \frac{u^* - (z_j - 1/z_j)^2}{u^* + (z_j - 1/z_j)^2} = 1. \tag{C.3}$$

The possible values of u_l's are fixed by (C.1b) which is a rational function in variable u after substituting the $z_j^{(\pm)}$'s of the groundstate solution. Whether the consistency condition eq. (C.2) gives $z_j^L = 1$ or $z_j^L = -1$ depends on the number of domain walls, and if $u = \infty$ is part of the solution or not.

- $+1$ equation:
  - even k, all the u_l's form complex conjugate pairs
  - odd k, $u_1 = \infty$, the rest of the u_l's form c.c. pairs
- -1 equation:
  - even k, $u_1 = 0$, $u_2 = \infty$, and the rest of the u_l's are c.c. pairs
  - odd k, $u_1 = 0$ and the other u_l's are c.c. pairs

We have to take into account that the self consistency condition (C.2) has different number of solutions depending on z_j's. If $z_j^L = -\mathrm{i}^{-L/2}$, it has $2n$ solutions for even n's, and $2n-1$ for odd ones. Out of these solutions, $2n-2$ are nonzero c.c. pairs, one is the $u = \infty$ solution, and for even number of solutions, $u = 0$ is also a solution.

The self consistency condition induced by $z_j^L = +\mathrm{i}^{-L/2}$ has $2n-1$ solutions for even n's, and $2n$ for odd ones. Out of these solutions, $2n-2$ are nonzero c.c. pairs, one is the $u = \infty$ solution, and for odd number of solutions, $u = 0$ is also a solution. We have to count the number of u solutions in c.c. pairs, as the degeneracy is from the possible choices among them, while we use $u = 0$ and $u = \infty$ to "tune" (C.1a) to ± 1.

In order to construct new groundstate solutions in the $(2n,\, k)$ sectors, we have to find self consistent solutions: we have to find a set of u_l's which give the expected $+1$ or -1 for (C.1a), and compute the degeneracy case by case. We have to distinguish eight cases: even or odd n, even or odd k, $+1$ or -1 equation and discuss these case by case:

- n even, k even, -1 equation: In order to get the -1 equation with even number of u_l's, $u_1 = 0$, $u_2 = \infty$, and the rest form c.c. pairs. The degeneracy is $\binom{n-1}{(k-2)/2}$.
- n even, k odd, -1 equation: To get the -1 equation, $u_1 = 0$, and the other $k-1$ u_l's form c.c. pairs. The degeneracy is $\binom{n-1}{(k-1)/2}$.
- n odd, k even, -1 equation: To get the -1 equation with even number of u's, we should have $u_1 = 0$, $u_2 = \infty$, but in this sector $u = 0$ is not a solution. Consequently, there is no consistent solution.
- n odd, k odd, -1 equation: To get the -1 equation with odd number of u's, we should have $u_1 = 0$, but in this sector $u = 0$ is not a solution. Consequently, there is no consistent solution.
- n even, k even, $+1$ equation: The k u's have to form $k/2$ c.c. pairs. No 0 or ∞ is involved. The degeneracy is $\binom{n-1}{k/2}$.
- n even, k odd, $+1$ equation: To satisfy the $+1$ equation, $u_1 = \infty$ and the rest form c.c. pairs. The degeneracy is $\binom{n-1}{(k-1)/2}$.
- n odd, k even, $+1$ equation: The k u's have to form $k/2$ c.c. pairs. No 0 or ∞ is involved. The degeneracy is $\binom{n-1}{k/2}$.
- n odd, k odd, $+1$ equation: To satisfy the $+1$ equation, $u_1 = \infty$ and the rest form c.c. pairs. The degeneracy is $\binom{n-1}{(k-1)/2}$.

Based on this, we can count the states in a certain sector. Instead of counting the explicit results, we would like to point out that summing over k results in a degeneracy proportional to 2^n. The exact number is not so interesting because this is only a partial degeneracy, with other symmetries, we can construct more states, however the exact number seems to be complicated to find.
Based on the numerical studies, we give the following conjecture for the degeneracy of the groundstate with $L = 4n$ system size

$$\#\text{ of GS:}\quad 2^{\frac{L}{2}+1} \tag{C.4}$$

For $L = 4n - 2$ systems, the previous degeneracy gives the degeneracy of the highest level state, which –according to eq. (4.118)– equals with the degeneracy of the groundstate of the antiperiodic system.

Summary

This thesis is centered around three topics, sharing integrability as a common theme. This thesis explores different methods in the field of integrable models. The second and third chapters are about integrable lattice models in statistical physics. The fourth chapter describes an integrable quantum chain. Integrable lattice models and quantum chains are closely related, both by the motivation to study them and by method to probe them. Typically, the Hamiltonian of the quantum chain is the logarithmic derivative of the transfer matrix of the corresponding lattice model: $H = \frac{d}{d\lambda} \log T(\lambda)|_{\lambda=0}$. One reason which makes these models interesting is exact solvability. They are typically strongly correlated systems which are impossible to approach with perturbation theory in interaction strength. In the context of statistical physics, integrable models can be used to compute universal quantities. They are also used as toy-models to learn about new phenomena, e.g. spin-charge separation is observed in the one-dimensional Hubbard-model. Low-dimensional systems with tunable parameters are realized in laboratories recently, giving direct experimental relevance to integrable systems.

Spin-1 current in the dilute $O(n = 1)$ loop model

In the second chapter, we considered the dilute $O(n = 1)$ loop model on a strip, with open boundary conditions. It is a lattice model, built up on the following face configurations

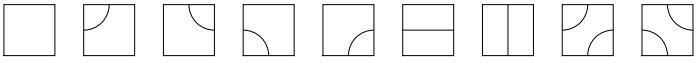

The interaction with the left boundary is described by the following plaquettes, by the elements of the left K-matrix

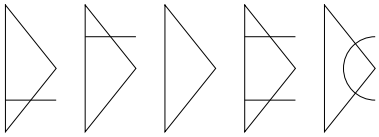

Interaction with the right boundary is described by the five vertically mirrored plaquettes. This model describes the statistical ensemble of dilute closed loops, possibly connected to the boundaries, with $n = 1$ loop weight. The model is treated in the framework of Sklyanin's double row transfer matrix, with inhomogeneous weights depending on rapidities (spectral parameters). At this special point, the largest eigenvalue of the T-matrix is simple, and the elements of the groundstate vector are polynomials in the rapidities. The quantum Knizhnik-Zamolodchikov equations (more precisely, an equivalent set of equations, which are loosely also called qKZ equations) are used to derive the groundstate elements.

We compute the spin-1 boundary to boundary current on a strip with finite width and infinite height. The spin-1 property means that each path between the two boundaries carries a unit current which –depending on the configuration– contributes to the mean current with a relative $\pm$ sign. The current passing between two arbitrary points is additive, consequently, it is sufficient to compute the current through a horizontal and vertical edge. We denote these quantities by X and Y, respectively. We find closed expressions for X and Y, in terms of rational functions in the rapidities. The expression for Y involves the partition sum, and symmetric in the rapidities, meaning that the current is translation invariant. The expression for X is substantially simpler, however it is not symmetric.

We explicitly calculated these expressions for small systems. Based on recursion relations, and some technical assumption we proved the form of the current for general system size. The technical assumptions are slightly different for X and Y. For X, we did not prove some of the symmetry in the rapidities, and used it as an assumption. We proved recursion relations in the width of the strip. The interaction with a boundary is characterized by a parameter, the so called boundary rapidity. It plays a similar role to the rapidities, and we observed for small systems that the symmetry in the rapidities includes the boundary rapidities also. For both X and Y, we assumed the symmetry between the normal and boundary rapidities. We constructed the K-matrix weights by the insertion of a line, which explains for certain other quantities the symmetry, however the proof does not apply for the current. We give numerical evidence

of the symmetry by computing small but highly nontrivial cases.

Fused RSOS models and finitized characters

In the third chapter, we considered the $n \times n$ fused $RSOS(m, m')$ models, further parametrized by the crossing parameter $\lambda = (m' - m)\pi/m'$. RSOS models are lattice models, where height variables on the vertices take values in a restricted range. Fusion is a construction by which one forms new solvable models from existing ones by effectively keeping only the variables of a sublattice of the original lattice. By $n \times n$ fusion, we consider the $n \times n$ blocks of the original lattice.

At criticality, the unfused $n = 1$ RSOS models are described by the minimal models, the simplest rational conformal field theories. At higher RSOS fusion level n, the continuum limit is expected to be described by higher n' fusion level coset models. Note that n and n' are different parameters. The parameter n characterizes the fused RSOS model which is constructed by the fusion of $n \times n$ faces of the unfused model. The parameter n' characterizes the level of the diagonal coset construction. Previous research by Tartaglia and Pearce conjectured that for $0 < \lambda < \frac{\pi}{n}$, $n \times n$ RSOS models are related to $n = n'$ coset models. The conjectured is based on computations performed for the $n = 2, 3$ cases.

Based on the Corner Transfer Matrix method, one-dimensional sums are computed in the low-temperature limit. With increasing size, the one-dimensional sums approximate the Virasoro characters of the corresponding conformal field theory. We use the same method to compute the $n = 2$ case for $\frac{\pi}{2} < \lambda < \pi$, and we find the finitized characters. Based on our computations, the corresponding conformal theories for the RSOS$(m, m')_{2\times 2}$ models are the $\mathcal{M}(m, m')$ minimal models. For both cases, closed expressions for the one-dimensional sums are found which we call finitized characters. The correspondence between the RSOS model and the CFT is proven, if based on the recursion relation and initial conditions, the one-dimensional sums are proven to be in the conjectured form. The proof is not complete for either case, as some further one-dimensional sums (not corresponding to finitized characters) are needed.

Jacob and Matthieu studied certain one-dimensional sums corresponding to paths with half-integer steps. These one-dimensional sums reproduce the Virasoro characters of the $\mathcal{M}(m, 2m + 1)$ models. By a bijection, we showed that the underlying lattice models of their one-dimensional sums are the 2×2

fused RSOS(m, $2m+1$) models.

Supersymmetric fermion chain

In Chapter 4 we introduce a new supersymmetric chain model, based on the M_1 model of Fendley, Schoutens and de Boer. The M_1 model describes spinless lattice fermions on a chain which interact via repulsion, i.e. the fermions are separated by at least one lattice site. It is an exactly solvable supersymmetric model with $\mathcal{N}=2$ supercharges.
We consider a fermion–hole symmetric modification of the model. The characteristics of the model change to a large extent, however some properties remain. All the energy levels become highly degenerate, and the fermion number is not a conserved quantity anymore. The degeneracy of all energy levels seems to be extensive, i.e. the degeneracy is a power of two with an exponent growing linearly in the system size. We give counting evidence that the degeneracy of the groundstate is extensive, and give the conjecture that it is exactly $2^{\frac{L}{2}+1}$. Supersymmetry and integrability are kept, providing powerful tools to solve the model.
We solved the model by means of the nested coordinate Bethe ansatz. We give the Bethe equations. This reduces the problem of diagonalizing a $2^L \times 2^L$ matrix to solving $\mathcal{O}(L)$ coupled nonlinear algebraic equations. The Bethe ansatz gives the solution in terms of the Bethe roots. As for the supersymmetric chain the fermion number is not conserved, it is not a good quantum number for the Bethe ansatz. We notice that the number of domain walls –separating strings of fermions from string of empty sites– is conserved. There are two types of domain walls, domain walls on even or odd site of the dual lattice, which are separately conserved. Hence, the Bethe ansatz is nested, and there are two sets of Bethe roots, $\{z_j\}_{j=1}^m$ and $\{u_l\}_{l=1}^k$. Both types of domain walls carry variable z, while odd domain walls also have variable u associated with them. We study the completeness of the Bethe solution by probing two explicit cases, the full spectrum of $L=6$ and the most degenerate $\Lambda=6$ eigenvalue at $L=10$. We find that the Bethe solution does not give the full spectrum, rather utilizing various symmetry transformations gives the full degeneracy of all the energies. The used symmetry transformations seems to be *ad hoc*, we do not know the complete symmetry group.
We study the symmetries characterizing the model, and give an exhaustive list of them. We explain the extensive degeneracy in terms of Cooper pair like excitations which are pairs of odd domain walls with u and $-u$ roots. Such new solutions do not change the eigenenergy, as the energy only depends on the z's.

We find the exact groundstate and first excited state solutions for the Bethe equations, for $L = 4n,\ n \in \mathbb{N}$. The energy follows for these cases, as $\Lambda_0 = 0$ and $\Lambda_1 = 4(1 - \cos(\pi/2n))$. This also shows that in the large size limit, the gap disappears as $\sim 1/L^2$, which is a characteristic of the classical diffusive systems.

Samenvatting

Dit proefschrift behandelt drie onderwerpen, die integreerbaarheid als een gemeenschappelijke thema gemeen hebben. Verschillende methodes uit de theorie van integreerbare modellen worden verkend. De hoofdstukken 2 en 3 gaan over integreerbaar roostermodellen in klassieke statistische fysica. Het laatste hoofdstuk behandelt een integreerbare quantumketen. Klassieke roostermodellen in twee dimensies en quantumketens zijn zeer verwant, zowel in de motivatie om ze te bestuderen als in de manier om ze te onderzoeken. Voor integreerbare roostermodellen geldt dat de Hamiltoniaan van de quantumketen de logaritmische afgeleide is van de transfermatrix van het overeenkomstige roostermodel naar de zogenaamde spectrale parameter λ: $H = \frac{\mathrm{d}}{\mathrm{d}\lambda} \log T\big|_{\lambda=0}$. De spectrale parameter kenmerkt een familie van onderling commuterende transfermatrices. De eigenvectoren hangen dus niet af van λ, maar de eigenwaarden (het spectrum) wel, vanwaar de naam spectrale parameter.
De belangrijkste reden waarom deze modellen interessant zijn, is de oplosbaarheid of ook wel integreerbaarheid, het feit dat eigenschappen berekend kunnen worden zonder benadering. Het zijn typisch sterk gecorreleerde systemen, die niet benaderd kunnen worden met een storingsreeks in wisselwerkingssterkte, zodat exacte oplossing overblijft als methode voor analyse. In de context van kritieke verschijnselen worden integreerbare modellen gebruikt om universele grootheid te berekenen. Voor universele grootheden is het geen bezwaar als de realistische beschrijving van microscopische details van de wisselwerkingen wordt opgeofferd aan integreerbaarheid. Ook worden integreerbare modellen gebruikt als *toy-models* om over nieuwe verschijnselen te leren, zoals de scheiding van spin en lading die wordt waargenomen in het ééndimensionale Hubbard-model. Laag-dimensionale systemen met instelbare parameters worden steeds vaker gerealiseerd in laboratoria, een nieuwe link tussen integreerbare systemen en het experiment. Zo is ook de vraag in hoeverre integreerbare systemen uitzonderlijk zijn in hun fysische eigenschappen experimenteel toegankelijk.

Spin-1 stroom in het verdunde O(n=1) lussenmodel

Het onderwerp van het tweede hoofdstuk is het verdunde O(n=1) lussenmodel op een strip, met open randvoorwaarden. De naam O(n) verwijst naar de orthogonale groep, de symmetriegroep van spinmodellen waarvan dit lussenmodel een herformulering is. De lussen zijn gesloten paden op het rooster, en het model wordt verdund genoemd, omdat de paden maar een fractie van de roosterplaatsen bezoeken. De configuraties van het roostermodel zijn opgebouwd met één van de volgende figuren op elk veld van het vierkante rooster

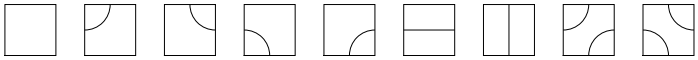

De interactie met de linker rand wordt beschreven door de volgende figuren

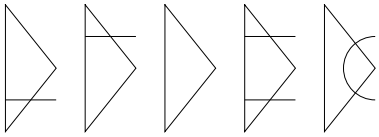

Deze figuren laten toe dat de paden eindigen op de rand. De interactie met de rechter rand wordt beschreven door de vijf analoge figuren, gespiegeld ten opzichte van die aan de linker rand.
Dit model beschrijft een statistische verdeling van paden, die gesloten lussen vormen, of eindigen op de randen. Het gewicht van elk pad is n. Het model wordt behandeld met behulp van Sklyanin's twee-rij-transfermatrix. De transfermatrix hangt af van de spectrale parameter, en daarnaast van een vrije parameter op elke roosterplaats, ook wel rapiditeit genoemd, omdat het analoog is aan een snelheid. Deze plaatsafhankelijkheid maakt het model inhomogeen. In het hier bestudeerde geval $n = 1$, is de grootste eigenwaarde van de T-matrix voor elke systeemgrootte eenvoudig uit te drukken, en zijn de elementen van de grondtoestandsvector polynomen in de rapiditeiten. De quantum Knizhnik-Zamolodchikov vergelijkingen (een reeks vergelijkingen, die ook qKZ vergelijkingen genoemd worden) worden gebruikt om de elementen van de grondtoestandsvector van de transfermatrix af te leiden.
We berekenen de verwachtingswaarde van de locale stroom tussen de twee randen op een strip met eindige breedte en oneindige hoogte, waarbij elk pad dat de twee randen verbindt, een eenheidsstroom voert van de linker naar de rechter rand. Voor elke configuratie van paden, zal dit, door een gegeven georienteerde link, resulteren in een stroom van grootte 0 of ± 1. Deze grootheid wordt ook wel

spin-1 stroom genoemd, om te benadrukken dat de stroom een vector grootheid is en de stroom door een gegeven link van teken omkeert als het pad dat de stroom voert, de link in omgekeerde richting passeert. De stroom die tussen twee willekeurige punten passeert is additief, d.w.z. de stroom tussen punten A en C is de som van de stroom tussen de punten A en B, en die tussen de punten B en C. Daarom is het voldoende om de stroom door een willekeurige horizontale en een willekeurige verticale link te berekenen. Deze twee grootheden duiden we aan met respectievelijk X en Y. Ons belangrijkste resultaat is een gesloten uitdrukking voor X en Y, in de vorm van van rationale functies in de rapiditeiten. De uitdrukking voor Y is symmetrisch onder verwisseling van de rapiditeiten en hangt ook af van de spectrale parameter. De symmetrie impliceert translatie invariantie, dit ondanks het feit dat het model inhomogeen is. De uitdrukking voor X is aanmerkelijk simpeler, en is symmetrisch in de rapiditeiten uitgezonderd de rapiditeit van de link waardoor de stroom wordt gemeten.
We hebben deze uitdrukkingen expliciet berekend voor kleine systemen (i.e. smalle strips). We hebben recursierelaties aangetoond in de breedte van de strip. Hiermee en met enkele technische veronderstellingen, vinden we daaruit de stroom voor willekeurige systeemgrootte. Over de technische veronderstellingen het volgende. Voor X hebben we de symmetrie in de rapiditeiten niet volledig bewezen, maar hebben volledige symmetrie verondersteld op basis van observatie. De interactie met een grens wordt gekenmerkt door een parameter, de zogenaamde grensrapiditeit. Deze speelt een soortgelijke rol als de rapiditeiten, en we zagen in kleine systemen, dat de symmetrie in de rapiditeiten ook de grensrapiditeit bevat. Daarom is voor zowel X als Y hebben we de symmetrie tussen de normale en grens rapiditeiten verondersteld. We hebben de randgewichten geconstrueerd door een lijn in te voegen, die voor bepaalde andere grootheden de symmetrie verklaart, maar net niet voor de stroom.
Tenslotte hebben we de veronderstelling van symmetrie door een numerieke berekening ondersteund.

Gefuseerde RSOS modellen en finitized characters

In het derde hoofdstuk, beschouwen we $n \times n$ gefuseerd $RSOS(m, m')$ modellen, met een belangrijke rol voor de *crossing* parameter $\lambda = (m' - m)\pi/m'$. RSOS modellen zijn roostermodellen, waar hoogtevariabelen op de vertices van een rooster waarden in een beperkt bereik aannemen. Fusie is een constructie waarmee nieuwe oplosbare modellen uit bestaande worden gemaakt, door alleen de variabelen van een subrooster van het oorspronkelijke rooster te behouden. De parameters in het oorspronkelijke model worden zo gekozen dat de overige

variabelen kunnen worden uitgesommeerd. Door een $n \times n$ fusie beschouwen we de $n \times n$ blokken van het oorspronkelijke rooster.
De oorspronkelijke $n = 1$ modellen hebben een kritiek punt waarin de schaallimiet beschreven wordt door de zogenaamde minimale modellen, de eenvoudigste rationele conformale veldtheorieën. Na fusie van het RSOS model in $n \times n$ blokken, wordt verwacht dat de schaallimiet wordt beschreven door hogere n' level coset modellen. Merk op dat n en n' differente parameters zijn. De parameter n karakteriseert de fusie-constructie van het RSOS-model. De parameter n' karakteriseert het niveau van de diagonale coset constructie die de basis vormt voor de conforme veldentheorie. Eerder onderzoek door Tartaglia en Pearce heeft geleid tot het voorstel dat voor $0 < \lambda < \frac{\pi}{n}$, $n \times n$ RSOS modellen via de schaallimiet gerelateerd zijn aan $n' = n$ coset modellen, zodat beide parameters dezelfde waarde aannemen. In dit proefschrift wordt dat werk uitgebreid naar $\frac{\pi}{n} < \lambda < \pi$.
Op basis van de *corner transfermatrix* methode werden toestandssommen berekend in een limiet waarin lage temperatuur wordt gecombineerd met hoge anisotropie. In deze limiet wordt het model vrijwel ééndimensionaal. Met de toenemende grootte van het systeem benaderen de ééndimensionale toestandssommen de Virasoro-karakters van de bijbehorende conforme veldentheorie. We hebben deze methode gebruikt om het $n = 2$ geval voor $\frac{\pi}{2} < \lambda < \pi$ te berekenen en de karakters te vinden. Onze berekeningen laten zien dat voor de RSOS$(m,\, m')_{2\times 2}$ de corresponderende conforme theoriën de $\mathcal{M}(m,\, m')$ minimale modellen zijn. Voor beide zijden van de correspondentie worden gesloten uitdrukkingen gevonden voor de eindige ééndimensionale sommen, *finitized characters* genoemd. Dat de uitdrukkingen gelijk zijn is niet in alle gevallen volledig bewezen. Voor het bewijs zijn nog enkele ééndimensionale toestandssommen nodig die niet overeenkomen met finitized characters.
Voor de gevallen $(m, m') = (m, 2m + 1)$, is het bewijs wel volledig gevonden op basis van werk van Jacob en Matthieu. Zij bestudeerden bepaalde ééndimensionale sommen die overeenkomen met paden met halve integerstappen. Deze ééndimensionale sommen reproduceren de Virasoro karakters van de $\mathcal{M}(m,\, 2m + 1)$ modellen. Door een bijectie hebben we aangetoond dat de onderliggende roostermodellen van hun ééndimensionale sommen zijn de 2×2 gefuseerd RSOS$(m,\, 2m + 1)$ modellen.

Supersymmetrisch fermionketen

In het vierde hoofdstuk wordt een nieuwe supersymmetrische quantumketen ingevoerd, gebaseerd op het M_1-model van Fendley, Schoutens en de Boer. Het

M_1-model beschrijft spinvrije fermionen op een keten die inwerken op elkaar via afstoting, d.w.z. de fermionen worden tenminste gescheiden door één lege roosterplaats. Het is een exact oplosbaar supersymmetrisch model met $\mathcal{N} = 2$ supercharges.

Hier wordt het model M_1 gemodificeerd om de gat-deeltje symmetrie te herstellen. De kenmerken van het model veranderen sterk, maar sommige eigenschappen blijven overeind. Alle energie niveaus zijn sterk gedegenereerd, en het fermion nummer is niet meer een behouden grootheid. Terwijl in het M_1 model de generieke energie-niveaus tweevoudig ontaard zijn, is hier de ontaardingsgraad van elk niveau steeds een macht van twee, met een exponent die lineair lijkt te groeien met de systeemgrootte. Voor de ontaardingsgraad van de grondtoestand hebben we argumenten dat deze gelijk is aan $2^{\frac{L}{2}+1}$ is. Supersymmetrie en integreerbaarheid zijn beide van toepassing, zodat krachtige instrumenten beschikbaar zijn om het model te analyseren.

We bestuderen het model door middel van de geneste coördinaten Bethe Ansatz. We hebben de Bethe vergelijkingen uitgewerkt. Deze vergelijkingen alleen al reduceren het probleem van het diagonaliseren van een $2^L \times 2^L$ matrix tot het oplossen van $\mathcal{O}(L)$ gekoppelde niet-lineaire algebraische vergelijkingen. De Bethe Ansatz geeft de eigenwaarden van de Hamiltoniaan in termen van de oplossingen van die vergelijkingen, de Bethe-wortels. Omdat voor de supersymmetrische keten het fermiongetal niet behouden is, is het ook geen goed quantumgetal voor de Bethe Ansatz. Wat wel behouden blijkt is het aantal domeingrenzen tussen bezette en onbezette posities. Als we de domeingrenzen op even en oneven posities onderscheiden, blijken beide aantallen afzonderlijk behouden te zijn. Als gevolg hiervan is de Bethe Ansatz genest, en er zijn twee sets van Bethe-wortels, $\{z_j\}_{j=1}^m$ and $\{u_l\}_{l=1}^k$. Beide soorten domeingrenzen worden gekarakteriseerd door de parameter z, terwijl oneven domeingrenzen tevens een tweede parameter u voeren.

We bestuderen de volledigheid van de Bethe-oplossing door twee gevallen te onderzoeken, het volledige spectrum van $L = 6$ en de meest ontaard $\Lambda = 6$ eigenwaarde bij $L = 10$. We hebben gevonden dat de Bethe-oplossingen wel het volledige spectrum, maar niet de volledige ontaardingsgraad geeft. Door gebruik te maken van verschillende symmetrieën wordt toch de volledige ontaardingsgraad gevonden. De preciese structuur van de symmetriegroep blijkt erg gecompliceerd te zijn.
Een groot aandeel in de ontaardingsgraad is het gevolg van tweetallen van domeingrenzen op oneven posities met tegengestelde waarden van de variabele u. In analogie met supergeleiding hebben we deze tweetallen Cooperparen genoemd. We hebben een operator geconstrueerd die twee even domeingrenzen omzet in

oneven domeingrenzen, en aldus een Cooperpaar creëert. Dergelijke nieuwe oplossingen veranderen de eigenwaarde voor de energie niet, omdat de energie bepaald wordt door de z-variabelen. We hebben de Bethe-oplossing voor de grondtoestand en de eerste aangeslagen toestand gevonden voor $L = 4n,\ n \in \mathbb{N}$. De energie volgt voor deze gevallen, als $\Lambda_0 = 0$ en $\Lambda_1 = 4(1 - \cos(\pi/2n))$. Dit impliceert dat de eerste aangeslagen toestand een energie heeft $\mathcal{O}(L^{-2})$ boven die van de grondtoestand. Het is opmerkelijk dat deze SUSY keten deze eigenschap gemeen heeft met een klassiek diffusief systeem.

Contribution to publications

Here, I give a detailed overview on my contribution to the publications, this basis is based on.

1. G. Z. Feher and B. Nienhuis. Currents in the dilute $O(n = 1)$ model. 2015, math-ph/1510.02721., *preprint*
   Exact closed formulae for the X and Y current. Numerical and analytical check of the symmetry of the expressions. Proof based on the recursion relation. Construction of the K-matrix via insertion of the rapidity line. Proof of the fusion equation.

2. György Z. Feher, Paul A. Pearce, and Alessandra Vittorini-Orgeas. One-dimensional sums and finitized characters of 2×2 fused RSOS models. 2016, *unpublished*
   Construction of fused face weights. Local energy functions without gauge modification. Exact expressions for the finitized characters. Numerical checks for the finitized characters.

3. Jan de Gier, Gyorgy Z. Feher, Bernard Nienhuis, and Magdalena Rusaczonek. Integrable supersymmetric chain without particle conservation. 2015, math-ph/1510.02520, *J. Stat. Mech. (2016) 023104*
   Little modification of Bethe equations. Completeness of Bethe equations. Certain symmetries, including the domain wall–non-domain wall symmetry, and the reflection of the spectrum. Exact Bethe solution for the groundstate, and the first excited state. Large system asymptotics of the system. Systematic counting of groundstates, conjecture on groundstate degeneracy.

Bibliography

[1] GZ Feher and B Nienhuis. Currents in the dilute $O(n = 1)$ model. *arXiv preprint arXiv:1510.02721*, 2015.

[2] György Z. Feher, Paul A. Pearce, and Alessandra Vittorini-Orgeas. One-dimensional sums and finitized characters of 2×2 fused RSOS models. Unpublished, 2016.

[3] Jan de Gier, Gyorgy Z Feher, Bernard Nienhuis, and Magdalena Rusaczonek. Integrable supersymmetric chain without particle conservation. *Journal of Statistical Mechanics: Theory and Experiment*, 2016(2):023104, 2016.

[4] Hans Bethe. Zur theorie der metalle. *Zeitschrift für Physik*, 71(3-4):205–226, 1931.

[5] LD Faddeev. How algebraic Bethe ansatz works for integrable model. *arXiv preprint hep-th/9605187*, 1996.

[6] Ernst Ising. Beitrag zur Theorie des Ferromagnetismus. *Zeitschrift für Physik A Hadrons and Nuclei*, 31(1):253–258, 1925.

[7] Harold NV Temperley and Elliott H Lieb. Relations between the 'percolation' and 'colouring' problem and other graph-theoretical problems associated with regular planar lattices: some exact results for the 'percolation' problem. In *Proceedings of the Royal Society of London A: Mathematical, Physical and Engineering Sciences*, volume 322, pages 251–280. The Royal Society, 1971.

[8] Richard Brauer. On algebras which are connected with the semisimple continuous groups. *Annals of Mathematics*, pages 857–872, 1937.

[9] Uwe Grimm and FY Wu. Dilute algebras and solvable lattice models. In *Proceedings of the Satellite Meeting of STATPHYS-19 on Statistical Models, Yang-Baxter Equation and Related Topics, edited by ML Ge and FY Wu (World Scientific, Singapore, 1996)*, pages 110–117, 1996.

[10] Elliott H Lieb. Residual entropy of square ice. *Physical Review*, 162(1):162, 1967.

[11] AB Zamolodchikov and VA Fateev. Model factorized S-matrix and an integrable spin-1 Heisenberg chain. *Sov. J. Nucl. Phys.(Engl. Transl.);(United States)*, 32(2), 1980.

[12] AG Izergin and VE Korepin. The inverse scattering method approach to the quantum Shabat-Mikhailov model. *Communications in Mathematical Physics*, 79(3):303–316, 1981.

[13] VV Bazhanov and AG Shadrikov. Trigonometric solutions of triangle equations. Simple Lie superalgebras. *Theoretical and Mathematical Physics*, 73(3):1302–1312, 1987.

[14] Bernard Nienhuis. Critical spin-1 vertex models and $O(n)$ models. *International Journal of Modern Physics B*, 4(05):929–942, 1990.

[15] Bernard Nienhuis. Critical and multicritical $O(n)$ models. *Physica A: Statistical Mechanics and its Applications*, 163(1):152–157, 1990.

[16] William H Mills, David P Robbins, and Howard Rumsey. Alternating sign matrices and descending plane partitions. *Journal of Combinatorial Theory, Series A*, 34(3):340–359, 1983.

[17] Vladimir E Korepin. Calculation of norms of Bethe wave functions. *Communications in Mathematical Physics*, 86(3):391–418, 1982.

[18] Anatoli G Izergin. Partition function of the six-vertex model in a finite volume. In *Soviet Physics Doklady*, volume 32, page 878, 1987.

[19] Anatoli G Izergin, David A Coker, and Vladimir E Korepin. Determinant formula for the six-vertex model. *Journal of Physics A: Mathematical and General*, 25(16):4315, 1992.

[20] Greg Kuperberg. Another proof of the alternative-sign matrix conjecture. *International Mathematics Research Notices*, 1996(3):139–150, 1996.

[21] Alexander V Razumov and Yu G Stroganov. Spin chains and combinatorics. *Journal of Physics A: Mathematical and General*, 34(14):3185, 2001.

[22] MT Batchelor, J De Gier, and B Nienhuis. The quantum symmetric XXZ chain at Δ=-1/2, alternating-sign matrices and plane partitions. *Journal of Physics A: Mathematical and General*, 34(19):L265, 2001.

[23] Alexander V Razumov and Yu G Stroganov. Combinatorial nature of the ground-state vector of the $O(1)$ loop model. *Theoretical and mathematical physics*, 138(3):333–337, 2004.

[24] Luigi Cantini and Andrea Sportiello. Proof of the Razumov–Stroganov conjecture. *Journal of Combinatorial Theory, Series A*, 118(5):1549–1574, 2011.

[25] Philippe Di Francesco and Paul Zinn-Justin. Around the Razumov-Stroganov conjecture: proof of a multi-parameter sum rule. *Journal of Combinatorics*, 12(1):R6, 2005.

[26] P Di Francesco and Paul Zinn-Justin. The quantum Knizhnik–Zamolodchikov equation, generalized Razumov–Stroganov sum rules and extended Joseph polynomials. *Journal of Physics A: Mathematical and General*, 38(48):L815, 2005.

[27] Stanislav Smirnov. Conformal invariance in random cluster models. I. Holmorphic fermions in the Ising model. *Annals of mathematics*, pages 1435–1467, 2010.

[28] Bernard Nienhuis. Exact critical point and critical exponents of $O(n)$ models in two dimensions. *Physical Review Letters*, 49(15):1062, 1982.

[29] HWJ Blote and B Nienhuis. Critical behaviour and conformal anomaly of the $O(n)$ model on the square lattice. *Journal of Physics A: Mathematical and General*, 22(9):1415, 1989.

[30] Hugo Duminil-Copin and Stanislav Smirnov. Conformal invariance of lattice models. *Probability and statistical physics in two and more dimensions*, 15:213–276, 2012.

[31] MA Rajabpour and John Cardy. Discretely holomorphic parafermions in lattice Z_N models. *Journal of Physics A: Mathematical and Theoretical*, 40(49):14703, 2007.

[32] Yacine Ikhlef and John Cardy. Discretely holomorphic parafermions and integrable loop models. *Journal of Physics A: Mathematical and Theoretical*, 42(10):102001, 2009.

[33] John Cardy. Discrete holomorphicity at two-dimensional critical points. *Journal of Statistical Physics*, 137(5-6):814–824, 2009.

[34] Yacine Ikhlef and Mohammad Ali Rajabpour. Discrete holomorphic parafermions in the Ashkin–Teller model and SLE. *Journal of Physics A: Mathematical and Theoretical*, 44(4):042001, 2010.

[35] M Tanhayi-Ahari and S Rouhani. Discrete holomorphic parafermions in the eight vertex model. *arXiv preprint arXiv:1209.4253*, 2012.

[36] IT Alam and MT Batchelor. Integrability as a consequence of discrete holomorphicity: the Z_N model. *Journal of Physics A: Mathematical and Theoretical*, 45(49):494014, 2012.

[37] Jan De Gier, Alexander Lee, and Jørgen Rasmussen. Discrete holomorphicity and integrability in loop models with open boundaries. *Journal of Statistical Mechanics: Theory and Experiment*, 2013(02):P02029, 2013.

[38] Jan De Gier, Bernard Nienhuis, and Anita Ponsaing. Exact spin quantum Hall current between boundaries of a lattice strip. *Nuclear Physics B*, 838(3):371–390, 2010.

[39] Vadim Gorin and Greta Panova. Asymptotics of symmetric polynomials with applications to statistical mechanics and representation theory. *The Annals of Probability*, 43(6):3052–3132, 2015.

[40] Rodney J Baxter. *Exactly solved models in statistical mechanics*. Elsevier, 1982.

[41] Evgeni K Sklyanin. Boundary conditions for integrable quantum systems. *Journal of Physics A: Mathematical and General*, 21(10):2375, 1988.

[42] Oskar Perron. Zur Theorie der Matrices. *Mathematische Annalen*, 64(2):248–263, 1907.

[43] Ferdinand Georg Frobenius. Über Matrizen aus nicht negativen Elementen. 1912.

[44] Igor B Frenkel and N Yu Reshetikhin. Quantum affine algebras and holonomic difference equations. *Communications in mathematical physics*, 146(1):1–60, 1992.

[45] Feodor A Smirnov. Form factors in completely integrable models of quantum field theory, 1992.

[46] Alexandr Garbali and Bernard Nienhuis. The dilute temperley-lieb O(n = 1) loop model on a semi infinite strip: the sum rule. *arXiv preprint arXiv:1411.7160*, 2014.

[47] Alexandr Garbali and Bernard Nienhuis. The dilute Temperley-Lieb O(n = 1) loop model on a semi infinite strip: the ground state. *arXiv preprint arXiv:1411.7020*, 2014.

[48] Subir Ghoshal and Alexander Zamolodchikov. Boundary S matrix and boundary state in two-dimensional integrable quantum field theory. *International Journal of Modern Physics A*, 9(21):3841–3885, 1994.

[49] Alexander A Belavin, Alexander M Polyakov, and Alexander B Zamolodchikov. Infinite conformal symmetry in two-dimensional quantum field theory. *Nuclear Physics B*, 241(2):333–380, 1984.

[50] George E Andrews, Rodney J Baxter, and Peter J Forrester. Eight-vertex SOS model and generalized Rogers-Ramanujan-type identities. *Journal of Statistical Physics*, 35(3-4):193–266, 1984.

[51] Peter J Forrester and Rodney J Baxter. Further exact solutions of the eight-vertex SOS model and generalizations of the Rogers-Ramanujan identities. *Journal of statistical physics*, 38(3-4):435–472, 1985.

[52] Daniel Friedan, Zongan Qiu, and Stephen Shenker. Conformal invariance, unitarity, and critical exponents in two dimensions. *Physical Review Letters*, 52(18):1575, 1984.

[53] David A Huse. Exact exponents for infinitely many new multicritical points. *Physical Review B*, 30(7):3908, 1984.

[54] Harold Riggs. Solvable lattice models with minimal and nonunitary critical behaviour in two dimensions. *Nuclear Physics B*, 326(3):673–688, 1989.

[55] Tomoki Nakanishi. Non-unitary minimal models and RSOS models. *Nuclear Physics B*, 334(3):745–766, 1990.

[56] Lars Onsager. Crystal statistics. I. A two-dimensional model with an order-disorder transition. *Physical Review*, 65(3-4):117, 1944.

[57] Barry M McCoy and Tai Tsun Wu. *The two-dimensional Ising model*. Courier Corporation, 2014.

[58] Robert B Griffiths. Thermodynamics near the two-fluid critical mixing point in He 3-He 4. *Physical Review Letters*, 24(13):715, 1970.

[59] M Blume, VJ Emery, and Robert B Griffiths. Ising model for the λ transition and phase separation in He 3-He 4 mixtures. *Physical review A*, 4(3):1071, 1971.

[60] Michael Lässig, Giuseppe Mussardo, and John L Cardy. The scaling region of the tricritical Ising model in two dimensions. *Nuclear Physics B*, 348(3):591–618, 1991.

[61] Andreas Klümper and Paul A Pearce. Analytic calculation of scaling dimensions: tricritical hard squares and critical hard hexagons. *Journal of statistical physics*, 64(1-2):13–76, 1991.

[62] Chen-Ning Yang and Tsung-Dao Lee. Statistical theory of equations of state and phase transitions. I. Theory of condensation. *Physical Review*, 87(3):404, 1952.

[63] Michael E Fisher. Yang-Lee edge singularity and ϕ 3 field theory. *Physical Review Letters*, 40(25):1610, 1978.

[64] John L Cardy. Conformal invariance and the Yang-Lee edge singularity in two dimensions. *Physical review letters*, 54(13):1354, 1985.

[65] Zoltan Bajnok, Omar el Deeb, and Paul A Pearce. Finite-volume spectra of the Lee-Yang model. *arXiv preprint arXiv:1412.8494*, 2014.

[66] PP Kulish, N Yu Reshetikhin, and EK Sklyanin. Yang-Baxter equation and representation theory: I. *Letters in Mathematical Physics*, 5(5):393–403, 1981.

[67] E Date, M Jimbo, A Kuniba, T Miwa, and M Okado. Exactly solvable SOS models II: Proof of the star-triangle relation and combinatorial identities. *Yang-Baxter Equation In Integrable Systems. Series: Advanced Series in Mathematical Physics, ISBN: 978-981-02-0120-3. WORLD SCIENTIFIC, Edited by Michio Jimbo, vol. 10, pp. 509-614*, 10:509–614, 1990.

[68] P Goddard, Adrian Kent, and David Olive. Virasoro algebras and coset space models. *Physics Letters B*, 152(1-2):88–92, 1985.

[69] Peter Goddard, Adrian Kent, and David Olive. Unitary representations of the Virasoro and super-Virasoro algebras. *Communications in Mathematical Physics*, 103(1):105–119, 1986.

[70] VV Bazhanov and N Yu. Reshetikhin. Critical RSOS models and conformal field theory. *International Journal of Modern Physics A*, 4(01):115–142, 1989.

[71] Andreas Klümper and Paul A Pearce. Conformal weights of RSOS lattice models and their fusion hierarchies. *Physica A: Statistical Mechanics and its Applications*, 183(3):304–350, 1992.

[72] Anne Schilling. Multinomials and polynomial bosonic forms for the branching functions of the $\widehat{su}(2)_M \times \widehat{su}(2)_N/\widehat{su}(2)_{M+N}$ conformal coset models. *Nuclear Physics B*, 467(1):247–271, 1996.

[73] Elena Tartaglia and Paul A Pearce. Fused RSOS lattice models as higher-level nonunitary minimal cosets. *Journal of Physics A: Mathematical and Theoretical*, 49(18):184002, 2016.

[74] P Jacob and P Mathieu. A new path description for the $\mathcal{M}(k+1)m\,2k+3$ models and the dual $\mathbb{Z}_k$ graded parafermions. *Journal of Statistical Mechanics: Theory and Experiment*, 2007(11):P11005, 2007.

[75] Julius Wess and Bruno Zumino. Consequences of anomalous Ward identities. *Physics Letters B*, 37(1):95–97, 1971.

[76] Edward Witten. Global aspects of current algebra. *Nuclear Physics B*, 223(2):422–432, 1983.

[77] Edward Witten. Non-abelian bosonization in two dimensions. *Communications in Mathematical Physics*, 92(4):455–472, 1984.

[78] Sergei P Novikov. Multivalued functions and functionals. An analogue of the Morse theory. In *Soviet Math. Dokl*, volume 24, pages 222–226. Citeseer, 1981.

[79] Al B Zamolodchikov. Higher-order integrals of motion in two-dimensional models of the field theory with a broken conformal symmetry. *ZhETF Pisma Redaktsiiu*, 46:129, 1987.

[80] AB Zamolodchikov. Integrals of motion in scaling 3-state Potts model field theory. *International Journal of Modern Physics A*, 3(03):743–750, 1988.

[81] AB Zamolodchikov. Integrable field theory from conformal field theory. 1990.

[82] R Jo Baxter. Corner transfer matrices of the eight-vertex model. I. Low-temperature expansions and conjectured properties. *Journal of Statistical Physics*, 15(6):485–503, 1976.

[83] RJ Baxter. Corner transfer matrices of the eight-vertex model. II. The Ising model case. *Journal of Statistical Physics*, 17(1):1–14, 1977.

[84] Rodney J Baxter. *Exactly solved models in statistical mechanics*. Courier Corporation, 2007.

[85] Omar Foda and Trevor A Welsh. On the combinatorics of Forrester-Baxter models. In *Physical combinatorics*, pages 49–103. Springer, 2000.

[86] Masaki Kashiwara and Tetsuji Miwa. *Physical combinatorics*, volume 191. Springer Science & Business Media, 2012.

[87] S Ole Warnaar. Fermionic solution of the Andrews-Baxter-Forrester model. I. Unification of TBA and CTM methods. *Journal of statistical physics*, 82(3-4):657–685, 1996.

[88] S Ole Warnaar. Fermionic solution of the Andrews-Baxter-Forrester model. II. Proof of Melzer's polynomial identities. *Journal of statistical physics*, 84(1-2):49–83, 1996.

[89] Goro Hatayama, Atsuo Kuniba, Masato Okado, Taichiro Takagi, and Zengo Tsuboi. Paths, crystals and fermionic formulae. In *MathPhys Odyssey 2001*, pages 205–272. Springer, 2002.

[90] P Jacob and P Mathieu. Particles in RSOS paths. *Journal of Physics A: Mathematical and Theoretical*, 42(12):122001, 2009.

[91] Pierre Mathieu. Paths and partitions: combinatorial descriptions of the parafermionic states. *Journal of Mathematical Physics*, 50(9):095210, 2009.

[92] Giovanni Feverati, Paul A Pearce, and Nicholas S Witte. Physical combinatorics and quasiparticles. *Journal of Statistical Mechanics: Theory and Experiment*, 2009(10):P10013, 2009.

[93] Michio Jimbo and Tetsuji Miwa. *Algebraic analysis of solvable lattice models*, volume 85. American Mathematical Soc., 1994.

[94] E Date, M Jimbo, A Kuniba, T Miwa, and M Okado. Exactly solvable SOS models: local height probabilities and theta function identities. *Nuclear Physics B*, 290:231–273, 1987.

[95] E Date, M Jimbo, A Kuniba, T Miwa, and M Okado. One-dimensional configuration sums in vertex models and affine Lie algebra characters. *letters in mathematical physics*, 17(1):69–77, 1989.

[96] George E Andrews and Rodney J Baxter. Lattice gas generalization of the hard hexagon model. III. q-Trinomial coefficients. *Journal of statistical physics*, 47(3-4):297–330, 1987.

[97] George E Andrews. *The theory of partitions*. Number 2. Cambridge university press, 1998.

[98] DA Kastor, EJ Martinec, and SH Shenker. RG flow in $N = 1$ discrete series. *Nuclear Physics B*, 316(3):590–608, 1989.

[99] Zongan Qiu. Supersymmetry, two-dimensional critical phenomena and the tricritical Ising model. *Nuclear Physics B*, 270:205–234, 1986.

[100] Omar Foda. A supersymmetric phase transition in Josephson-tunnel-junction arrays. *Nuclear Physics B*, 300:611–636, 1988.

[101] Hubert Saleur and Nicholas P Warner. Lattice models and $N = 2$ supersymmetry. In *Quantum Field Theory and String Theory*, pages 335–377. Springer, 1995.

[102] Paul Fendley, Kareljan Schoutens, and Jan de Boer. Lattice models with $N = 2$ supersymmetry. *Physical review letters*, 90(12):120402, 2003.

[103] Paul Fendley, Bernard Nienhuis, and Kareljan Schoutens. Lattice fermion models with supersymmetry. *Journal of Physics A: Mathematical and General*, 36(50):12399, 2003.

[104] Liza Huijse, Kareljan Schoutens, et al. Supersymmetry, lattice fermions, independence complexes and cohomology theory. *Advances in Theoretical and Mathematical Physics*, 14(2):643–694, 2010.

[105] G Misguich, D Serban, and V Pasquier. Quantum dimer model on the kagome lattice: Solvable dimer-liquid and ising gauge theory. *Physical review letters*, 89(13):137202, 2002.

[106] Paul Fendley and Kareljan Schoutens. Exact results for strongly correlated fermions in $2+1$ dimensions. *Physical review letters*, 95(4):046403, 2005.

[107] Hendrik van Eerten. Extensive ground state entropy in supersymmetric lattice models. *Journal of mathematical physics*, 46(12):123302, 2005.

[108] Paul Fendley and Kareljan Schoutens. Cooper pairs and exclusion statistics from coupled free-fermion chains. *Journal of Statistical Mechanics: Theory and Experiment*, 2007(02):P02017, 2007.

[109] Chen-Ning Yang. Some exact results for the many-body problem in one dimension with repulsive delta-function interaction. *Physical Review Letters*, 19(23):1312, 1967.

[110] M Gaudin. Un systeme a une dimension de fermions en interaction. *Physics Letters A*, 24(1):55–56, 1967.

[111] Leon N Cooper. Bound electron pairs in a degenerate Fermi gas. *Physical Review*, 104(4):1189, 1956.

[112] AN Kirillov. Combinatorial identities, and completeness of eigenstates of the heisenberg magnet. *Journal of Mathematical Sciences*, 30(4):2298–2310, 1985.

[113] Anatol N Kirillov and Nadejda A Liskova. Completeness of Bethe's states for the generalized XXZ model. *Journal of Physics A: Mathematical and General*, 30(4):1209, 1997.

[114] RJ Baxter. Completeness of the Bethe ansatz for the six and eight-vertex models. *Journal of statistical physics*, 108(1-2):1–48, 2002.

[115] Paul H Ginsparg. Applied conformal field theory. *arXiv preprint hep-th/9108028*, 63, 1988.

[116] Philippe Di Francesco, Pierre Mathieu, and David Sénéchal. *Conformal Field Theory*. Springer Science & Business Media, 1997.

[117] Changrim Ahn, Stephen-wei Chung, and S-H Henry Tye. New parafermion, SU(2) coset and N=2 superconformal field theories. *Nuclear Physics B*, 365(1):191–240, 1991.

[118] Alexander Berkovich, Barry M McCoy, Anne Schilling, and S Ole Warnaar. Bailey flows and Bose-Fermi identities for the conformal coset models $(A_1^{(1)})_N \times (A_1^{(1)})_{N'}/(A_1^{(1)})_{N+N'}$. *Nuclear Physics B*, 499(3):621–649, 1997.

[119] Victor G Kač and Dale H Peterson. Infinite-dimensional Lie algebras, theta functions and modular forms. *Advances in Mathematics*, 53(2):125–264, 1984.

[120] M Jimbo and T Miwa. *Irreducible Decomposition of Fundamental Modules for A*** and C***, and Hecke Modular Forms*. Kyoto University. Research Institute for Mathematical Sciences [RIMS], 1983.

[121] Doron Gepner and Zongan Qiu. Modular invariant partition functions for parafermionic field theories. *Nuclear Physics B*, 285:423–453, 1987.

[122] Jacques Distler and Zongan Qiu. BRS cohomology and a Feigin-Fuchs representation of Kač-Moody and parafermionic theories. *Nuclear Physics B*, 336(3):533–546, 1990.

[123] K Huitu, D Nemeschansky, and S Yankielowicz. $N = 2$ supersymmetry, coset models and characters. *Physics Letters B*, 246(1):105–113, 1990.

Acknowledgements

When I started my PhD in Amsterdam, I imagined it as an adventure, and I never thought that reality will outperform my expectations. I consider myself very lucky, as I had the chance to experience this particular four years.
I will never forget the warm and welcoming atmosphere that I received at the University of Amsterdam. The community welcomed me with a warm heart and made my integration smooth and easy. My first and utmost thanks goes to my supervisor, Bernard, who always treated me as an equal partner, and who was always there to answer my questions. Doing research with him is always fun and inspiring. He always gave me freedom, which -hopefully- helped me to be a better researcher.
I would like to thank Sasha Garbali for the many discussions, explanations, questions, and parties. He broke down the qKZ equations to me in a way that I could finally understand it. I am grateful for the numerous discussion I had with the colleagues from the math department, with Kayed Al-Qasimi and Jasper Stokman. It was a pleasure and to meet all the amazing people at IoP, including Kareljan Schoutens, Jean-Sébastien Caux, Sebas Eliëns, Jacopo De Nardis, Balázs Pozsgay, who helped me during the first times in A'dam, Omar El Araby, with whom we shared fun moments shooting videos, Rogier Vlijm, Enej Ilievski, Eoin Quinn, Michael Bjerngaard, who pushed me to run faster, even if I wanted to die, Ido Niesen, Ana Oliveira Silva, Jasper, Phillipe Corboz, Moos van Caspel, Diego Cohen, Irfan Ilgin, Laurens Kabir, Eva Llabres Llambias, Artem Nikitin, Yu Pan, Alona Tytarenko, Ari Turner.
Rianne van den Berg, Bram Wouters, Sergio Tapias Arze, it was always fun to share an office with you, and from time to time, escape work with tea-breaks.
I am very thankful for the work of Anna-Marieke Crommentuijn, Joost van Mameren, Fatima Ouzza, Natalie Wells, who took care of all the bureaucratic duties I couldn't have take care of, and answered all my dull questions with patience.
Life is not the same without friends, cheers to the "Dallasz" group: Teodóra

Bán, Blanka Zombori, Réka Ács, the people of Utrecht: Martina Radli, Hanna Zorandy, Zoltán Jeszenszky, and of course to Daniel Ignatius Jagadisan, Ke Tran, Péter Kovács, Bence Márkus, Ildikó Herczeg, Danilo Lewanski, Jule Kuhn, Istvan Zsolt Kulcsar, Gábor Szávai, and the whole "Túrórudi" group.
My PhD would have been a very different experience without my visit to Melbourne, which wouldn't have been possible without Jan de Gier and Paul Pearce. Thank you for your generosity and hospitality. Alessandra Vittorini Orgeas, Elena Tartaglia, it was always fun to do research with you. I met amazing people in Melbourne, both in and out of the math department, including Anita Ponsaing, Anthony Mays, with whom we learnt that busking is not so simple, Michael Wheeler, Omar Foda, Andrea Bedini, Joe Chan, Georgia Tsambos, David Diaz, Iriss Lam, Kathy Palmer, Mark Beltran. Riyan, Dinali, Elton, Manami, Abby, we know that GH rocks.
I would like to thank Elena Tartaglia, Sasha Garbali and Yein Oh for reading and commenting on my thesis.
I'm thankful for Paul Zinn-Justin and Gábor Takács for their hospitality while writing up my PhD.
I would like to thank Jean-Bernard Zuber and Paul Zinn-Justin for their valuable comments on my thesis.